Magdalena Wit

Protein Kinase D2 in the regulation of lipid droplet metabolism in enterocytes of the small intestine

PhD thesis
Completed in the Dioscuri Centre for Metabolic Diseases
at the Nencki Institute of Experimental Biology
Polish Academy of Sciences

SUPERVISOR
Dr. Grzegorz Sumara, Ph.D., D.Sc.

Warsaw, 2026

This study was supported by: Dioscuri Grant (Dioscuri Centres of Scientific Excellence), a program initiated by the Max Planck Society, jointly manager with the National Science Centrein Poland, and mutually funded by the Polish Ministry of Education and Science and the German Federal Ministry of Education and Research to Grzegorz Sumara, Polish National Science Centre OPUS grant (2022/45/B/NZ4/02175) to Grzegorz Sumara and Polish National Science Centre PRELUDIUM grant (2022/45/N/NZ4/02452) to Magdalena Wit.

ACKNOWLEDGEMENTS

I want to express my special thanks to:

My PhD supervisor, Dr. Grzegorz Sumara, for allowing me to start my research work in his laboratory, for scientific freedom and advice, support in testing new ideas, and all resources.

All members, past and present, of the Dioscuri Centre for Metabolic Diseases – you made that PhD journey a meaningful and good chapter. Thank you for being great colleagues in the lab and outside – Kasia, Filip, Angel, Toufic, Iza, Katia, Gosia, Dominika, Andrei, Rehab, Fareeha, Bartosz, Vishnu, Wiktoria, Jakub, Mythreyi, Maria.

Other members of the Nencki Community – whole team of Animal House, especially Kasia and Ola, for your patience and care (to the mice and Anibio), members of the Laboratory of Tissue Structure and Function – Natalia, Artur, Małgorzata - for help in darkness to see the bright colours.

Colleagues from other labs that I met throughout these years, especially members of the Dioscuri Centre for Chromatin Biology and Epigenomics. Eryk, thank you for always being there!

All collaborators and granting institutions.

Finally, to my Family and Friends: Ola, Kasia, Agnieszka, Paweł, my Grandparents, Brother, Mum and Dad.

I dedicate this work to all those taking their first steps in the scientific path – to keep brave and optimistic about facing the unknown.

ABSTRACT

Excessive consumption of energy-dense, lipid-rich foods promotes the development of obesity, diabetes, and atherosclerosis. Moreover, a high-fat diet increases the incidence of inflammatory bowel disease (IBD) and constitutes a significant risk factor for the development of colorectal cancer. Intestinal lipid absorption is a complex, multistep process initiated by the micellization of dietary fats by bile acids, followed by their digestion in the intestinal lumen, primarily by pancreatic lipase, the uptake of fatty acids (FA) and glycerol by enterocytes, and the subsequent resynthesis of triglycerides (TG) in the endoplasmic reticulum (ER). Following resynthesis, TGs may either be directed for secretion into the systemic circulation in specialized particles known as chylomicrons or stored in lipid droplets (LD) within intestinal epithelial cells. Aberrant activation of signalling cascades and hormonal imbalances are triggered by dietary fat overconsumption, and members of the Protein Kinase D (PKD) family have been found to be involved in several mechanisms mediating metabolic homeostasis. In our previous study, we identified that inhibition of protein kinase D2 in the intestine protects against the development of obesity due to reduced output of chylomicrons from the intestine. In the presented work, we aimed to identify additional mechanisms involved in lipid processing by intestinal epithelial cells, and we focused on pathways regulating lipid storage in lipid droplets (LD) and dependent on PKD2. We found that LDs in enterocytes forming in response to acute lipid challenge are bigger in size in the absence of PKD2 compared to wild-type mice, and their clearance is impaired. That is in line with aberrant trafficking of LD-associated lipases, which do not associate with LDs. We show that Golgi-resident PKD2 together with Golgi apparatus-resident proteins co-localize with LDs in PKD2-intact enterocytes, while kinase depletion results in Golgi apparatus disruption. Moreover, we identified that ingestion of dietary lipids physiologically triggers proteolysis of a rate-limiting lipase, ATGL, both *in vivo* and in mouse intestinal organoids, but it is prevented in enterocytes depleted of PKD2. We identify PKD2 as a novel regulator of LD metabolism, which indirectly controls lipolysis via enabling ATGL trafficking from the Golgi apparatus to LDs in enterocytes of the small intestine. Identification of the physiological event of ATGL degradation induced by dietary fat ingestion brings a novel insight into the metabolic adaptation capacity of intestinal epithelium. We hope that the data presented in this work not only contribute to a better understanding of mechanisms that govern intestinal lipid metabolism, but in a long term-perspective also lead to the discovery of novel therapeutic targets for pharmacological intervention in the treatment of obesity, diabetes, atherosclerosis, and IBD.

STRESZCZENIE

Nadmierne spożycie wysokoenergetycznej żywności bogatej w lipidy sprzyja rozwojowi otyłości, cukrzycy i miażdżycy. Ponadto dieta wysokotłuszczowa zwiększa częstość występowania nieswoistych chorób zapalnych jelit (IBD; z ang. *inflammatory bowel diseases*) oraz stanowi istotny czynnik ryzyka rozwoju raka jelita grubego. Wchłanianie lipidów w jelicie jest złożonym, wieloetapowym procesem, zapoczątkowanym przez micelizację tłuszczów pokarmowych przez kwasy żółciowe, a następnie ich trawienie w świetle jelita, głównie przez lipazę trzustkową, wychwyt kwasów tłuszczowych (FA; z ang. *fatty acids*) i glicerolu przez enterocyty oraz wtórną syntezę triglicerydów (TG; z ang. *triglycerides*) w retikulum endoplazmatycznym (ER; z ang. *endoplasmic reticulum*). Po resyntezie TG mogą być kierowane do wydzielania do krążenia ogólnego w wyspecjalizowanych cząstkach zwanych chylomikronami lub magazynowane w kroplach lipidowych (LD; z ang. *lipid droplets*) w komórkach nabłonka jelitowego. Nadmierne spożycie tłuszczów pokarmowych prowadzi do nieprawidłowej aktywacji kaskad sygnałowych oraz zaburzeń hormonalnych, a wykazano, że przedstawiciele rodziny kinaz białkowych D (PKD; z ang. *Protein Kinase D*) uczestniczą w wielu mechanizmach pośredniczących w utrzymaniu homeostazy metabolicznej. W naszych wcześniejszych badaniach wykazaliśmy, że hamowanie kinazy białkowej D2 (PKD2) w jelicie chroni przed rozwojem otyłości na skutek ograniczenia wydzielania chylomikronów z jelita. W niniejszej pracy skupiono się na dodatkowych mechanizmach zaangażowanych w metabolizm lipidów przez komórki nabłonka jelitowego, koncentrując się na zależnych od PKD2 szlakach regulujących magazynowanie lipidów w LD. Wykazano, że LD powstające w enterocytach w odpowiedzi na posiłek wysokotłuszczowy są większe u myszy pozbawionych PKD2 niż u myszy dzikiego typu, a ich usuwanie jest upośledzone. Zjawisku temu towarzyszy nieprawidłowy transport lipaz związanych z LD, które nie ulegają prawidłowej rekrutacji do kropli lipidowych. Wykazano również, że w enterocytach z zachowaną ekspresją PKD2 kinaza ta, zlokalizowana w aparacie Golgiego, wraz z innymi białkami rezydującymi w tym organellum, kolokalizuje z LD, podczas gdy delecja kinazy prowadzi do dezorganizacji aparatu Golgiego. Ponadto stwierdzono, że spożycie lipidów pokarmowych fizjologicznie indukuje proteolizę ATGL, kluczowej lipazy LD, zarówno in vivo, jak i w mysich organoidach jelitowych, jednak proces ten nie zachodzi w enterocytach pozbawionych PKD2. Uzyskane wyniki pozwalają zidentyfikować PKD2 jako nowy regulator metabolizmu LD, który pośrednio kontroluje lipolizę poprzez umożliwienie transportu ATGL z aparatu Golgiego do LD w enterocytach jelita cienkiego. Identyfikacja fizjologicznego zjawiska degradacji ATGL

indukowanej spożyciem tłuszczów pokarmowych dostarcza nowych informacji na temat zdolności nabłonka jelitowego do adaptacji metabolicznej. Przedstawione w tej pracy dane nie tylko przyczyniają się do lepszego zrozumienia mechanizmów regulujących metabolizm lipidów w jelicie, lecz także mogą w dłuższej perspektywie umożliwić identyfikację nowych celów terapeutycznych dla interwencji farmakologicznych w leczeniu otyłości, cukrzycy, miażdżycy oraz IBD.

TABLE OF CONTENTS

List of abbreviations

ACC – acetyl-CoA carboxylase

AMPK – AMP-activated protein kinase

APOA1 – apolipoprotein A1

APOA4 – apolipoprotein A4

APOB48 – apolipoprotein B48

ARFRP1 - ADP-ribosylation factor-related protein 1

ARL1 - ADP-ribosylation factor-like protein 1

ATGL – adipose triglyceride lipase

ATP – adenosine triphosphate

BAT – brown adipose tissue

BSA – bovine serum albumin

CB – cacodylate buffer

CCK – cholecystokinin

CD36 – cluster of differentiation 36

CE – cholesteryl esters

CES2 – carboxylesterase 2

CHX - cycloheximide

CGI-58 – comparative gene identification-58

CIDEB - cell death-inducing DFFA-Like Effector B

CM – chylomicron

CMA – chaperone-mediated autophagy

COP I/II – coat protein complex I/II

DAG – diacylglycerol

DGAT 1/2 – diacylglycerol acyltransferases ½

DMSO – dimethylsulfoxide

ECM – extracellular matrix

ER – endoplasmic reticulum

ERAD – endoplasmic reticulum-associated degradation

FABP – fatty acid binding protein

FATP4 – fatty acid transport protein 4

FBS – fetal bovine serum

FFD – fat-free diet

GAPDH - glyceraldehyde 3-phosphate dehydrogenase

GI - gastrointestinal

GIP – gastric inhibitory peptide

GLP-1/2 – glucagon-like peptide 1/2

GLUT2/5 – glucose transporter 2/5

GPAT4 – glycerol-3-phosphate acyltransferase 4

GRASP55 - Golgi reassembly-stacking protein of 55 kDa

HBSS – Hank's balanced salt solution

HDL – high density lipoprotein

HILPDA – hypoxia lipid droplet associated protein 2

HSL – hormone sensitive lipase

HSC70 – heat-shock protein 70

IBD – inflammatory bowel disease

IF – immunofluorescence

IHC – immunohistochemistry

LAL – lysosomal acid lipase

LAMP1 – lysosome-associated membrane protein 1

LAMP2A – lysosome associated membrane protein 2A

LC/MS – liquid chromatography/mass spectrometry

LC3 – microtubule-associated protein 1A/1B-light chain 3

LD – lipid droplet

LDAF1 – lipid droplet-associated factor 1

LDL – low density lipoprotein

LIR – LC3-interacting region

LPA – lysophosphatidic acid

LPAAT – lysophosphatidic acid acyltransferase

MAG – monoacylglyceride

MCFA – medium chain fatty acid

MGAT1/2 – monoacylglycerol acyltransferase 1/2

MGL – monoglyceride lipase

MMP 2/9 – matrix metalloproteinase 2/9

mTORC1 – mechanistic target of rapamycin complex 1

MTTP – microsomal triglyceride transfer protein

NAFLD – non-alcoholic fatty liver disease

OA – oleic acid

PA – palmitic acid

PBS – phosphate buffered saline

PBST - phosphate buffered salt solution with 0.05% Tween

PCTV – pre-chylomicron transport vesicle

PFA – paraformaldehyde

PKA – protein kinase A

PKD1/2/3 – protein kinase D1, 2, 3

PL – phospholipids

PLC – phospholipase C

PLIN1/2/3/5 – perilipin 1/2/3/5

PNPLA3 – patatin-like phospholipase domain-containing protein 3

PUFA – polyunsaturated fatty acid

PtdIns4P - phosphatidylinositol-4-phosphate

RFU – relative fluorescence unit

SCD1 – stearoyl-CoA desaturase 1

SCN – suprachiasmatic nucleus

SFA – saturated fatty acid

SGLT1/2 – sodium-glucose co-transporter 1/2

SREBP1C – sterol regulatory element-binding transcription factor 1

SQSTM1/p62 – sequestome 1

TBST – Tris buffered salt solution with 0.05% Tween 20

TEM – transmission electron microscopy

TG – triglyceride

TGN – trans-Golgi network

TGN46 – transgolgin 46

TLC – thin-layer chromatography

TMT – tandem mass tag

UCP1 – uncoupling protein 1

UPS – ubiquitin-proteasome system

VLDL – very low density lipoprotein

VPS - vacuolar protein sorting 13 homolog B

WAT – white adipose tissue

WB – western blotting

INTRODUCTION

Energy metabolism and organ coordination

Energy metabolism comprises the biochemical processes through which nutrients are transformed into usable cellular energy, primarily ATP, to sustain all vital functions (1). At the cellular level, this network includes glycolysis, the tricarboxylic acid cycle, oxidative phosphorylation, fatty acid oxidation, and, under certain physiological conditions, ketone body metabolism (1). These pathways do not operate independently because their activity is continuously adjusted to nutrient availability, hormonal signals, and tissue-specific energy demand (1). At the whole-body level, energy homeostasis depends on the integration of energy intake, storage, expenditure, and long-term disruption of this balance promotes excess adiposity and metabolic disease (2,3). For this reason, energy metabolism should be understood as a multi-organ process rather than as an isolated activity of particular tissues (1). The organism must continuously coordinate nutrient uptake after feeding, mobilization of stored substrates during fasting, and adaptive changes in fuel demand during exercise, cold exposure, or illness (1,2). Several systems play a key role in shaping of energy metabolism. The major one is the central nervous system as it integrates endocrine, neural, and nutrient-related signals that influence feeding behavior and energy expenditure (2). Signals related to nutritional state help the brain adapt appetite and metabolism to both short-term nutrient availability and longer-term energy stores (2). This central regulation is essential for maintaining body weight stability over time, although compensatory mechanisms may also oppose weight loss once obesity has developed (2,3).

Adipose tissue also plays a central role in systemic energy metabolism as it stores surplus energy and releases fuel when demand increases (1). In periods of positive energy balance, excess energy is deposited predominantly as triglycerides (TG), whereas fasting and increased energetic demand stimulate substrate mobilization from stored reserves (1,3). In addition to its storage function, adipose tissue contributes to metabolic regulation through endocrine and paracrine signaling that influences whole-body fuel handling (1).

Metabolically distinct from white adipose but also involved in energy balance is brown adipose tissue, and its primary function is heat production rather than long-term energy storage (4). Through thermogenic mechanisms, brown adipose tissue dissipates chemical energy and contributes to non-shivering thermogenesis, particularly during cold exposure (4). This process

links adipose tissue directly to energy expenditure and has attracted strong interest in metabolic research because it may influence systemic glucose and lipid handling as well as total energy dissipation (4). Skeletal muscle is another major determinant of energy metabolism because it accounts for a large share of substrate oxidation, especially during physical activity (1). During exercise or increased contractile activity, skeletal muscle adjusts its use of carbohydrate and lipid fuels according to oxygen availability, exercise intensity, and hormonal conditions (1). The liver functions as a metabolic hub that helps maintain nutrient availability across feeding and fasting cycles (1). It coordinates glycogen synthesis and breakdown, gluconeogenesis, lipogenesis, fatty acid oxidation, and ketone production, thereby stabilizing circulating fuel supply for other organs (1). In this way, hepatic metabolism supports the transition between absorptive and postabsorptive states and contributes to the balance between substrate storage and use (1). Lastly, the gastrointestinal tract also contributes to energy metabolism beyond its role in digestion and absorption (2) (Fig. 1). Nutrient sensing in the gut participates in the regulation of appetite, metabolic adaptation, and the coordination of postprandial responses (2). Thus, energy homeostasis emerges from reciprocal communication between the brain, adipose tissue, liver, muscle, and intestine rather than from the action of any single organ alone (1,2).

At the intracellular level, energy metabolism is shaped by regulatory systems that balance ATP production with biosynthetic demand (1). When energy is scarce, pathways that promote substrate oxidation and ATP generation are favored, whereas nutrient abundance supports anabolic processes and energy storage (1). The ability to shift appropriately between these states is often described as metabolic flexibility, and impairment of this readiness is a characteristic feature of obesity-related metabolic dysfunction (2,3).

Disturbance of coordinated energy metabolism contributes to the pathogenesis of obesity and its complications, known collectively as metabolic syndrome (3). Chronic positive energy balance promotes storage of excess energy, while adaptive physiological responses may simultaneously counteract weight gain by altering intake and expenditure patterns (2,3). As a result, abnormalities in energy metabolism are reflected in clinical conditions affecting human populations worldwide - such as insulin resistance, dyslipidemia, fatty liver disease, and atherosclerosis (1,3).

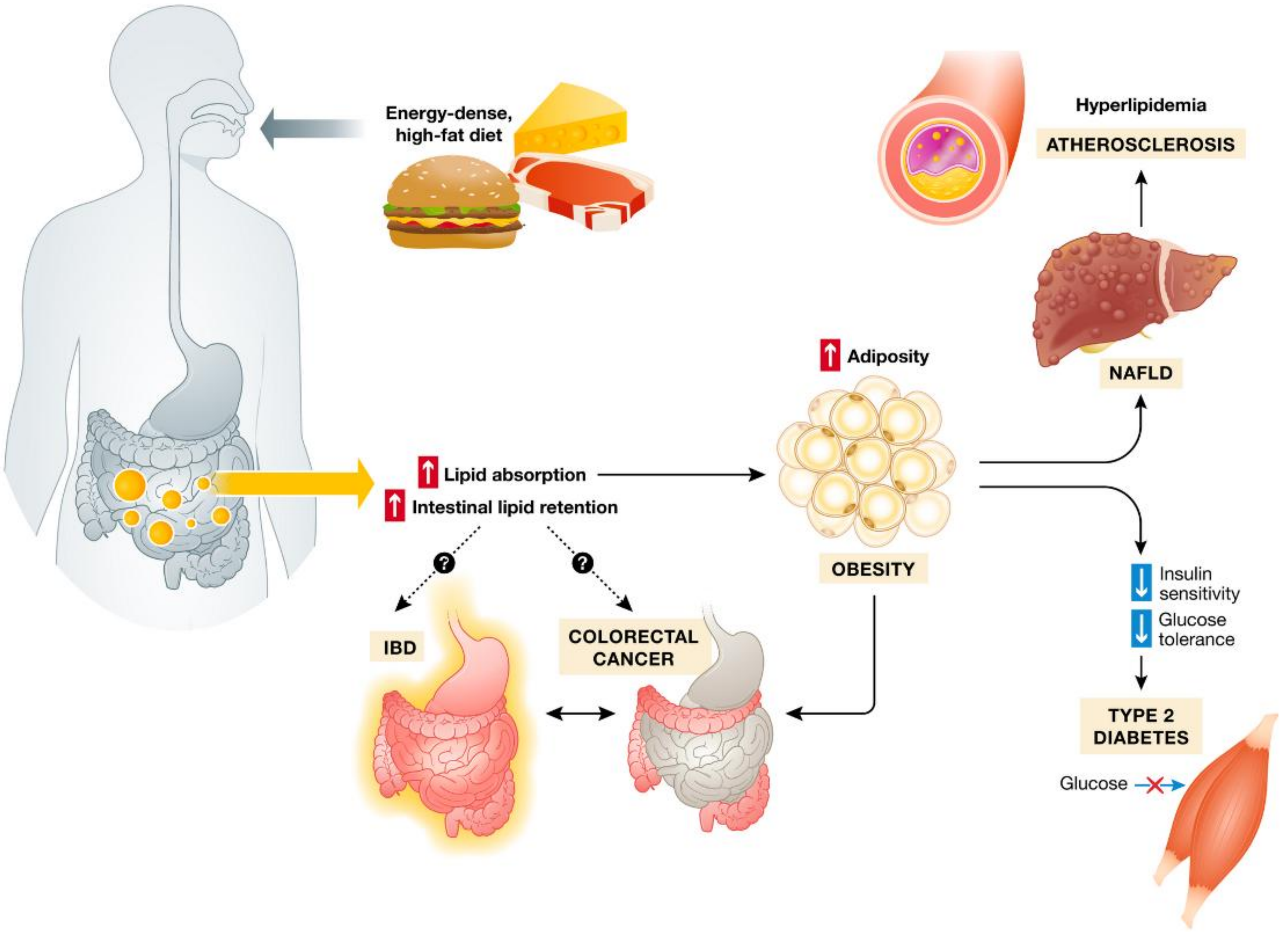

Fig. 1. The role of dietary lipids overload in the development of metabolic diseases. Dietary fats are absorbed in the small intestine and distributed to peripheral tissues; when supplied in excess, they are stored in adipose tissue, increasing fat mass. Excess fatty acid flux to the liver promotes non-alcoholic fatty liver disease (NAFLD), while adipose-derived fatty acids and inflammatory mediators contribute to insulin resistance, beta-cell dysfunction, and type 2 diabetes. Hyperlipidemia also favors atherosclerotic plaque formation, and intestinal lipid overload may further promote colorectal cancer and inflammatory bowel disease. (From: Wit et al., 2022, with permission from EMBO Press)

Digestive system – general anatomy and function

The digestive tract is a continuous, regionally specialized tube composed of hierarchically: oral cavity, larynx, esophagus, stomach, small intestine, large intestine, and ending at the anal canal, with the teeth, tongue, salivary glands, liver, gallbladder, and pancreas functioning as accessory organs that support digestion (5). Each segment of the digestive tract has its contribution to digestion and nutrient absorption, the key events associated with these processes are executed in the small and large intestine. At the tissue level, the mucosa that lines the tube of the alimentary canal forms a selectively regulated barrier at the interface with the external environment, so the system must balance transport with protection and mucosal defense (6). Within this framework, the small and large intestines perform related but distinct tasks. The small intestine is the segment most closely tied to digestion and absorption across the mucosa, and the GI system as a whole is responsible for the digestion and absorption of ingested food and liquids (6,7). The large intestine, by contrast, is the terminal segment of the tract and is functionally narrower, serving mainly to complete fluid handling and prepare residual material for excretion rather than to carry the bulk of nutrient processing (5). Neural control also differs by region: vagal afferents signal mainly from upper gastrointestinal regions, whereas pelvic afferents signal mainly from the colorectal region, underscoring the different motor and sensory demands of proximal and distal bowel (8).

As mentioned before, the small intestine is one of the central integrative organs for whole-body energy homeostasis, acting not only as a site of nutrient absorption but also as a metabolic, endocrine, and immunological sensor that shapes systemic lipid handling and cardiometabolic risk (9–11) (Fig. 1). Its roles concern digestion and uptake of all nutrients, including dietary lipids, being of interest in presented study, intracellular lipid trafficking and oxidation, chylomicron assembly and secretion, gut–brain and gut–liver signaling, and crosstalk with the intestinal microbiota. All these, collectively determine postprandial lipid flux and long-term energy balance (11–14). Of note**,** dietary lipid overload is an independent risk factor for the development of inflammatory bowel disease (IBD) (15,16) and colorectal cancer (15). Additionally, diets rich in fat induce dysbiosis which might be one of the states involved in the pathogenesis of colon cancer (17,18) (Fig. 1). Therefore, small intestine is a first-line organ limiting the availability of food-derived lipids and interference with fat digestion might be an effective approach to combat obesity and its comorbidities such as type 2 diabetes, non-alcoholic

fatty liver disease, cardiovascular diseases, and possibly inflammatory disorders (IBD) as well as cancer. (Fig. 1)

Anatomical, histological and functional overview of the small intestine

The small intestine comprises the duodenum, jejunum and ileum, forming the principal site of macronutrient digestion and absorption in mammals. Enterocytes in the villus epithelium, supported by crypt stem cells and a rich vascular and lymphatic network, orchestrate nutrients from the lumen and their subsequent transport into portal blood (carbohydrates, aminoacids) or lymphatic circulation (majority of lipids) (19–21). The small intestine expresses a broad repertoire of carbohydrate, aminoacid, lipid and micronutrient transporters, fatty-acid oxidation enzymes and lipoprotein assembly factors, placing it as a metabolically active organ that both consumes and exports energy substrates (22–24). Spatial heterogeneity along the longitudinal axis leads to regional specialization, with the duodenum and jejunum dominating sugars, protein, triglyceride (TG) and cholesterol absorption while the distal ileum contributes to bile acid and vitamin B12 reabsorption.

Histologically, the small intestine is composed of, starting from the gut lumen: mucosa, submucosa, circular muscle layer, longitudinal muscle layer, and, most externally, serosa. The absorptive surface of small intestinal mucosa is greatly increased due to its foldings, called plicae circulares (Fig. 2). The small intestine is lined by a simple columnar epithelium organized into finger-like protrusions called villi and invaginations named crypts of Lieberkühn, a histological arrangement which is another adjustment to maximize absorptive surface while enabling continuous epithelial renewal and barrier protection (25,26). Each villus is equipped in one central, blindly-ended lymphatic vessel (lacteal) and a network of capillaries; arterioles, and venules responsible for absorbing lipids or glucose and amino acids from digested food, respectively (Fig. 2). The crypt–villus axis is sustained by intestinal stem cells located at the crypt base, which self-renew and generate progenitors that differentiate into the major epithelial lineages as they migrate toward the villus tip (25,26). This rapid cellular turnover is essential for preserving epithelial integrity under constant exposure to dietary, microbial, and mechanical

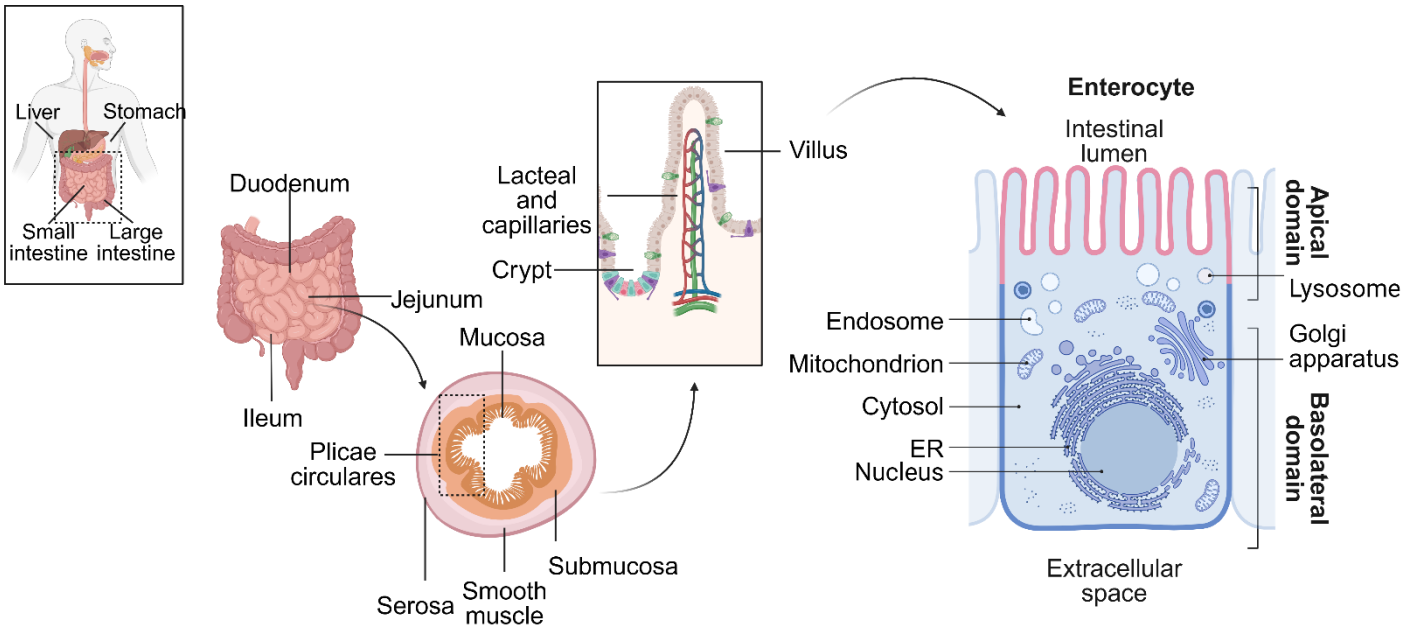

Fig. 2. Schematic anatomy of the small intestine, revealing organ build-up complexity. Gastrointestinal system is composed of several organs and small intestine can be subdivided into duodenum, jejunum and ileum. Following tissues are building the small intestine; mucosa (contacting with the gut lumen), submucosa, two layers of smooth muscles and serosa. Mucosa forms protrusions known as villi and invaginations called crypts. Surface of the villi are covered with epithelial cells and majority of them are absorptive enterocytes. (Modified from: Encyclopaedia Britannica, 2014), for description please see the text. Figure created with BioRender.

stress (27). Enterocytes are the most abundant epithelial cells and create the absorptive surface of the villi, where their brush-border forming microvilli additionally markedly increase the absorptive surface (25) (Fig. 2). Goblet cells are interspersed between enterocytes and secrete mucins that form the mucus layer, which lubricates the lumen and limits direct contact between microbes and the epithelium (28,29). At the crypt base reside Paneth cells, adjacent to stem cells, that contribute to host defense by secreting antimicrobial peptides such as defensins and lysozyme while also supporting the stem-cell niche (30,31). Enteroendocrine cells are relatively rare but highly specialized epithelial cells that sense luminal nutrients and release hormones regulating motility, digestion, insulin secretion (those are called ‘incretins’), and satiety (25). The key enteroendocrine cell types are K cells found in the duodenum, secreting gastric inhibitory peptide (GIP), an incretin, which also supports TG storage, L cells that secrete glucagon-like peptide 1 (GLP-1, an incretin), peptide YY, oxyntomodulin, and glucagon-like

peptide-2 (GLP-2). L cells are primarily found in the ileum. In the first segment of the small intestine are also present I cells which secrete cholecystokinin (CCK), a peptide hormone that promotes the secretion of pancreatic juice from the pancreas and bile from the gallbladder. Another relatively rare epithelial lineage are Tuft cells, which exert chemosensory functions via detecting luminal metabolites and initiate type 2 immune responses (32). Together, these epithelial populations form an integrated histological system in which absorption, mucus production, antimicrobial defense, endocrine signaling, and tissue regeneration are tightly coordinated (25,32).

General physiology of nutrient absorption

Nutrient absorption in the small intestine relies on subsequent processes of luminal digestion, epithelial transport across the brush-border and basolateral membranes, and eventually distribution via the portal circulation or lymphatic system (33). The digestion process starts already in the mouth, where salivary amylase breaks down starches into simpler sugars and lingual lipase initiates TG breakdown (34). In the stomach, an acidic environment provided by secreted hydrochloric acid is needed to activate pepsin, an enzyme that digests proteins to polypeptides. To a minor extent, digestion of TG by gastric lipase continues in the stomach as well. Duodenum receives pancreatic juice produced by the exocrine part of the pancreas and containing trypsin, chymotrypsin, and elastase, breaking down proteins and polypeptides to peptides and amino acids, respectively, while pancreatic amylase digests complex carbohydrates to simple sugars. Pancreatic juice is enriched in bicarbonates, which neutralize the acidic pH of the contents from the stomach. Bile salts, synthesized in the liver and secreted directly from the gall bladder to the duodenum, emulsify fats, forming micelles, while pancreatic lipase, with colipase and cholesterol esterase, executes TG and cholesteryl esters hydrolysis (35). Epithelial cells of mucosa are also equipped with a set of digestive enzymes such as amylase, peptidases, lipases, or nucleases, which, upon release to the gut lumen, provide a continuation of nutrient digestion locally, on a brush border of enterocyte (36). The uptake of nutrients and water by enterocytes is mediated by several mechanisms, specific to the considered compound, and includes: passive diffusion, facilitated diffusion, active transport, and transport via osmotic gradient. Glucose, the major product of carbohydrate digestion, is taken up via active transport by sodium-dependent glucose cotransporter (SGLT1) and facilitative transporters (GLUT2), while fructose utilizes GLUT5, and both sugars, once crossing the basolateral membrane, are released into the portal vein (33). Unidirectional

transport of sodium and glucose drives an osmotic gradient promoting water absorption via diffusio. Proteins are hydrolyzed by pancreatic and brush-border peptidases to oligopeptides and amino acids that enter enterocytes through specific peptide transporters (e.g., PEPT1) and amino acid carriers, and, similarly to sugars, are transferred to the portal circulation (33). In contrast, the absorbed dietary lipids and fat-soluble vitamins (A, D, E, K) leave the intestine via the lymphatics as chylomicrons, a class of lipoproteins whose synthesis is a multi-step process requiring enterocyte-specific enzymes and coat proteins (37,38). That emphasizes that lipid absorption follows a distinct anatomical and metabolic route compared with hydrophilic nutrients, which is a matter of more detailed description in the following section. (37).

Luminal lipid digestion and micellar solubilization

Efficient lipid absorption starts with the emulsification and enzymatic hydrolysis of dietary TG, phospholipids, and cholesteryl esters in the upper small intestine (33,37). Gastric lipase initiates TG digestion in the stomach, but most hydrolysis occurs in the duodenum and jejunum through pancreatic triglyceride lipase and its cofactor colipase, as well as phospholipase A2 and cholesterol esterase (33,37). Bile acids, secreted into the duodenum, act as biological detergents that emulsify fat droplets and form mixed micelles containing monoglycerides, free fatty acids, cholesterol, and lysophospholipids, greatly enhancing their diffusion to the brush border (33,37,39). Mouse and human studies demonstrate that defects in bile acid secretion or composition markedly reduce micellar solubilization, leading to fat malabsorption, steatorrhea, and deficiencies in fat-soluble vitamins (33,37).

Apical uptake of lipid digestion products

Lipid uptake across the apical membrane involves a combination of passive diffusion and protein-mediated transport (33,40,41). Long-chain fatty acids are taken up via scavenger receptor CD36, fatty acid transport protein 4 (FATP4), and other long-chain fatty acid transporters, while fatty acid-binding proteins within the cytosol (I-FABP, L-FABP) chaperone them to intracellular sites of further processing (11,40) (Fig. 3). Cholesterol absorption is mediated predominantly by Niemann–Pick C1-like protein 1 (NPC1L1) and counterbalanced by apical efflux transporters such as ABCG5/ABCG8, and modulation of these pathways in humans has direct effects on plasma LDL-cholesterol and cardiovascular risk (42). Genetic and pharmacological manipulation of these transport systems in mice—including CD36, FATP4,

I-FABP, and L-FABP—alters intestinal fat uptake, postprandial lipemia, and susceptibility to diet-induced obesity, highlighting their central role in shaping systemic lipid exposure (11,40).

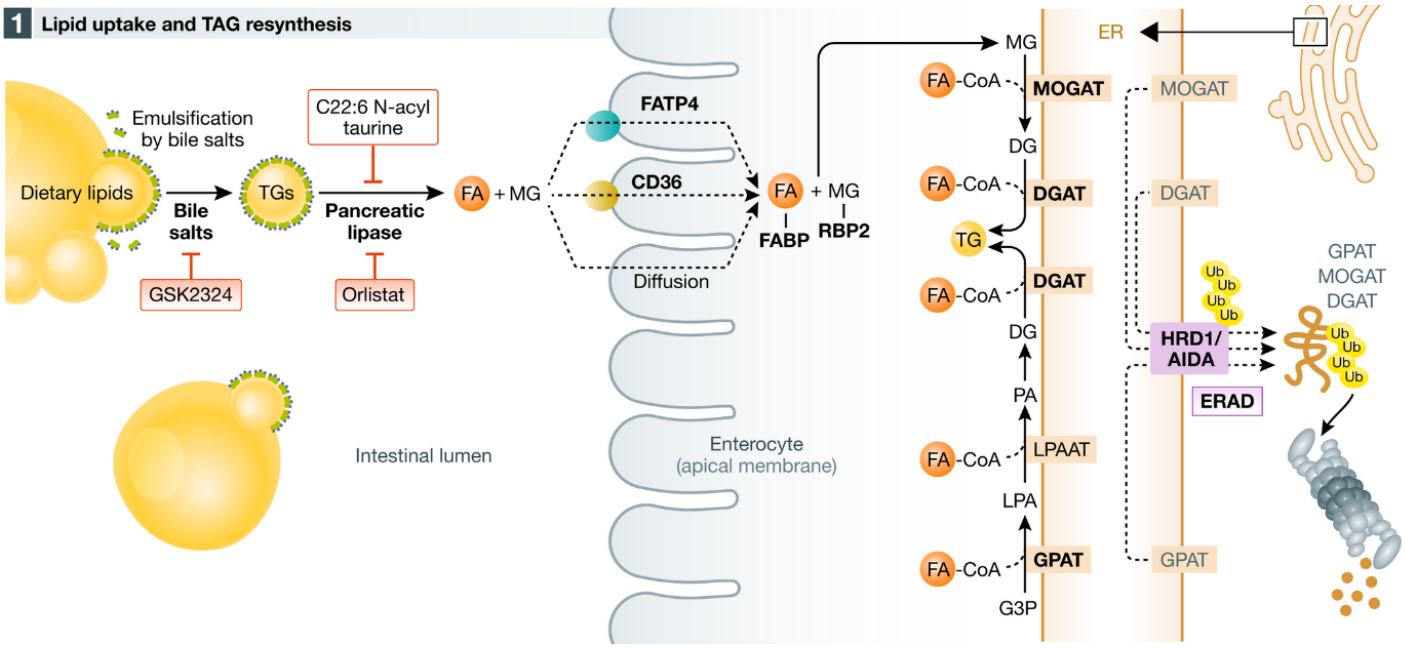

Fig. 3. Dietary lipid uptake, and TG resynthesis in enterocytes. (Modified from: Wit et al., 2022, with permission from EMBO Press). For the description, see the sub-chapters above and below.

Intracellular re-esterification and lipid droplet formation

Once inside the enterocyte, absorbed monoglycerides and fatty acids are rapidly re-esterified to triglycerides in the endoplasmic reticulum via the sequential actions of monoacylglycerol acyltransferases (MGATs) and diacylglycerol acyltransferases (DGAT1 and DGAT2) (33,40). Diacylglycerol (DAG) utilized in TG resynthesis can also be derived from the glycerol-3 phosphate pathway (G3P). Here, endogenous G3P is acylated by glycerol-3-phosphate - acyltransferase (GPAT), to produce lysophosphatidic acid (LPA), which is further acetylated by lysophosphatidic acid acyltransferase (LPAAT) results in phosphatidic acid (PA) synthesis, which is converted into DAG (Fig. 3). TG resynthesis can be inhibited by targeted degradation of GPAT, MGAT, and DGAT1/2 enzymes via the endoplasmic reticulum. Primarily, the newly re-synthesized TGs are immediately directed toward chylomicron assembly, whereas another fraction accumulates in cytoplasmic lipid droplets (LDs), which serve as transient storage

organelles that buffer fluctuations in dietary fat intake (43,44). LDs are coated by structural proteins such as perilipin 2 (PLIN2) and perilipin 3 (PLIN3), and their size and turnover are regulated by lipases and lipophagy, processes that have been dissected in chapter ‘1.2. Lipid droplets of the presented work (11,40). The detailed description of the synthesis and transport of the enterocyte-unique product – chylomicron, is a subject of a section below.

Chylomicron biogenesis and export

Chylomicrons are highly complex lipoprotein particles composed of TGs, cholesterol, phospholipids, apolipoproteins, and additional lipid species (45). CM biosynthesis begins in the ER with the formation of a nascent particle, termed the pre-chylomicron (pre-CM), and this process is critically dependent on microsomal triglyceride transfer protein (MTTP) (45,46). MTTP facilitates the translocation and lipidation of apolipoprotein B48 (APOB48), thereby initiating lipoprotein assembly, and it also promotes the transfer of lipids into the newly formed pre-CM (45) (Fig. 3). The importance of this pathway is underscored by the severe hypolipidemic phenotypes associated with impaired MTTP-dependent lipoprotein production and by evidence that intestine-specific *Mttp* deletion exacerbates experimental colitis and increases tumor burden in models of colitis-associated cancer (47). Although pharmacological inhibition of MTTP with lomitapide has been explored as a strategy to reduce lipid transport, systemic inhibition is associated with substantial adverse effects, which limit its applicability for obesity treatment. In this context, PRAP1 has emerged as an intestine-enriched lipid-binding protein that facilitates MTTP-mediated lipid transport and promotes TG loading into pre-chylomicrons. Consistent with this role, deletion of *Prap1* reduces the formation and lipidation of APOB-containing lipoproteins and decreases intestinal TG absorption (48). APOB48 is a core apolipoprotein defining the CM, while several other (exchangeable) apolipoproteins decorate the particle’s coat. One of them is APOC-III, whose main established role is in metabolism rather than assembly of chylomicrons since apoC-III inhibits lipoprotein lipase-mediated TG hydrolysis and also reduces hepatic uptake of CM remnants (49). Apolipoprotein A4 (APOA4) is another important apolipoprotein associated with CMs. Although it is produced mainly by enterocytes and secreted together with chylomicrons, APOA4 is also present in high-density lipoproteins (HDL), very-low-density lipoproteins (VLDL), and CM remnants, suggesting a broader role in lipoprotein remodeling and peripheral lipid metabolism. Increased APOA4 abundance has been linked to enhanced dietary lipid absorption, increased TG packaging, and larger CM size (50). However, other studies have shown that *Apoa4* deficiency

can reduce plasma TG and cholesterol levels despite increasing CM size, indicating that APOA4 abundance does not correlate in a simple linear manner with net intestinal lipid absorption (51). This complexity is further illustrated by studies of our group on protein kinase D2 (PKD2). Loss of PKD2 in mice increases circulating APOA4 levels while reducing lipid absorption and body weight gain, and this phenotype is accompanied by improved metabolic parameters and a more favorable intestinal microbial profile (52). Notably, APOB48 abundance was not altered, suggesting that the phenotype does not reflect reduced CM number but rather altered APOA4 function (52). Because PKD2 directly phosphorylates APOA4, the lack of this post-translational modification may underlie the observed effects (52). In addition, pharmacological inhibition of PKD signaling with CRT0066101 reduces intestinal lipid absorption, ameliorates obesity-associated metabolic abnormalities, and improves insulin sensitivity, while PKD2 activity in the small intestine of obese patients correlates positively with plasma TG levels (52). Collectively, these findings suggest that both APOA4 abundance and its enzymatic modification may be of therapeutic relevance in obesity and hyperlipidemia. After assembly in the ER, pre-CM are exported to the cis-Golgi in specialized pre-chylomicron transport vesicles (PCTVs) (45) (Fig. 3). This transport is coatomer complex II (COPII)-dependent and constitutes a critical step in intracellular TG trafficking during CM biogenesis (45). Once inside the Golgi apparatus, pre-CMs undergo further lipidation and acquire additional apolipoproteins, including apolipoprotein A1 (APOA1) (Fig. 3). Their progression through the Golgi requires the coordinated action of golgins and small GTPases that regulate cargo maturation and trafficking. Among these regulators, ADP-ribosylation factor-related protein 1 (ARFRP1) appears to be of particular importance. Activated ARFRP1 recruits ARL1 to the Golgi, where ARL1 interacts with Golgin-245 and Rab2 to promote CM lipidation and subsequent intra-Golgi transport (53) (Fig. 3). Intestinal deletion of *Arfrp1* causes growth retardation, reduced plasma TG levels, impaired lipid absorption, and reduced APOA1 secretion, demonstrating that Golgi-associated processing events directly influence both CM composition and the efficiency of dietary lipid absorption (53). The terminal stages of CM release from enterocytes remain less well understood. Nevertheless, available data indicate that the trafficking of CM-containing secretory vesicles is regulated by DENND5B, a transmembrane member of the DENN family involved in Rab-dependent vesicular transport (54) (Fig. 3). Mice lacking DENND5B exhibit reduced intestinal TG absorption, lower body weight, improved metabolic homeostasis, and reduced circulating cholesterol (55). Ultrastructural studies have shown that DENND5B deficiency impairs fusion of CM secretory vesicles with the basolateral plasma membrane, thereby interfering with delivery of CMs to the

lamina propria (55). In addition, efficient intestinal lipid absorption appears to depend not only on intracellular lipoprotein assembly and vesicle trafficking, but also on epithelial and endothelial fluid handling. Studies in *Aqp1*-deficient mice demonstrated that these animals are viable and develop normally on a low-fat chow diet, but exhibit steatorrhea, increased fecal lipase activity, serum hypotriglyceridemia, and impaired body weight gain when challenged with a high-fat diet, particularly at a young age (56). This phenotype has been interpreted as being at least partly consistent with impaired CM transport into lacteals, although the exact underlying mechanisms remain incompletely defined (56). More recent evidence further supports the concept that lacteal permeability and lymphatic uptake are actively regulated components of intestinal lipid transport rather than passive downstream events. Nevertheless, from lacteals, chylomicrons are transported via the lymphatic system to the thoracic duct and systemic circulation, allowing dietary lipids to reach adipose tissue and muscle before first-pass hepatic metabolism (37,57). Importantly, not all taken-up free fatty acids are subjected to chylomicron-mediated transport to the circulation. Medium-chain fatty acids (MCFA; such as lauric acid, capric acid, or caprylic acid, found in palm oil or coconut oil) are absorbed directly into the liver via the portal vein as an immediate energy source. In conditions causing chylomicron malformation and fat malabsorption, such as chylomicron retention disease caused by mutations in the *SAR1B* gene (58) or familial hypobetalipoproteinemia caused by mutations in *APOB* gene (59), dietary supplementation with MCFA is an established therapeutic approach to provide lipid supply (60).

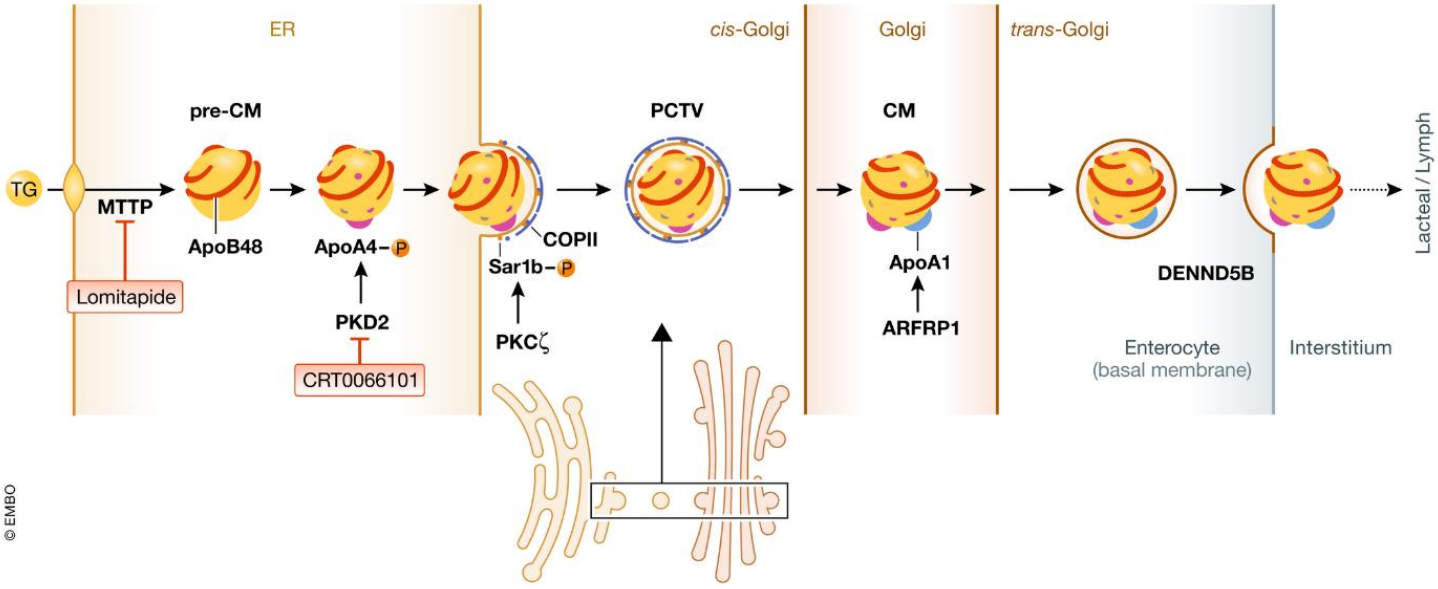

Fig. 4. Chylomicron synthesis and maturation; scheme description is provided in the text (From: Wit et al, 2022, with permission from EMBO Press).

Interplay between chylomicrons and lipid droplets (LD)

LD and CM represent interconnected arms of enterocyte lipid handling, with LD serving as a flexible reservoir that can supply TG for CM assembly or sequester excess lipid when secretory pathways are saturated (11,44). In lymph-fistula and tracer studies, experimental modulation of apolipoproteins (e.g., apoC-III) in mice reduces chylomicron secretion and particle size despite normal total fat absorption, accompanied by substantial alterations in LD abundance and composition, indicating that CM output can be uncoupled from uptake via changes in LD metabolism (61). Vice versa, genetic ablation of LD-associated proteins such as PLIN2 or CIDEB (which is a protein promoting LD fusion) leads to excessive TG retention in LDs and impaired chylomicron secretion, demonstrating that proper droplet formation and remodeling are prerequisites for efficient lipoprotein export (62,63). Moreover, human studies in obese and insulin-resistant subjects show increased enterocyte LD content and exaggerated postprandial TG responses, consistent with a maladaptive expansion of the LD compartment and enhanced chylomicron production in metabolic disease (20,64).

Biogenesis of LD

Lipid droplets are now recognized as dynamic, ER-derived organelles rather than passive fat inclusions, consisting of a neutral-lipid core surrounded by a phospholipid monolayer and a unique protein coat (65,66). TG in LD core is built of fatty acids either synthesized in the cell via *de novo* lipogenesis [controlled largely by SREBP1c and its downstream target genes such as acetyl-coA carboxylase (*ACC*), fatty acid synthase (*FASN*), and stearoyl-CoA desaturase 1 (*SCD1*)] or taken up externally (67). LD biogenesis begins in the ER, where TG and steryl esters are synthesized by ER-associated enzymes and accumulate within the hydrophobic region of the bilayer (65,66). When the local concentration of these neutral lipids exceeds a critical threshold, they demix from surrounding phospholipids and condense between the two ER leaflets into a lens-like structure, indicating that LD formation is a phase-separation process governed by membrane dynamics (65,66). Therefore, the nascent LD should not be viewed as a classical membrane vesicle but rather as a neutral-lipid phase that emerges from the ER and acquires its coating by a phospholipid monolayer derived from the cytosolic leaflet of the ER membrane (65,66). Current models further indicate that this process is spatially regulated and does not occur uniformly across the entire ER (66,68). The probability of droplet nucleation is strongly influenced by local membrane properties, including phospholipid composition,

diacylglycerol abundance, curvature, and membrane tension, all of which can alter the energetic threshold required for neutral-lipid condensation (66). In particular, highly curved ER tubules appear to provide a favorable physical environment for lens formation, suggesting that ER architecture is itself an active determinant of lipid droplet biogenesis (66). This view joins the biophysical and cell-biological perspectives by proposing that lipid droplet formation is lipid-driven at its core, but selectively permitted at specialized ER subdomains (65,66). Among the proteins implicated in this process, seipin has emerged as the principal organizer of LD nucleation sites (65,66). Seipin appears to lower the kinetic barrier for droplet formation, stabilize early neutral-lipid assemblies, and maintain a functional ER-lipid droplet junction during the earliest stages of growth (66,68). Seipin-associated factors, including LDAF1, together with proteins such as FIT2, further modulate the partitioning of neutral lipids within the membrane and help ensure that lipid accumulation results in an organized droplet rather than chaotic lipid deposition within the ER bilayer (65,66). The importance of these regulators is underscored by the fact that their dysfunction leads to delayed nucleation, abnormal LD size, or ectopic LD formation, which altogether support the idea that proteins determine the spatial organization of that event (65,66). Following nucleation, the neutral-lipid lens expands through continued lipid influx and expands toward the cytosol, thereby generating a nascent droplet that often remains connected to the ER through a persistent lipidic bridge (65,66). This continuity with the ER is mechanistically important because it provides a route for ongoing lipid transfer, surface monolayer expansion, and selective recruitment of proteins required for maturation and metabolic specialization (65,68). LD biogenesis should therefore be understood not as a single budding event but as a continuum encompassing neutral-lipid synthesis, phase separation, nucleation-site selection, ER emergence, and subsequent growth (65,66).

Protein trafficking to LD

LD proteins can be classified into two groups based on the trafficking routes they utilize to access the surface of LD: one involves proteins that first insert into the ER and subsequently redistribute to LDs (also known as class I proteins, ER-to-LD, or ERTOLD), whereas the other involves proteins that are recruited directly from the cytosol to the LD surface after droplet formation (also denoted as class II proteins, cytoplasm-to-LD, or CYTOLD) (65,69). This distinction reflects the challenge posed by the LD monolayer, which lacks a classical translocon-based import system and therefore favors targeting mechanisms based on membrane partitioning, surface recognition, and protein-protein interactions rather than canonical

vesicular delivery alone (65,66). In this model, the trafficking route is determined largely by protein structure, particularly whether a protein contains a hydrophobic hairpin embedded in the ER membrane or instead carries amphipathic motifs that can bind the droplet surface from the cytosol (69,70). Proteins that traffic from the ER to LDs generally contain hydrophobic hairpin motifs that insert into the ER membrane without fully traversing it, thereby allowing them to remain in the cytosolic leaflet and later partition into the nascent LD monolayer (65,69). This pathway is mechanistically consistent with the current model of LD biogenesis, in which neutral lipids accumulate within the ER bilayer, phase-separate into an oil lens, and bud toward the cytosol while preserving continuity with the ER during early stages of growth (65,66). GPAT4 (glycerol-3-phosphate acyltransferase 4) is one of the best-described examples of this ER-to-LD trafficking route, because it is first localized to the ER and later accumulates on a subset of expanding LDs, where it supports local glycerolipid synthesis and droplet growth (69). Mechanistic studies showed that successful LD targeting of GPAT4-like motifs depends on specific sequence features within the hydrophobic region, especially deeply inserted tryptophan residues and positively charged residues near the predicted hairpin hinge (69). These residues appear to favor partitioning into the LD environment because they become energetically more compatible with the oil-water interface of the monolayer than with an ordinary phospholipid bilayer (69). DGAT2 represents a related but mechanistically more nuanced example of ER-associated LD targeting (69,71). DGAT2 localizes to both the ER and LDs and contributes to triacylglycerol synthesis at sites of droplet growth, supporting the idea that LD expansion is fueled in part by local neutral-lipid synthesis on or near the droplet surface (71). However, comparative analysis of membrane motifs indicated that the isolated DGAT2 hydrophobic segment is not by itself sufficient for efficient early LD targeting in the same manner as the GPAT4 motif, suggesting that full-length DGAT2 likely relies on additional determinants or cellular context for robust LD localization (69). This distinction is important because it shows that not all ER-derived LD proteins follow exactly the same trafficking logic, even when they participate in related metabolic pathways (69).

A second major route to LDs involves proteins that are recruited directly from the cytosol to the droplet surface after LD formation (70). These proteins typically recognize the distinctive physicochemical properties of the LD monolayer, including lipid-packing defects, surface curvature, and the unusual interface between phospholipid headgroups and the neutral-lipid core (65,66). Amphipathic helices are particularly well suited to this mode of targeting because they can insert shallowly into the monolayer and stabilize association without requiring

transmembrane passage (70). Cytosolic recruitment, therefore, depends on a match between protein surface properties and LD monolayer organization rather than on conventional membrane insertion machinery (65,66).

The perilipin (PLIN) family provides the classic example of cytosolic LD targeting and surface retention (70). PLINs are major structural proteins of mammalian LDs, and different family members are expressed according to cell type and metabolic state, with PLIN 2 and 3 commonly associated with small LDs in many cell types, whereas PLIN 1, 4, and 5 are more prominent in specialized lipid-storing tissues (70). In addition to stabilizing the LD surface, PLINs regulate lipolysis by controlling the access of lipases and lipase cofactors to neutral-lipid substrates, thereby linking LD targeting to metabolic regulation (70). The PLINs therefore demonstrate that LD trafficking is not merely a matter of reaching the organelle, but also of establishing a functional and persistent surface scaffold that can determine droplet behavior (70). Protein trafficking to LDs must also be considered a dynamic and metabolically responsive process (66,71). During nutrient excess, LD growth is accompanied by recruitment of lipid-synthetic enzymes and protective coat proteins, whereas during lipolytic stimulation, the composition of the LD surface changes to favor enzyme access and lipid mobilization (70,71). This remodeling implies that proteins continuously cycle between the ER, cytosol, and LD surface, with retention depending not only on initial targeting but also on protein stability, local lipid composition, and regulatory protein-protein interactions (65,71). In this respect, LD protein trafficking is better described as a regulated equilibrium than as a one-time delivery event (65,66).

Lipolysis and lipases

The best-characterized pathway of LD catabolism is cytosolic lipolysis, a stepwise hydrolytic cascade in which adipose triglyceride lipase (ATGL/PNPLA2) initiates TG breakdown, hormone-sensitive lipase (HSL) preferentially hydrolyzes DAG, and monoacylglycerol lipase (MGL) completes the release of glycerol and FFA (72,73) (Fig. 5). Liberated FFA can be either utilized in mitochondrial beta-oxidation as a fuel or re-esterified into TG, and such recurrent lipolysis-re-esterification cycles were recently proposed to remodel TG composition in adipocytes (74) ATGL is composed of a patatin domain (N-terminus) with a catalytic site, while the C-terminus inserts into LD. ATGL reaches the LD surface via a well-described route, from ER-Golgi intermediate compartment (ERGIC) and via SAR1-COPII ATGL and GBF1-ARF1-COPI protein complexes (75,76). It is thus classified as a late class I LD protein. ATGL is

strongly activated by CGI-58 (also known as ABHD5), which increases lipase activity by about 20-fold. Accessibility of CGI-58 for ATGL is regulated by competitive binding with PLIN1 on the LD surface in adipose tissue, creating a molecular switch that determines whether the LD is protected from hydrolysis or opened to lipase access (77–79). On the other hand, ATGL activity can be inhibited by the binding of G0S2 (80) and HILPDA proteins (81) (Fig. 5). PLIN5 in adipose tissue was also shown to inhibit lipolysis by independently binding ATGL and CGI-58, and in the liver, PNPLA3 protein lowers lipolysis rate by restricting CGI-58 from ATGL binding. (82) (Fig. 5)

Hormonal control of lipolysis is dominated by catecholamine-induced cAMP signaling, which activates protein kinase A, promotes phosphorylation of PLINs and HSL, and enhances mobilization of stored fatty acids (83). Another hormonal stimulus that promotes lipolysis is glucagon, activating phospholipase A and ATGL together with cAMP-PKA signaling and HSL-mediated lipolysis (84). By contrast, insulin suppresses lipolysis in the fed state and therefore restrains the release of circulating FFA (85). This balance is crucial for systemic metabolic homeostasis, since broad evidence shows that excessive or dysregulated lipolysis contributes to ectopic lipid deposition, insulin resistance, and hypertriglyceridemia (86,87).

Mouse genetic studies established that ATGL and HSL play complementary but nonidentical roles in LD catabolism, with ATGL acting at the first hydrolytic step and HSL making a major contribution to downstream hydrolysis and stimulated lipolysis (72,86). Human studies broadly support this model but also indicate that the relative contribution of each enzyme depends on the adipocyte model and metabolic context (88,89).

LD-associated proteins also exert strong regulatory control over lipolysis because they influence lipase recruitment, cofactor availability, and substrate accessibility at the organelle surface (68,78,79). Transgenic mouse models further demonstrate that perturbation of lipases or LD-coating proteins causes profound changes in adiposity, ectopic lipid storage, and insulin sensitivity, underscoring that LD lipolysis is a determinant of whole-body energy metabolism rather than a purely local degradative event (86). More recent evidence indicates that ATGL- and HSL-dependent reactions also regulate the release of bioactive lipid species, linking LD catabolism to inflammatory and metabolic signaling pathways in addition to fuel mobilization (90).

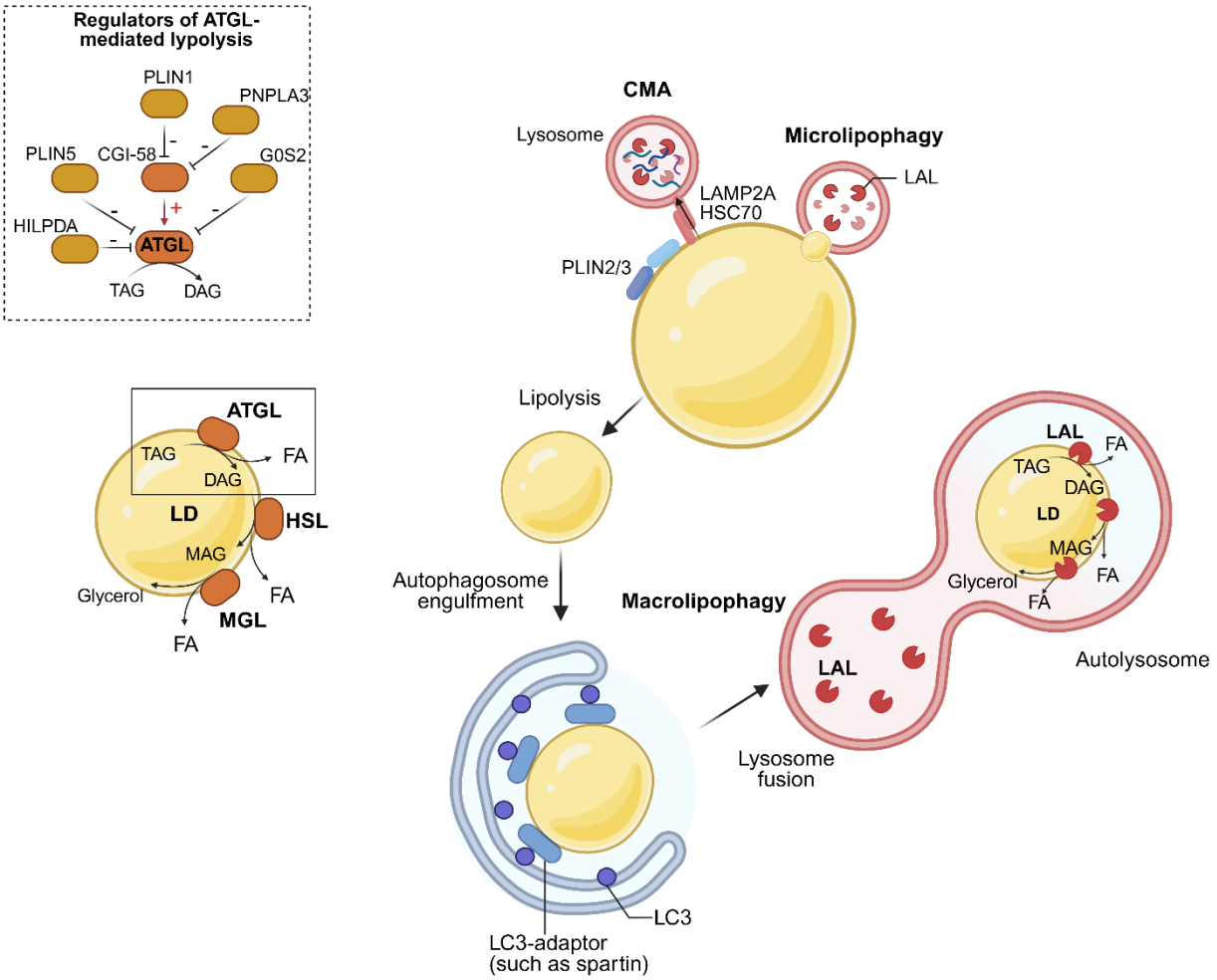

Fig. 5. Catabolic regulation of LD via lipolysis and lipophagy. Lipolysis of triacylglycerols (TAGs) stored in lipid droplets (LDs) proceeds sequentially through ATGL, HSL, and MGL, with ATGL acting as the rate-limiting enzyme. ATGL activity is stimulated by CGI-58 and modulated by multiple regulatory proteins, including direct inhibitors (G0S2 and HILPDA) and proteins that inhibit ATGL-CGI-58 interaction (PLIN1, PLIN2, and PNPLA3). LDs are also degraded through macrolipophagy and microlipophagy, which deliver whole LDs or LD fragments to lysosomes. In macrolipophagy, degradation of PLIN2 and PLIN3 facilitates autophagic membrane recruitment, autolysosome formation, and subsequent lipid breakdown, whereas microlipophagy enables direct lysosomal uptake independent of autophagy machinery. Lysosomal acid lipase (LAL) hydrolyzes lysosomal lipids, including TAGs and sterol esters. (modified from: Mathiowaetz & Olzmann, 2024 (68)). Figure created with BioRender.

Autophagic degradation of LD

In addition to classical lipolysis, LDs can be degraded by autophagy, a process commonly referred to as lipophagy (91,92). In this pathway, LDs or fragments of LDs are delivered to lysosomes, where lysosomal acid lipase (LAL) and other hydrolases liberate fatty acids and sterols for reuse by the cell (91,92). Lipophagy may occur via macroautophagy-like sequestration into autophagosomes or, i.e. macrolipophagy or by related lysosomal routes such as chaperone-mediated autophagy (CMA) and microlipophagy (91,93).

Lipophagy is particularly important during nutrient deprivation and cellular stress, as it provides an additional pathway for lipid mobilization when energetic demand rises or when cytosolic lipolysis alone is insufficient (68,92). At the same time, autophagic LD degradation contributes to lipid quality control by helping cells remove damaged droplets and adapt to ER stress or organelle dysfunction (68,92). Execution of macrolipophagy involves receptors (such as p62 or lysosome-associated membrane protein 2A; LAMP2A) and adaptors that provide physical binding of autophagosomal membranes with target cargo localized on the LD surface (94). One of the recently described potential LD-specific autophagic adaptors may be spartin, which was shown to directly recruit and LC3-decorated autophagic membranes via its LC3-interacting region (LIR) and thereby promoting lipophagy (95). CMA supports macrolipophagy in LD size reduction, and this mechanism is employed to degrade PLIN2 and PLIN3, which facilitates lipase recruitment to the LD surface and lipolysis (96,97) (Fig. 5). Lastly, microlipophagy relies on a direct transfer of small portions of TG directly to the lysosome, omitting recruitment of autophagosomal membranes (94) (Fig. 5). Overall, lipophagy complements surface lipolysis rather than duplicating it, integrating LD turnover with the broader autophagic network (91,98). The liver is one of the best-studied examples of physiologically relevant lipophagy where autophagic LD degradation restrains steatosis and supports fasting adaptation in hepatocytes (91,99). When autophagic flux is impaired, hepatocytes accumulate LDs, promoting the progression of fatty liver disease (99). Comparable lysosome-dependent mechanisms also contribute to cholesterol mobilization from macrophage LDs and therefore influence foam-cell biology and atherogenesis (91,100).

A study concerning the role of lipophagy in the gut revealed that in wild-type mice, feeding increased the intestinal LC3-II/I ratio and LAMP1 and decreased p62, consistent with activation of intestinal autophagy, whereas these responses were largely lost in SHP- and FGF15-KO mice. The same study reported that postprandial intestinal TG and APOB48 were higher in

SHP-KO and FGF15-KO mice, supporting the idea that intestinal lipophagy normally limits the lipid pool available for chylomicron secretion after a meal. (101) A more detailed description of protein degradation mechanisms – ubiquitin-proteasome system and autophagy is provided below.

Ubiquitin-proteasome system (UPS) and autophagy – two major routes for protein degradation.

Intracellular protein degradation in eukaryotic cells is mediated primarily by two complementary systems: the ubiquitin–proteasome system (UPS) and lysosome-dependent autophagic pathways. These systems differ in substrate spectrum and molecular machinery, yet together they maintain proteostasis by eliminating short-lived regulatory proteins and damaged or misfolded polypeptides (102,103). In general, the UPS is optimized for selective degradation of soluble proteins and dynamically regulated enzymes, whereas autophagy-dependent pathways are more important for long-lived proteins, protein aggregates, and membrane-bound cargo, including LD-associated components and organelle fragments (102,104).

In the UPS, target proteins are marked by covalent ubiquitin conjugation through the sequential action of E1 activating enzymes, E2 conjugating enzymes, and substrate-selective E3 ligases. Polyubiquitylated proteins, often modified by Lys48-linked ubiquitin chains (but also by Lys-63, Lys-100), are recognized by the 26S and translocated into the 20S catalytic core for proteolysis (102). By contrast, autophagy-dependent degradation culminates in lysosomal hydrolysis and is initiated under nutrient deprivation via AMPK activation and mTORC1 inhibition, which allows activation of the ULK1 complex and downstream stimulation of the Beclin-1–VPS34 nucleation machinery. Autophagosomal membrane elongation then requires ATG proteins - ATG5, ATG7 and LC3/ATG8 conjugation systems, while lysosomal cathepsins finalize protein degradation after autophagosome–lysosome fusion (103,104).

The distinction between these pathways seem particularly relevant in the context of LD biology, where both the LD proteome and lipolytic enzymes are post-translationally regulated. As already briefly mentioned in a previous section, PLIN2 represents a well-characterized example of a LD-associated protein undergoing regulated degradation. The cytosolic, LD-unbound pool of PLIN2 is degraded via the ubiquitin–proteasome pathway, involving substrate recognition by the E3 ligase TEB4, indicating that droplet association protects PLIN2 from rapid cytosolic turnover (105,106). In parallel, PLIN2 and PLIN3 can also undergo CMA, in which HSC70

recognizes both PLINs and delivers them to LAMP2A at the lysosomal membrane. Functionally, degradation of these PLINs facilitates access of lipolytic and autophagic machinery to the LD surface (96).

ATGL itself is a subject of tightly regulated protein degradation. Current evidence indicates that ATGL is degraded mainly by the UPS rather than by lysosomal mechanisms, as proteasome inhibition with MG132 increases ATGL abundance and ubiquitinated ATGL species, whereas lysosomal inhibition with bafilomycin A1 has little or no effect on endogenous ATGL levels in the same settings (107). Mechanistically, several E3 ligases have been implicated in ATGL turnover depending on the context and organ. In hepatocytes, COP1 E3 ligase recognzes ATGL and promotes its Lys48-linked polyubiquitylation, thereby targeting ATGL for proteasomal degradation and reducing fatty acid mobilization and oxidation; conversely, COP1 depletion ameliorates hepatic steatosis in experimental models (108). More recently, the N-end rule pathway was shown to regulate ATGL stability through the E3 ligases UBR1 and UBR2, which recognize the destabilizing N-terminal phenylalanine of ATGL and promote proteasome-dependent turnover; notably, the N-end rule-resistant ATGL (F2A) mutant exhibits increased stability and enhanced lipolytic activity, and Lys100 again emerged as an important determinant of ATGL ubiquitylation and protein half-life (107). Additional regulation has been linked to the peroxisomal E3 ligase PEX2, which polyubiquitylates ATGL in both LD and cytosolic fractions and thereby suppresses lipolysis in response to changes in intracellular fatty acid metabolism (109). Furthermore, pigment epithelium-derived factor (PEDF) has been identified as an upstream physiological signal that decreases ATGL stability by promoting its COP1-dependent proteasomal degradation, including enhanced nuclear import of ATGL prior to degradation in hepatocytes, and PEDF was also reported to shorten ATGL half-life through a ubiquitin-dependent proteasomal pathway in adipocytes (110,111). Turnover of intestinal ATGL in the context of the proteasome has not been studied so far.

According to current literature data, ATGL is generally linked to autophagy not primarily as an autophagic substrate, but as a functional regulator of lipophagy. In hepatocytes, ATGL activity promotes expression of autophagy-related genes, increases LC3-II and LAMP1 abundance, reduces p62 accumulation, and enhances colocalization of LD with lysosomes, indicating that ATGL supports autophagic flux and lipophagy-dependent lipid catabolism rather than being cleared mainly by lysosomes itself (112). Thus, ATGL occupies a mechanistically interesting position at the interface of the two degradative systems: its own protein abundance is likely

controlled via proteasomal degradation, while its lipase activity facilitates lipophagy-driven LD breakdown.

Taken together, these findings indicate that LD homeostasis depends on coordinated proteolytic remodeling of both structural droplet coat proteins and lipolytic enzymes. Proteins such as PLIN2 and PLIN3 can be eliminated by proteasomal or lysosomal routes depending on their molecular state and cellular context, whereas ATGL appears to be controlled mainly by UPS-mediated turnover involving COP1, UBR1/UBR2, PEX2, and upstream modulators such as PEDF (96,107–110).

Functions of LD in health and disease

In healthy tissues, LDs perform at least three fundamental functions: they store excess fatty acids in a neutral and osmotically safe form, supply substrates for energy production and membrane synthesis, and protect cells from lipotoxic stress by sequestering potentially harmful lipids (68,98). These functions are particularly important in adipose tissue, where LDs provide the principal reservoir for organismal energy storage and protect nonadipose organs from lipid overload. However, when LD biogenesis, expansion, or degradation becomes dysregulated, LDs can actively contribute to disease pathogenesis (68,98).

In the liver, excessive LD accumulation is a hallmark of steatotic liver disease, and increasing evidence indicates that disease progression depends not only on the quantity of stored fat but also on LD proteome composition and degradative capacity (113–115). In adipose tissue, disturbed LD turnover alters lipolysis and increases fatty acid spillover into the circulation, thereby promoting insulin resistance and dyslipidemia (86,116). In macrophages, LD-rich foam cells play an important role in atherogenesis through altered cholesterol storage and inflammatory activation (117,118).

LD biology is gaining more attention in the context of the nervous system, as LD accumulation in neural cells is increasingly associated with oxidative stress, mitochondrial dysfunction, and neurodegenerative disease (119–121). Current evidence suggests that LDs may initially protect neural cells by buffering excess fatty acids, but persistent accumulation or impaired degradation may become maladaptive and contribute to diseases such as Alzheimer’s disease and Parkinson’s disease (121–123). In skeletal muscle, LDs participate in oxidative metabolism and

may influence cell fate, regeneration, and metabolic flexibility, although their role depends strongly on localization and physiological context (124–126).

Characteristics of LD in enterocytes of the small intestine

The small intestine constitutes a distinctive organ-specific model of LD biology since, during the postprandial period, absorbed lipids are partitioned between CM incorporation and temporary storage in LD. (38,127,128) A rapid droplets' appearance after an oral fat challenge, followed by subsequent depletion, indicates that they function as transient metabolic reservoirs rather than inert depots (127,129). Regional analyses have further shown that LD abundance and morphology differ along the proximal-to-distal axis of the small intestine, consistent with spatial specialization in lipid buffering and trafficking (130). In parallel, proteomic studies in mouse enterocytes have identified LD-associated proteins involved in apolipoprotein handling, membrane trafficking, and lipid remodeling, supporting the concept that intestinal LD operate as active platforms for postabsorptive lipid processing (131). Chronic dietary lipid excess also remodels intestinal lipid droplet morphology and proteome, producing larger droplets and altered droplet-associated protein composition during acute fat exposure in obese mice (132). On the other hand, in humans, GLP-2 acutely increases circulating TG and CM without significantly reducing duodenal LD abundance, indicating that enhanced lipid export can occur without overt depletion of LD pools (133). This finding suggests that LD turnover, chylomicron assembly, and lymphatic transport are coordinated but at least partially dissociable processes within intestinal lipid handling (133,134).

Among the best-characterized structural regulators of LD are the PLIN family proteins, which coat the droplet surface and influence access of lipases to the neutral lipid core (128). In murine intestinal mucosa, PLIN2 and PLIN3 are the principal proteins associated with enterocyte LD and decorate them after dietary fat exposure (128). Available data suggest that PLIN 3 is involved primarily in early droplet biogenesis, whereas PLIN 2 contributes more strongly to stabilization of mature droplets, although the consequences of enterocyte-specific PLIN protein dysfunction for TG partitioning between chylomicron secretion, oxidation, and storage remain insufficiently defined (128).

Lipolytic mobilization of TG stored in the small intestine requires coordinated action of LD-associated hydrolases (135). ATGL and its co-activator CGI-58 initiate TG hydrolysis, while downstream enzymes, including HSL and MGL, complete sequential degradation of DAG and

MAG intermediates, respectively (135). Intestine-specific deletion of ATGL causes marked accumulation of LD in enterocytes, yet does not impair overall triglyceride absorption to the extent expected if this stored TG pool were a major obligatory substrate for CM production (136).

Subsequent work has refined this interpretation by showing that ATGL and CGI-58 are critical for catabolism of a distinct intestinal lipid droplet pool, particularly one derived from basolaterally acquired fatty acids, rather than for direct provision of substrate for chylomicron synthesis (135). These findings indicate that not all enterocyte LDs are metabolically equivalent and support the existence of functionally distinct pools with different substrate origins and physiological fates (135). CGI-58 deficiency in the intestine has also been associated with enlarged lipid droplets and impaired postprandial lipid handling, further underscoring the importance of regulated droplet lipolysis in intestinal lipid trafficking.

Additional evidence for the role of lipid droplet lipolysis in chylomicron assembly comes from studies of GRASP55, a Golgi-resident protein required for proper trafficking of certain lipid droplet-associated lipases, including ATGL and MGL, to the droplet surface (137). GRASP55 deficiency impairs fat absorption, reduces CM secretion, and promotes the formation of abnormally large enterocyte LD, indicating that lipase targeting to LD is necessary for sustained substrate supply to the secretory pathway (137). These observations support the view that intracellular membrane trafficking machinery can influence intestinal lipid export indirectly through control of LD catabolism (137).

Carboxylesterase 2c (CESC2) is another important contributor to enterocyte neutral lipid hydrolysis (138). Intestine-specific overexpression of CES2C enhances fatty acid oxidation in enterocytes and promotes metabolic protection against obesity and fatty liver disease, while preserving overall fat absorption (138). Notably, altered intestinal CES2 activity changes the spatial distribution of lipid uptake along the intestine and increases chylomicron particle size, suggesting that intracellular lipolysis can reshape both enterocyte metabolism and lipoprotein output (138).

Overall, current evidence indicates that enterocyte LDs are highly dynamic and functionally heterogeneous organelles that integrate lipid storage, regulated mobilization, oxidative metabolism, and lipoprotein secretion (128,134,135). Their biology is shaped by droplet-coating proteins, lipases, membrane trafficking factors, and extracellular regulatory pathways,

and disruption of these systems has consequences not only for postprandial lipid transport but also for obesity, fatty liver disease, and intestinal inflammation (137–140). Actively debated is also the impact of aberrations in small intestine lipid metabolism on cancer and inflammation-related conditions, which is a subject of the following chapter.

Contribution of the intestinal lipid metabolism to the development of cancer and inflammatory diseases

Intestinal fat absorption, although classically regarded as a nutritional function, is increasingly recognized as a determinant of intestinal homeostasis and disease susceptibility because it governs epithelial exposure to dietary lipids, modulates bile acid metabolism, and influences host-microbiota interactions (141,142).
Consequently, disturbances in intestinal lipid handling may contribute directly to the pathogenesis of both intestinal inflammatory disorders and intestinal neoplasia (141–143), while excessive intestinal fat absorption remains a key risk factor predetermining the development of metabolic syndrome (discussed earlier in this chapter).

In the context of intestinal cancer, there is substantial evidence regarding colorectal carcinogenesis. High dietary fat intake increases the demand for bile acid secretion to facilitate intestinal lipid absorption, and a fraction of these bile acids escapes enterohepatic recovery and undergoes bacterial conversion in the colon to secondary bile acids, including deoxycholic acid and lithocholic acid (141,144,145). These metabolites are of particular pathological relevance because they promote epithelial stress, alter proliferative signaling, enhance local inflammatory response, and thereby create an environment that may favour tumor initiation (141,146,147). Thus, excessive intestinal fat absorption may support colorectal cancer development indirectly through bile acid-driven and microbiota-dependent mechanisms, while established colorectal tumors also exhibit profound lipid metabolic reprogramming that further sustains proliferation, invasion, and immune remodeling within the tumor microenvironment (141,143). A related but distinct pathological axis links intestinal lipid handling to inflammatory disorders, namely, inflammatory bowel disease (IBD). Chronic intestinal inflammation is characterized by epithelial barrier dysfunction, abnormal innate and adaptive immune activation, and persistent mucosal injury, all of which may be exacerbated by altered lipid exposure and metabolism (142). Within this pathogenic model, intestinal LD may be a functionally important organelle. As described before, in enterocytes, LD serve to buffer postprandial lipid flux, coordinating chylomicron production, and limiting acute exposure of cellular membranes and organelles to

unesterified fatty acids (127–129). This buffering role is highly relevant to initiate pathological state since LD may protect intestinal epithelial cells against lipid overload under physiological conditions, whereas failure of this adaptive capacity may favor accumulation of toxic lipid intermediates, which trigger endoplasmic reticulum stress, mitochondrial dysfunction, oxidative injury, and inflammatory signaling (11,129,148). Moreover, intestinal LD has also been implicated in host-pathogen interactions, further supporting the concept that they participate broadly in mucosal defense and inflammatory regulation (149).

The concept of lipotoxicity may provide a mechanistic bridge connecting disordered, i.e. excessive, intestinal fat absorption with both inflammation and carcinogenesis. Lipotoxicity refers to the deleterious cellular effects caused by excessive accumulation of non-neutral lipid species, especially when lipid storage and disposal mechanisms become saturated (148,150). In the intestine, such lipotoxic stress may disrupt epithelial integrity, stimulate reactive oxygen species production, activate inflammasome-related or pyroptotic pathways, and thereby intensify mucosal inflammation and enhance epithelium turnover rate, therefore conditions often preceeding neoplastic transformation (142,151). Accordingly, the transition from physiological lipid trafficking to pathological lipid overload may be a critical point in the initiation of chronic intestinal inflammatory states or cancer, although more studies oriented to test that link more directly are needed (141,151).

Protein Kinase D2 in the regulation of lipid metabolism

General structure and mechanism of PKDs activation

Obesity and related metabolic dysfunction are either a cause or a consequence of rewired signalling pathways involved in metabolism regulation. One protein cluster has been proven in recent years to profoundly contribute to glucose, amino acid, carbohydrate, and lipid metabolism across different organs, and also being of interest of presented work are protein kinase D (PKD) family members. PKDs belong to the serine/threonine kinases and Ca2+/calmodulin-dependent protein kinase superfamily. Mammalian cells express three PKD isoforms, PKD1, PKD2, and PKD3, each encoded by a distinct gene, but all sharing a conserved structure composed of cysteine-rich C1 domains, an autoinhibitory pleckstrin homology domain, and a C-terminal catalytic kinase domain. As members of the calcium/calmodulin-

dependent kinase superfamily, PKDs are activated downstream of both G protein-coupled receptors and receptor tyrosine kinases in response to hormones, growth factors, neurotransmitters, and nutrient-associated stimuli (67). A canonical activation of PKD starts upon membrane receptor-dependent activation of phospholipase C (PLC). PLC hydrolyzes phosphatidylinositol 4,5-bisphosphate to generate inositol 1,4,5-trisphosphate and DAG, with the latter serving as the key lipid signal that recruits both protein kinase C (PKC) and PKDs to membrane compartments. Following membrane recruitment, PKDs are activated through PKC-dependent phosphorylation of conserved serine residues within the activation loop, followed by autophosphorylation of serine sites, which are: for PKD1 at Ser738/Ser742, PKD2 at Ser706/Ser710, and PKD3 at Ser731/Ser735 (67,152). The intracellular localization of PKDs is dictated by DAG availability and includes the plasma membrane, Golgi complex, cytoplasm, nucleus, and mitochondria, indicating that PKD activity is shaped by the local lipid environment rather than by a single universal activation site. Importantly, DAG can be produced by several cellular pathways, but not every DAG pool is equally capable of triggering the PKC/PKD axis (67,152). In particular, sn-1,2 DAG is regarded as the major PKC-activating form and therefore the DAG species most relevant for subsequent PKD activation. That species is generated mostly through phospholipase C-mediated phosphoinositide hydrolysis and can also arise during sphingomyelin synthesis at the plasma membrane, while PKC-responsive DAG is also abundant within the ER and Golgi compartments. By contrast, DAG derived from lipolysis mediated by ATGL and HSL is enriched in rac-1,3 and sn-2,3 isomers produced but these species are poor activators of the PKC/PKD pathway (67,152). This distinction is especially relevant in the intestine, where we showed that PKD2 is involved in dietary fat handling. Although PKD2 is activated in enterocytes during fat absorption and promotes chylomicron-mediated lipid transport, it remains uncertain whether this response is driven directly by transient DAG accumulation at the endoplasmic reticulum during fatty-acid re-esterification. Nevertheless, current evidence supports the view that disturbed DAG signaling and PKDs activation contribute to metabolic pathology, including obesity and related systemic dysfunction, but due to non-redundant roles of PKD isoforms, each kinase shapes a tissue-specific phenotype. (52,67,152).

PKDs in the control of glucose, amino acid, and lipid metabolism.

In pancreatic β-cells, PKD1 supports stimulated insulin exocytosis and cell survival, whereas the stress kinase p38δ suppresses this pathway through inhibitory phosphorylation of PKD1. Consequently, p38δ-deficient mice show enhanced insulin secretion and improved glucose tolerance, placing PKD1 as a regulatory kinase within a glucose-homeostatic circuit (153). In adipose tissue, PKD1 also acts as a brake on energy expenditure via suppressing AMP-activated protein kinase (AMPK). Adipocyte-specific PKD1 deletion increases mitochondrial fragmentation, biogenesis, and respiration, promotes beigeing of adipose tissue, and protects mice from HFD-induced adiposity while improving systemic insulin sensitivity (154).

PKD3 is particularly important in the liver, where it integrates fasting and nutrient-overload signals. A phosphoproteomic study showed that glucagon activates PKD3 and that PKD3 amplifies PKA-dependent hepatic programs, thereby increasing glucose output and promoting tyrosine production from phenylalanine, which connects this isoform to both glucose metabolism and amino acid metabolism during fasting (155). By contrast, under lipid-rich conditions, PKD3 provides negative feedback on insulin signaling in hepatocytes by suppressing AKT and mTORC1/2 activity, which restrains SREBP-driven cholesterol and triglyceride synthesis. Loss of hepatic PKD3 in mice therefore improves insulin signaling but promotes steatosis and lipid accumulation (156).

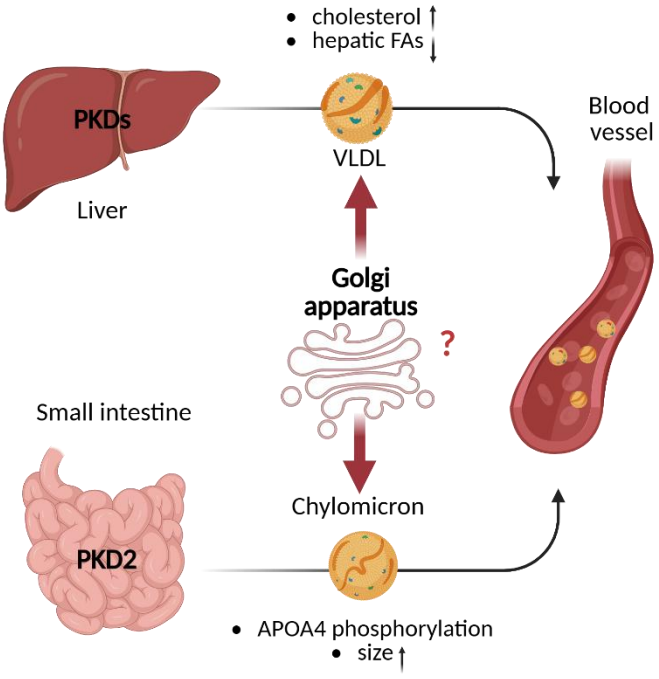

Fig. 6. PKDs in lipoprotein-mediated lipid secretion. PKDs contribute to synthesis of VLDL in the liver and CM in the intestine. Hepatic PKDs (non-defined isoform) promote cholesterol packing into VLDL and limit the accumulation of free fatty acids (FAs) in the organ. In enterocytes of the small intestine, PKD2 promotes chylomicron secretion, possibly via APOA4. The role of the Golgi apparatus, modified by PKDs, in shaping these phenotypes is speculative. (modified from Wit et al., 2024). Figure created with BioRender.

Among the PKD family members, PKD2 is currently the clearest example of a direct control of intestinal lipid flux. PKD2 is activated during enterocyte dietary fat uptake and promotes CM-mediated TG transport from the intestine, thereby promoting postprandial lipid delivery to the circulation and contributing to obesity *in vivo* under high-fat diet feeding conditions. (52,67) (Fig. 6). Mechanistically, PKD2 does not primarily appear to interfere with fatty-acid uptake itself; rather, it enhances the efficiency of net lipid output by increasing CM size, i.e., particle lipidation (52). That is associated with reduced abundance of APOA4, and our published data suggest that PKD2 may regulate APOA4 directly, possibly through phosphorylation, a post-translational modification which may suppress APOA4 stability and thereby enhance TG packaging into nascent chylomicrons (52,67). Accordingly, PKD2 deficiency or inactivation leads to smaller CM, diminished intestinal TG export, lower circulating TG, and protection from high-fat diet-induced obesity and glucose intolerance, highlighting intestinal PKD2 as a determinant of whole-body lipid homeostasis (52). Important - from a translational point of view - is also a fact that orally administered inhibitor of PKD, CRT0066101, to C57BL6 wild type mice, provides a similar obesity-protective phenotype, highlighting the position of PKD2 as a targettable node for potential future anti-obesogenic therapies, especially for patients with liver or kidney insufficiencies as CRT0066101 acts specifically in the intestine, and largely omits clearance pathways in abovementioned organs. Data from humans also suggest that decreased PKD2 activity correlates with a healthier blood metabolic profile, i.e. lower TG and glycated hemoglobin (HBa1c; a long-term glucose levels marker) and higher high-density lipoproteins (HDL). While CM is an enterocyte-unique class of secreted lipoprotein, specific for the liver are very low-density lipoproteins (VLDL), also enriched in TG. Reducing the activity of all three PKD isoforms in that organ lowers VLDL and cholesterol output, which is proposed to be connected with PKDs function in regulating vesicular transport from the TGN to the plasma membrane (157). Considering lipoproteins, both CM and VLDL, as secretory

cargoes traversing through TGN and controlled by PKD proposes a new mechanistic investigation, possibly linking the relevance of Golgi apparatus architecture with lipid absorption and secretion a direction which has not yet been explored. (Fig. 6)

Overall, PKD1, PKD2, and PKD3 control distinct but complementary aspects of nutrient metabolism where PKD1 tunes insulin secretion and adipocyte energy dissipation, PKD3 coordinates hepatic glucose, amino acid, and lipogenic signaling, and PKD2 governs the efficiency of CM assembly and intestinal lipid export as collectively depicted on Fig. 7 (52,153–156).

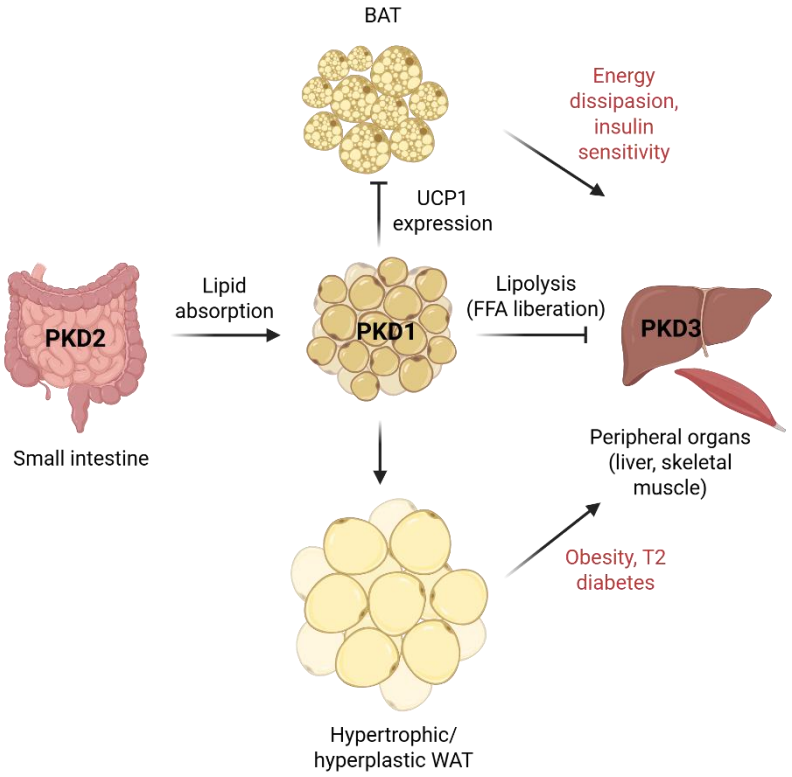

Fig. 7. PKDs in the integration of lipid metabolism across organs. PKD2 promotes lipid absorption from the intestine, which, if in surplus, is stored in WAT. PKD1 in WAT promotes lipid storage, suppresses UCP1 expression, and energy dissipation (beiging of adipose tissue). Lipolysis-derived FFA are taken up by hepatocytes, where PKD3 protects from lipid deposition. BAT; brown adipose tissue, UCP1; uncoupling protein 1, T2 diabetes; type 2 diabetes, WAT; white adipose tissue. Figure created with BioRender.

AIMS OF THE STUDY

As described above, the postprandial handling of absorbed lipids in enterocytes of the small intestine refers to a dynamic balance between chylomicron secretion and storage of lipids in LD. Research conducted previously in our laboratory showed a profound role of Protein Kinase D family members in lipid and amino acid metabolism across various organs (52,154–156). Particularly for the study described herein, intestinal PKD2 was shown to promote TG absorption via increasing the size of secreted chylomicrons which, mechanistically, is likely due to APOA4 phosphorylation. In line, genetic or pharmacological inactivation of PKD2 resulted in reduced TG output from the intestine and protection from obesity in mice fed with an HFD. However, whether PKD2 impacts the other aspect of lipid handling in the intestine, the metabolism of LD and via that mechanism regulates intestinal lipid absorption, was not tested before. Based on our previous findings regarding the role of different PKD isoforms in the regulation of fat accumulation in the liver and adipose tissue, as well as the established role of PKD2 in chylomicron (CM) formation, we hypothesized that PKD2 may also be a regulator of lipid storage and secretion in enterocytes.

Thus, the first aim of this study was to determine the role of PKD2 in the turnover of intestinal LDs formed in response to both acute (via olive oil gavage) and prolonged dietary lipid load (through feeding with a high-fat diet). Moreover, we aimed to elucidate the PKD2-dependent molecular mechanisms regulating LD dynamics. During the course of this study, we also identified an unexpected phenomenon. Specifically, we observed a rapid degradation of a cluster of LD-associated proteins (lipases) in response to lipid ingestion into the intestinal lumen. Therefore, an additional objective was to characterize this previously unreported physiological process and to define the role of PKD2 in its regulation. The molecular characterization of this process thus became the third specific aim of the PhD project.

MATERIALS AND METHODS

Animal models

All animal experiments performer in this thesis were approved by the local animal ethical committee and conducted according to the guidelines and state regulations. Experiments were performed under animal protocol number 1797/2025 approved by 1st Local Ethical Committee for Animal Experiments in Warsaw. Mice were maintained in specific-pathogen-free facility, in individually ventilated cages (IVC), with the ambient temperature set at 22°C and 55% air humidity, in a 12 h light-dark cycle and provided ad libitum access to water and standard chow diet. As indicated in certain experimental procedures, the chow diet was exchanged to high-fat diet (HFD) or fat-free diet (FFD). Mice were kept in gropus up to 5 mice per IVC cage. Euthanasia was performer via cervical dyslocation, in a separate area, away from alive animals. No animals died or got injured/ill during experimental procedures. All experiments were carried out with male mice.

The generation of mice bearing a specific deletion of intestinal PKD2 was achieved by crossbreeding Villin-Cre mice (B6.Cg-Tg(Vil1-cre)1000Gum/J) with Pkd2 flox/flox mice (courtesy of Prof. Yamasaki, Osaka University) (249).

Mouse line carrying a whole-organism PKD2 inactivation (Pkd2 knock-in) were generated in the laboratory of Prof. Cantrell (250). These mice presented point mutations of Ser707 and Ser711 into alanines (Pkd2ki/ki) by the homologous recombination of the PGK-NeoR cassette in C57BL/6J embryonic stem cells which were microinjected into C57BL/6 blastocysts. Mice were maintained in a C57BL/6 background.

Mice genotyping

DNA extraction

Fingers of mice were clipped and the tissue was lysed in 0.5 mL of buffer composed of 10 mM Tris pH 8, 100 mM EDTA pH 8, 0.5% SDS, 2.5 uL Proteinase K and left for overnight digestion at 55°C. Next, 100 uL of 5 M NaCl was added and centrifuged at 13000 rpm 10 min at 4°C. DNA was precipitated from the supernatant by addition of 300 µL of isporopanol, cooling at -20°C for 30 min., followed by centrifugation. The obtained pellet was washed with 70% ethanol, air-dried and suspended in 30 µL of ultra pure water.

PCR conditions for genotyping

PCR reaction was composed of 1.5 µL of DNA and :

Component	Volume (µL)
Thermo 10x Buffer with KCl	2.5
Each primer (10 µM)	1
Thermo dNTPs (5 µM)	2
Thermo MgCl2 (10x)	2.5
Thermo Taq Polymerase (5 U/µL)	0.5
Total amount (completed with water)	23.5

The PCR cycling conditions were as following:

a) *Pkd2$^{flox/flox}$* genotyping

Step 1. 94°C 2 min

Step 2. 94°C 30 sec

Step 3. 60°C 30 sec

Step 4. 68°C 30 sec

Step 5. go to Step 2, repeat 40x

Step 6. 72°C 10 min

Step 7. 4°C hold

b) Villin Cre genotyping

Step 1. 94°C 2 min

Step 2. 94°C 20 sec

Step 3. 65°C 15 sec -0,5°C per cycle decrease

Step 4. 68°C 10 sec

Step 5. go to Step 2, repeat 10x

Step 6. 94°C 15 sec

Step 7. 60°C 15 sec

Step 8. 72°C 10 sec

Step 9. Go to step 6, repeat 28x

Step 10. 72°C 10 sec

Step 11. 4°C hold

c) Pkd2 ki genotyping

Step 1. 94°C 3 min

Step. 2 94°C 30 sec

Step. 3 65°C 20 sec

Step. 4 68°C 40 sec

Step. 5 go to Step 2, repeat 10x

Step. 6 94°C 30 sec

Step. 7 50°C 20 sec

Step. 8 70°C 40 sec

Step 9. go to Step 6, repeat 25x

Step. 10 72°C 2 min

Step 11 10°C hold

Agarose gel electrophoresis

The product of PCR reaction was mixed with 6x loading dye and loaded into 3 % agarose gel composed of 3 g agarose per 100 mL Tris-acetate-EDTA buffer, boiled in a microwave followed by adding 7.5 μL of Midori Green to stain DNA. The samples and 100 bp ladder were run at 120 V for ~1 h and bands were visualized under ultraviolet light. For each genotyping the resulting bands were:

a) *Pkd2*$^{flox/flox}$ wildtype = 350 bp flox = 450 bp

b) Villin Cre transgene = 150 bp internal positive control = 182 bp

c) *Pkd2*$^{ki/ki}$ wildtype = 280 bp knockin = 340 bp

Lipids, glucose and casein oral challenge

Mice were fasted overnight (16 h) or 6 h (from 8 am to 2 pm) and a defined dosage of oil [olive oil, coconut oil or linseed oil; 10 μL/g of body weight (if not stated otherwise)] or isocaloric dosage of 50% glucose solution or casein powder water suspension were administered orally with a feeding needle intragastrically.

***In vivo* experiments with Orlistat, Pluronic L-81, MG132 and Bafilomycin A1**

On the day of the experiment, C57BL6J mice were transferred to cages with fresh bedding, without access to food, but with free access to drinking water for 6 h (from 8:00 a.m. to 2:00 p.m.). For oral gavage studies, animals received Orlistat, a pancreatic lipase inhibitor, at a dose of 60 mg/kg body weight, in accordance with published data (251). Orlistat was dissolved in

DMSO according to the manufacturer's instructions (Sigma-Aldrich), and the dose adjusted to each mouse's body weight was brought to a final volume of 250 μL with sterile drinking water at room temperature. Another group received a mixture of DGAT1 and DGAT2 inhibitors, PF04620110 and PF07202954, respectively, at doses of 3 mg/kg and 7.5 mg/kg body weight, as previously described to inhibit intestinal triglyceride re-esterification (252). Both compounds were dissolved in sterile DMSO according to the manufacturer's instructions (Sigma-Aldrich), combined in a single syringe in amounts adjusted to body weight, and the final volume was brought to 250 μL with sterile drinking water at room temperature. Mice assigned to the corresponding control groups received 1% aqueous DMSO, also at a volume of 250 μL, corresponding to 2.5 μL of pure DMSO per mouse, a dose reported not to produce adverse effects (253). In a separate set of animals, a group received Pluronic L-81, a surfactant that inhibits chylomicron synthesis, by oral gavage as a 3% solution in drinking water at a dose of 10 mL/kg, according to the available literature (254); Pluronic L-81 purchased from Sigma-Aldrich was used as supplied. The corresponding control group received sterile drinking water at the same volume (10 mL/kg). One hour after substances administration, the animals were gavaged with olive oil (10 μl/g b.w.) and sacrificed via cervical dislocation 30 min after the gavage.

In a separate experiment, mice received a single subcutaneous injection of the proteasome inhibitor MG132 at a dose of 7.5 mg/kg body weight, as described previously (255). MG132 (Sigma-Aldrich) was supplied as a powder and was dissolved in DMSO according to the manufacturer's instructions. The appropriate amount for each mouse was then diluted with sterile saline to a final volume of 100 μL. Control mice received 1% DMSO in sterile saline by subcutaneous injection, using the same procedure and final volume (100 μL).

In another experiment, mice received a single intraperitoneal injection of the autophagy inhibitor bafilomycin A1 at a dose of 0.1 mg/kg body weight, according to published protocols (256,257). Bafilomycin A1 (Sigma-Aldrich) was supplied as a powder and dissolved in sterile DMSO according to the manufacturer's instructions. The dose, adjusted to each mouse's body weight, was then diluted with sterile saline at room temperature to a final volume of 100 μL. The injection was performed in the right lower quadrant of the abdomen using a 25 G needle. Control mice received 1% DMSO in sterile saline (100 μL) intraperitoneally, using the same procedure as for the bafilomycin A1-treated animals.

Fasting-refeeding experiments

For fasting-refeeding experiments, mice were fasted 6 h (from 8 am to 2 pm) followed by 3 hours of free access to food (diets defined in experimental procedures: chow, high-fat, fat-free diet). After that period, mice were euthanized via cervical dislocatiion and organs of interest were collected for further analysis.

Microcopy methods

Immunohistochemistry (IHC)

For immunohistochemical analysis of intestinal tissues, jejunum was isolated, fixed in 4% neutral-buffered formalin overnight and embedded in a paraffin block. Paraffin sections of the jejunum were cut transversely at 5 µm thickness, deparaffinized with xylene, rehydrated by immersing in gradiently increasing ethanol (50%, 70%, 95% and 100%) solutions and antigen retrieval was performed by heat treatment. Non-specific binding sites were blocked with 5% goat serum and 1% BSA in PBS for 1 h. The indicated primary antibodies were diluted in 5% goat serum in PBS and applied overnight at 4 °C. After washing three times with PBS with 0.05 % Tween, tissues were treated with fluorophore-dye conjugated secondary antibodies diluted in 5 % goat serum for 1 h at RT, followed by 3 washes with PBS and nuclei were stained with DAPI. Mounted with ProLong™ Diamond Antifade Mountant, the images were captured using a laser scanning confocal microscope with a 63x oil objective (SP8, Leica).

Immunoblotting

Tissues and cells were lysed in RIPA buffer supplemented with Protease and Phosphatase Inhibitor. Tissues were lysed with a TissueLyser (Qiagen) and grinding beads (2 min, 30 frequency) and cells were homogenized with a pestle and then a passed through a syringe needle (25 G). Homogenized samples were centrifuged (16000 g, 4°C), protein-enriched supernatant was collected to a fresh tube and protein concentration was determined with Pierce™ BCA Protein Assay Kit. Equal amount of protein (50 µg) was adjusted to equal volume with RIPA buffer, mixed with 2x Laemmli buffer and boiled 5 min at 95°C). Samples were loaded into a SDS-PAGE gel (10%) and run at 120V, tranferred onto a nitrocellulose membranes at constant 80 V, 1.5 h, 4°C. Membranes were blocked either in milk 5% in TBST or BSA 5% in TBST for 1 h (for detection of phosphorylated proteins, washed three times with TBST and incubated with primary antibodies (1:1000 in 5% BSA in TBST) overnight at 4°C. The membrane was washed three times with TBST and then incubated with HRP-conjugated secondary antibody for 1h at

4°C (1:5000 in 5% milk in TBST). After three more washes with TBST and one with TBS, the membrane was developed with ECL by using X-ray films or digitally in Amersham Imager 680.

Electron microscopy

Mice were euthanized via cervical dyslocation at indicated time points after olive oil challenge or upon a period of fasting only and excision of 0.5 cm of jejunum with cutting open was performed in 2% paraformaldehyde and 1% glutaraldehyde in 0.1 M cacodylate buffer (CB). Immediately afterwards, the samples were transferred for fixation to a buffer containing 1% glutaraldehyde and 1% osmium tetroxide in 0.1 M CB at 4°C 45 min. Samples were then washed twice in 0.1 M CB with two changes and total duration 20 min and transeffred to another fixative buffer (2% glutaraldehyde in 0.1 CB for 2 h at 4°C). After washing in 0.1 CB, the samples were postfixed and stained in 2% osmium tetroxide in CB for 2 h at 4°C, followed by washing in 0.1 M CB with four buffer changes and total duration over 1 h at 4°C. The samples were then rinsed and kept in CB until the processing could be resumed (typically 48-72 h). The following incubation steps were aided by a Pelco BioWave Pro+ (Ted Pella, Inc.). The samples were first incubated in 1% potassium ferrocyanide in CB. After rinsing with water, the tissues were incubated in 0.3% thiocarbohydrazide in water, rinsed and further incubated with 1% osmium tetroxide in CB. After rinsing and an overnight incubation in 1% uranyl acetate, samples were dehydrated with a graded ethanol series and infiltrated with increasing concentrations of Epon hard. Finally, the samples were polymerized at 60◦C for 48 h. The resin blocks were then sectioned using an ultramicrotome (Leica UC7) and 70 nm-thick sections were collected on formvar coated single-slot grids. The sections were imaged with a Jeol JEM-2100 Plus, with an acceleration voltage of 120kV, using the acquisition software SerialEM (Mastronarde, 2003). The imaging workflow was as follows: 1) low magnification images of the sections were acquired to identify the position of the tissue. 2) intermediate magnification montages were acquired to identify regions in which the tissue was cut perpendicular to the longest cell axis. So that the entire cross section of the cells could be visualized. 3) Cells that could be entirely imaged from the basal to the apical surface were targeted for higher resolution imaging. For each sample, we acquired at least 10 cells from at least 3 different villi.

Subcellular fractionation

Lipid droplets, cytosol and total membranes from intestinal epithelium were isolated as described by Ding et al. (258). In brief, jejunal scratches from about 15 cm piece of intestine were collected from mice sacrificed 2 h after olive oil gavage were placed in 1 mL of buffer A composed of 250

mM sucrose and 20 mM tricine (pH 7.8) with complete phosphatase and protease inhibitors and kept on ice for 20 min. Tissues were transferred in 10 mL of buffer A to a Dounce homogenizer a and broken by mechanical force (~20 dounces). Subsequently, the tissues were passed through a syringe 25 G (~10 times), transferred to 15 mL falcon and centrifuged 10 min at 3000 *g*, 4 °C. Obtained supernatant was collected as postnuclear superntatant (PNS) and 500 uL was saved in a separate microcentrifuge tube for later determination of fractions purity. PNS was transferred to an Open-Top Ultra Clear Tube (Beckmann Coulter), 3 mL of buffer B containing 20 mM HEPES, 100 mM KCl and 2 mM $MgCl_2$ (pH 7,4) was added on top and ultracentrifuged 182 000 *g* for 1 h, 4 °C with Optima XPN-100 ultracentrifuge using SW41 swinging-out rotor. The resulting top band of lipid droplets was carefully collected and kept on ice. The pellet was washed with buffer B and saved as total-membranes fraction. After collecting lipid droplets, 1 mL of solution from the middle was transferred to a micro-ultracentrifuge tube and ultracentrifuged using AT3 fixed-angle rotor and Thermo Scientific Sorvall WX 80+ ultracentrifuge at 270 000 *g* for 1 h, 4°C. Obtained supernatant was saved for further analysis as a cytosolic fraction. Lipid droplet fraction was delipidated and proteins were solubilized as described previously (259). Other organelles, *i.e.* Golgi apparatus and endoplasmic reticulum were isolated using commercial kits and following manufacturer's instructions (Minute™ Golgi Apparatus Enrichment Kit and Minute™ ER Enrichment Kit, respectively, from Invent Biotechnologies, Inc.). The proteins in all fractions were denaturated with 2x Laemmli buffer, protein concentration was determined with BCA Pierce™ BCA Protein Assay Kit (BCA) and equal amount of protein (25 ug) was used for immunoblotting.

Measurement of ATGL activity *in vitro*

Activity of ATGL in the intestines was measured using the EnzCheck lipase substrate (Thermo Fisher, cat. no. E33955). Jejunal scratches were isolated from *Pkd2*$^{flox/flox}$ and *Pkd2*$^{gu\Delta t/\Delta}$ male mice that underwent 16 h of fasting. Tissues were homogenized in a buffer containing 50 mM HEPES (pH 7.2), 100 mM NaCl, 5 mM $CaCl_2$, 0.5 mM DTT, 2% DMSO, 0.1% Triton X-100 using tissue lyser. The samples were centrifuged at 10000 g at 4ºC for 10 min. The supernatant was transferred to new tubes and protein concentration was measured using the BCA. Assays were performed in 96-well opaque black plates (Corning, #3915) containing 30 µg of tissue extract in a volume buffer A to bring 90 µl of total mixture with addition of ATGL specific inhibitor, Atglistatin (Sigma), at concentration 50 µM (from 1 mM stock; 5 µL per well) or equal volume of DMSO as control. After 30 min preincubation at room temperature with 700 rpm orbital shaking, 5 µl of 20 µM EnzChek lipase substrate working solution was added to each well to a

final concentration of 1 µM and the reaction was started at 37°C. Fluorescence was measured using a TECAN Infinite M200 Pro plate reader at 37ºC, with excitation/emission wavelengths of 485/510 nm, respectively. Fluorescence was recorded every 30 seconds for 90 minutes, with a 2-second shaking step preceding each reading. Initial 20 min was a time for reaction stabilization and discarded from AUC quantification. ATGL activity was calculated based on the slope of the fluorescence increase curve over time (x-axis), using the linear portion of the curve where fluorescence increased in a linear manner and using individual blank (sample with inhibitor added) for each sample. The procedure was analogical for an assay performed with Caco-2 cells which were grown in standard growth medium on 100 mm cell culture dishes until reaching the confluency, cell lysates were collected with assay buffer described above and homogenized by passing through a 25G needle. All following steps were as described above.

Organoid culture

Intestinal crypts isolation

Murine crypts were isolated from the jejunums of 8- to 12-week-old *Pkd2*$^{flox/flox}$ or *Pkd2*$^{gu\Delta t/\Delta}$ male mice. Animals were euthanized with cervical dislocation and the jejunum was harvested and flushed with ice-cold PBS. The intestine was cut longitudinally to expose the villous surface, chopped into 0.5 cm pieces and transferred to 50 mL falcon with fresh ice-cold PBS. The pieces were washed with PBS 20-25 times (10 mL per wash) or until the supernatant was clear. Subsequently, the intestinal fragments were submerged in 25 mL of 2 mM EDTA/PBS and left on a rocking platform 30 min at 4 °C. The supernatant was discarded and replaced with 10 mL of 1% FBS/PBS and pippeted up and down to release crypts and supernatant was filtered through cell-strainer (70 µm) and labeled as fraction 1. The procedure was repeated three more times and all fractions were centrifuged 5 min at 290 g, 4 °C. The obtained pellets were suspended in 2 mL of Advanced DMEM/F12 with 2 mM GlutaMax, 10 mM HEPES, 100 U/ml penicillin, 100 µg/ml streptomycin and 200 µg/ml normocin (Advanced DMEM/F12+++) and crypts were counted with haemocytometer. For seeding, crypts were suspended in 70% BME Cultrex Type 2 RGF/Advanced DMEM/F12+++ to a final concentration 900 crypts per 50 µL droplet that were plated into the wells of a 24 well plate and placed in a 37 °C for 20 min to polymerize. 500 µL of growth medium (composed of Advanced DMEM/F12+++ and 10% Noggin-conditioned medium, 5% R-spondin conditioned medium, 1x B27 supplement, 50 ng/ml EGF, 1 mM N-acetylcysteine, 3 µm CHIR99021, 1 mM valproic acid and 10 µM Y-27632 (only for first two

days after plating). Medium was changed every other day and organoids were splitted once per week by mechanical disruption.

R-spondin and Noggin-conditioned media production

HEK293-mNoggin-Fc and HEK293T HA-RspoI-Fc recombinant cell lines were used for production of biologically active Noggin- and R-spo1- conditioned media for organoid culture, respectively and both cell lines were a generous gift from prof. Helmuth Gehart (ETH Zurich). Cells were maintained in DMEM supplemented with 10% FCS, 1 mM sodium pyruvate, and penicillin/streptomycin, with selection during routine expansion (300 µg/mL Zeocin for R-spondin-1 producing cells and 500 µg/mL Geneticin/G418 for Noggin producing cells). After thawing, cells were expanded for two passages in T175 flasks at 37 °C and 5% CO_2. For conditioned medium production, cells were grown to full confluence and the growth medium was replaced with selection-free Ad+ medium consisting of Advanced DMEM/F-12 supplemented with GlutaMAX, 10 mM HEPES, and penicillin/streptomycin. Supernatants were collected after 5–7 days, clarified by centrifugation (5 min, 1000 rpm, RT), sterile-filtered through 0.22 µm filters, aliquoted, and stored frozen (-20 °C), avoiding repeated freeze-thaw cycles.

Organoid differentiation

To enrich the in absorptive enterocyte population, organoids were differentiated into enteroids. Ready to split, mature organoids were extracted from Matrigel with PBS and incubated in Cell Recovery Solution for 20 min at 4°C. The organoids were centrifuged 5 min at 290 g, 4 °C and the supernatant was removed. The pellet was resuspended in TrypLE for 5 min at 37°C to digest the organoids sinto single cells and material was passed through a 25 G needle about 10 times. Medium was added to stop the reaction and the mixture was centrifuged 5 min at 500 g, 4 °C. The cells were counted and seeded in Matrigel droplets at density 30000 cells/50 µL in complete growth medium with 10 µM Y-27632. After two days, medium was exchanged for differentiation medium composed of Advanced DMEM/F12+++ and 10% Noggin-conditioned medium, 5% R-spondin-conditioned medium, 1x B27 supplement, 50 ng/ml EGF, 1 mM N-acetylcysteine, 1 mM valproic acid and 2 µM IWP-2 and was maintained for next 5 days when experiments were performed.

Culture of apical-out enteroids

For generation of apical-out organoids, the Matrigel of young (3-4 days), grown from singular stem cells, basal-out organoids was broken with ice-cold Cell Recovery Solution and transferred

to microcentrifuge tube and left for incubation on a rocker for 20 min, 4 °C. The organoids were pelleted 3 min, 290 g at 4 °C and washed with ice-cold PBS. The supernatant was aspirated, pellet was resuspended in 1 mL of 5 mM EDTA/PBS, transferred to a 15 mL conical tube with 12 mL of 5 mM EDTA/PBS and left for 1 h on a rocker for incubation on ice. The organoids were centrifuged, washed with PBS and resuspended in a complete growth medium with 10 μM Y-27632 and placed onto an ultra-low attachment 24-well plate. After two days, the medium was exchanged for enterocyte-differentiation medium which composition is described above. The medium was changed every other day, until day 5-7 of culture when the experiments were performed.

Culture of 2D cell monolayers from 3D organoids

Basolateral-out enteroids were extracted from Matrigel with Cell Recovery Solution and incubated on ice for 20 min. The enteroids were pelleted and the supernatant was removed. The pellet was resuspended in TrypLE for 5 min at 37°C to digest the organoids into single cells and material was syringed through 25 G needle 10 times. Medium was added to stop the reaction and the mixture was centrifuged 5 min at 500 g, 4 °C. The pellet was resuspended in Advanced DMEM/F12 and cells were counted. Per one insert of a 24-well plate 100 000 cells were resupended in 100 μL of complete growth medium with 10 μM Y-27632 for first two days. For further culture, the medium was replaced with enterocyte differentiation medium.

Immunofluorescence of organoids and 2D monolyer

Apical-out enteroids were collected from wells to microcentrifuge tubes, centrifuged 290 g, 5 min at 4 °C, washed with PBS and fixed using 4% paraformaldehyde for 20 min at room temperature. Fixative was aspirated, organoids were washed with PBS and permeabilized with 0.3% Triton for 15 min at room temperature, followed by 1 h blocking in 10% goat serum in PBS at room temperature and overnight incubation in appropriate primary antibody diluted in 10 % goat serum/PBS at 4 °C. The following day, the enteroids were washed twice with PBS for 5 min and incubated with secondary antibody for 1.5 h at room temperature. The organoids were washed again twice with PBS for 5 min. The washing was followed by application of DAPI for nuclei staining diluted in PBS (1:500) for 20 min and, if indicated, for lipid droplets or cytoskeleton staining, LipidTox or Phalloidin at 1:200 were applied for 1 h at room temperature. The enteroids were transferred in 200 uL of PBS onto μ-Slide 8 Well Cell culture chamber slide and imaged with Leica SP8 confocal microscope using 63x water objective. Each organoid was scanned over 40 μm (1 μm between-stack distance). The images for each condition in experiment were taken using the same exposure time/laser power.

Real-time qPCR

Extraction of total RNA from about 20 mg of intestinal tissue was performed with 1 mL of QIAzol lysis reagent and following the instructions of its manufacturer upon tissue homogenization with tissue lyser. After RNA concentration measurement with NanoDrop, 1.5 μg of RNA was reversely transcribed with First cDNA Synthesis Kit according to manufacturer's protocol. cDNA was diluted five times before the qPCR was run with SYBR Green Master mix. The mix for the RT-qPCR contained:

2 μL of diluted cDNA
0.4 μL of each primer (forward and reverse) (10 pmol/μL)
5 μL PowerUp SYBR Green
2.2 μL UltraPure water

RT-qPCR conditions:
Step 1 95°C 10 min
Step 2 95°C 15 s
Step 3 60°C 1 min
go to step 2, 40x
Step 4 95°C 15 s
Step 5 60°C 1 min
Step 6 95°C 15 s (step 4-6 for melting curve)
The relative expression of genes using the mRNA was calculated using the comparative DDCT method normalized to the reference genes *Actb* and *Hprt* (upon the measurement of geometric mean). The sequences of primers are shown in Table 1.

Table 1. Sequences of primers used for qPCR (all for *Mus musculus* sp.)

Gene name	Forward serquence (5'-3')	Reverse sequence (3'-5')
Pnpla2	GGAACCAAAGGACCTGATGACC	ACATCAGGCAGCCACTCCAACA
Plin2	GACAGGATGGAGGAAAGACTGC	GGTAGTCGTCACCACATCCTTC
Lipe	GCTCATCTCCTATGACCTACGG	TCCGTGGATGTGAACAACCAGG

Abhd5	AGATGTGCCCTCAGGTTGGACA	ATCTGGTCGCTCAGGAAAACCC
Acc	GTTCTGTTGGACAACGCCTTCAC	GGAGTCACAGAAGCAGCCCATT
Hilpda	TGATGGAGTCCCTAGAGGGCTT	GCCAGTATGGAAGGAGGTCTTAT
G0S2	GCTAGTGAAGCTATACGTGCTGG	GGACTGCTGTTCACACGCTTCC
Seipin	GTCTGTGTTCCTCTATGGCTCC	CCAGTGAGACATTGGCAACAGG
Actn	TGCTGACAGAGGCACCACTGAA	CAGTTGTACGTCCAGAGGCATAG
Mogat2	CGGTTCTGCAGGTGTTCTTT	GGAATCCTGGGTCCGTTCA
Dgat1	GGTTCCGTGTTTGCTCTGGCAT	CCACTGACCTTCTTCCCTGTAG
Dgat2	CTGTGCTCTACTTCACCTGGCT	CTGGATGGGAAAGTAGTCTCGG
Fasn	CACAGTGCTCAAAGGACATGCC	CACCAGGTGTAGTGCCTTCCTC
Lipa	ATCCTGGTGAGGAACACTCGGT	TAGAATCTGCCAGCAAGCCGTG
Prkd2	GCTCTTCCAGAACAACACGACC	GTGACGATCTCAAAGCAGTGTGG
Mgll	GACACCATCCAGAAGGACTACC	GATTGGCAAGGACCAGAGGTGA
Hprt	CTGGTGAAAAGGACCTCTCGAAG	CCAGTTTCACTAATGACACAAACG
Plin3	GATGTGGCTGAGAAAGGCGTCA	AGGCTTTCCTGCAGTCTGTCCA

Lipid extraction and *thin layer chromatography* (TLC)

Lipids were extracted according to the method of Bligh and Dyer. In brief, about 20 mg of jejunal scratches were homogenized in a glass tube in 1 ml of chloroform: methanol (2:1) containing 0.01 % (*w*/*v*) butylated hydroxytoluene (BHT). Next, 0.5 ml of ddH_2O was added to each tube, followed by vortexing and centrifugation at 3000 rpm for 10 min at 4 ◦C. Lower phase containing lipids was collected with glass Pasteur pipette and loaded onto thin-layer chromatography (TLC) silica gel 60 plates (Merck). The TLC plates were developed in a heptane/isopropyl ether/glacial acetic acid (60/40/4, vol/vol/vol) mixture for neutral lipid separation. For the visualization of bands that corresponded to particular neutral lipid species, the plates were rinsed with 10% cupric sulfate in 8% aqueous phosphoric acid, allowed to dry for 10 min at room temperature, and then placed in a 140 ◦C oven for 20 min.

Caco-2 cell culture and freezing

Caco-2 cells were cultured in Dulbecco's modified eagle's medium (DMEM) High Glucose (4.5 g/L glucose), 10% fetal bovine serum (FBS), 1x GlutaMax, 1x non-essential amino acids (NEAA), 1 mM sodium pyruvate and 40 μg/mL gentamycin. Medium was changed every other

day and the cells were subcultured when reaching about 70% at 1:10 ratio by detaching the cells with 0.05% Trypsin for 5 min at 37°C. Cells were frozen once reached 70-80% confluency in a freezing medium composed of 50% DMEM High Glucose (4.5 g/L), 40% FBS and 10% DMSO. Cells were centrifuged, resuspended, counted (500000 cells/vial), aliquoted into cryuotubes (1 mL) and placed in a freezing chamber that was maintained in -80◦C for 24 h and afterwards the tubes were transferred to liquid nitrogen tanks.

HEK293T cell culture, transfection and generation of lentiviral particles

HEK293T cells were cultured in Dulbecco's modified eagle's medium (DMEM) High Glucose (4.5 g/L), 10% fetal bovine serum (FBS), 1x GlutaMax and 1x sodium pyruvate (Gibco) till reaching 70-80% confluence. Lentiviral vectors were transfected together with packaging vectors psPAX and pMD2.G (Addgene) with the help of transfection reagent DharmaFECT^{TM} Duo. Medium from transfected HEK293T cells was collected 48 and 72 h after transfection. Subsequently, the medium was filtered (45 µm) and mixed with polybrene (4 µg/mL, Sigma-Aldrich). The target cells (Caco-2) were spinfected (30 min, 32°C, 1800 rpm) with the medium and selected for 10 days with Puromycin (5 µg/mL, Thermo-Fisher).

Generation of stable cell lines expressing *shRNA*

Caco-2 cells at early passages (5-7) were spinfected with media containing lentiviral particles generated from HEK293T cells as described above. The cells were infected with lentiviral particles from pLKO.1 vector containing *shRNA* targeting either *Prkd2* or *Scramble* (non-targeting) and silencing efficiency was determined by immunoblotting with an antibody against PKD2.

LC/MS Lipidomic analysis

Lipid analysis was performed in collaboration with prof. Werner Schmitz from University of Wuerzburg, Germany. Briefly, to extract lipids, organelle pellets were mixed with 170 µl 10 mM HCl, 190 µl methanol, and 20 µl external standards (100 µM D7-cholesterol, 50 µM D7-7DHC, 10 µM each of D31-hexadecanoic acid, LPA-(17:0) and LPC-(17:0), Merck, Darmstadt, Germany) in chloroform/methanol (1/1, v/v). Successively, 90 and 100 µl of chloroform were added with thorough mixing in between. The resulting upper phase was re-extracted with 300 µl synthetical lower phase. The combined lower phases were evaporated under a stream of nitrogen

gas at 45°C. The dried sample extracts were redissolved in 75 µl of isopropanol and for further analysis 3 µl of samples were applicated to an Acclaim 120 C8 HPLC column (3 µm particles, 100 × 2.1 mm, Thermo Scientific). The LC separation (solvent A: MeOH/H2O/FA (5/94.9/0.1, v/v/v); solvent B: CH3CN/iPrOH/H2O/FA (45/45/9.9/0.1, v/v/v)) was performed at 45°C and a flow rate of 200 µl/min starting with 20% solvent B for 2 min followed by a linear increase to 100% solvent B within 10 min and maintaining it for 20 min, then returning to 20% solvent B within 1 min and keeping it for 5 min NH4OAc in CH3CN/H_2O (95/5, v/v) for 16 min, returning to 100% solvent B and then 20% B for 2 min. Before each injection, the column was equilibrated for 7 min in 20% solvent B. The eluent was directed to the HESI source of the Q Exactive mass spectrometer (Thermo Scientific) from 5 min to 48 min after sample injection. Usage of a high-resolution orbitrap instrument allowed analysis of ions with a sub-ppm accuracy enabling a semi-targeted, semi-quantitative method. Chromatograms were recorded in alternating negative and positive mode at 70000 resolution with a scan range of 190–1400 *m/z*. The peak areas originating from isomers differing in the position of double bonds were integrated as a whole. Peaks corresponding to the calculated monoisotopic metabolite masses (±3 mMU) were integrated using TraceFinder V5.1 software (Thermo Scientific).

LC/MS Proteomic analysis (TMT)

Sample preparation

Reduction of disulfide bonds on cysteine was performed with dithiothreitol (56°C, 30 min, 10 Mm in 50 mM HEPES, pH 8.5) followed by alkylation with 2-chloroacetamide (room temperature, in the dark, 30 min, 20 mM in 50 mM HEPES, pH 8.5). The SP3 protocol (260) was used for sample clean-up

and trypsin (sequencing grade, Promega) was added in an enzyme to protein ratio 1:50 for overnight digestion at 37°C (in 50 mM HEPES). Peptides were labelled with TMT10plex Isobaric Label Reagent (ThermoFisher) according to the manufacturer's instructions. In brief, of 0.8mg reagent dissolved in 42 ul acetonitrile (100%) 8 ul was added and incubated for 1h room temperature. The reaction was with 8 ul 5% hydroxylamine for 15 min. RT. Samples of a set were combined and desalted on a OASIS® HLB µElution Plate (Waters). Offline high pH reverse phase fractionation was carried out on an Agilent 1200 Infinity high-performance liquid chromatography system, equipped with a Gemini C18 column (3 µm, 110 Å, 100 x 1.0 mm, Phenomenex) installed with a Gemini C18, 4 x 2.0 mm SecurityGuard (Phenomenex) cartridge as a guard column. The binary solvent system consisted of 20 mM ammonium formate (pH 10.0)

(A) and 100% acetonitrile as mobile phase (B). The flow rate was set to 0.1 mL/min. Peptides were separated using a gradient of 100% A for 2 min, to 35% B in 59 min, to 85% B in another 1 min and kept at 85% B for an additional 15 min, before returning to 100% A and re-equilibration for 13 min. 48 fractions were collected which were pooled into 12 fractions. Pooled fractions were dried under vacuum centrifugation, reconstituted in 10 µL 1% formic acid, 4% acetonitrile and then stored at -80 °C until LC-MS analysis.

Mass spectrometry data acquisition

An UltiMate 3000 RSLC nano LC system (Dionex) fitted with a trapping cartridge (µ-Precolumn C18 PepMap 100, 5µm, 300 µm i.d. x 5 mm, 100 Å) and an analytical column (nanoEase™ M/Z HSS T3 column 75 µm x 250 mm C18, 1.8 µm, 100 Å, Waters) was coupled to an Orbitrap Fusion™ Lumos™ Tribrid™ Mass Spectrometer (Thermo) using the Nanospray Flex™ ion source in positive ion mode. The samples were applied onto the trapping column with a constant flow of 30 µL/min 0.05% trifluoroacetic acid in water for 6 minutes. After switching in line with the analytical column peptides were eluted at a constant flow of 0.3 µL/min. The gradient was as follows: 2% to 8% in 6 minutes (min), 8% to 25% in 99 min, 25% to 40% in min, 40-85% in 0.1 min, maintained at 85% B for 3.9 min and re-equilibrated to 2% B for 6 min. Peptides were introduced into an Orbitrap Fusion™ Lumos™ Tribrid™ mass spectrometer (Thermo Fisher Scientific) via a Pico-Tip emitter (360 µm OD × 20 µm ID; 10 µm tip, CoAnn Technologies) using an applied spray voltage of 2.4 kV. The capillary temperature was maintained at 275 °C. Full MS scans were acquired in profile mode over an m/z range of 375–1,500, with a resolution of 120,000 at m/z 200 in the Orbitrap. The maximum injection time was set to 50 ms, and the AGC target limit was set to ‘standard’. The instrument was operated in data-dependent acquisition (DDA) mode, with MS/MS scans acquired in the Orbitrap at a resolution of 30,000. The maximum injection time was set to 94 ms, with an AGC target of 200%. Fragmentation was performed using higher-energy collisional dissociation (HCD) with a normalized collision energy of 36%, and MS2 spectra were acquired in profile mode. The quadrupole isolation window was set to 0.7 m/z, and dynamic exclusion was enabled with a duration of 60 seconds. Only precursor ions with charge states 2–7 were selected for fragmentation.

MS data analysis

IsobarQuant with Mascot (v2.2.07) was used to process the
acquired data, which was searched against a mus musculus proteome database
(UP000000589, May 2016, 59550 entries) including contaminants and reversed sequences.

The following modifications were included into the search parameters: Carbamidomethyl on Cysteine and TMT10 on lysine as fixed modifications, protein N-term acetylation, oxidation on methionine and TMT10 on N-termini as variable modifications. For precursor ions a mass error tolerance of 10 ppm and for fragment ions 0.02 Da or 20 ppm was used. Trypsin was set as protease with a maximum of two missed cleavages. The minimum peptide length was set to seven amino acids. At least two unique peptides were required for a protein identification. The false discovery rate on peptide and protein level was set to 0.01.

Statistical analysis

The results are presented as mean values ± standard deviation (SD). Significances were assessed by using a Mann-Whitney non-parametric test for independent groups. P values of 0.05 or lower were considered as statistically significant (*$p<0.05$, **$p<0.01$, ***$p<0.001$, ****$p<0.0001$). Data were analysed using GraphPad Prism 9 sofware.

RESULTS

Overview of the used models

To study the impact of PKD2 deficiency on LD dynamics in murine intestine we decided to use two approaches (Fig. 8). In first experimental model, mice were gavaged with a single, intragastric bolus of olive oil at specified dose (10 µl per gram of body weight). The main advantage of that approach is a rapid and certain induction of LD formation in enterocytes. However, neither a route of lipid administration nor its dose do fully resemble the physiological conditions, required to draw conclusions in that kind of studies. Therefore, in parallel we used a model in which mice were subjected to feeding with a high-fat diet (HFD) for 4 weeks. That period is sufficient to induce chronic lipid overload of gastrointestinal tract which manifests, among others, with LD accumulation in enterocytes. Although that model does not provide a strict control over the amount of lipids consumed by the animal (mice are fed ad-libitum) and allows to conclude about long-term outcomes of PKD2 loss on LD turnover exclusively, it brings physiologically more relevant data compared to olive oil gavage procedure. To model the loss of PKD2 function, two genetic mouse lines were used, i.e. *Pkd2*$^{gut\Delta/\Delta}$ or *Pkd2*$^{ki/ki}$ mice with global point mutations in the catalytic domain (S707A/S711A). That allowed to distinguish between the consequences caused by the physical and functional absence of PKD2 specifically in the enterocyte and those resulting from whole-body (including intestine) lack of kinase activity for LD turnover, respectively.

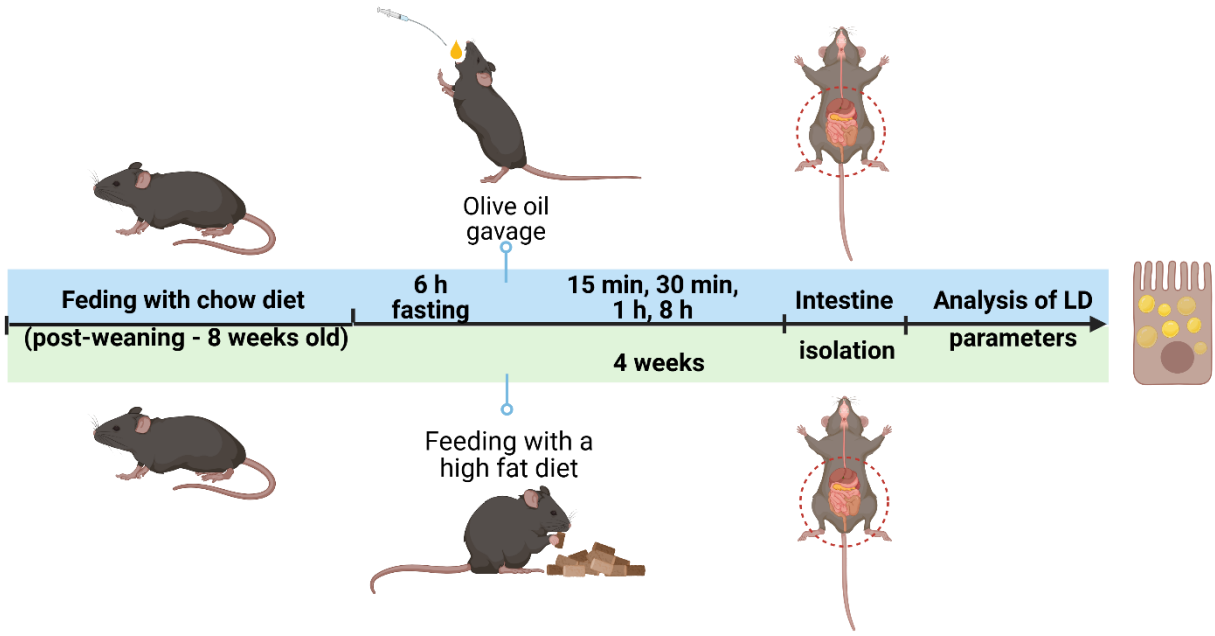

Fig. 8. Schematic presentation of two major experimental models used in the study. Upper panel (blue) presents the workflow to characterize the impact of PKD2 deficiency on LD turnover in response to acute dietary lipid challenge, lower (green) – to describe the epithelium's response to chronic exposure to feeding with HFD. For both approaches, male *Pkd2*$^{flox/flox}$ and *Pkd2*$^{gut\Delta/\Delta}$ or *Pkd2*$^{wt/wt}$ and *Pkd2*$^{ki/ki}$ mice of C57BL/6J strain background were used. Figure created with BioRender.

Although data obtained *in vivo* surpass, regarding their reliability, those obtained from simpler *in vitro* systems, the use of mouse as a model has its limitations. Many variables are uncontrollable or hidden (such as impact of hormones, microbiome or stress) resulting in difficult to extract cause-effect relationships. Mechanistic studies are therefore much cleaner and clearer using *in vitro* models. Another limitation is low scalability due to a time required for breeding, growth and completing experimental group as well due to ethical demand to limit the number of animals used in experimental procedures. To overcome these difficulties, we applied another model - crypt-derived mouse intestinal organoids, often called a bridge model since it combines the control of *in vitro* systems with a plethora of the structural and functional features of living tissue (Fig. 9). Mouse intestinal organoids are 3D mini-gut structures grown *in vitro* from intestinal stem cells (typically Lgr5^{+} cells) isolated from the intestinal crypts. When cultured in a supportive matrix (such as Matrigel) with the right growth factors, these cells self-organize into structures that mimic key features of the intestinal epithelium. They are applicable as a model to study lipid absorption in the gut as they contain fully functional enterocytes (the absorptive cells) which take up fatty acids and cholesterol, re-esterify them into TG, form LD and lipoproteins. Intestinal organoids are polarized structures, which means their cells have two distinct sites; apical membrane which *in situ* faces the gut lumen and basolateral membrane which faces the underlying tissue layers. One advantage of organoids is a controllable polarity of the cells. In standard, Matrigel-embedded organoids the basolateral membrane faces outward, to to media therefore lipids and other nutrients reach basal side first. To resemble the physiological process of lipid uptake, the polarity of organoid can be inverted by releasing from the extracellular matrix and when maintained in suspension culture organoids spontaneously open-up and expose their apical membranę to the media. Lastly, organoids can be also dissociated into singlar cells and when plated on porous membranes, they divide and form tight junctions serving thereby as simplified 2D model similar in handling to standard cell lines but derived from a healthy tissue. Figure 9 A presents schematically the workflow of 3D and 2D organoid culture, with their respective immunoflurescent images in Figure 9B and 9C..

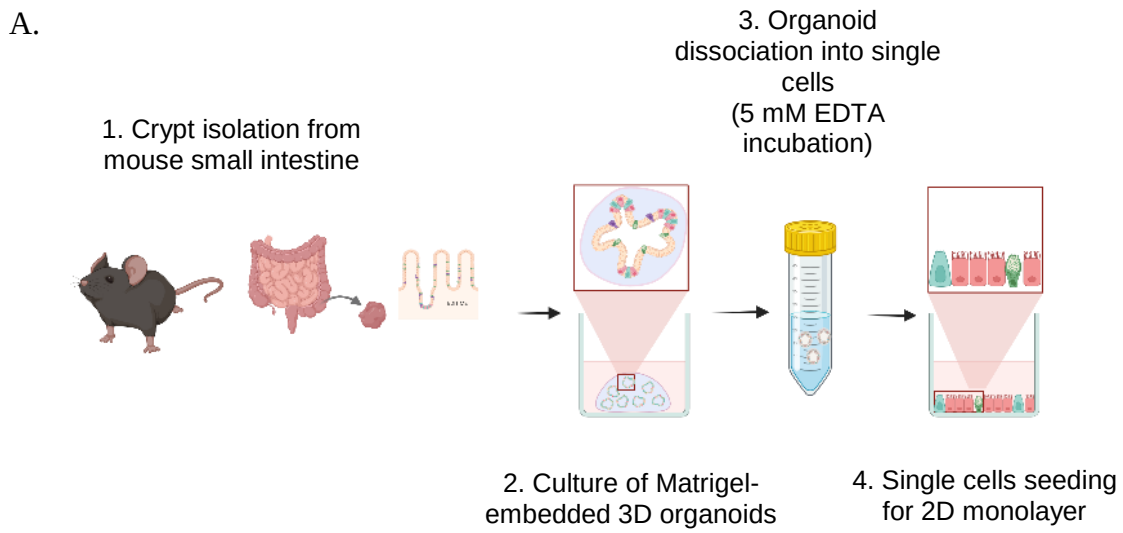

Fig. 9. Organoids as a model resembling the physiology of small intestine . A. Schematic workflow depicting the procedure of intestinal crypt isolation, organoid culture establishment and generation of 2D cell monolayers from 3D organoids. B. Confocal images showing a mature apical-out intestinal organoid and organoid-derived 2D cell monolayer below. Nuclei are in cyan (DAPI), cytoskeletal fibers are in magenta (Phalloidin 647) and in green are lipid droplets (LipidTox). Panel A of the figure was created with BioRender.

Lastly, we utilized Caco-2 cells as a well-established model of the intestinal epithelial barrier. This cell line, derived from a human colorectal adenocarcinoma, differentiates upon confluency into enterocyte-like cells that resemble those of the small intestine in terms of absorption and transport. Differentiated Caco-2 cells express a range of nutrient transporters and digestive enzymes and are capable of lipid handling, including the formation of LD and secretion of chylomicrons. Due to these properties, Caco-2 cells are widely used in pharmaceutical and

nutritional research to study the absorption of drugs and dietary compounds. However, this model represents a simplified system composed of a single cell type and lacks key features of the native intestinal epithelium, such as goblet, Paneth, and enteroendocrine cells. In addition, important components required for physiological lipid digestion and absorption - including mucus, bile acids, pancreatic enzymes, and peristalsis - are absent.

Overall, although Caco-2 cells provide a robust and reproducible platform for studying epithelial transport, caution is required when extrapolating findings to *in vivo* conditions.

Enterocytes in small intestine of *Pkd2*$^{gut\Delta/\Delta}$ mice accumulate more LD upon acute challenge with dietary fats

Whole-organism PKD2 inactivation or specific deletion in intestinal cells previously showed the importance of the kinase in the regulation of lipid absorption, specifically, via increasing the size of chylomicrons secreted postprandially to the circulation (52). To test whether other aspect of intestinal lipid metabolism, i.e. LD turnover is in parallel affected by PKD2, we subjected the *Pkd2*$^{gut\Delta/\Delta}$ mice and *Pkd2*$^{flox/flox}$ littermates as controls to 6 h of fasting followed by oral challenge with a bolus of olive oil and analyzed the LD morphology in intestinal cells using transmission electron microscopy (TEM). In enterocytes of mice of both genotypes that underwent 16 h of fasting only, we did not identify any lipid-enriched particles, i.e. neither chylomicrons nor LD (Fig. 10). High resolution of acquired images allowed to analyze the general morphology of the cells, in particular the appearance of the apical membrane with brush border and basolateral membrane with intercellular connections. As shown on the images and their zoomed regions below, none of these parameters seemed visually different between the genotypes. It suggests that, at least upon fasting and on macroscopic level, ablation of PKD2 does not impair cell integrity which would imply potential consequences for lipid absorption from the gut lumen (Fig. 10).

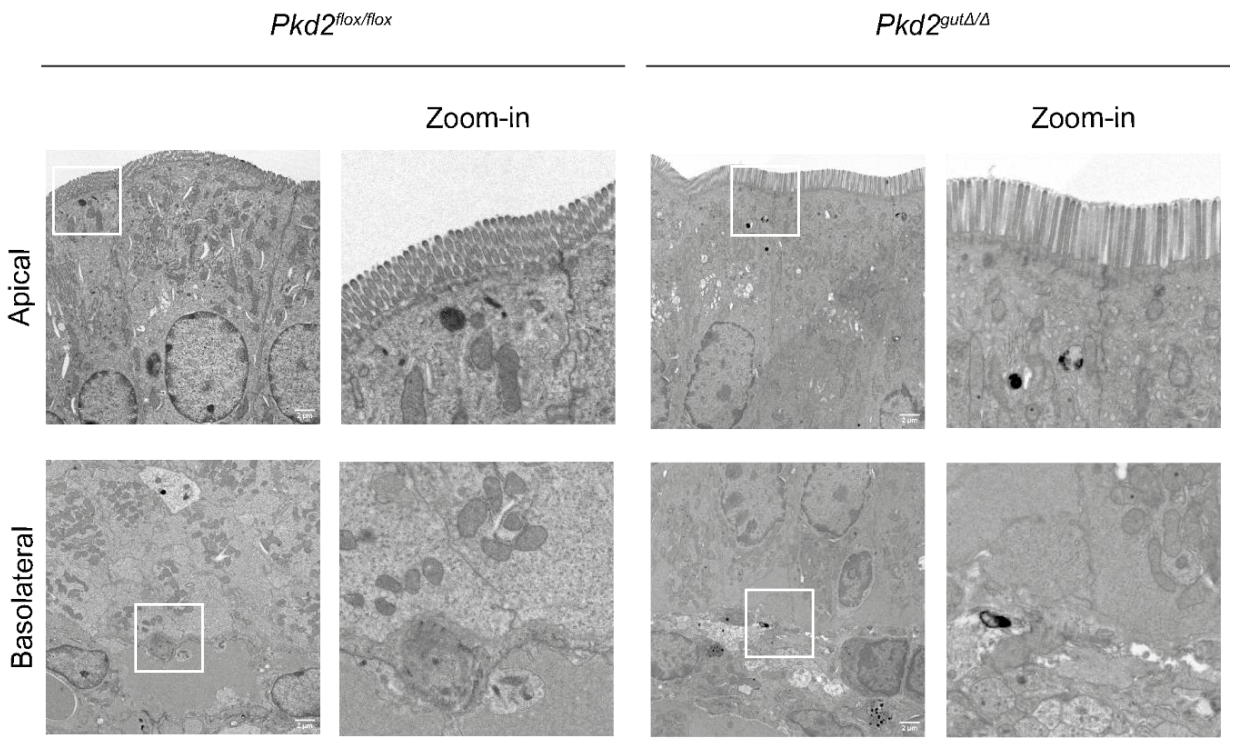

Fig. 10. General morphology of enterocyte is not changed upon ablation of intestinal PKD2. Representative TEM images of intestinal epithelia isolated from *Pkd2*$^{flox/flox}$ and *Pkd2*$^{gut\Delta/\Delta}$ mice after 16 h of fasting. For each genotype an image showing apical (with brush border) and basolateral part of the cell is shown, with respective zoom-in on the right. Scale bar on non-zoomed images is 2 µm.

In contrast, in jejunum harvested from *Pkd2*$^{gut\Delta/\Delta}$ animals at 2 h after olive oil gavage the enterocytes we found a massive accumulation of LD and quantitative analysis revealed that both the number and size of the organelles are significantly increased compared to *Pkd2*$^{flox/flox}$ (Fig. 11 B, C, D, E).

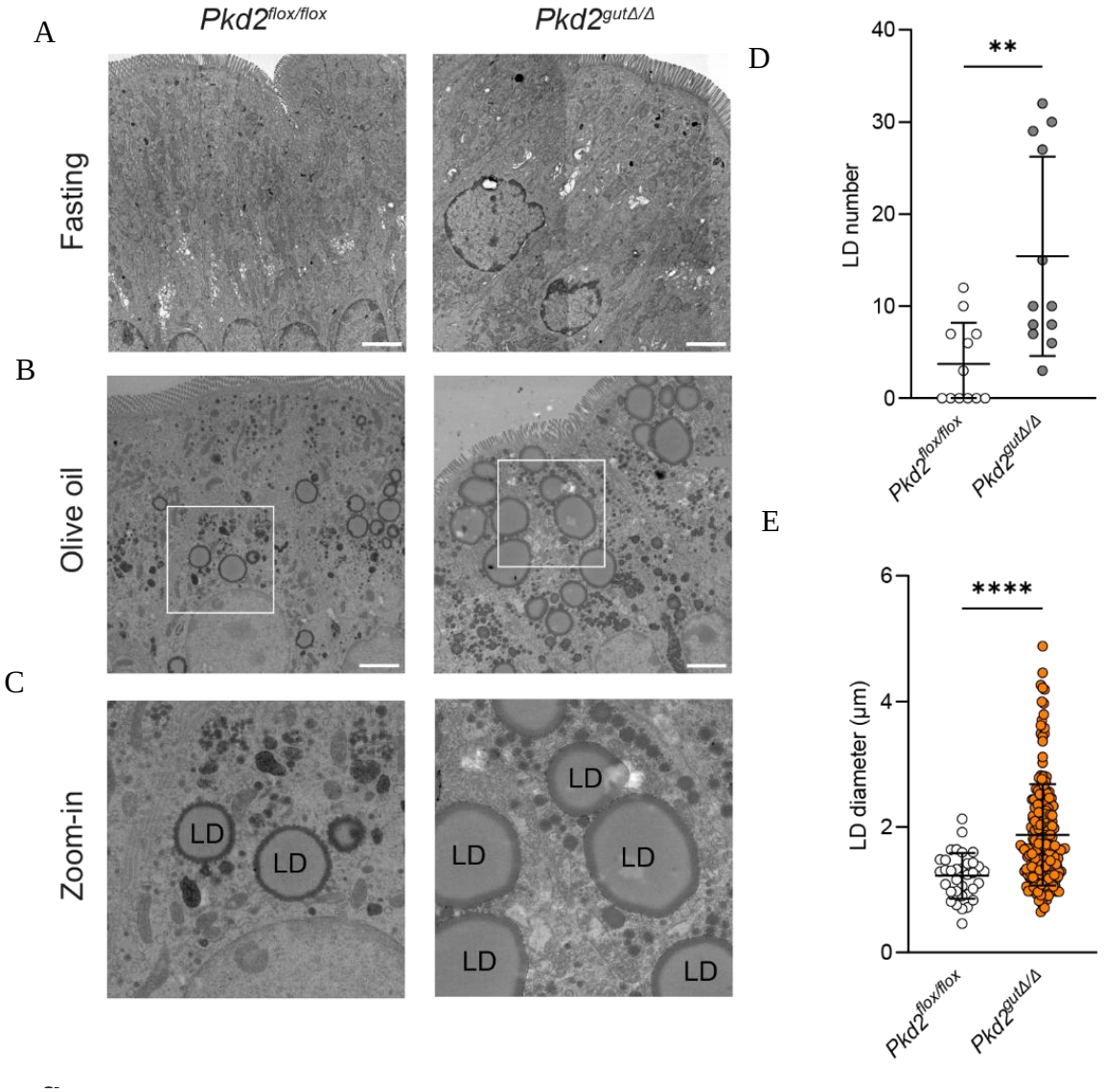

Fig. 11. LD are enlarged in enterocytes of *Pkd2*$^{gut\Delta/\Delta}$ after single gavage with olive oil. A. Representative TEM images of mouse jejunum after 16 hours of fasting or **B.** 2 hours after oral olive oil gavage (10 µl/g b.w.) isolated from *Pkd2*$^{flox/flox}$ and *Pkd2*$^{gut\Delta/\Delta}$ mice. **C.** Enlarged images depicting LDs from (B). **D.** Quantification of LD number from (B**)**. E. Quantification of LD size (diameter) from (B) (*n* = 4 male mice/genotype, 5 cells/mouse). Scale bar=2 µm, data represent mean ± SD. ***p<0.01, ****p<0.0001 by Mann-Whitney test*

The process of lipid absorption via intestine is highly dynamic with TG peak in plasma occurring about 2 h after lipid-enriched meal ingestion while within 4 h after lipid challenge serum TG reach again the pre-ingestion concentration (52). Therefore, one explanation for observed phenomena could be a delay in tissue clearance from dietary lipids. However, analogical TEM analyses of intestinal epithelia isolated at either 4 h and 8 h after oil gavage revealed a consistent phenotype and accumulation of LD in *Pkd2*$^{gut\Delta/\Delta}$ animals suggesting an impairment rather than a delay in postprandial lipid clearance (Fig. 12).

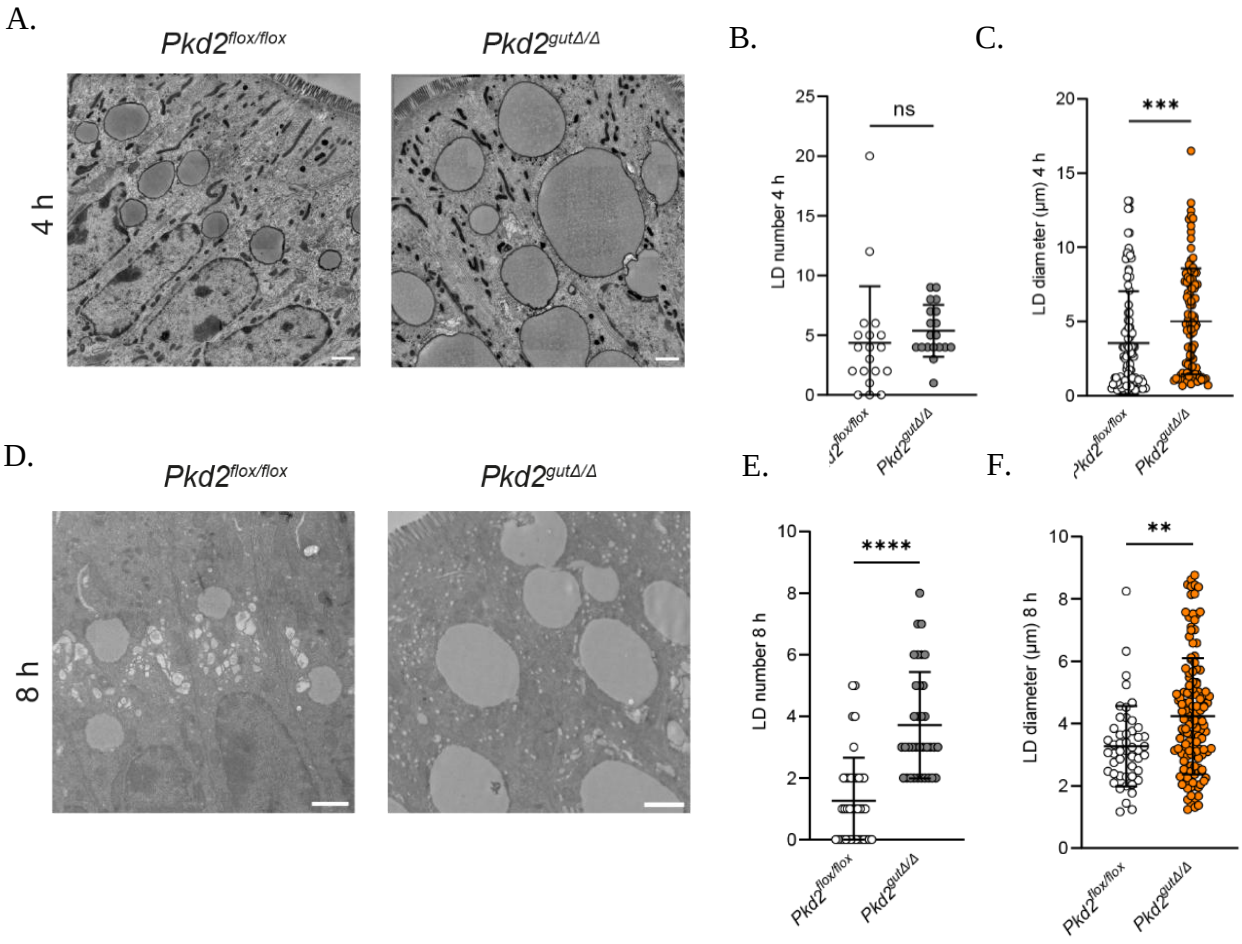

Fig. 12. LD remain enlarged in enterocytes of *Pkd2*$^{gut\Delta/\Delta}$ in extended time course after olive oil gavage. Representative TEM images of *Pkd2*$^{flox/flox}$ (left) and *Pkd2*$^{gut\Delta/\Delta}$ (right) intestinal epithelia isolated 4 h (**A**) and 8 h (**D**) after oral olive oil gavage (10 µl/g b.w.) depicting enlarged LD. **B.** Quantification of LD number from (**A**). **C.** Quantification of LD size (diameter) from (**A**). **E.** Quantification of LD number from (**D**).

F. Quantification of LD size (diameter) from (**E**). For both analyses *n*=5 male mice/genotype, 10 cells/mouse) Scale bar = 2 µm, data represent mean ± SD. Ns; non significant, ***p<0.01, ***p<0.001,****p<0.0001 by Mann-Whitney test*

Similarly to observed LD increase in *Pkd2*$^{gut\Delta/\Delta}$ mice throughout the time course after olive oil gavage, we found a consistent build-up of chylomicrons, mostly fulfilling the intercellular spaces in the epithelium of those mice. (Fig. 13). Stacking of chylomicrons in such localization indicates that PKD2 may not affect chylomicron production in the cell but rather their post-secretion traversing through lamina propria or extracellular matrix (ECM). Notably, that phase of fat absorption in the intestine is poorly described regarding its mechanistic regulation. Previously, it was shown that PKD2 regulates the secretion of matrix metalloproteases (MMPs), a class of enzymes responsible for cleaving the components of the extracellular matrix (collagens, laminins) and thus increasing its fluidity (159). It is also known that in postprandial phase the ECM in the small intestine increases its pores which facilitates the transport of chylomicrons. Therefore, one of the possible explanations for observed phenomenon might be a reduced release of MMPs resulting in increased stiffness of ECM. Testing of that hypothesis, however, is not a matter of current study which focuses on relation between PKD2 and LD dynamics exclusively.

A.

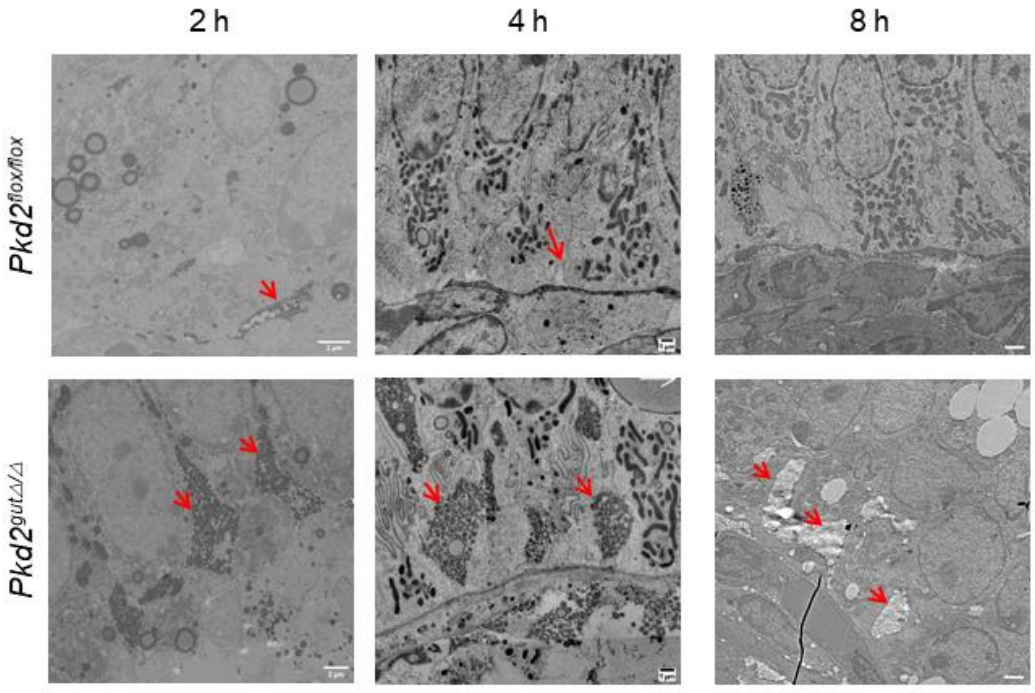

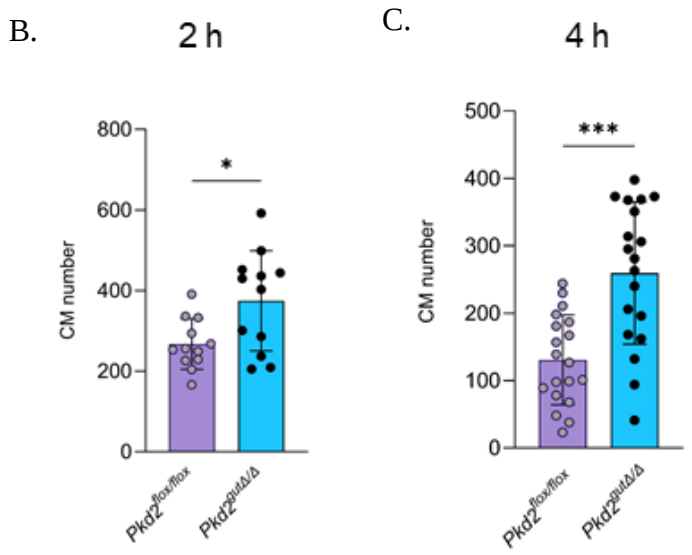

Fig. 13. Chylomicrons accumulate in the intercellular spaces of *Pkd2*$^{gut\Delta/\Delta}$ intestinal epithelia. A. Representative TEM images of basolateral part of intestinal epithelia isolated from *Pkd2*$^{flox/flox}$ and *Pkd2*$^{gu\Delta t/\Delta}$ mice at indicated time points after olive oil gavage, showing accumulation of chylomicrons in the intercellular spaces in PKD2-depleted animals (red arrows). **B**. Quantification of chylomicrons from 2 h and **C**. 4 h time points after olive oil gavage. N = 4-5 animals per genotype, chylomicrons were quantified from 5 adjacent cells per mouse. Data represent mean ± SD, **p<0.05, ***p<0.001, ***p<0.001 by Mann-Whitney test*

Apart from a visual proof, we confirmed an enhanced accumulation of neutral lipids in PKD2-depleted enterocytes with a few other approaches. We isolated the intestinal scratches from *Pkd2*$^{flox/flox}$ and *Pkd2*$^{gut\Delta/\Delta}$ after oral olive oil gavage (2 h), extracted lipids and subjected them to a thin-layer chromatography (TLC)-based separation to analyze the abundancy of cholesteryl esters (CE), TG, FFA, DAG (diacylglycerol) and PL (phospholipids). The results revealed that TG appeared to be enriched in intestinal epithelia of *Pkd2*$^{gut\Delta/\Delta}$ mice compared to control animals, whereas other classes of lipids did not show any differences between the genotypes.

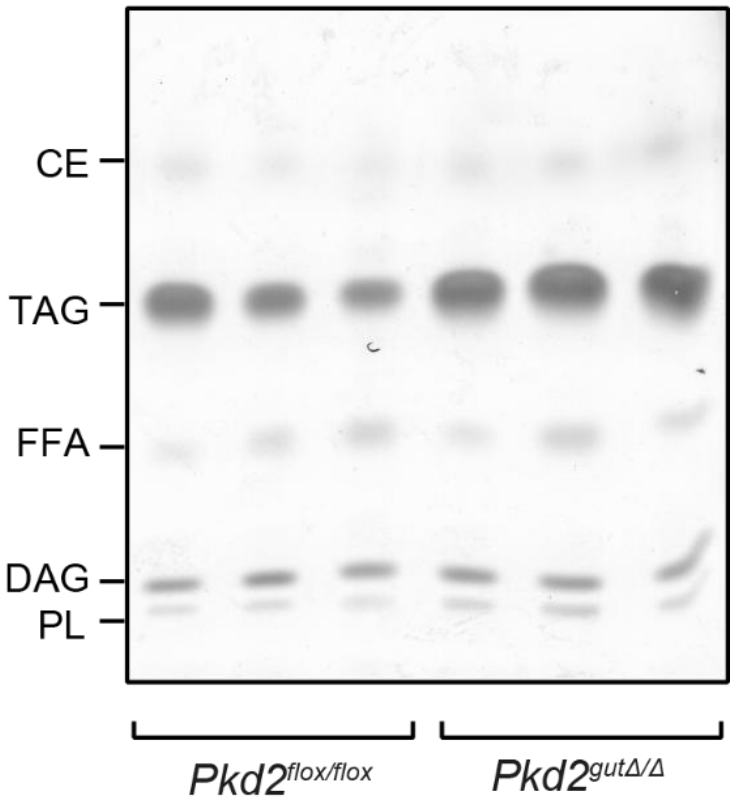

Fig. 14. TG accumulatation in intestines of PKD2-depleted mice is evidenced with thin-layer chromatography (TLC). TLC resolving CE, TG, FFA, DAG in jejunal scrapings from *Pkd2*$^{flox/flox}$ and *Pkd2*$^{gut\Delta/\Delta}$ isolated 2 h after olive oil gavage.

The next approach which we used to specify the lipid profile upon intestinal PKD2-deletion was via liquid chromatography-mass spectrometry lipidomic analysis. We isolated LD, endoplasmic reticulum, Golgi apparatus, Golgi-derived vesicles from mouse intestinal epithelial scratches and analyzed different classes of lipids in the organelles. (Fig. 15 A, B, C).

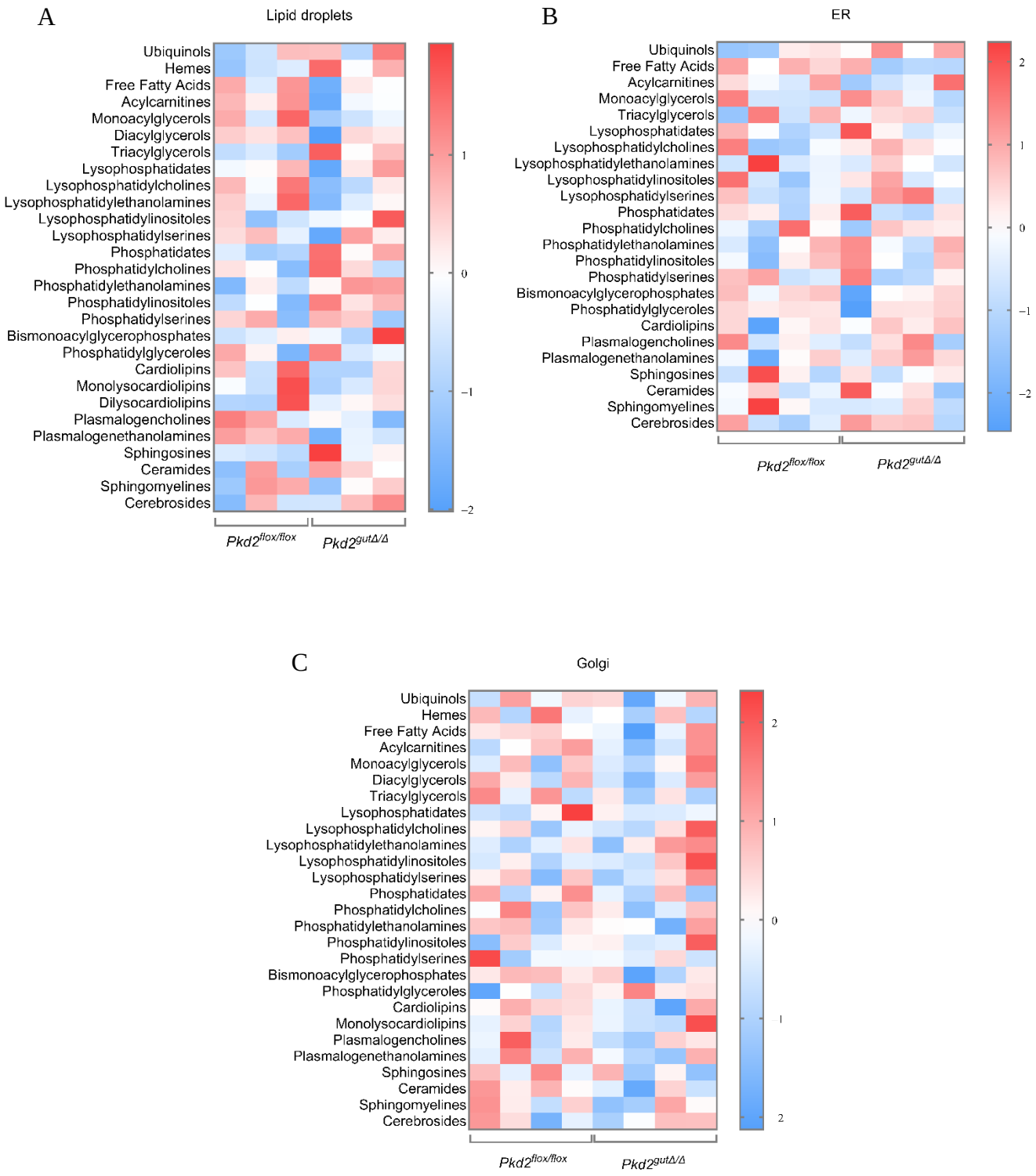

Fig. 15. Lipidomic analysis of different organelles of enterocytes revals organelle-specific differences in lipid composition between *Pkd2*$^{flox/flox}$ and *Pkd2*$^{gut\Delta/\Delta}$. A. Heatmap showing the clustering of identified lipid classes by untargeted lipidomic analysis in LD (A), endoplasmic reticulum (ER) (B), Golgi apparatus (C) from jejunal scrapings isolated from *Pkd2*$^{flox/flox}$ and *Pkd2*$^{gut\Delta/\Delta}$ 2 h after oral oil gavage (n = 3 for LD and n = *4* male mice/genotype for other

organelles). The intensity of the blue color indicates a lower presence of lipids in analyzed organelle, while the intensity of the red color indicates a higher presence, in reference to white color (=0) calculated as an arithmetic mean of m/s peaks from all tested animals combined together.

Unlike other cell compartments, we found a significant increase in abundancy of all identified (seventeen) TG species in LD derived from *Pkd2*$^{gut\Delta/\Delta}$ animals and that were consistent among all compared animals (Fig. 17A). Among other lipid classes within LD fraction that showed a differences between genotypes, although not statistically significant, were acylcarnitines, phosphatidates, phosphatidylinositoles and plasmalogenethanolamines and hemes (Heme B) (Fig. 15A). Acylcarnitines are fatty acid metabolites derived from l-carnitine and play an essential role in β-oxidation of fatty acids. They are built in the inner membrane of mitochondria and aid the transport of long-chain fatty acids from the inter-membrane mitochondrial space to the matrix (160). Mitochondria are frequently found in close proximity with LD, especially in organs extensively relying on oxidative respiration (161,162) and it is commonly recognized that maintenance of LD-mitochondria contacts facilitate the flux of LD-derived fatty acids to mitochondria for β-oxidation (161,162). Of note, recently the importance of mitochondria in enterocytes was shown in the context of intestinal fat absorption while abrogation of mitochondrial function results in reduced chylomicron secretion, lowered circulating TG and intestinal LD accumulation (163). As uniquely present in mitochondria, the reduced abundance of acylcarnitines within LD fraction in *Pkd2*$^{gut\Delta/\Delta}$ enterocytes, may, hypothetically indicate at either reduced number of LD-mitochondria contact sites or overall reduced mitochondria number or size in the cell. That finding from lipidomics analysis prompted us to determine mitochondrial parameters in enterocytes using TEM images used previously for LD and chylomicron quantification in a time course experiment with olive oil. Macroscopically, the mitochondria in *Pkd2*$^{gut\Delta/\Delta}$ enterocytes did not show any aberrations in morphology regarding, for instance, inner and outer membrane continuity, cristae structure, presence of mitophagic figures (Fig. 16A). Quantification of mitochondria area revealed, however, an upregulation in *Pkd2*$^{gut\Delta/\Delta}$ at fasting and at 4 h after oil gavage due to increased organelle length. Width of mitochondria was also increased at 4 h time point. Mitochondria elongation is observed, among others, during metabolic stress or as a starvation response (164,165) which could be an interesting point for further study in the context of retention of enlarged LD in PKD2-deficient cells. Lack of consistency in obtained results between

relatively short time points allows, however, to draw only a conclusion that we do not observe any major morphological differences in mitochondria affected by PKD2 deficiency.

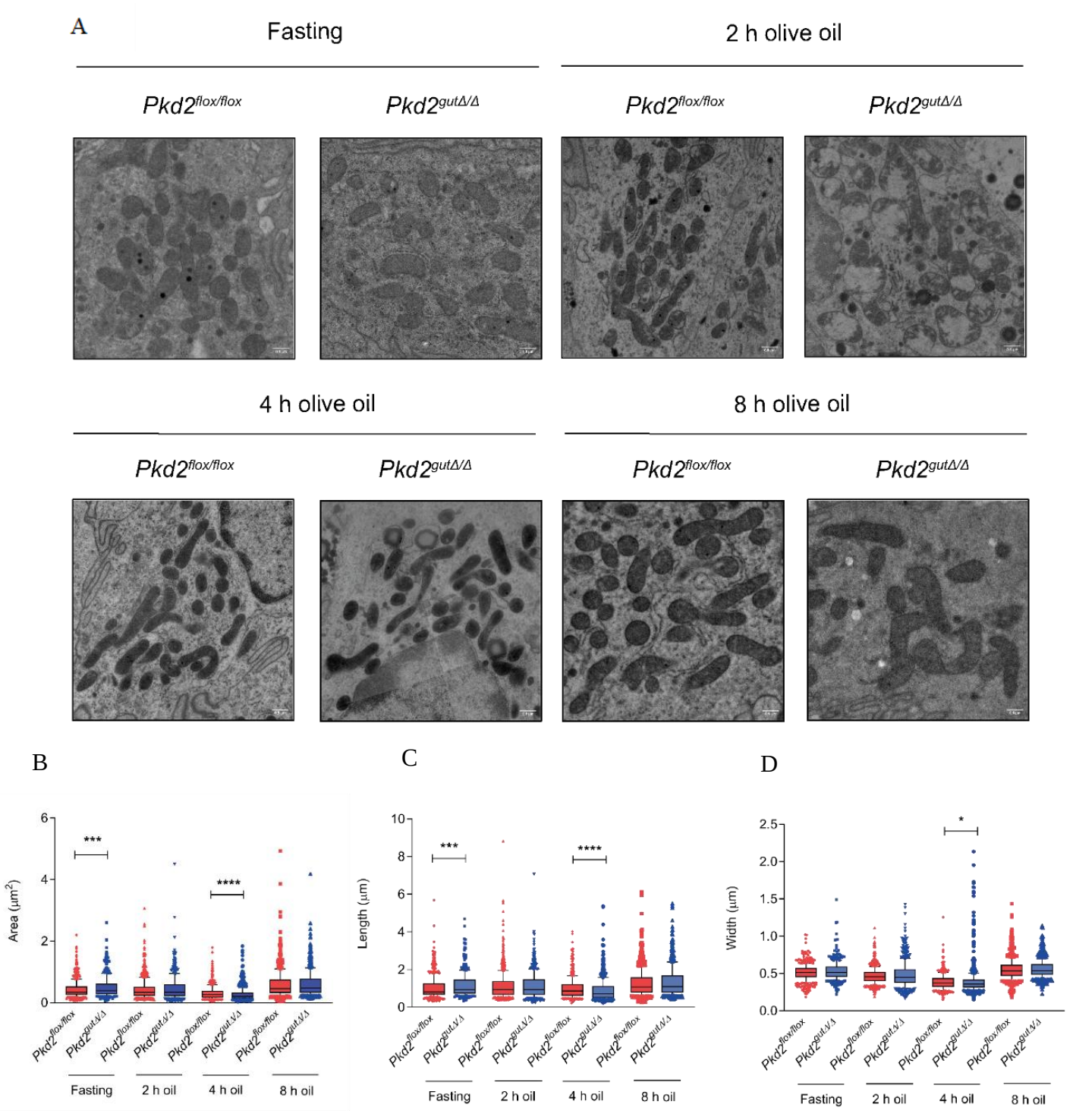

Fig. 16. Analysis of mitochondria morphological parameters in enterocytes of *Pkd2$^{flox/flox}$* and *Pkd2$^{gutΔ/Δ}$* mice. A. TEM images showing the mitochondria in enterocytes of *Pkd2$^{flox/flox}$* and *Pkd2$^{gutΔ/Δ}$* at different time points after olive oil gavage used for quantification of indicated organelle parameters area (B), length (C) and width (D). *n* = 4 or 5 mice per genotype, each

dot represents an individual mitochondrion and mitochondria were quantified from 5 cells per animal. Data represent mean ± SD. *ns* - non significant, ***p<0.01, ***p<0.001, ****p<0.0001 by Mann-Whitney test.*

Phosphatidates and phosphatidylinositoles are one of the components of each eukaryotic cellular and organelle membrane, including phospholipid monoloayer surrounding the LD core (68). The increased content of these lipids within LD from PKD2-depleted mice could be a result of collectively increased LD-coating phospholipid monolayer abundancy, in line with general increase of LD content. It has to be noted, however, that we observed specifically accumulation of large LD in which the ratio of phospholipid surface to volume is reduced compared to small LD of the same collective volume. Therefore, verification of proposed hypothesis would require a different approach, e.g. fractionation of phospholipids and neutral LD core from intact LD, followed by adjusted quantitative analysis. All described above differences were not found in any other tested organelles except for LD, thereby underscoring the specificity of PKD2 function in organelle lipid homeostasis.

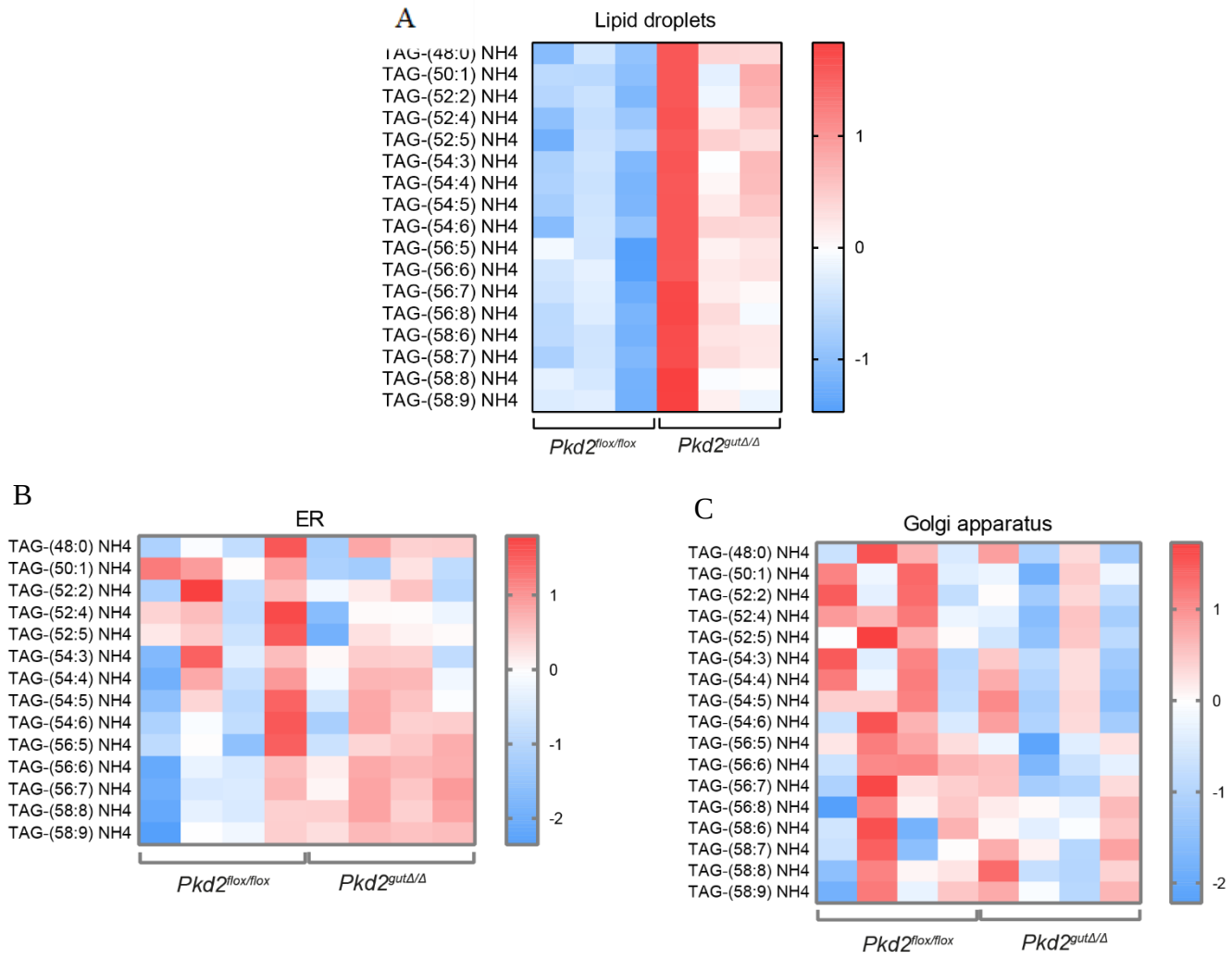

Fig. 17. **Lipidomic analysis reveals that TG accumulate specifically in LD but not other organelles in enterocytes of *Pkd2*$^{gut\Delta/\Delta}$ mice.** A. Heatmap showing the clustering of TG by untargeted lipidomic analysis in LD (A), endoplasmic reticulum (ER) (B), Golgi apparatus (C) from jejunal scrapings isolated from *Pkd2*$^{flox/flox}$ and *Pkd2*$^{gut\Delta/\Delta}$ 2 h after oral oil gavage (*n*=3 for LD and *n=4* male mice/genotype for other organelles). The intensity of the blue color indicates a lower presence of lipids in analyzed organelle, while the intensity of the red color indicates a higher presence, in reference to white color (=0) calculated as an arithmetic mean of m/s peaks from all tested animals combined together.

As described previously in the 'Introduction', LD-resident proteins can be classified in the context of the pathway mediating their delivery to LD, therefore CYTOLD- or ERTOLD-dependent proteins can be distinguished. Perilipins (PLINs) which represent CYTOLD pathway are one of the constitutive LD-resident proteins, involved in the regulation of their metabolism and therefore – LD size. Among five members of the protein family (PLIN1-5), PLIN2 and PLIN3 were described to associate with enterocyte LD and marking different LD populations; while PLIN3 is known to target LD forming in response to acute dietary lipid challenge, PLIN2 decorates LD found upon chronic feeding with a high-fat diet. We therefore performed immunofluorescent staining of intestinal sections obtained from *Pkd2*$^{flox/flox}$ and *Pkd2*$^{gut\Delta/\Delta}$ 8 h after oral olive oil gavage with anti-PLIN2 and anti-PLIN3 antibodies to determine whether PKD2 affects a certain population of LD. The results indicate that both, the size and number of either PLIN2 or PLIN3-positive LDs are uniformly increased in *Pkd2*$^{gut\Delta/\Delta}$ enterocytes (Fig.18 A-F). Similarly to our findings from intestine-specific PKD2 deletion, I found a vast accumulation of LD in mice carrying a whole-body inactivation of the kinase (*Pkd*$^{ki/ki}$) compared to control group (*Pkd2*$^{wt/wt}$) in tissue sections stained against both Perilipins and isolated 1 h after olive oil gavage (Fig. 19).

\

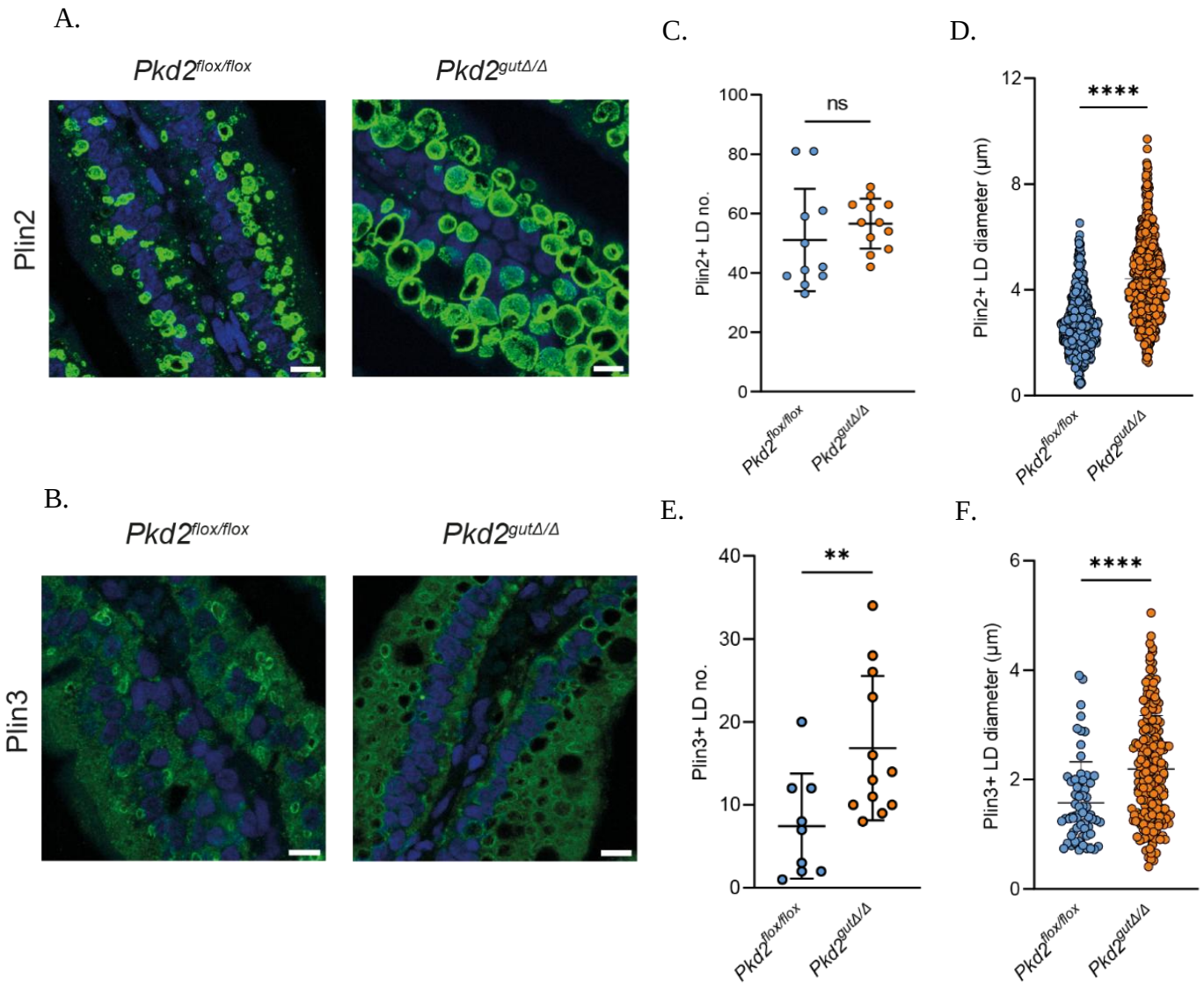

Fig. 18. LD morphology *Pkd2*$^{flox/flox}$ and *Pkd2*$^{gut\Delta/\Delta}$ revealed by immunofluorescent staining against PLIN2 and PLIN3 proteins. **A, B.** Representative immunofluorescent images of jejunal sections from *Pkd2*$^{flox/flox}$ and *Pkd2*$^{gut\Delta/\Delta}$ mice isolated 8 hours after olive oil gavage and stained against PLIN2 and PLIN3. C. Quantification of PLIN2 – coated LDs' number from (A). D. Quantification of PLIN2– coated LDs' size from (A). E. Quantification of PLIN3 – coated LDs' number from. (B). Quantification of PLIN3 – coated LDs' size from (B). *n* = 4 per genotype and 4-5 villous areas 40 x 40 µm per mouse were quantified, scale bar is 10 µm. Data represent mean ± SD. *ns* - non significant, ***p<0.01, ***p<0.001, ****p<0.0001 by Mann-Whitney test.*

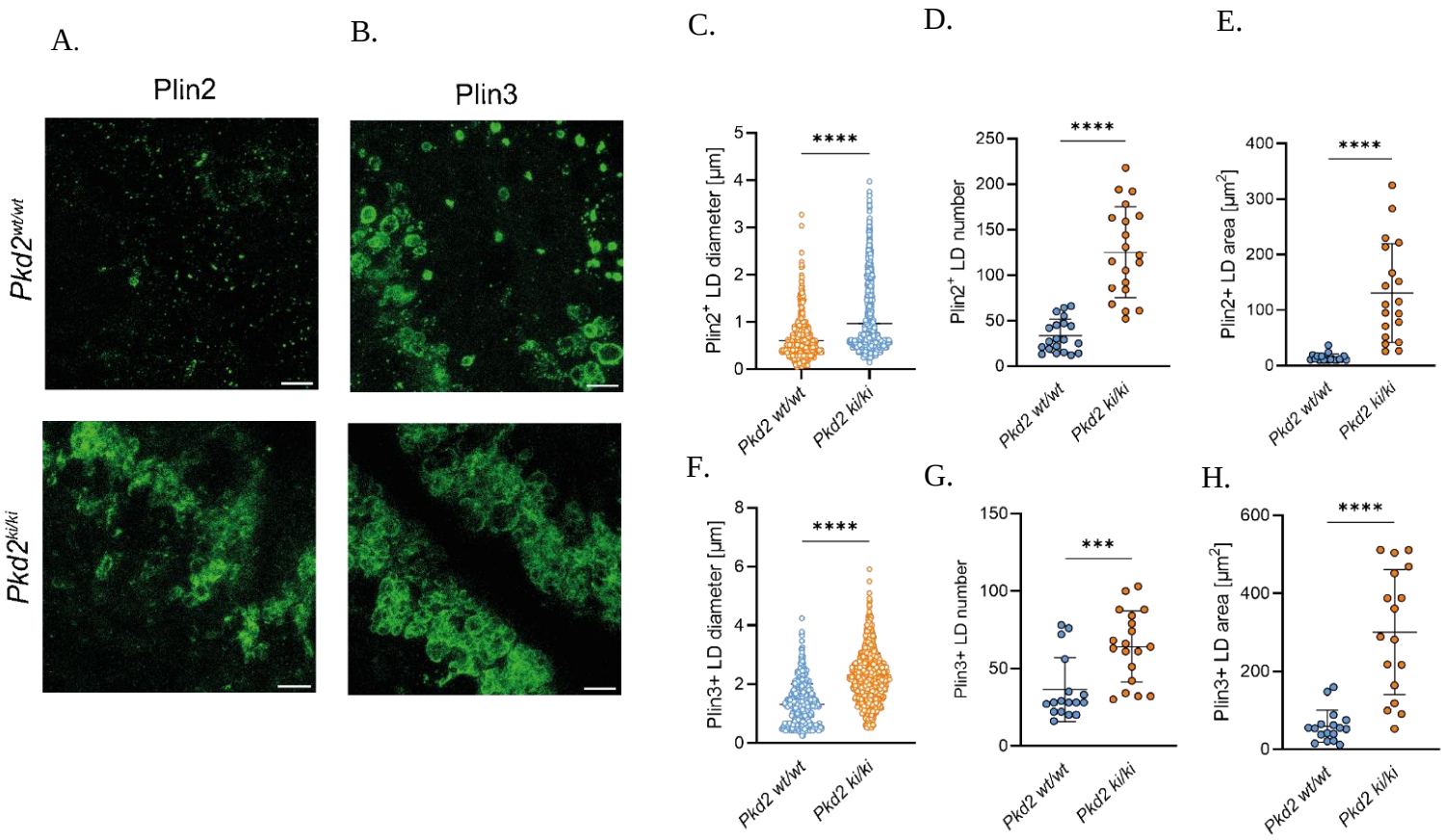

Fig. 19. PLIN2- and PLIN3-coated LD are enlarged in intestine of *Pkd2$^{ki/ki}$* compared to *Pkd2$^{wt/wt}$* mice. A. Representative immunofluorescent z-stacked images of intestinal sections from PKD2-inactive (*Pkd2$^{ki/ki}$*) and control male mice (*Pkd2$^{wt/wt}$*) stained against Plin2 (A) and Plin3 (B) (1h after oil challenge). Quantification of LD diameter (C, F), number (D, G) total LD area (E, H). *n* = 4 and 4-5 areas 40 x 40 µm per mouse were taken for quantification, scale bar is 5 µm. Data represent mean ± SD. ****p<0.001, *****p<0.0001 by Mann-Whitney test.*

Enlarged LD may result from either intensified LD synthesis, reduced catabolism or both processess. We therefore tested first if on a transcriptional level any of the genes encoding the proteins involved in LD biogenesis or degradation are affected by the lack of PKD2 (Fig. 20). The majority of genes which expression was measured with qPCR was not not changed between the genotypes under conditions of acute lipid load (2 h after gavage), except for *Seipin*, encoding an ER -integral membrane protein that is involved in LD biogenesis and expansion which was significantly upregulated in PKD2-deficient mice, in line with the general appearance of LDs..

Another target which expression was statistically significantly elevated in PKD2-deficient animals was *Pnpla2* encoding ATGL protein, the main LD-degrading enzyme.

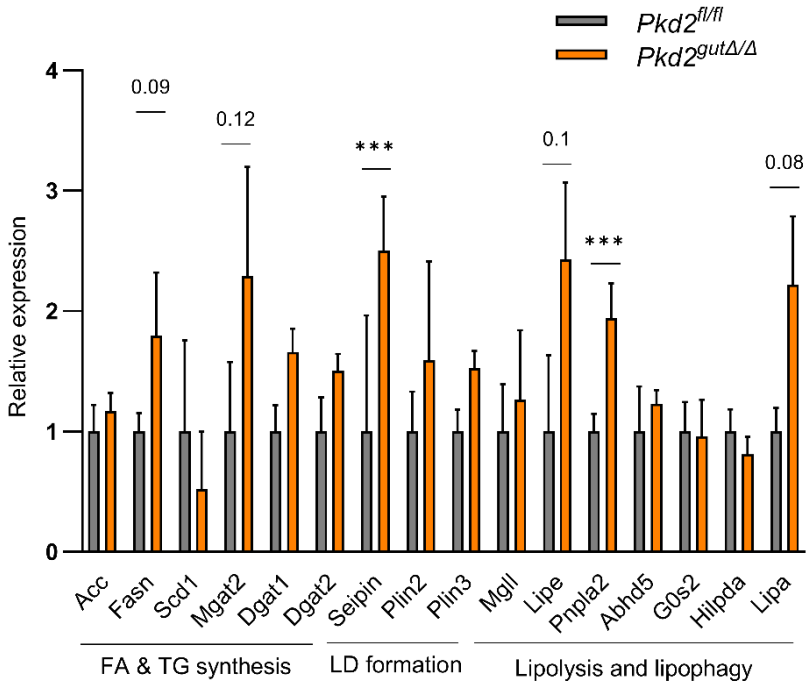

Fig. 20. **Relative expression of key genes encoding proteins regulating LD biogenesis and metabolism in intestinal scratches collected from *Pkd2*$^{flox/flox}$ and *Pkd2*$^{gut\Delta/\Delta}$ male mice 2 h after olive oil challenge.** N = 8 per genotype, data represent mean ± SD. ****p<0.001*.

Therefore, we next checked the expression of a set of proteins regulating LD metabolism in the intestinal lysates, hypothesizing a post-translational impact of PKD2 on LD-associated proteins stability, at the same conditions of 2 h after oral challenge with olive oil as previously for gene expression analysis. Due to a low efficiency of tested antibodies in lipid-loaded tissue homogenates, we were able to determine the abundancy of merely few LD-related proteins, including key lipases – ATGL and HSL and PLINs 2 and 3. Western blot analysis of indicated proteins did not reveal significant differences in protein levels, except for ATGL which expression was slightly higher in PKD2-depleted animals and as evidenced with quantification (Fig. 21 A, B)

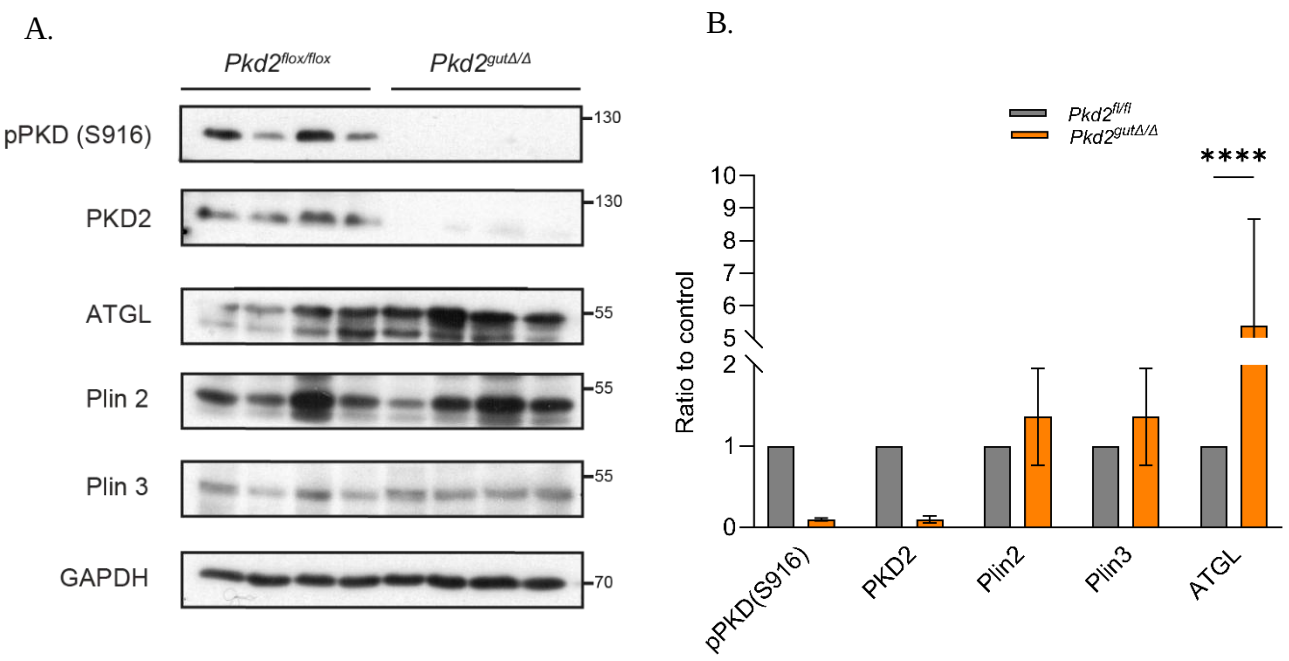

Fig. 21. .PKD2-deficiency in mouse intestine is associated with elevated ATGL protein level. A.Western blot analysis and B. quantification of phosphorylated PKD2 (PKD2 S916), total PKD2, ATGL, Plin 2, Plin 3 and GAPDH as internal control in intestinal homogenates from *Pkd2*$^{flox/flox}$ and *Pkd2*$^{gut\Delta/\Delta}$ male mice 2 h after olive oil challenge. n = 4 per genotype, data represent mean ± SD. ***$p<0.001$.

A major lipase of LD - ATGL is physiologically degraded during fat absorption but not in the absence of PKD2.

It is well described in the literature as well as proved with our TEM data from olive oil treatment time-course experiments that LD formation is a highly dynamic and efficient process (128,131). Since 2 h post ingestion is sufficient timing to observe a tremendous difference in LD morphology between *Pkd2*$^{flox/flox}$ and *Pkd2*$^{gut\Delta/\Delta}$ mice which correlated with altered ATGL protein expression, we sought to investigate if there exists any functional link between these two PKD2-dependent events. First, we determined whether observed difference in ATGL expression has a time-dependent character. We checked lipases abundance at earlier phase, 30 minutes after olive oil ingestion and compared them with fasting conditions (Fig. 22 A). While in mice that did not receive a bolus of olive oil we did not observe a varied lipases' expression

between the genotypes, in intestines collected 30 min after oil gavage we found a profound decrease in ATGL and HSL levels in *Pkd2*$^{flox/flox}$ but stable, comparable to fasting conditions, expression of these proteins in *Pkd2*$^{gut\Delta/\Delta}$ mice. That finding prompted us to study the physiological dynamics of LD-associated proteins turnover in response to olive oil ingestion in a time-course experiment, thus wild-type C57/BL6 mice were used for that purpose and each mouse sacrificed at indicated time point after oil gavage was paired with an animal given an isovolumetric bolus of drinking water. (Fig. 10). Due to a rate-limiting role of ATGL in lipolysis regulation we focused our attention primarily on ATGL lipase.

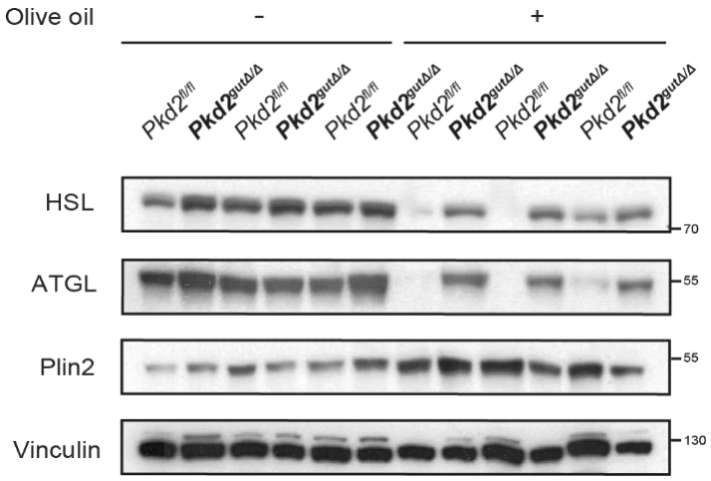

Fig. 22. **ATGL protein is subjected to degradation in intestine of *Pkd2*$^{flox/flox}$ but not *Pkd2*$^{gut\Delta/\Delta}$ mice upon olive oil gavage.** Western blot analysis of ATGL, HSL, Plin 2 and Vinculin as internal control in intestinal homogenates from *Pkd2*$^{flox/flox}$ and *Pkd2*$^{gut\Delta/\Delta}$ male mice upon fasting (left part; '-') or 30 min (right; '+') after olive oil challenge.

A. B

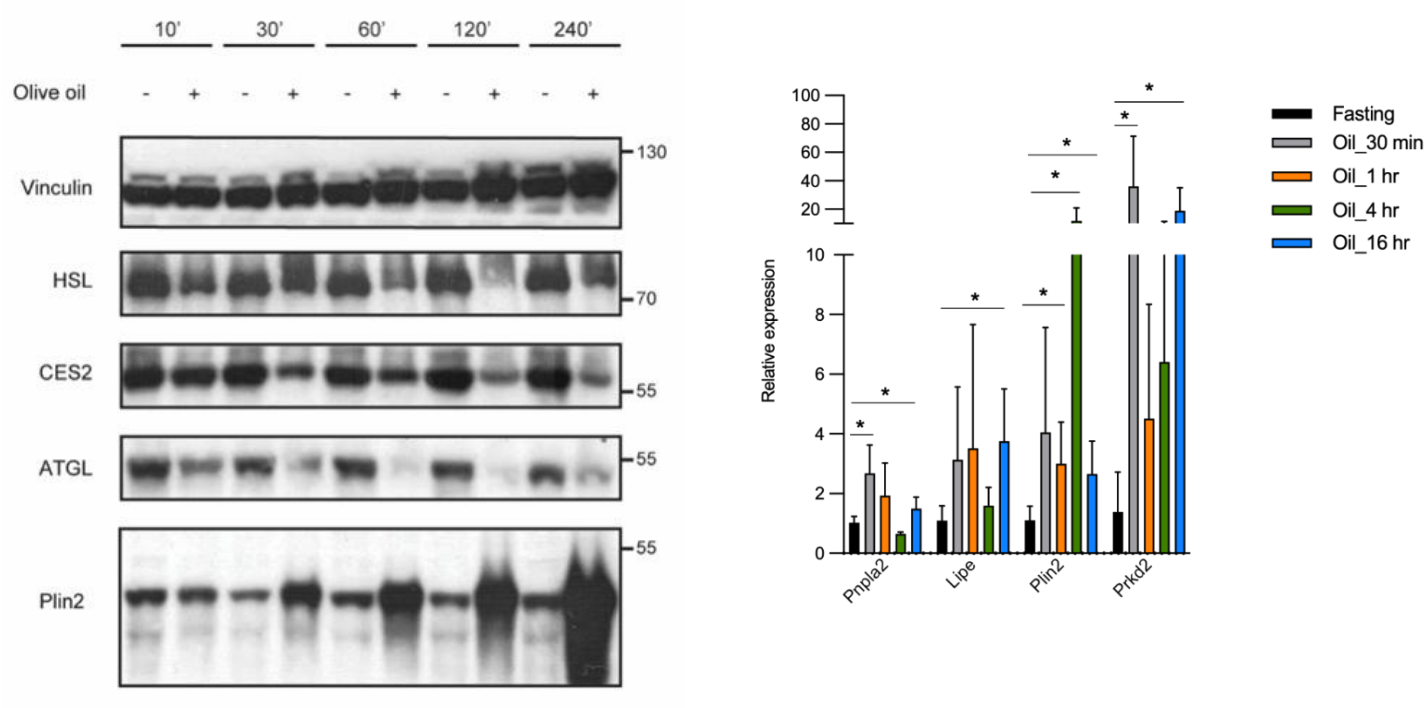

Fig. 23. Abundance of LD-associated proteins in C57/BL6 mouse intestine is affected by olive oil gavage and changes over time after the gavage. A. Western blot analysis of ATGL, Plin 2, CES2 protein expression levels and Vinculin as internal control in intestinal homogenates from C57/BL6 male mice that underwent 6 h fasting followed by intragastric gavage with a bolus of drinking water ('-') or olive oil ('+') and sacrificed at indicated time points after oil gavage. B. qPCR gene expression analysis of Pnpla2 (encoding ATGL), Lipe (encoding HSL) and Prkd2 (encoding PKD2) in C57/BL6 subjected to 6 h of food withdrawal followed by gavage with olive oil and sacrificed at indicated time points after fat ingestion. *n*= 4, data represent mean ± SD. *p<0.005 by Mann-Whitney test.

Strikingly, as soon as 10 minutes after olive oil gavage was sufficient timing to observe a reduced level of ATGL in jejunal homogenates compared to water-treated mouse and that effect progressess in time, with the lowest protein expression at 60 minutes after oil intake, while ATGL recovers at 4 h after lipid ingestion (Fig. 23A). Similarly, the expression of two other proteins involved in TG breakdown, i.e. HSL and CES2 dropped in response to olive oil intake. Our experiments with olive oil gavage coloured with Evans blue revealed that within 10

minutes, liquid content travels till the end of ileum, indicating that observed alteration of protein expression may be mediated directly by lipids being absorbed rather than a neuronal or endocrinological signal from the upper part of gastrointestinal tract (e.g., stomach or duodenum) sent to the jejunum (data not shown). In contrast, PLIN2 revealed an inverted pattern of expression, with abundancy increasing in time and reaching its peak at latest time point, 4 h after oil challenge (Fig. 23A). The analysis of protein levels was complemented with qPCR gene expression assesment and showed a coherent increase in *Plin2* copies, linear in time after gavage, but also *Pnpla2* and *Lipe,* while encoded proteins (ATGL and HSL respectivly) dropped rapidly (Fig. 23B). This result suggest that removal of ATGL and HSL after oil ingestion may be regulated via post-translational mechanisms. Worth noting is also an increase in *Prkd2* (encoding for PKD2), although we did not find this to correspond with total protein abundance (data not shown), it is in line line with previously shown activation of PKD2 after oil gavage and underscores a positive correlation between lipid ingestion and PKD2 (52)
In summary, these data indicate that a subset of enzymes directly involved in the liberation of triglycerides (TGs) from lipid droplets (LDs) in enterocytes is degraded in response to lipid ingestion into the intestinal lumen. At the same time, the transcription of these enzymes is upregulated to replenish their levels. To gain more insight into some key physiological determinants of ATGL degradation in small intestine we carried out a set of experiments with C57BL/6J mice.

Uncovering the mechanisms mediating ATGL degradation in response to lipid ingestion

First, we asked whether observed event is specific to a type of ingested nutrient and to this end we administered an isovolumetric and isocaloric (i.e., to olive oil) bolus of either glucose solution (as carbohydrate) or casein suspension (as protein representative) and drinking water as control, followed by ATGL protein abundance assessment 30 min after intake. Western blot analysis did not reveal any substantial differences between the groups, with only a subtle drop in glucose bolus - treated samples (Fig. 24 A). To resolve it, we carried out an experiment with glucose solution gavage in a wider time scope which, however, did not reveal any variation in ATGL levels compared to control animals (Fig. 24 B). We therefore concluded that ATGL removal is specific to dietary lipids intake.

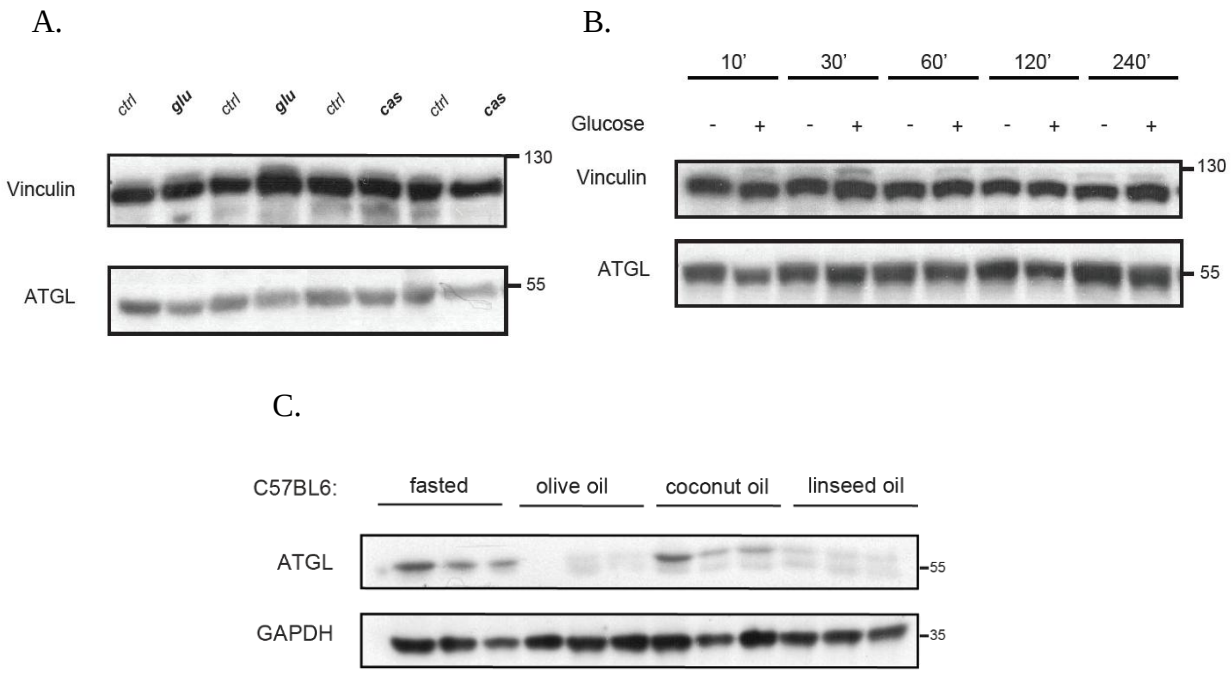

Fig. 24. ATGL degradation is specific to lipid ingestion in mouse intestine. A. Western blot analysis of ATGL and Vinculin (as loading control) expression level in small intestinal epithelium harvested 30 min after oral gavage with glucose solution (glu), casein suspension (cas) or drinking water as control in male C57/BL6J mice. B. Western blot analysis of ATGL and Vinculin (as loading control) expresion level in small intestinal epithelium harvested at indicated time points after oral gavage with glucose solution (+) or drinking water as a control (-). C. Western blot analysis of ATGL protein expression in small intestinal epithelium harvested 30 min after oral gavage with olive oil, coconut oil, linseed oil or drinking water (fasted) as control.

We further asked if the specificity of protein removal is restricted to olive oil only or it applies to other types of dietary fats as well. Olive oil is a vegetable oil, primarily composed of TG (~99%), with a high concentration of monounsaturated and long chain fatty acids —mainly oleic acid (55–83%) — and to a lesser extent palmitic and linoleic acids. We therefore gavaged the C57BL/6J mice with oils of dissimilar fatty acid composition, i.e. coconut oil, containing ~80-90% of saturated fat, with lauric acid as a principal fatty acid compound (about 40–50%), which is saturated and medium chain. Other experimental group received linseed oil which

among natural vegetable oils is characterized by the highest content of long chain, polyunsaturated fatty acids dominated by linolenic acid, which makes up 50%–60% of its total composition but also enriched in monounsaturated fatty acids (oleic acid, ~15-20%).

Interestingly, ATGL protein expression levels were comparably reduced after linseed oil gavage as after olive oil standing as a positive control. In coconut oil treated animals protein abundance remained unchanged compared to fasted animals (negative control) (Fig. 24 C). That result implies that lipid-induced loss of ATGL may be driven with a certain selectivity, which is promoted by mono- and/or polyunsaturated fatty acids rather than medium-chain and saturated fatty acids. Throughout all conducted so far experiments a one, established dose of olive oil was used (10 ul/g b.w). We determined if there exists a dose dependent correlation by administering a decreasing dose of olive oil to wild-type mice at maintained total volume of bolus by adjusting it with drinking water. We confirmed a negative correlation between ATGL levels and the amount of oil ingested, while observing a drop in ATGL abundance already upon ingestion of nutrient at the lowest of tested doses (1 ug/g b.w.) (Fig. 25).

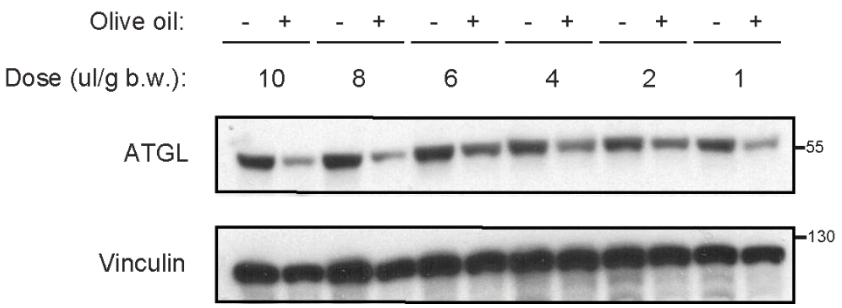

Fig. 25. **Degradation of ATGL in murine intestine has an olive oil dose-dependent character.** Western blot analysis of ATGL expression levels in jejunum of C57BL6J wild-type mice gavaged with different doses of olive oil or drinking water as control and harvested 30 min later. Vinculin was blotted as internal control.

Further specification of an oil compund(s) evoking the protein diappearance would require a large scale treatments with a variety of individual compounds present as a mixture in oil, such as different TG and DG species, fatty acids, fat-soluble vitamins, which due to the limitations

of mouse model, was unfeasible. To narrow a range of substances possibly involved in the ATGL degradation and get an insight into a general mechanism, we administered orally to the mice Orlistat, followed by gavage with olive oil. Orlistat is a pancreatic lipase inhibitor, blocking the breakdown of TG in gut lumen (166), thereby inhibiting the uptake of FFA, lipid absorption and is registered as a medication to manage obesity in humans (167).

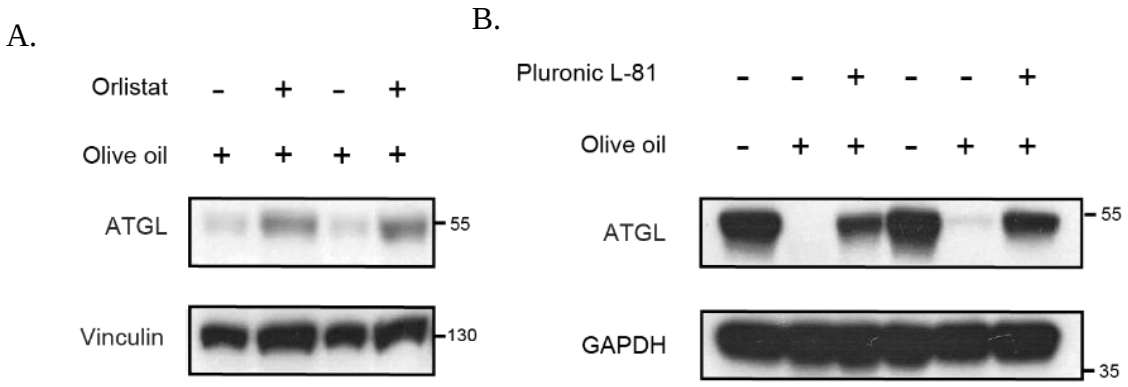

Fig. 26. ATGL degradation requires FFA uptake and is co-ordinated with chylomicron synthesis. A. Western blot analysis of ATGL and Vinculin (as loading control) expresion levels in small intestinal epithelium harvested 30 min after oral gavage with olive oil, preceeded with oral administration of single dose of pancreatic lipase inhibitor Orlistat (60 mg/kg b.w.). B. Western blot analysis of ATGL and Vinculin (as loading control) expression levels in small intestinal epithelium harvested 30 min after oral gavage with olive oil, preceeded with oral administration of single dose of Pluronic L-81 (10 mL/kg b.w.) to inhibit chylomicron synthesis.

As shown on Fig. 26 A, pre-gavage with single dose of Orlistat successfully prevented ATGL loss despite the following ingestion of olive oil. It suggests that TG breakdown is required for that event, however, leaves open a question if products uptake into the enterocyte is required too or the signal towards protein removal is mediated via cell membrane-localized receptor. It is also worthnoting that pregavage with Pluronic L-81, a surfactant which blocks chylomicrons synthesis (at prechylomicron stage in ER, via inhibiting MTTP function) also rescued ATGL removal (Fig. 26 B). The relation between ATGL stability and chylomicron production has not been further studied but is an interesting field for investigation considering also a fact that coconut oil which, as shown, does not trigger ATGL removal is mainly composed of medium

chain fatty acid which largely bypass packaging into chylomicrons and are directly absorbed via hepatic portal vein. Lipid abosprtion is inevitably associated with LD synthesis in enterocyte. We therefore asked if that event is also a prerequisite for ATGL degradation by blocking LD formation followed by olive oil gavage. LD synthesis was inhibitetd via administering the inhibitors of diacylglycerol acyltransferases 1 and 2 (DGAT1 and 2), key enzymes responsible for TG resynthesis with compounds known as PF04620110 and PF07202954, respectively (168,169). The efficiency of the inhibitors was validated also in the organoids via LD staining by treatment at doses and time according to previously reported data (170) (Fig. 27 A). As shown with Fig. 27 B incjection of inhibitors alone did not alter ATGL levels, while DGATs inhibitors with following olive oil gavage in wild-type mice prevented ATGL loss. That result pinpoints the another physiological determinant of lipid-induced ATGL degradation and indirectly indicates that it might be associated with lipolytic function of ATGL, specifically at LD.

A.

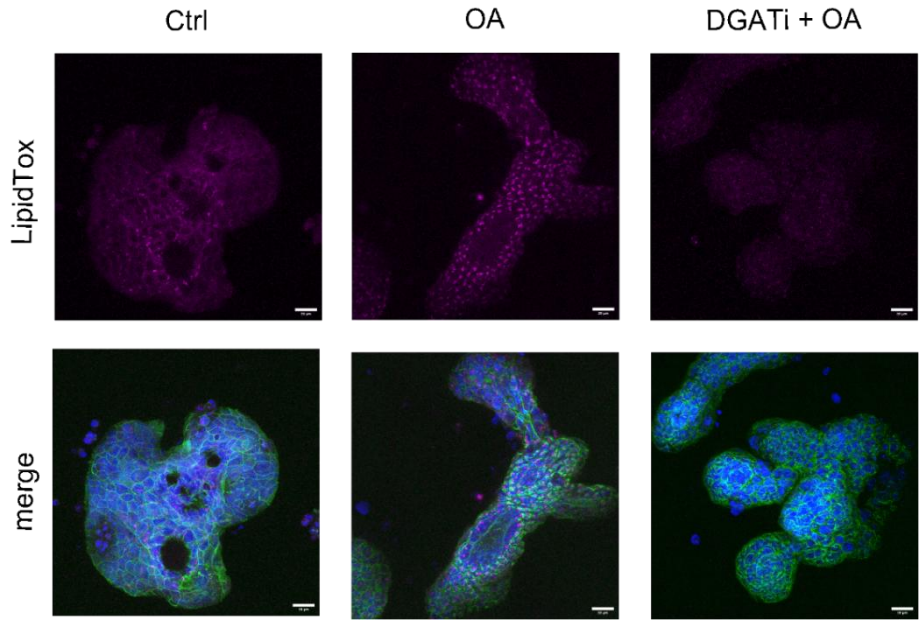

B.

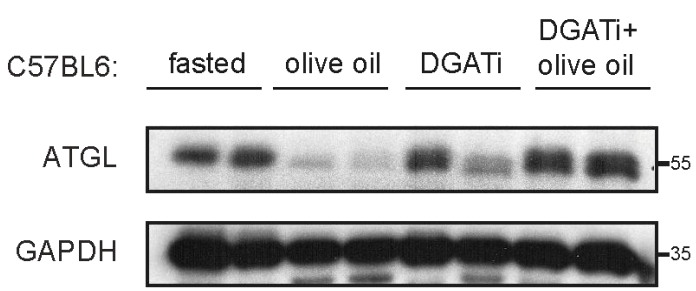

Fig 27. LD formation is required for ATGL degradation following uptake of FFA. A. Representative immunofluorescent images of apical-out organoids derived from C57BL6J mouse and maintained either in complete medium (ctrl) or additionally supplemented with 1 mM oleic acid for 3 h (OA) or preincubated with DGAT 1 and 2 inhibitors (DGATi) for 24 h (PF04620110 and PF07202954, at 10 μM and 7.5 μM, respectively) with following OA treatment for 6 h. LD were stained with Lipidtox, (magenta), nuclei with DAPI (blue) and actin fibers with Phalloidin 488 (green), scale bar is 20 μm. B. Western blot analysis of ATGL and GAPDH protein level in C57BL6J mice that were fasted for 6 h (fasted), additionally gavaged with olive oil and sacrificed 30 min later (olive oil), injected intraperitoneally with PF04620110 and PF07202954 (at 3 mg/kg b.w. and 7.5 mg/kg b.w, respectively) (DGATi) and sacrificed after 1 h or injected with DGAT inhibitors, gavaged with olive oil and sacrificed 30 min after gavage.

It is plausible that ATGL degradation is an enterocyte-autonomous response since similarly to our *in vivo* findings, we confirmed a rapid reduction in protein expression level in mouse intestinal organoids which are built of epithelial cells exclusively (Fig 28). We treated organoids isolated from C57/BL6J mice with oleic acid, the most abundant fatty acid present in olive oil, which also evoked ATGL degradation already 10 minutes after adding to cell culture media. That outcome was observed either in the apical-out as well as in basal-out organoids. These two models were used to determine whether the route of entrance of fatty acid (i.e., via apical versus basolateral membrane) determines the ATGL susceptibility to degradation. In basal-out organoids, embedded in basement membrane matrix, the fatty acid reaches the cytosol by entering through the basal membrane, opposite to apical-out organoids, which resemble the physiological route of nutrient uptake in small intestine. Each membrane of enterocyte is equipped in a distinct set of proteins/transporters which may participate in a signal transduction towards degradation. However, observing ATGL removal in both cases allows to hypothesize that this event is not mediated by a membrane-specific transporter.

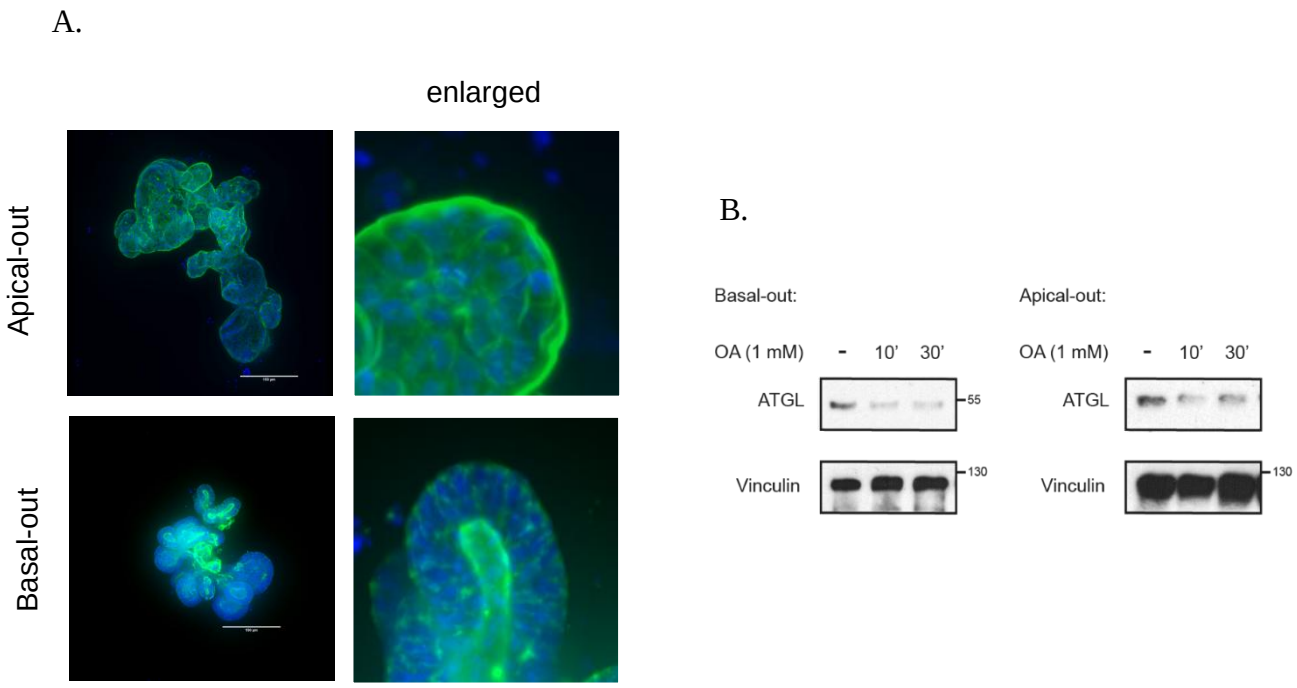

Fig. 28. Oleic acid triggers degradation of ATGL in intestinal organoids. A. Immunofluorescent confocal images of apical-out (upper panel) and basal-out (lower panel) organoids derived from C57BL6J mouse B. Western blot analysis of ATGL protein levels (and Vinculin as a loading control) in protein extracts collected from basal out (left) and apical-out (right) organoids treated with oleic acid (OA) at 1 mM, conjugated with BSA for 10, 30 minutes or BSA alone as control (-).

Intriguied by finding such a robust and rapid changes concerning only two tested proteins playing a well established role in maintenance of LD metabolism, we wondered how fat ingestion may affect enterocyte proteome globally. To this end, we performed LC/MS tandem mass tag (TMT) proteomic analysis of intestinal scratches isolated 30 minutes after olive oil or drinking water (as control) gavage from C57/BL6 male mice (Fig. 28 A). Within this short time, the abundance of 107 out of 6803 identified proteins was markedly changed (Fig. 28 B). In line with previous results, the abundance of some LD-associated proteins was significantly affected (reduced as in case of MGL or markedly increased as in case of PLIN2). Gene-ontology (GO) enrichment analysis conducted in the context of biological process or molecular function revealed that, among others, a cluster of mitochondrial respiration and function – related proteins were significantly upregulated (Fig. 28 C, D). This list includes *Atp5j*, *Ndufb10*, *Coa3*,

Cox6c, *Cox7c*, *Etfdh*, *Letm1*, *Oxa1L*, *Slc25a20* and *Ucqrh*. These results are in line with a study from other group revealing the importance of mitochondrial respiration in fueling CM synthesis and fat absorption (163). On the other hand, a group of proteins involved in organization and function of extracellular matrix was among the most downregulated. These results indicate that lipid ingestion evokes a rapid remodeling of enterocytes' proteome which is, at least partially, dependent on the function of PKD2. Due to a short time between oil gavage and observed impact on the proteome, it is likely that observed changes result from post-translational modifications.

A.

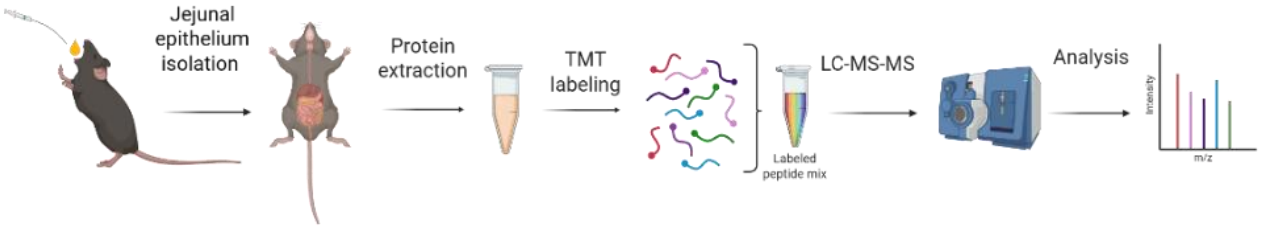

B.

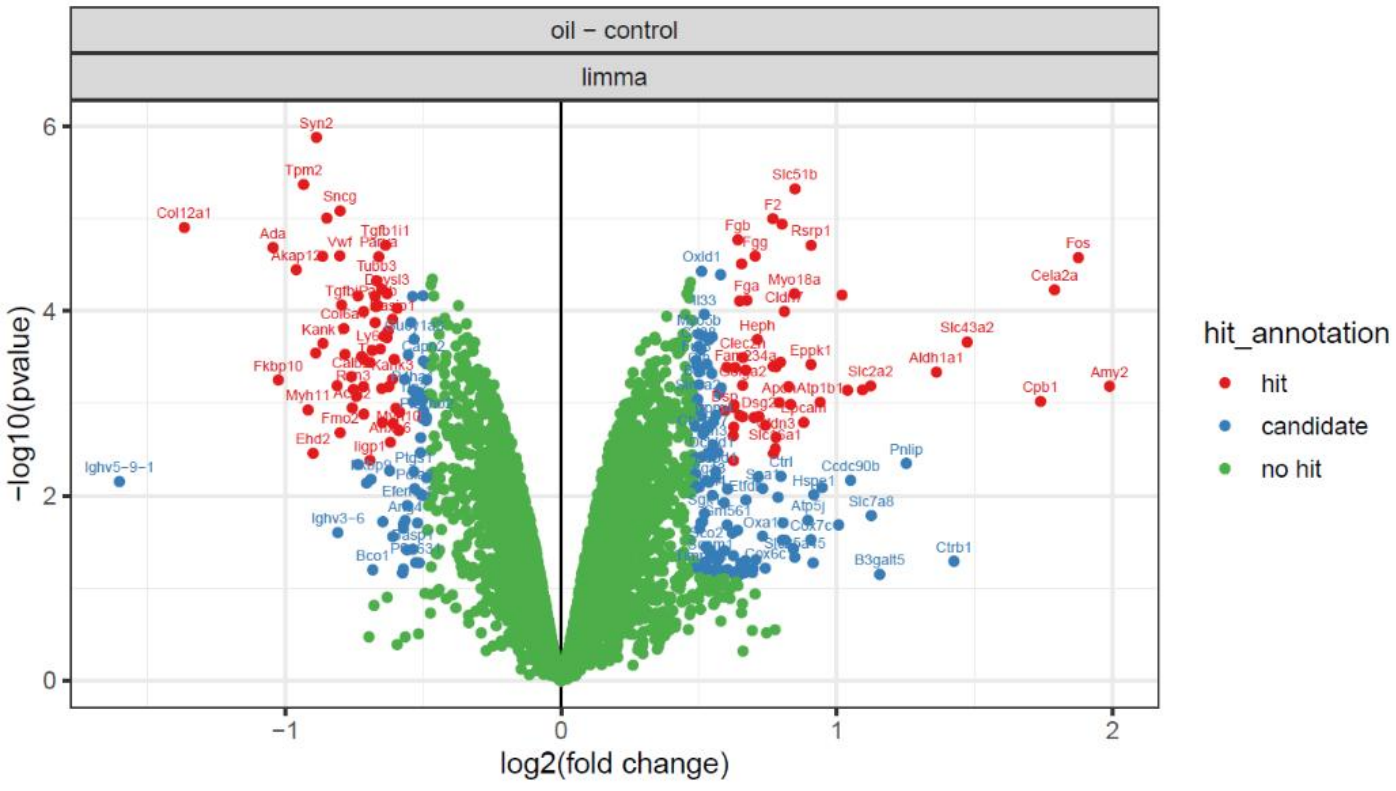

C.

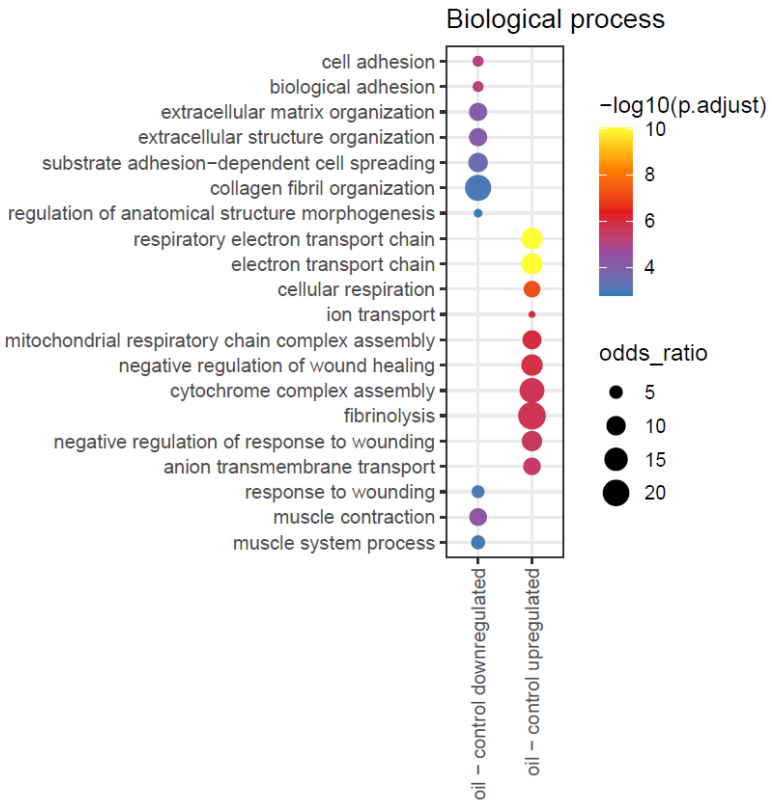
Biological process
cell adhesion
biological adhesion
extracellular matrix organization
extracellular structure organization
substrate adhesion−dependent cell spreading
collagen fibril organization
regulation of anatomical structure morphogenesis
respiratory electron transport chain
electron transport chain
cellular respiration
ion transport
mitochondrial respiratory chain complex assembly
negative regulation of wound healing
cytochrome complex assembly
fibrinolysis
negative regulation of response to wounding
anion transmembrane transport
response to wounding
muscle contraction
muscle system process
oil − control downregulated
oil − control upregulated
−log10(p.adjust)
10
8
6
4
odds_ratio
5
10
15
20

D.

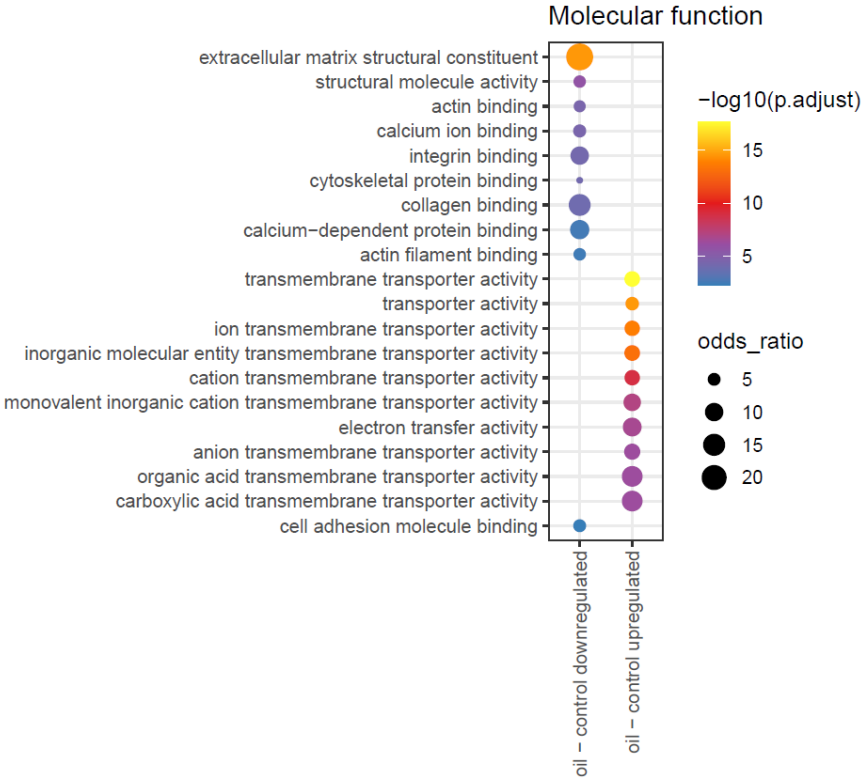
Molecular function
extracellular matrix structural constituent
structural molecule activity
actin binding
calcium ion binding
integrin binding
cytoskeletal protein binding
collagen binding
calcium−dependent protein binding
actin filament binding
transmembrane transporter activity
transporter activity
ion transmembrane transporter activity
inorganic molecular entity transmembrane transporter activity
cation transmembrane transporter activity
monovalent inorganic cation transmembrane transporter activity
electron transfer activity
anion transmembrane transporter activity
organic acid transmembrane transporter activity
carboxylic acid transmembrane transporter activity
cell adhesion molecule binding
oil − control downregulated
oil − control upregulated
−log10(p.adjust)
15
10
5
odds_ratio
5
10
15
20

Fig. 28. **Lipid ingestion evokes global changes in intestinal proteostasis.** A. Schematic workflow for TMT proteomic analysis of intestinal tissues harvested from C57/BL6 mice. B. Volcano plot showing the relative abundance of proteins in the epithelium of the intestine of fasted C57/BL6 mice gavaged with olive oil (10 µl per gram of body weight of mice) and sacrificed 30 min later. C. GO enrichment analysis of proteins identified in (A) and clustered according to biological processes and D. molecular functions.

LD accumulate in enterocytes of PKD2-deficient mice under a chronic exposure to feeding with a high-fat diet.

All described above data refer to a phenotype of LD of intestinal epithelia observed upon acute and large in quantity exposure to lipids. However, typically, the crude fat content in commercially available mouse diet is about 4-6 %. Therefore it might be speculated whether results obtained from a challenge with a bolus containing dietary lipids exclusively at a dose 10 ml/kg b.w. would reflect the intestine's response as under spontaneous feeding conditions. It has to be noted, however, that olive oil gavage at indicated dose is a widely accepted procedure to mimic a high-fat meal ingestion in laboratory rodents (52,171,172). Another commonly accepted procedure for metabolic studies in mice is feeding with a high-fat diet which typically provides 20-60% of calories from fat. It was also described in the literature that prolonged exposure to a high-fat diet promotes LD deposition in enterocytes of murine small intestine. Therefore, I decided to subject *Pkd2*$^{gut\Delta/\Delta}$ and *Pkd2*$^{flox/flox}$ animals to feeding with a high-fat diet for 1 month and starting the diet at the age of 8 weeks to determine whether the impact of PKD2 on LD metabolism may be also found in more physiologically valid conditions regarding the dietary fat intake. It is well described that feeding with a high fat diet causes a range of morphological adaptations in small intestine, including villi shortening, stem cells enrichment, epithelial cells degeneration as well as functional changes, primarily, enhanced capacity towards lipid absorption. On a day of completion of feeding with experimental diet, mice were fasted 6 h followed by 3 h of refeeding with a high fat diet. Analogically to a set of analyses performed for acute lipid challenge experiments, I determined the size and abundance of LDs by immunofluorescent staining of intestinal sections against Plin 2- and Plin 3-decorated LDs. Strikingly, the elevation in both parameters for each LD population in *Pkd2*$^{gut\Delta/\Delta}$ mice-derived specimens was even more pronounced compared to acute oil challenge conditions (Fig. 29 A-F).

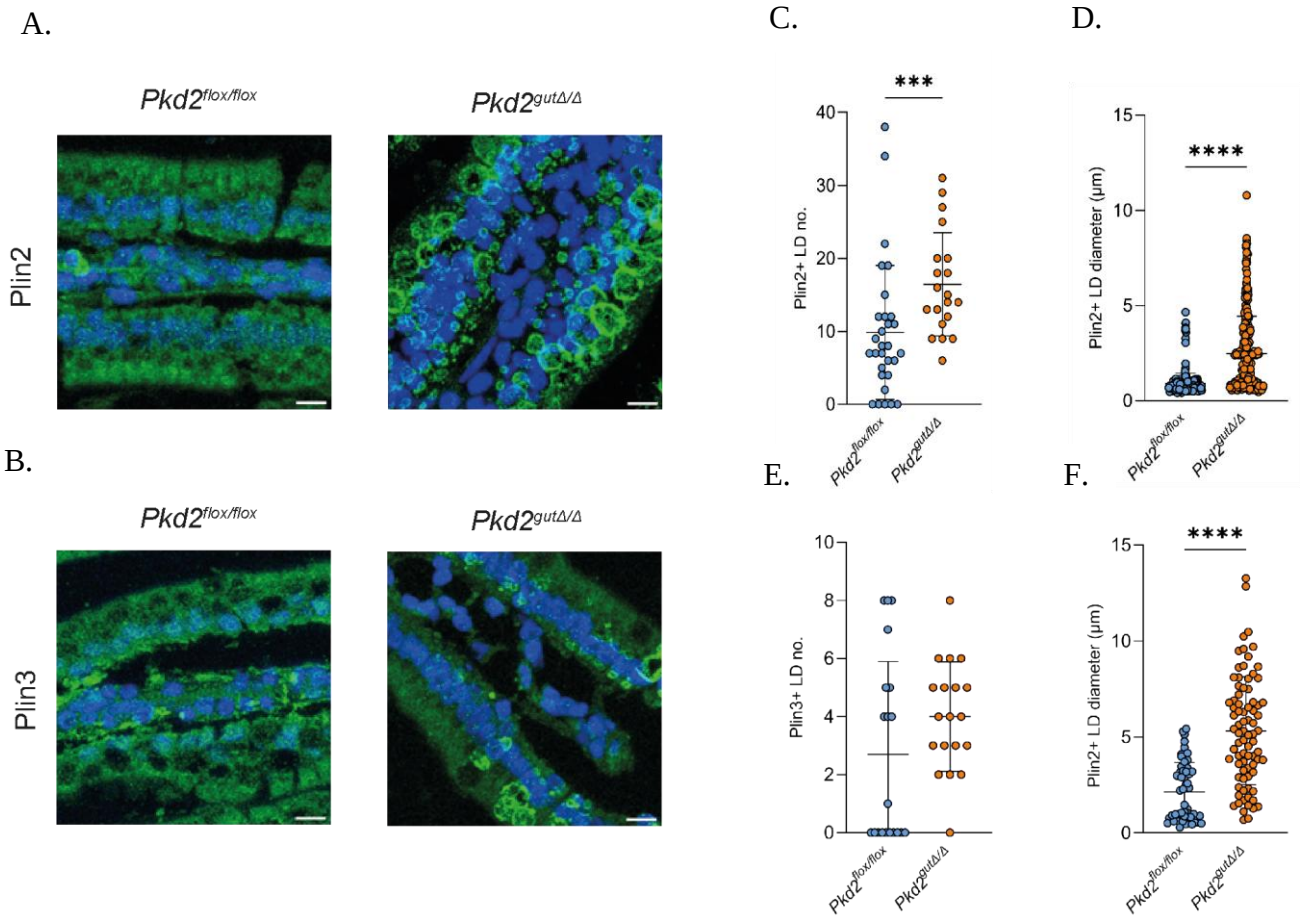

Fig. 29. **LD are enlarged in enterocytes of *Pkd2$^{gutΔ/Δ}$* mice exposed to feeding with a high-fat diet (HFD)**. A, B. Representative immunofluorescent images of jejunal sections harvested from *Pkd2$^{flox/flox}$* and *Pkd2$^{gutΔ/Δ}$* mice that underwent 1 month of feeding with a high fat diet and stained against Plin 2 and Plin 3. C. Quantification of Plin 2 – coated LDs' number from (A). D. Quantification of Plin 2– coated LD size from (A). E. Quantification of Plin 3 – coated LD number from. (B). Quantification of Plin 3 – coated LD size from (B). *n* = 5 per genotype and 4 villous areas 40 x 40 µm per mouse were quantified, scale bar is 10 µm. Data represent mean ± SD. *Ns* – non significant, ***p<0.01, ***p<0.001, ****p<0.0001 by Mann-Whitney test.*

Gene expression analysis revealed that several factors involved in either FA and TG synthesis (*Acc*, *Dgat1*), LD formation (*Plin 3*), lipolysis suppression (*G0S2, Hilpda*) were significantly

upregulated in *Pkd2*$^{gut\Delta/\Delta}$ samples, in line with observwed LD accumulation. In contrast, however, stands the greatest upregulation of *Abhd5* encoding CGI-58 protein, a co-activator of ATGL, in those animals compared to control (Fig. 30).

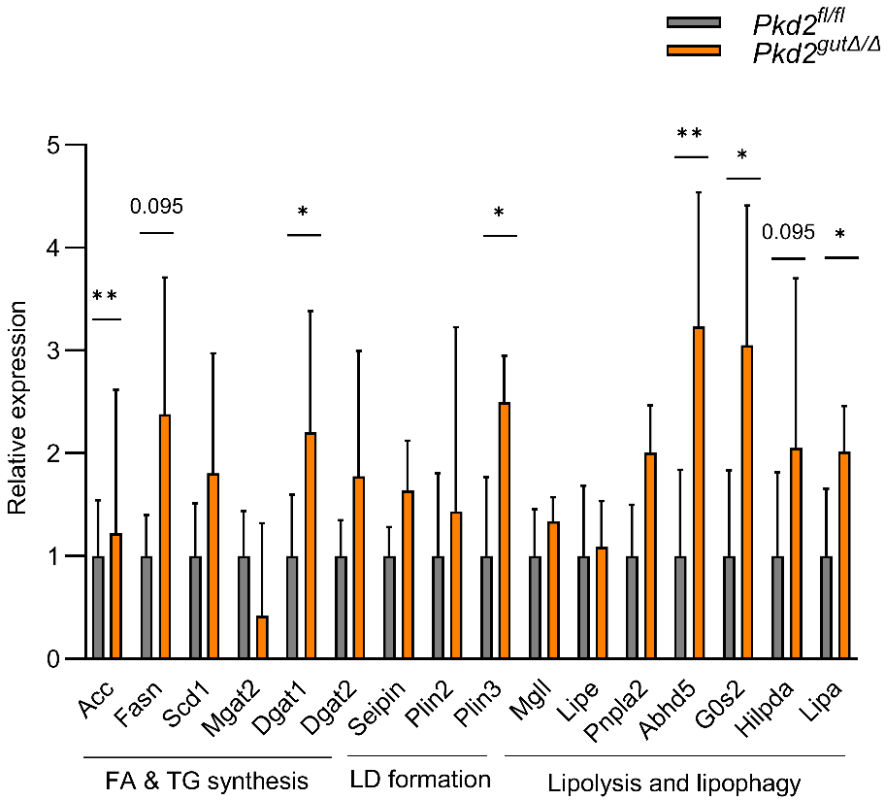

Fig. 30. Relative expression of key genes encoding proteins regulating LD biogenesis and metabolism in intestinal scratches collected from *Pkd2*$^{flox/flox}$ and *Pkd2*$^{gut\Delta/\Delta}$ male mice that underwent 1 month of feeding with a high fat diet (HFD), fasted 6 h, followed by refeeding with a HFD for next 3 h. *n* = 5 per genotype, data represent mean ± SD, *p<0.005 by Mann-Whitney test..

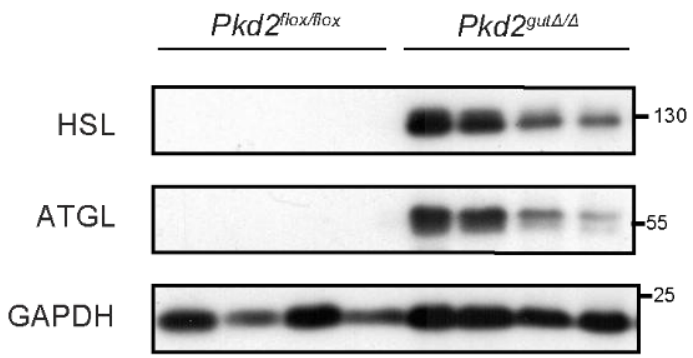

Fig. 31. ATGL and HSL protein levels are elevated in small intestine of *Pkd2*$^{gut\Delta/\Delta}$ mice fed with a high-fat diet. Western blot analysis of indicated proteins associated with LD function – ATGL and HSL - in mouse protein extracts isolated from *Pkd2*$^{flox/flox}$ and *Pkd2*$^{gut\Delta/\Delta}$ male mice intestines that underwent 1 month of feeding with a high-fat diet (ATGL, HSL and, GAPDH as a loading control).

On a protein level, similarly to acute challenge with olive oil, refeeding with HFD led to loss of ATGL and HSL in the epithelium of *Pkd2*$^{flox/flox}$ but not *Pkd2*$^{gut\Delta/\Delta}$ mice (Fig. 31). Observation of profound impact of PKD2 on LD morphology under spontaneous feeding conditions together with elevated ATGL and HSL expression in *Pkd2*$^{gut\Delta/\Delta}$ versus *Pkd2*$^{flox/flox}$ specimens only confirmed the relevance of kinase's function in physiology. That outcome also prompted us to study ATGL turnover pattern in wild-type C57BL6J mice fed ad libitum with different diets. As shown on Fig. 32 A, refeeding with HFD for 3 h preceeded with 6 h food withdrawal leads to ATGL loss as after olive oil gavage. Under both conditions PKD2 is subjected to activatory phosphorylation, and simultaneous increase in Plin2 levels suggests enhanced LD formation. ATGL and also HSL loss were further confirmed in another independent HFD refeeding experiment, while not revealing any differences in CGI-58, functionally related with ATGL (Fig. 32 B), underscoring thereby a narrow specificity of proteins degraded upon lipid ingestion. In contrast, refeeding with a diet containing no fat did not evoke any changes in ATGL expression compared to control, fasted animals (Fig. 32 C). Altogether, these data provide a strong evidence for physiological occurrence of LD-associated proteins degradation in the presence of dietary fat. These also allow to postulate that not a rapidness and massiveness of influx of dietary fat may be a direct trigger of protein loss (as achieved with forced olive oil gavage) but rather a cumulative quantity of lipids being absorbed (as proved by the effect of spontaneous feeding).

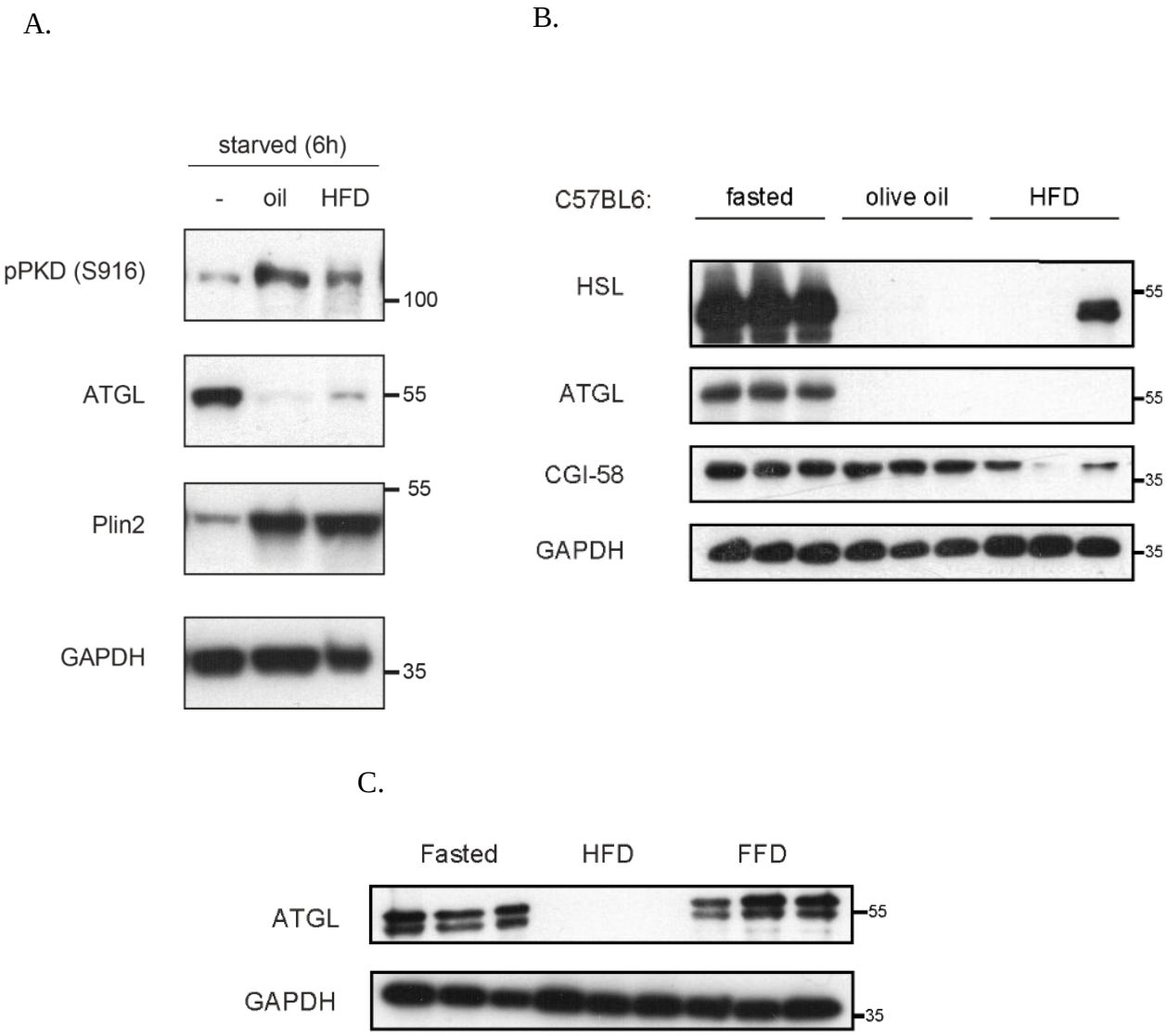

Fig. 32. ATGL is degraded during spontaneous feeding with a high-fat diet in C57BL6J mice. A. Western blot analysis of phosphorylated PKD (at Ser 916), ATGL, Plin2 and GAPDH in jejunal epithelium of C57BL6J mice that underwent 6 h of fasting, followed by oral gavage with olive oil (and sacrificed 30 min later) or given free access to high-fat diet (HFD) for 3 h. B. Western blot analysis of phosphorylated PKD (at Ser 916), HSL, ATGL, CGI-58, GAPDH in jejunal epithelium wild-type C57BL6J mice, fasted 6 h and gavaged with olive oil or refed with HFD for 3 h. C. Western blot analysis of ATGL and GAPDH (as a loading control) expression levels in wild-type animals, that were either fasted 6 h, fasted 6 h followed by refeeding with high-fat diet (HFD) or fat-free diet (FFD) for next 3 h.

Another interesting physiological finding was a correlation between ATGL expression pattern with a circadian rhytm. It is a in internal, approximately 24-hour internal clock that controls cycles of sleep, wakefulness, hormones, body temperature, and other biological processes**.** Mice are nocturnal rodents meaning that they are characterized by high activity during the dark phase and sleep during the light phase. Their master clock, the suprachiasmatic nucleus (SCN) in hypothalamus, is synchronized by primarily light, but mice can also entrain to food, temperature, and social cues (173) (Fig. 33 A). In our housing conditions, beginning of the dark phase was set at 7 p.m., with 12 h duration (Fig. 33 B). Low ATGL protein levels in the jejunum of wild-type mice at the end of the dark phase when animals were given a free access to food (chow-diet) are in line with previously postulated cumulative impact of food-derived fat ingestion on ATGL expression (Fig. 33 C). We also found a positive correlation between the duration of fasting (starting from 7 a.m.) with ATGL abundance in the intestine (Fig. 33 C). Surprisingly that was also followed by an increase in PLIN2, despite supposed depletion of LD during fasting. Of question is, however, if observed dependencies are regulated via food intake and withdrawal only or an independent, central control from SCN and key circadian rhythm-associated proteins (such as CLOCK**,** BMAL1**,** PER and CRY**)** plays a role here as well.

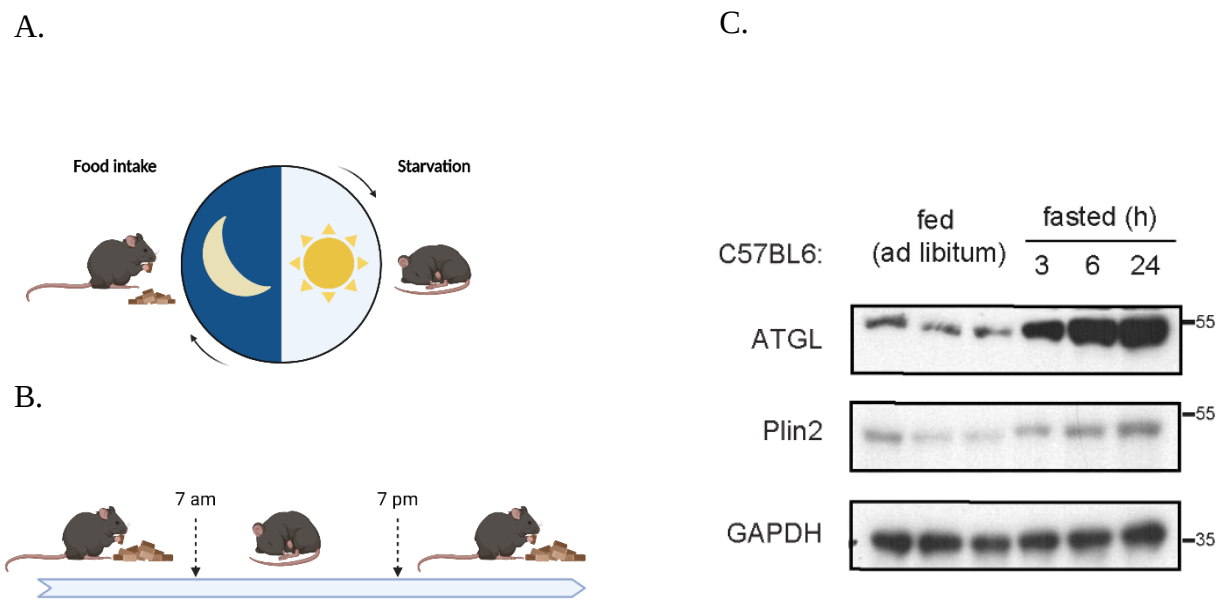

Fig. 33. ATGL expression pattern is associated with circadian rhytm and fasting duration in mouse intestine. A. Schematic representation of mouse feeding behavior in a day-night cycle. B. Schematic representation of light-night cycle in applied mice-housing

conditions. C. Western blot analysis of ATGL, Plin2 and GAPDH as loading control in jejunum of C57BL6J mice fed ad libitum with chow diet at the end of the active phase (fed) or after indicated period of fasting.

Data coming from described above experiments strongly indicate that the phenotype of LD accumulation in PKD2-depleted enterocytes is present under voluntary feeding conditions and thereby enhancing the physiological relevance of PKD2 in LD turnover. We show that a key trigger to reveal that phenotype can be either acute (olive oil gavage) or chronic (HFD feeding) lipid overload of the intestine. Of note, same prerequisite can be postulated regarding the event of dietary fat-mediated ATGL degradation, which loss, *nota bene*, is also prevented in *Pkd2*$^{gut\Delta/\Delta}$ mice fed with HFD.

UPS and autophagy may be involved in ATGL degradation

Confirmation of the data regarding the link between fat ingestion, ATGL stability and PKD2 obtained in a set of experiments described above with different diets (as fully physiological settings) justified the use of olive oil gavage as a model to study further the mechanism responsible for ATGL loss. A rapidness of the indicated that ATGL may be subjected to degradation. Two major mechanisms responsible for clearance of the proteins in the cell via their degradation are ubiquitin-proteasome system (UPS) and lysosome-related pathways (macro- and micro-autophagy and chaperone-mediated autophagy) (174), both more widely described in the 'Introduction'. Other specialized systems include caspase- and calpain-mediated or extracellular degradation (175). We focused our attention primarily on distinguishing between potential involvements of UPS and autophagic machinery by pretreatment of the animals with respective inhibitors – MG132 which reversibly inhibits the proteolytic activity of the 26S proteasome and Bafilomycin A1 – which blocks the late stage of autophagy via inhibiting the vacuolar-type H^+-ATPase (V-ATPase) (176)**,** a proton pump responsible for acidifying the lysosomes. We carried out first a pilot experiment in which we included a range of conditions, i.e. C57BL6J wild-type fasted or gavaged with olive oil animals, PKD2 knock-in animals either fasted or treated with olive oil and wild-type mice pre-injected with DMSO (control) or MG132 subcutaneously, followed by olive oil gavage. Apart from confirmation of phenotypes found before, we found that MG132 rescued ATGL

from degradation despite fat intake (Fig. 34). These data suggest that UPS may be involved in dietary fat-mediated degradation of ATGL.

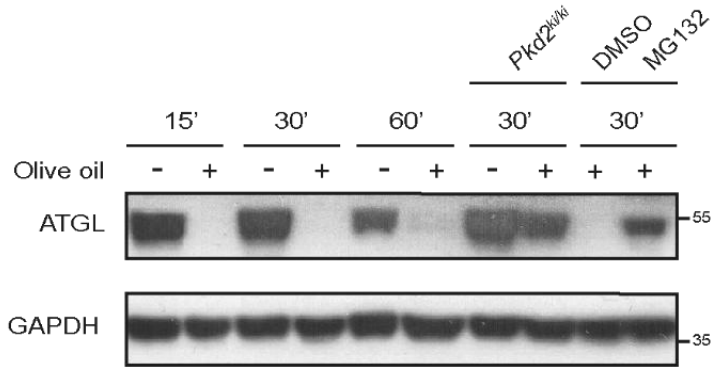

Fig. 34. Inhibition of proteasome activity with MG132 protects from ATGL degradation in mouse intestine. Western blot analysis of ATGL and GAPDH expression in jejunum of, describing from the left: fasted versus challenged with olive oil wild-type C57BL6J mice sacrificed at indicated time points after gavage, in PKD2 knock-in mice fasted or gavaged with olive oil and wild-type mice preinjected with DMSO or MG132, followed by olive oil gavage and sacrificed 30 min later.

We analogically approached an experiment with Bafilomycin A1 pretreatment, given that proved efficiency of MG132 does not exclude the involvement of autophagic machinery and both systems may cooperate to degrade a protein (177). Interestingly, Bafilomycin A1 also rescued ATGL loss after olive oil challenge, indicating at the complexity of that phenomenon (Fig. 35 A). Reduced band of p62, one of the key autophagy adaptor protein (178), indicates at enhanced autophagic flux, while its upregulation after Bafilomycin A1 treatment with oil gavage – at effective autophagy inhibition. One of the most widely used markers to monitor autophagy is LC3 (microtubule-associated protein 1A/1B-light chain 3), a protein which associates with autophagosomal membranes (179). Measurement of LC3 puncta (dots) with fluorescent microscopy may indicate at either enhanced autophagic flux (enhanced autophagy) or autophagosomes accumulation and blockage of late stages of degradation (180). Staining of intestinal sections from *Pkd2*$^{wt/wt}$ and *Pkd2*$^{ki/ki}$ mice 1 h after oil gavage against LC3 and ATGL revealed an accumulation of LC3 puncta, partially co-localizing with ATGL signal (Fig. 35 B, C, D). A resistance to degradation in PKD2-inactive or deficient enterocytes

shown with Western blot allows to hypothesize that observed LC3 puncta increased size and number may rather indicate at autophagy blockage.

A.

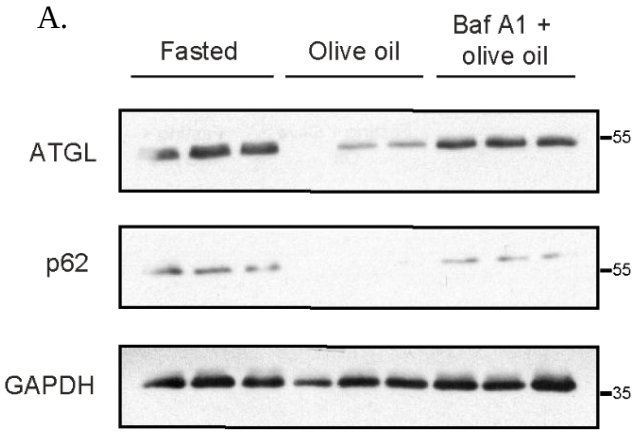

B.

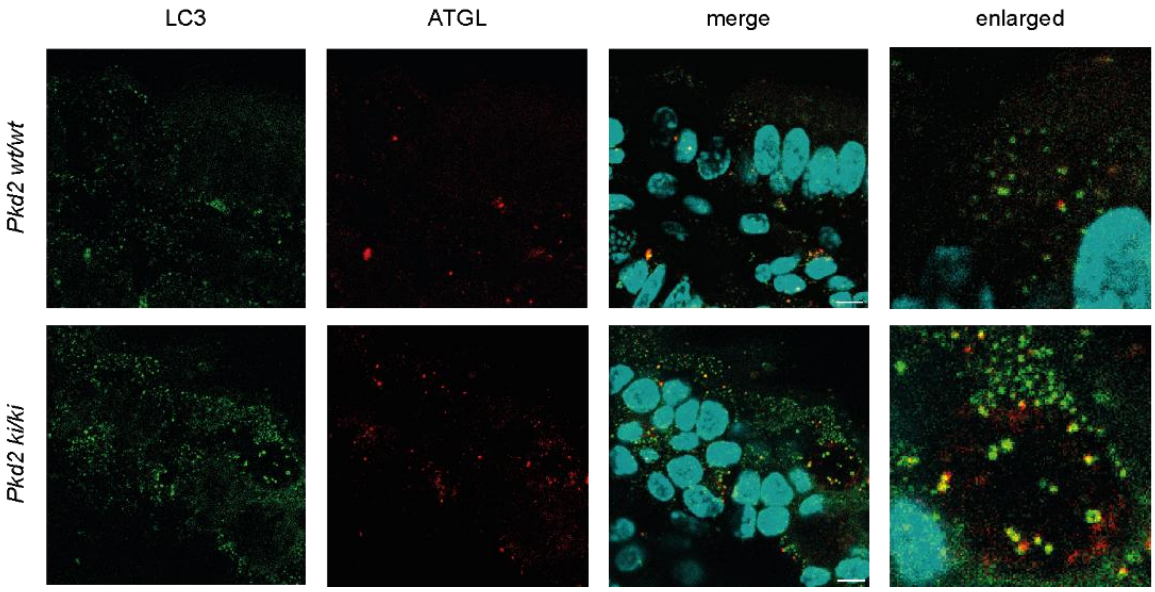

C.

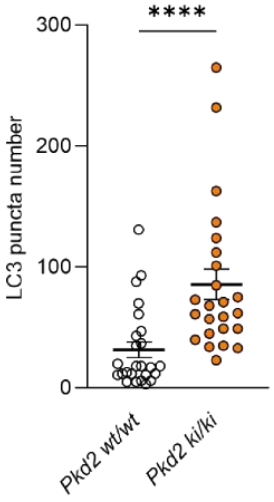

D.

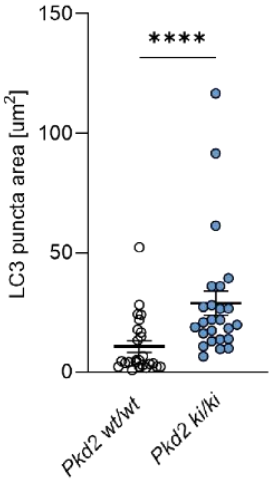

Fig. 35. **Blockage of autophagy with Bafilomycin A1 rescues ATGL from degradation**.A. Western blot analysis of ATGL, p62 and GAPDH in wild-type mouse jejunum that were fasted, gavaged with olive oil or injected intraperitoneally with Bafilomycin A1 (100 ug/g b.w.) with following olive oil gavage. B. Immunofluorescent images of intestinal sections of *Pkd2*$^{wt/wt}$ and *Pkd2*$^{ki/ki}$, 1 h after oil gavage and stained against LC3 (green) and ATGL (red), nuclei are in cyan. C. Quantification of LC3 puncta and area (D), from images shown representatively panel A. *n* = 4, LC3 puncta were quantified in 4 areas (40 x 40 um) in each animal, scale bar is 5 µm.

For further studies we aimed to use an in vitro model of Caco-2 cell line which would offer a wider experimental capacity regarding molecular description of ATGL degradation. First, we sought to determine the validity of that model, i.e. to verify whether ATGL degradation also occurs in response to fatty acid treatment and whether it is blocked in cells depleted from PKD2. To this end we generated a stable cell lines expressing either *shScramble* or *shPkd2* using lentiviral vector. Cells were treated with oleic acid and protein level was evaluated in cell lysates at time points indicated on Fig. 36. We confirmed the silencing of PKD2 in *shPkd2* cell line and its rapid activation in *shScramble* cells after adding oleic acid, occurring with a wave propagation, expected for the kinase (181). Unexpectedly, we found a relatively low level of ATGL under basal conditions (complete medium) in *shScramble*, with oleic acid promoting its abundance, proportionately to the time of incubation (Fig. 36). In contrast, cells depleted from PKD2 revealed increased ATGL level already in non-stimulated conditions, with no further change after adding oleic acid (Fig. 36). In spite of discrepancy between in vitro and in vivo findings, there are however, two common points for these models. First, we observe that oleic acid (or olive oil) modulates the bundance of ATGL in wild-type or *shScramble* variant and second, depletion of PKD2 disrupts that relation and overall increases the abundance of ATGL.

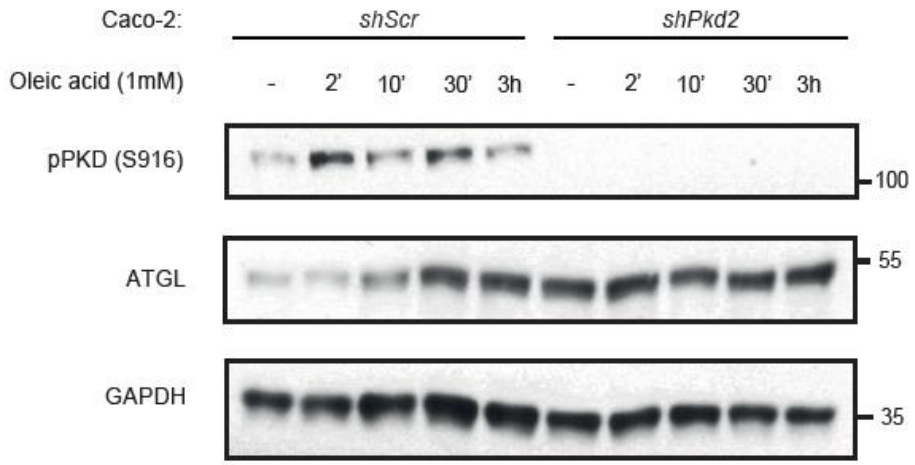

Fig. 36. **Oleic acid treatment increases ATGL level in Caco-2 *shScr* cells but does not affect lipase abundance in *shPkd2* cells.** Western blot analysis of phosphorylated PKD (at Ser 916), ATGL and GAPDH as loading control in Caco-2 cells *shScramble* and *shPkd2* maintained in complete growth medium (-) or additionally treated with oleic acid (at 1 mM) for indicated time.

It was previously reported that ATGL turnover rate *in vitro* is regulated via proteasomal degradation (107,108,182,183). We tested if that scenario applies to Caco-2 (using wild type cells) as well in a cycloheximide pulse-chase experiment to monitor the fate of existing protein (184). Indeed, MG132 stabilized ATGL levels, analogically as did oleic acid (Fig. 37 A and B, respectively), and an line with *in vitro* data from hepatic cell line (183).

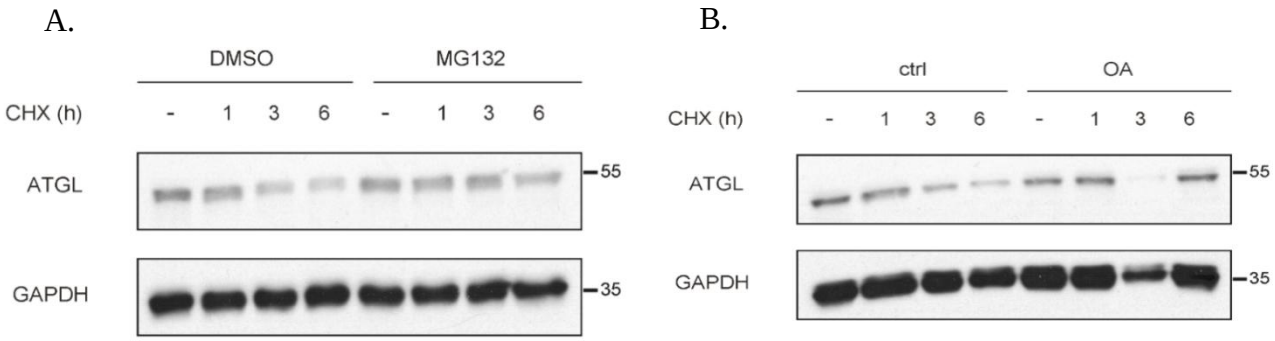

Fig. 37. Inhibition of proteasome with MG132 and oleic acid treatment stabilize ATGL levels in Caco-2 cells. A. Western blot analysis of ATGL and GAPDH (as loading control) levels in Caco-2 cells treated with cycloheximide (at 50 mg/mL) and DMSO (control) or MG132 (at 10 µg/µL) for indicated time points. **B.** Western blot analysis of ATGL and GAPDH (as loading control) levels in Caco-2 cells treated with cycloheximide (at 50 mg/mL) and BSA (control) or oleic acid – BSA conjugate (at 1 mM) for indicated time points.

The notion that ATGL level in Caco-2 cells maintained in a complete growth medium is very low resembled a phenotype observed in wild type mice fed ad libitum (Fig. 33 C). We hypothesized that compound(s) present in medium may evoke a protein degradation. Analogically as it was investigated in vivo, we depleted cell culture media from particular nutrients and observed how it affects ATGL abundance, either in PKD2-intact and PKD2-deficient cells (Fig. 38). Of note, at any of the conditions applied, i.e. all nutrients (maintained in Hank's balanced salt solution; HBSS), glucose (Glc), all aminoacids (AA), glutamine (Glu) or fetal bovine serum (FBS) deprivation for 6 h we observed an elevation of ATGL band in *shScramble* cells compared to complete medium, while the most pronounced increase was found when FBS was depleted (Fig. 38). Notably, that is the only variant in which we modified lipids availability exclusively, recalling, again, a negative correlation between ATGL protein level and external lipids abundance found *in vivo* first. Lipase expression remained largely unchanged in *shPkd2* Caco-2 cells throughout all tested starvation conditions compared to complete medium, however, a slight increase was observed upon FBS removal. Another lipase, HSL, also presented elevated level in PKD2-deficient cells, at any of the conditions tested. Interestingly, phospho-p70 S6 kinase (at Thr 389), a downstream target of mTORC1, showed increased level in *shPkd2*, especially in complete medium-kept cells (Fig. 38), opening a way to hypothesize that nutrient sensing- related signaling may be altered due to PKD2 deficiency.

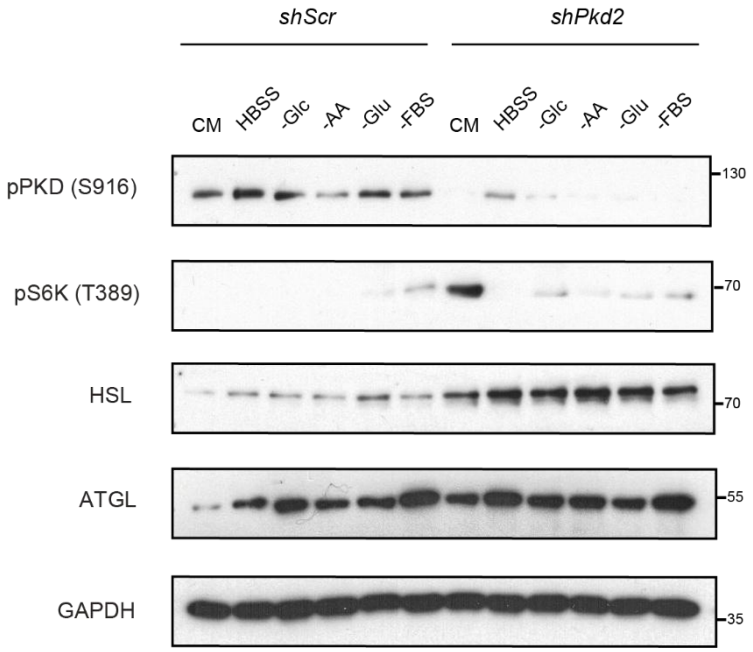

Fig. 38. Nutrients deprivation increases ATGL abundance in *shScr* but not *shPkd2* Caco-2 cells. Western blot analysis of phosphorylated PKD (at Ser 916), phosphorylated p70 S6 kinase (at Thr 389), HSL, ATGL and GAPDH as loading control in PKD2-intact (*shScr*) or deficient (*shPkd2*) cells maintained in complete medium (CM), Hank's balanced salt solution (HBSS), complete growth medium depleted from glucose (Glc), aminoacids (AA), glutamine (Glu) or fetal bovine serum (FBS) for 6 h.

Having found the conditions in which we can boost ATGL expression *in vitro*, i.e. by FBS starvation, we aimed to test whether such a starvation with subsequent treatment with fatty acids may evoke ATGL loss, which would bring a rationale for further use of Caco-2 cells as a model to study the mechanism of ATGL degradation. Caco-2 *shScramble* or *shPkd2* were thus treated either with oleic acid (the main fatty acid constituent of olive oil and which proved to evoke ATGL loss in organoids) or with palmitic acid (the most abundant fatty acid present in high-fat diet and refeeding with which also proved to be a trigger for degradation). None of the treatments, at any of indicated time points did not reduce ATGL level in *shScr* upregulated after FBS starvation (Fig. 39). As expected, ATGL in *shPkd2* cells remained unchanged all over the treatments. Worth noting is however, a constitutive enhanced phopsphorylation of p70 S6K at Thr 389 in *shPkd2* and selective activatory potential of

palmitic acid in *shScr* cells (Fig. 39). These data did not justify the further use of Caco-2 to explain the mechanism of ATGL degradation despite a clear influence lipid/fatty acid availability in media on ATGL abundance in cells with functional PKD2 and lack of such dependence in kinase-depleted cells. One possible explanation for inefficiency of fatty acid treatment to evoke degradation might be the fact that Caco-2 is an immortalized cell line derived from colon adenocarcinoma while our previously used models represent healthy intestinal epithelium. If ATGL degradation is a physiological response, it is plausible to expect that such a response would be altered in metabolically altered state which is cancer transformation. Thus, it would interesting to rather investigate whether ATGL resistance to degradation serves as as cancer-related metabolic adaptation., which is however, beyond the scope of presented study.

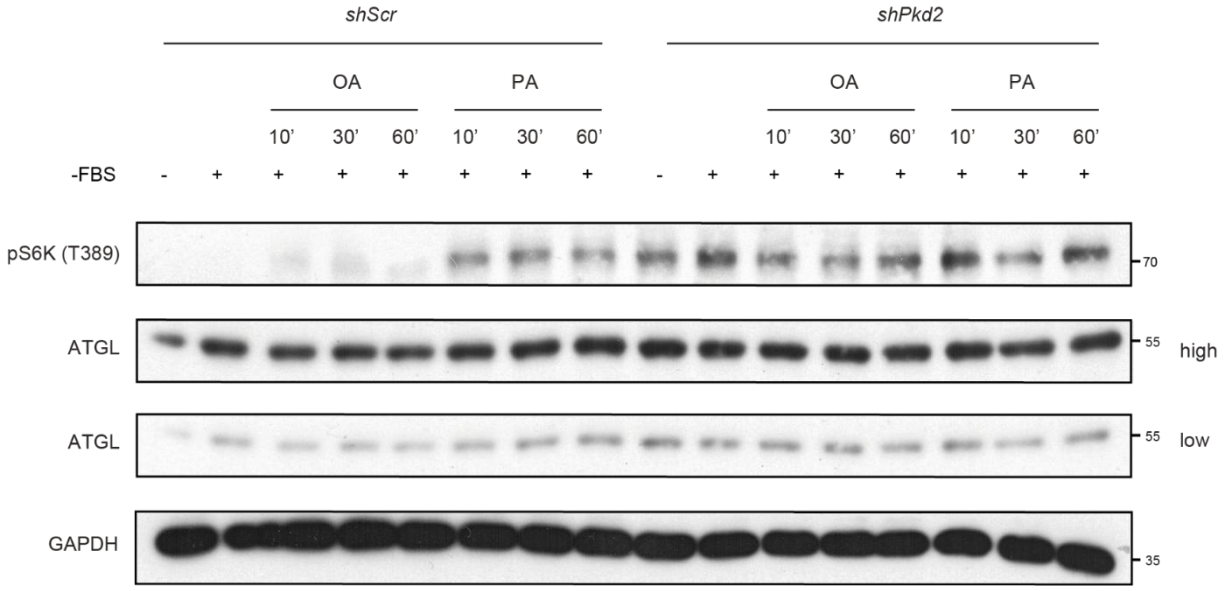

Fig. 39. Fatty acid treatment does not evoke ATGL degradation in Caco-2 cells. Western blot analysis of phosphorylated p70 S6 kinase, ATGL (at different exposures) and GAPDH as loading control in Caco-2 *shScr* and *shPkd2* cell lysates at following conditions (from left): kept in complete growth medium, serum (FBS) starved for 6 h, serum starved with following treatment with oleic (OA)- or palmitic acid (PA) - BSA conjugates (at 1 mM) and cell lysates were collected at indicated time points.

PKD2 determines ATGL trafficking to LD

Overall, using *in vivo* model we were able to prove that lipid mediated ATGL degradation may require ubiquitin-proteasome system and autophagic machinery. While keeping consequent with the model used we decided to focus on explanation why LD are enlarged upon PKD2 deficiency and if that is related to ATGL resistance to degradation. We hypothesized that LD accumulation may be a result of either intensified TG synthesis or impaired LD catabolism. Since previously we did not identify any significant differences regarding the expression of genes involved in fatty acid and TG synthesis as well as in protein levels, we directly focused on LD catabolism in the context of ATGL and PKD2 function. Effective ATGL-mediated lipolysis has two requirements; an enzyme needs to be localized on LD surface and be functionally competent. Despite high ATGL abundance in PKD2-deficient enterocytes these two features were not defined. ATGL is synthesized at rough ER and translocalized to LD by the Golgi-ER transport protein complex GBF1-Arf1-COPI. (described with more details in the 'Introduction'). PKD2 is primarily active at the *trans*-Golgi network (TGN), where it regulates the formation and release of transport carriers destined for various cellular compartments (ref). It also plays a pivotal role in the maintenance of the Golgi apparatus architecture itself (described in the 'Introduction' section). We aimed to determine if PKD2 contributes to proper ATGL delivery to LD by performing subcellular fractionation of intestinal epithelia harvested from $Pkd2^{flox/flox}$ and $Pkd2^{gut\Delta/\Delta}$ mice and pulled. That experiment was conducted at several time points after olive oil gavage to gain a perspective on ATGL trafficking in time. At 15 minutes after oil gavage, an overall ATGL abundance in all compartments (i.e., LD, cytosol, and membranes containing ER and Golgi) in $Pkd2^{flox/flox}$ was lower compared to $Pkd2^{gut\Delta/\Delta}$ however, a weak band of ATGL was observed in LD of $Pkd2^{flox/flox}$, but not in $Pkd2^{gut\Delta/\Delta}$ in which a protein redistribution to the cytosol was observed (Fig. 40 A). Interestingly, we found a differential expression of LC3 within the LD fraction, with an increased level of LC3B (lower band) in $Pkd2^{flox/flox}$ mice, suggesting an enhanced autophagic flux in that compartment. Similarly, in an experiment carried out at 2 h post oil gavage, ATGL was found much more abundantly in LDs collected from $Pkd2^{flox/flox}$ animals (Fig 40 B). Worth noting is also the fact that phosphorylated PKD2 was detected not only in the Golgi apparatus but in the LD fraction as well (Fig. 40 B). Presence of the kinase supports a postulated relevance of PKD2 for LD homeostasis. That may also indicate that the Golgi apparatus, a primary location for PKD2, is in close proximity to LD, as suggested by the presence of the Golgi marker proteins (Syntaxin 6 and RCAS1) within. That finding is also in line with previously reported Golgi-to-LD and PKD3-to-LD translocation

in liver (185). Lastly, data obtained from fractionation at 4 h after olive oil confirmed our findings from earlier time points and, as expected, revealed the highest ATGL level at LD (Fig. 40 C) due to supposed protein recovery (please look at Fig. 23 A). Altogether, these data suggest that PKD2 may be required for ATGL delivery to the LD surface, which would explain increased LD size due to impaired lipolysis.

A.

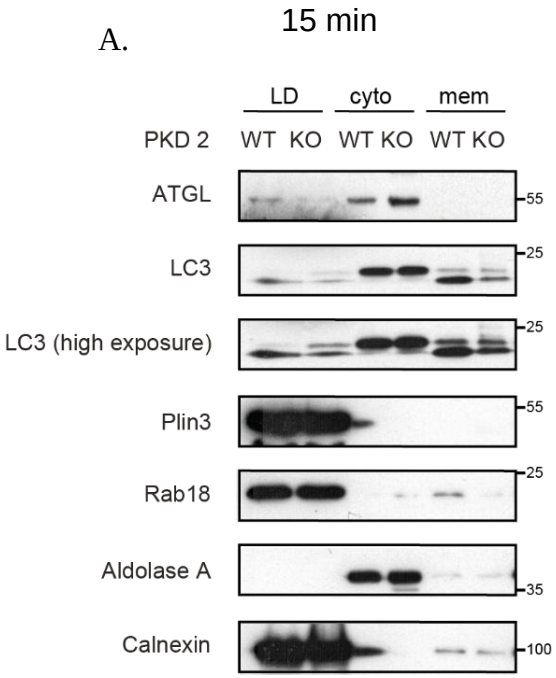

B.

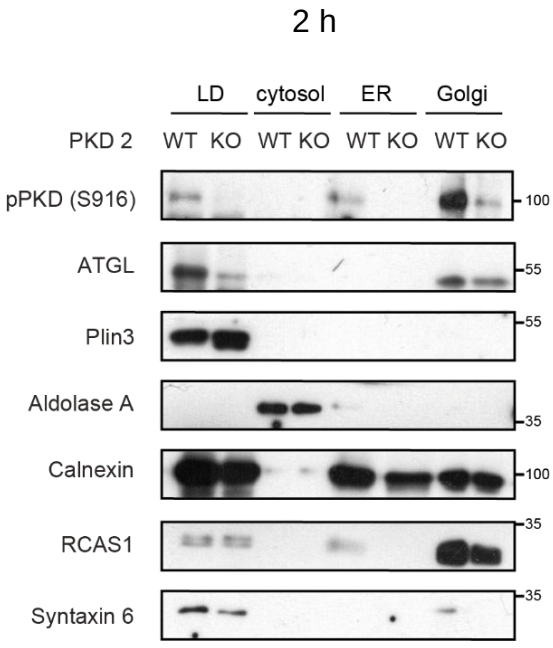

C.

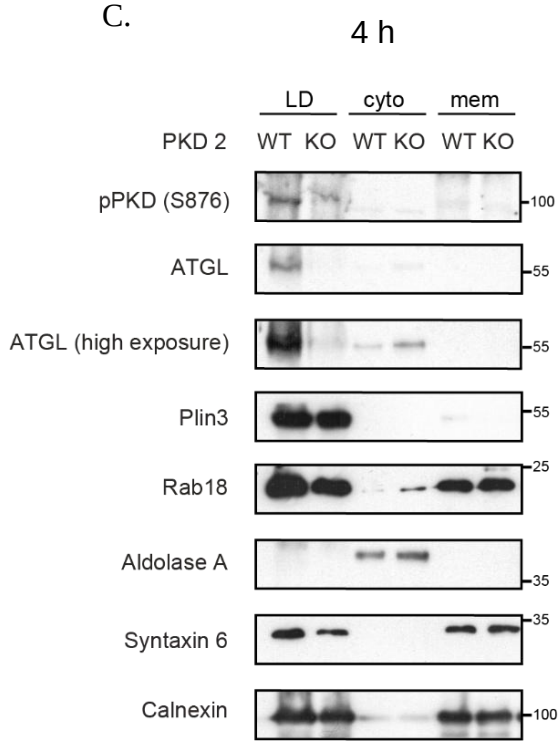

Fig. 40. **PKD2 deficiency impairs ATGL trafficking to LD in enterocytes of mouse intestine.** A. Western blot analysis of ATGL, LC3 and phosphorylated PKD2 subcellular localization in *Pkd2*$^{flox/flox}$ (WT) versus *Pkd2*$^{gut\Delta/\Delta}$ (KO) in jejunal epithelia collected at indicated time points after oil intake and material from 3 (for 15 min and 4 h time points) or 4 (in case of 2 h) mice per genotype was pooled. Plin 3 and Rab 18 were used as LD fraction marker (LD), Aldolase A as cytosol marker (cyto), Calnexin as total membranes (mem) or ER marker, Syntaxin 6 and RCAS1 served as the Golgi apparatus or total membranes marker.

Golgi apparatus morphology is altered in enterocytes depleted from PKD2

It was already described by others that maintenance of the Golgi apparatus is crucial for ATGL-to-LD delivery and its fragmentation due to a lack of one of the proteins partitioning in cargo sorting, namely, GRASP55, results in LD accumulation in the mouse small intestine and reduced lipid absorption (137). We tested whether, analogically, PKD2 deficiency leads to the Golgi apparatus dispersal that could potentially explain a default ATGL trafficking. We took advantage of TEM images of intestinal epithelia used for LD and CM assessment, and we analyzed Golgi apparatus morphology at higher magnification. Under basal, unstimulated conditions, the Golgi apparatus appeared morphologically unaltered, and the number of cisternae was not affected by deletion of PKD2 (Fig. 41 A and B). However, upon the olive oil challenge, the Golgi apparatus in enterocytes from control animals remained well organized, compact, flattened, and tightly stacked. In contrast, in the absence of PKD2, the Golgi apparatus appeared more dilated, irregular, and displayed a tubular-vesicular organization. Moreover, the Golgi apparatus was less stacked in PKD2-deficient enterocytes, and fewer cisternae could be detected per unit area of the Golgi apparatus (Fig. 41 C and D).

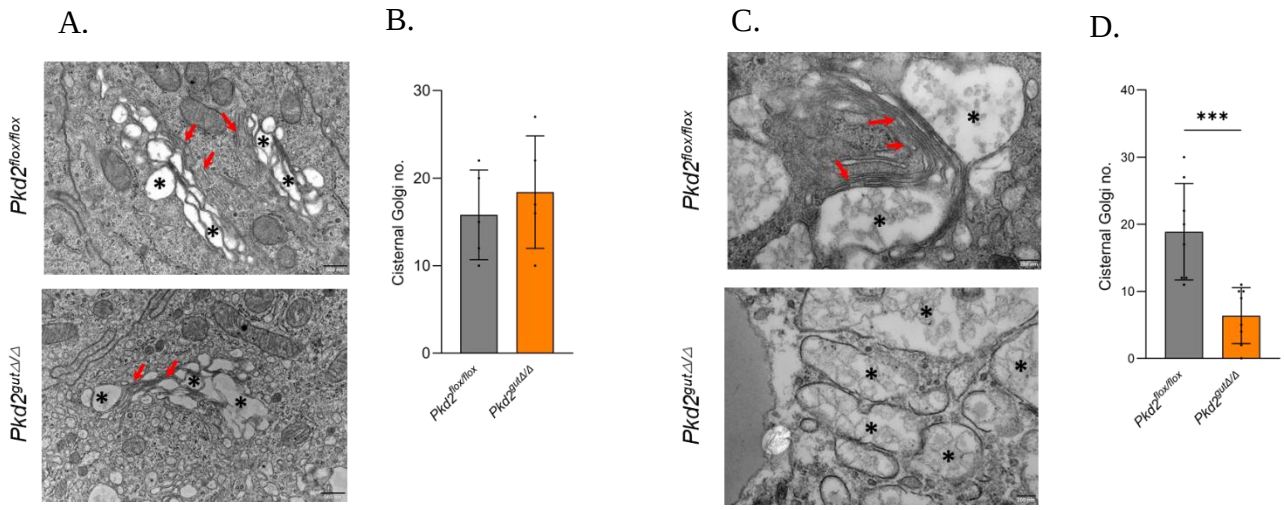

Fig. 41. Golgi apparatus in *Pkd2*$^{gut\Delta/\Delta}$ enterocytes lacks typical, cisternal structure. Representative TEM images of intestinal epithelial cells enlarged at the Golgi apparatus and isolated from *Pkd2*$^{flox/flox}$ or *Pkd2*$^{gut\Delta/\Delta}$ mice after (**A**) 16 h of food withdrawal or at (**C**) 8 h after intragastric olive oil gavage. Red arrorws indicate stacks of Golgi cisternae and black asterisks – Golgi-derived vesicles. Panel **B** and **D** show the quantification of Golgi apparatus with present stacks of cisternae at either 16 h of fasting or at 8 h after olive oil gavage, respectively. Golgi apparatus were quantified in 13-20 cells per mouse and 4 – 5 mice per genotype were used for experiment; each dot represents a summed number of Golgi apparatus per mouse. Scale bar is 500 nm, data represent mean ± SD, *** p <0.001 by Mann-Whitney test

Further, Golgi morphology was evaluated by immunofluorescent staining of Syntaxin 6, a TGN-specific marker, in 2D monolayers derived from *Pkd2*$^{flox/flox}$ or *Pkd2*$^{gut\Delta/\Delta}$ intestinal organoids. In *Pkd2*$^{flox/flox}$ enterocytes, Syntaxin 6 revealed a compacted, arched pattern concentrated around the nucleus, while in *Pkd2*$^{gut\Delta/\Delta}$ an overall signal intensity was lower and dispersed throughout the cytosol (Fig. 42), confirming thereby a grand role of PKD2 in maintenance of the Golgi apparatus architecture in enterocytes of murine small intestine.

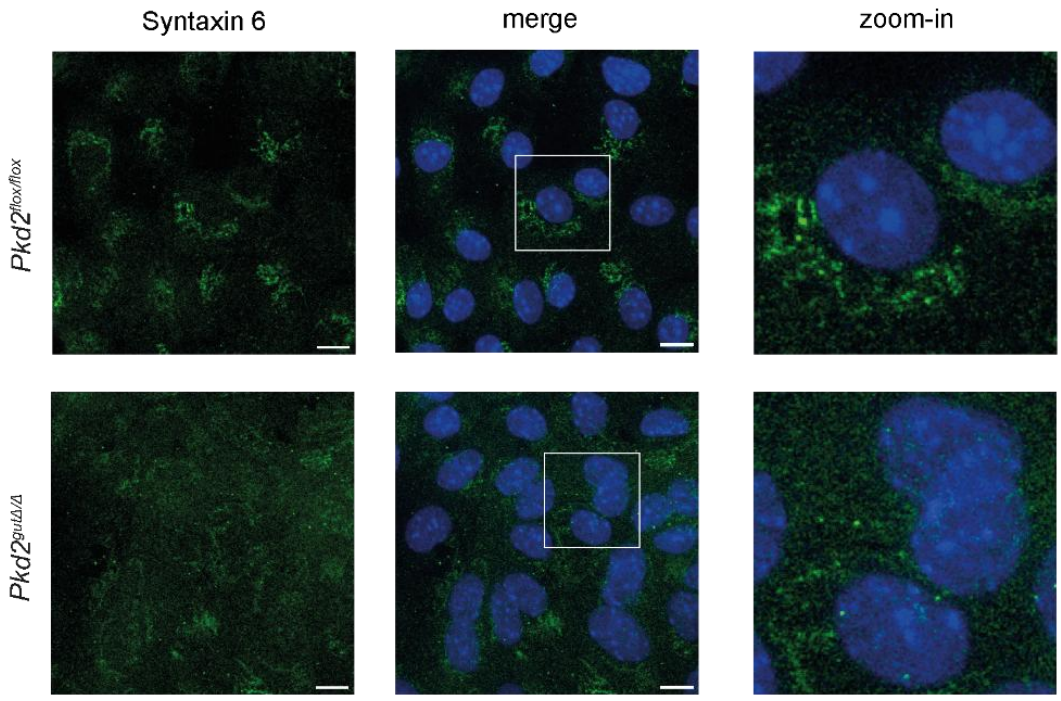

Fig. 42. Immunofluorescence staining reveals disrupted morphology of the Golgi apparatus in organoid-derived enterocytes. Representative immunofluorescent images of 2D monolayers derived from *Pkd2*$^{flox/flox}$ or *Pkd2*$^{gut\Delta/\Delta}$ intestinal organoids, enterocyte-differentiated and stained against Syntaxin 6 (in green); nuclei are in blue, stained with DAPI. Scale bar is 5 µm.

Analogically, we visualised the *trans*-Golgi network in Caco-2 cells using anti-transgolgin 46 (TGN46) antibody which revealed substantial difference in staining pattern. In Caco-2 *shScr* the signal appeared as dotted, strongly concentrated around the cell nucleus, while in *shPkd2* its overall intensity was lower and less nucleus-centered (Fig. 43). That is another feature linking *in vitro* and *in vivo* model, determined, likely, by PKD2 function exclusively and not affected by environmental cues.

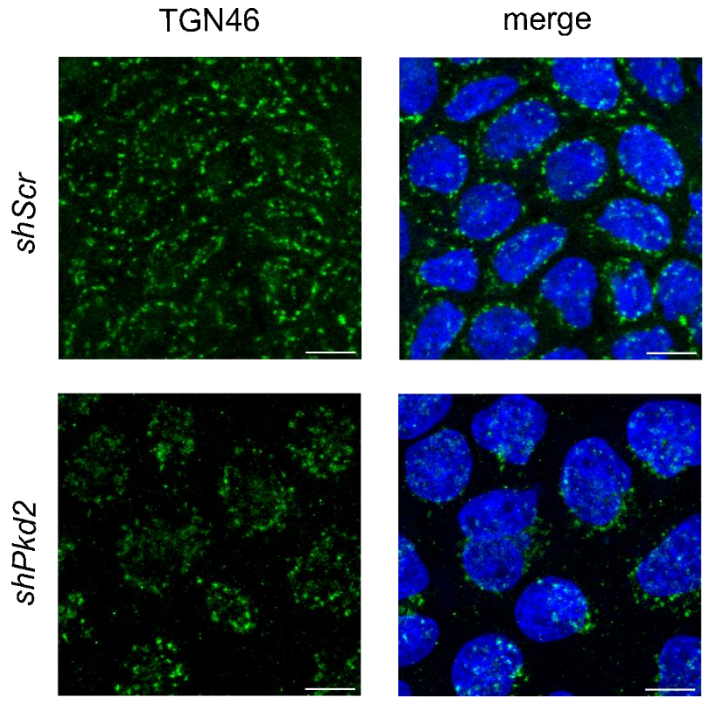

.

Fig. 43. PKD2 deficiency distorts Golgi apparatus structure in Caco-2 cells. Representative immunofluorescent images of *shScr* and *shPkd2* Caco-2 cells stained with anti-TGN46 antibody (green) as a *trans*-Golgi network marker, depicting morphological organelle aberration. Nuclei are in blue, stained with DAPI. Scale bar is 10 µm.

Identification of Golgi-specific proteins within the LD fraction and at higher levels in *Pkd2*$^{flox/flox}$ specimens compared to *Pkd2*$^{gut\Delta/\Delta}$ previously in subcellular fractionation experiments (Fig. 40) prompted us to also look more closely at LD-Golgi contact sites. Although generally less described than ER-LD contacts, the Golgi-LD contacts were proven to be involved in efficient lipid homeostasis and in the secretion pathway of VLDL (186), with increasing organelle contact numbers under stimulated conditions like oleic acid (OA) treatment (186). So far, barely a few proteins have been described to maintain LD-Golgi contact sites specifically, such as Rab2 or VPS13B (186,187). By quantification of LD-Golgi contact sites, we aimed to determine if PKD2 could be another candidate as a tethering protein.

A.

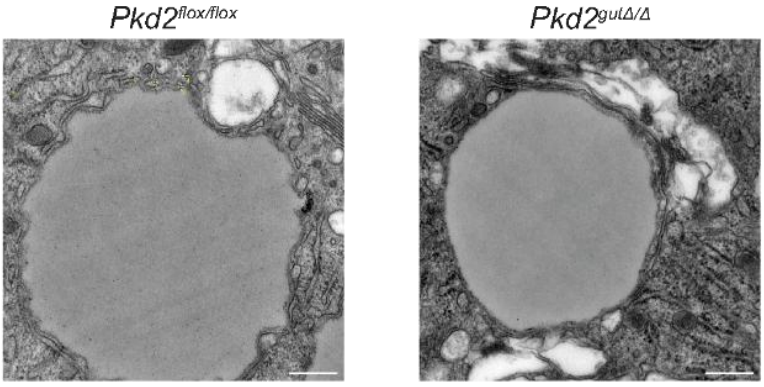

B.

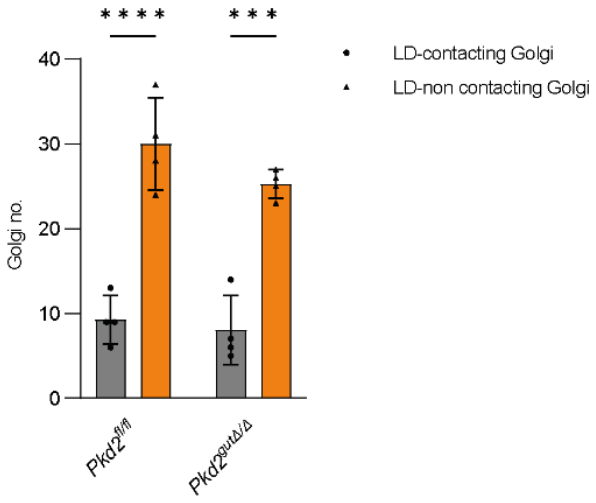

Fig. 44. LD-Golgi contact sites number are not affected by the lack of PKD2 in mouse enterocytes. A. Representative TEM images showing LD surrounded by Golgi cisternae in enterocytes of mouse jejunum, collected 8 h after olive oil gavage, scale bar is 1 µm.

B. Quantification of Golgi apparatus contacting with LD (grey) and distanced from LD (orange). N = 4 mice per genotype, in each mouse Golgi were quantified in 22-25 cells, each dot represents a total count from one animal. Data represent mean ± SD, *** p <0.001, **** p <0.0001by Mann-Whitney test.

We analyzed a set of TEM images of mouse epithelia taken at the 8 h time point after oil gavage (Fig. 44) and quantified both the number of Golgi apparatus contacting with LD and the distanced from LD. As expected, the Golgi count not contacting with LD was in the majority (in both genotypes), we did not find, however, that PKD2 deficiency would diminish the Golgi-LD contact sites (Fig. 44 B). Although our data do not support the idea that PKD2 might be a candidate as a tethering protein for LD-Golgi contacts, it should be noted that for clearer statements, a wider time lapse (i.e., different time points after olive oil gavage or upon exposure to feeding with HFD) analysis should be carried out, especially knowing the organelles' dynamics.

PKD2 deficiency contributes to reduced ATGL lipolytic activity

ATGL acquires its enzymatic competency throughout the trafficking route from the ER, via Golgi to LD, and finally, its activity is regulated directly on the LD coat via posttranslational modifications, for instance, via AMPK-mediated phosphorylation at Ser406, which increases ATGL activity (188). We sought to determine if altered ATGL subcellular localization due to the lack of PKD2 is also associated with a difference in enzymatic activity. To this end, we measured lipase activity *in vitro* using protein extracts from jejunal scratches of fasted $Pkd2^{wt/wt}$ and $Pkd2^{ki/ki}$ animals. A drawback of that assay is the measurement of total lipase activity, to extract ATGL activity levels from the readout, an ATGL-specific inhibitor, Atglistatin, was included. As shown in Fig. 30 A and B, total lipase activity was significantly lower in extracts from $Pkd2^{ki/ki}$ mice, and it is likely that this reduction results from impaired ATGL competence, since while preincubation of protein extracts with Atglistatin in $Pkd2^{wt/wt}$ led to activity decrease, it did not further reduce the lipase activity levels in $Pkd2^{ki/ki}$. We partially reproduced

these data in an assay performed with protein extracts from fasted *Pkd2*$^{flox/flox}$ and *Pkd2*$^{gut\Delta/\Delta}$, namely, Atglistatin reduced lipase activity in *Pkd2*$^{flox/flox,}$ while no significant drop was found in *Pkd2*$^{gut\Delta/\Delta}$. Only a slight, statistically non-significant reduction in activity of *Pkd2*$^{gut\Delta/\Delta}$, was recorded, however, in basal conditions. A different model used might be associated with a slightly different mechanism of ATGL activity impairment, moreover, uncontrollable variations prior to experiment (e.g. slightly different housing conditions, satiety levels) could have also contributed to the obtained difference in basal conditions.

Since no other inhibitors of particular lipases were used in the assay, it cannot be excluded that altered activity of different enzymes have a part in the overall decrease in lipase capacity upon PKD2 inactivation. One other drawback of the applied approach is the fact that lipase activity is measured without a context of subcellular localization, i.e., with proteins released from the organelles, the spatial functionality cannot be described with that method. We postulate, however, that PKD2 deficiency has a negative impact on ATGL activity, but to gain a more precise perspective regarding that aspect, analogous assays performed with isolated organelles (crucially LD, ER, or Golgi) should be carried out (189).

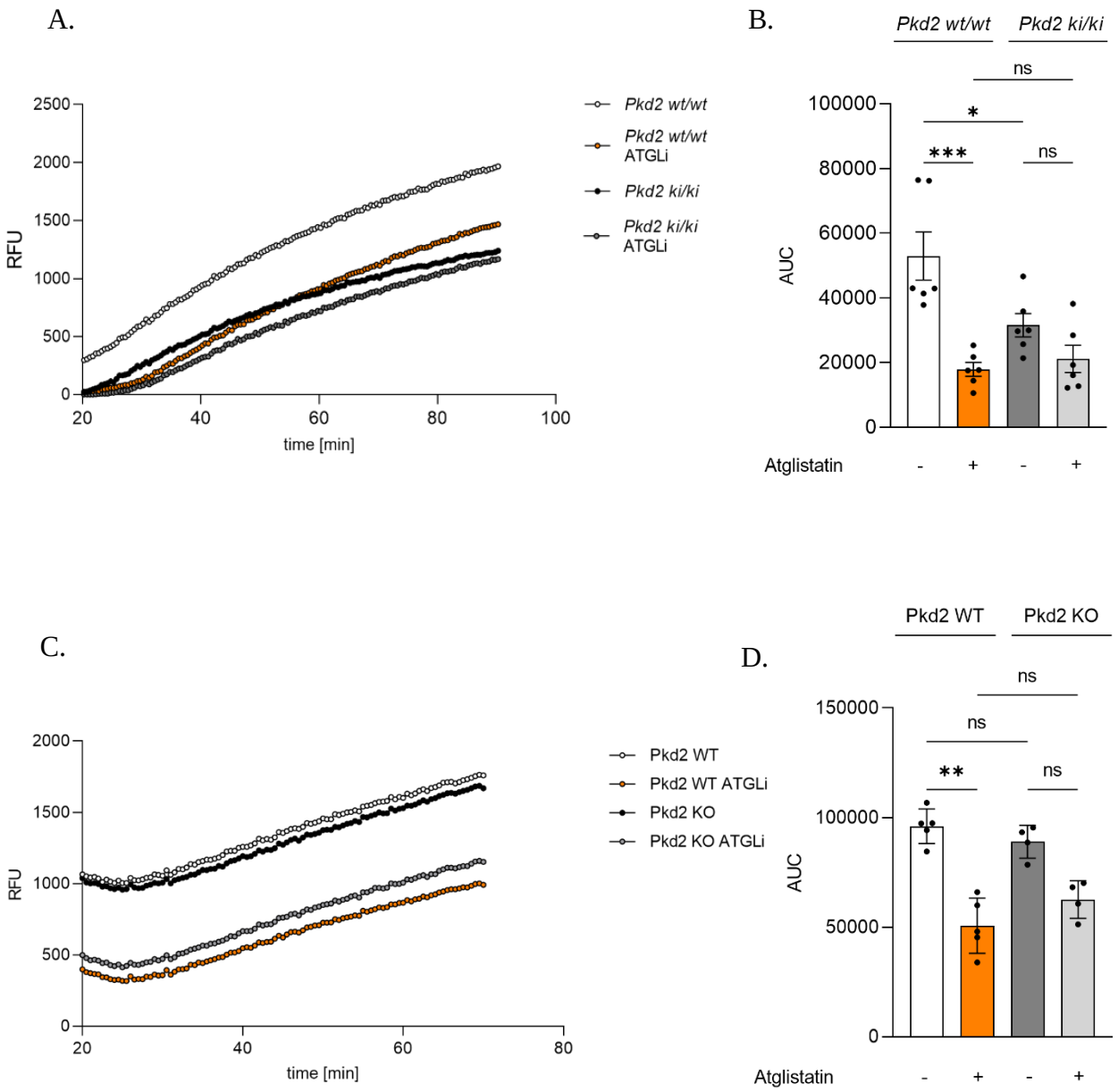

Fig. 45. **Lipase activity is reduced in intestinal epithelium of *Pkd2*$^{gut\Delta/\Delta}$ mice.** A. Readout of lipase activity, expressed in relative fluorescence units (RFU) in jejunal protein extracts from *Pkd2*$^{wt/wt}$ and *Pkd2*$^{ki/ki}$ animals and C. in *Pkd2*$^{flox/flox}$ (Pkd2 WT) and *Pkd2*$^{gut\Delta/\Delta}$ (Pkd2 KO) mice. To block ATGL activity specifically, Atglistatin (ATGLi) at 50 µM concentration was added to lysate 30 min prior the start of an assay. B and C panels represent the quantification of area under the curve from an assay shown on A. and C., respectively, *n* = 4 mice per genotype, data represent mean ± SD. *Ns* – non significant, **p<0.05,**p<0.01, ***p<0.001 by Mann-Whitney test.*

Lipase activity was also evaluated with an in vitro model of Caco-2 cells. Silencing of PKD2 in these cells by shRNA resulted in a reduction of recorded readouts; however, since no human ATGL-specific inhibitor is commercially available (Atglistatin exerts inhibitory affinity towards murine ATGL), only the total lipase activity was compared between *shScr* and *shPkd2* Caco-2. Similar to the previous model, a significant reduction in activity was found in lysates from PKD2-depleted cells (Fig. 46). Again, despite a range of dissimilarities between *in vitro* and *in vivo* set-up, this result indicates that impaired ATGL-mediated lipolysis is another common point between these two models.

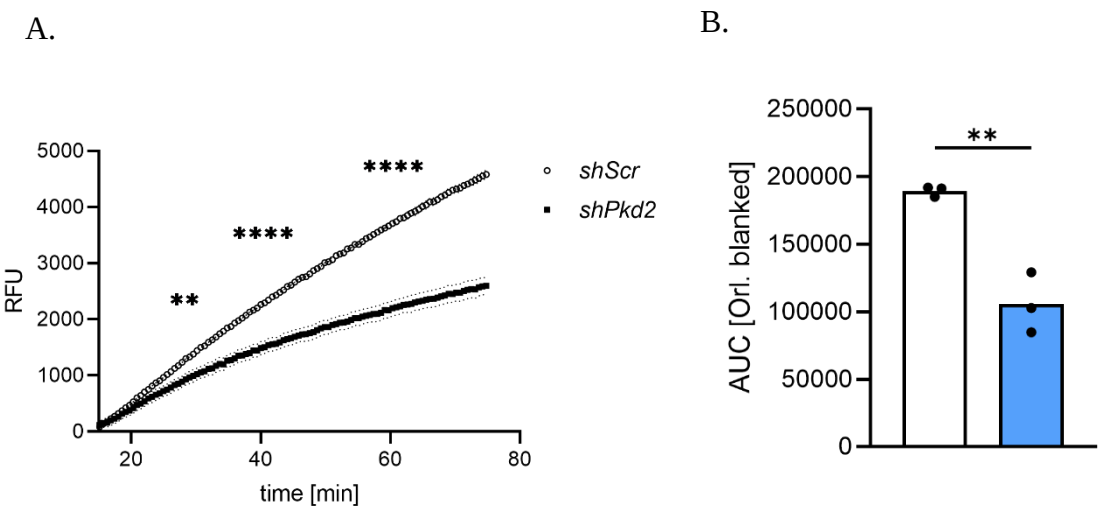

Fig. 46. **PKD2 deficiency decreases lipase activity in Caco-2 cells.** A readout of lipase activity, expressed in relative fluorescence units (RFU) in protein extracts from *shScr* and *shPkd2* Caco-2 cell lysates. Asterisks indicate at statistically significant difference at 30, 40 and 60 min time points of an assay. B. A graph of area under the curve quantified from, as a blank for the readout, the values from cells treated with Orlistat to inhibit the activity of all lipases were used '[Orl. Blanked]'. *n* = 3 biological replicates, ***p<0.01, ****p<0.0001 by Mann-Whitney test.*

LD are enlarged in *Pkd2*$^{gut\Delta/\Delta}$ enterocytes due to impaired ATGL-mediated lipolysis

To test directly if increased LD size in PKD2-depleted enterocytes is due to inefficient ATGL-mediated LD catabolism, we monitored LD turnover by confocal imaging in apical-out, enterocyte-differentiated organoids derived from *Pkd2*$^{flox/flox}$ and *Pkd2*$^{gut\Delta/\Delta}$ mice, treated with oleic acid (OA) or OA and Atglistatin. As expected, LD content was significantly elevated in *Pkd2*$^{gut\Delta/\Delta}$ organoids incubated with OA) for 16 h, but also under basal conditions in control medium (Ctrl) (Fig. 47 A, B). While the addition of Atglistatin to *Pkd2*$^{flox/flox}$ organoids, together with OA stimulation, resulted in significant LD accumulation, it had no further impact on LD abundance in *Pkd2*$^{gut\Delta/\Delta}$ compared to OA treatment alone. These data, together with previous findings, strongly indicate a key role of impaired ATGL-mediated LD catabolism in shaping the phenotype of increased LD size in PKD2-deficient enterocytes.

A.

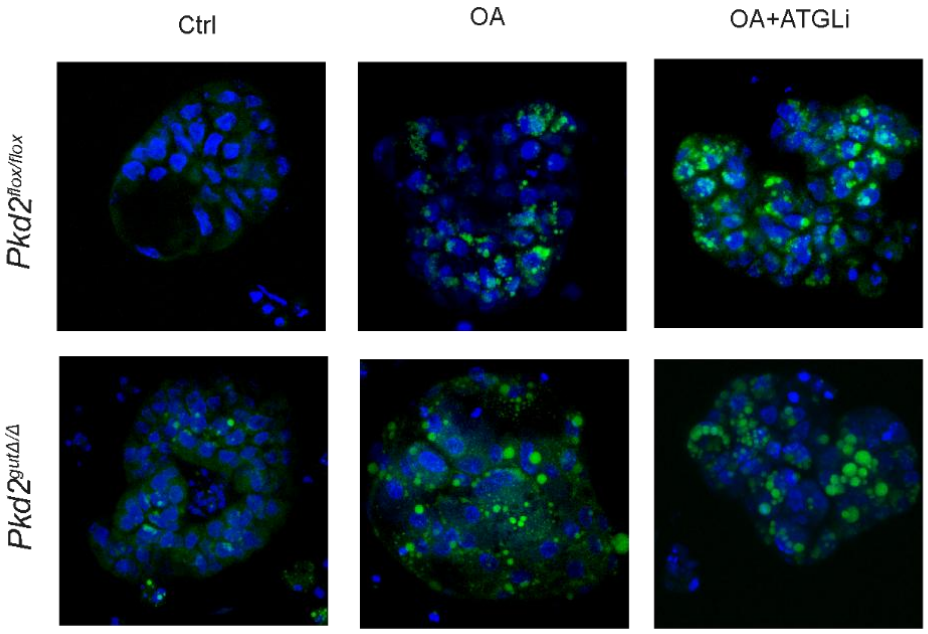

B.

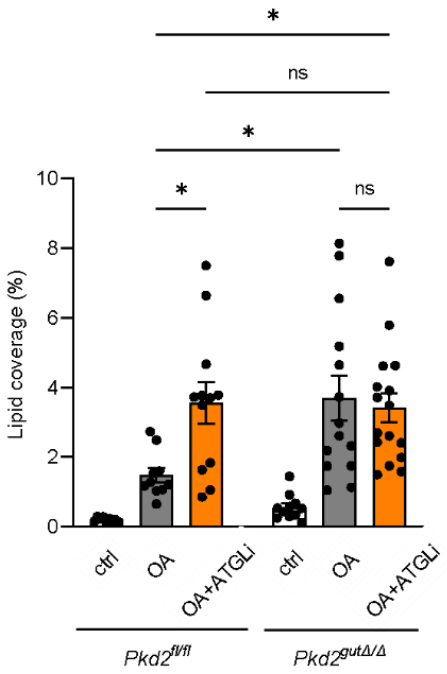

Fig. 47. A. Representative immunofluorescent images of enteroids isolated from *Pkd2*$^{fl/fl}$ and *Pkd2*$^{gut\Delta/\Delta}$ mice and maintained in control medium (Ctrl) or additonally treated with oleic acid (OA; 16 h, 200 µM) or OA with Atglistatin (OA+ATGLi; 16 h, 50 µM) showing LD in green (LipidTox) and nuclei in blue (DAPI). B. Quantification of percentage of lipid droplet content per organoid (relative to DAPI), n = 12 organoids per condition from three independent experiments. Ns – non significant, **p<0.05 by Mann-Whitney test*

DISCUSSION

Maintenance of lipid homeostasis in the gut is increasingly recognized not only as a determinant of lipid absorption efficiency but also considered in the context of disorders of intestinal tissue itself, such as IBD or cancer transformation. Better understanding of mechanisms coordinating lipid handling in this organ may therefore help to develop novel anti-obesity therapeutic strategies and reduce the burden of lipid accumulation-triggered conditions. Given the dichotomic nature of lipid handling in the intestine, i.e. secretory function via chylomicron synthesis and fat storage in LD, it is also of particular interest to identify the molecular switches that combine these two pathways.

Our previous study clearly identified PKD2 as a novel player promoting intestinal fat absorption via increasing the size of secreted chylomicrons that can be targeted to combat obesity (ref) and here, we complement these findings by uncovering the role of PKD2 in maintenance of LD homeostasis in the gut. We identified, using several techniques, that PKD2 deficiency leads to a massive LD accumulation in enterocytes caused, at least to certain extent, by default ATGL-mediated lipolysis. In parallel we show that thi key lipase, ATGL, is physiologically subjected to degradation in the intestine after dietary fat ingestion. The presented work may therefore serve as a complimentary in a better understanding of mechanisms dictating lipid homeostasis in the gut. The data obtained prompt to ask multiple following next questions, while other raise certain concerns – which altogether are a matter of discussion below.

One of the missing points and a solid direction to investigate is to quantitatively define whether the phenotype of PKD2-depleted enterocytes relies on a simple lipid redistribution from secretion towards storage. There are available literature data with the use of mouse genetic models, proving the existence of such a switch. For instance, in *Grasp55*−/− mice, which exhibit fewer chylomicrons and abnormally large intestinal lipid droplets following acute lipid challenge (137). Of note, GRASP55 is a Golgi apparatus-associated protein, defining the organelle architecture, similary as PKD2 does. Moreover, *Cideb* deficiency impairs CM lipidation, decreases lipoprotein secretion, and increases lipid retention in enterocytes (62). Conceptually similar data come from studies in liver which also shares a role of lipid secreting (as VLDL) and storing organ. *Cideb*-null mice exhibit reduced secretion VLDL together with increased hepatic LD accumulation, whereas hepatocyte-specific LAP1 or torsinA deficiency

causes defective VLDL secretion accompanied by hepatic steatosis and LD accumulation (194,195).

Although the net lipid output is markedly reduced in the absence of PKD2 with concomitant LD accumulation in the epithelial cells, our TEM data reveal that *Pkd2*$^{gut\Delta/\Delta}$ intestines are abundant in CM, which are, however, stacked in the intercellular spaces. That may suggest that PKD2 does not affect CM synthesis alone but is somewhat involved in post-synthesis-associated steps in CM export, which unravels – to our best knowledge – a previously not-described kind of phenotype. For that reason, it would require a quantitative approach in which TG incorporated into CM are separated from those LD-derived and compared between *Pkd2*$^{flox/flox}$ and *Pkd2*$^{gut\Delta/\Delta}$ animals. With our current data, we cannot state whether PKD2 defines the partitioning of absorbed dietary fats between secretion and storage. It is also possible that CM and LD-associated phenotypes are two independent scenarios, regulated by distinct functions of PKD2 in the cell. Hypothetically, selective depletion of LD in *Pkd2*$^{gut\Delta/\Delta}$ (e.g., via *Seipin* silencing in the gut) followed by measurement of lipid secretion as CM would help to, at least indirectly, clarify that issue.

We proved that reduced ATGL-governed lipolysis is largely responsible for increased LD size upon PKD2 deficiency in Atglistatin-treated organoids experiment. We did not focus, however, on the potential involvement of other lipases (such as HSL, MGL, CES2 or LAL) in shaping that phenotype. Especially, examination of HSL functionality would be valuable given that this lipase expression pattern shared certain similarities with ATGL behaviour in enterocytes of *Pkd2*$^{gut\Delta/\Delta}$ mice (i.e., resistance to degradation, impaired trafficking to LD). Given the rate-limiting role of ATGL in lipolysis performance, it is plausible to claim that declined function of that particular lipase plays a pivotal role in favouring LD storage upon PKD2 ablation. For a full perspective, however, a lipophagic degradation of LD should be evaluated in studied model as well. Data concerning the stimulatory influence of nutrient absorption on lipophagy in the gut are in scarce (101), yet given the availability of LAL-specific inhibitor (Lalistat) that issue is relatively easy to dissect. Interestingly, in the small intestine, LAL deficiency is characterized by massive neutral-lipid accumulation in lamina propria macrophages, lipid malabsorption, reduced CM secretion, increased fecal lipid loss, and the presence of lipid-containing lysosomes in duodenal enterocytes, while selective enterocyte LAL deficiency alone does not reproduce the full intestinal phenotype, indicating that infiltrating macrophages are the major drivers (196).

One other aspect which has not been thoroughly evaluated by us in this study is the impact of PKD2 on LD biogenesis rate. We confronted with that subject only via measurement of mRNA expression levels of *de novo* lipogenesis- and LD synthesis-associated genes (such as *Acc*, *Scd1*, *Fasn*, *Mgat2*, *Dgat1*, *Dgat2*, *Seipin*) while not-identyfying a significant differences between the genotypes, it does not allow us to draw any statements regarding PKD2 role in LD synthesis. It was shown that enhanced lipid synthesis appears sufficient to promote LD accumulation in vivo, by liver-specific overexpression of active SREBP-1c, which induces hepatic lipogenesis and LD deposition (197), and by hepatic DGAT2 overexpression, which drives severe hepatic steatosis (198). Interestingly, intestinal overexpression of DGAT2 was reported to increase intestinal TG secretion while leaving enterocyte TG accumulation similar to control animals (199). In fact, for the purpose of our study, the measurement of MGAT2, DGAT1 or DGAT2 enzymes abundance or activity would be rather non-feasible given an overlapping function of these enzymes in TG resynthesis that are designated for both, CM and LD formation. More informative would be, instead, to focus on relation between PKD2 and Seipin function and abundance, a protein that is uniquiely associated with LD synthesis.
Additionally, for a general overview of LD synthesis rate in the absence of PKD2, for example, an approach utilizing a synthetic construct termed LiveDrop, a marker of newly formed neutral lipid-poor LDs, based on the membrane-embedded hairpin motif from glycerol-3-phosphate acyltransferase 4 (GPAT4) linked to a fluorescent tag might be useful. (65).

By subcellular fractionation, we found that ATGL access to LD is restrained by the lack of PKD2 – which would logically explain a partial impairment of lipolysis. The trafficking pathway of ATGL, from protein synthesis till reaching LD surface, is well described (please see “Introduction; Lipolysis and lipases” chapter for more details). Maintenance of the Golgi apparatus structure and secretory function is essential in that process, since ATGL targeting to the LD surface appears to depend on early secretory trafficking machinery linked to that organelle. Specifically, ATGL delivery requires the GBF1-ARF1-COPI/COPII pathway, consistent with sorting at ER exit sites or the ER-Golgi intermediate compartment rather than classical trafficking through the entire Golgi stack (75). Direct binding between ATGL and GBF1 further supports a model in which Golgi-associated trafficking regulators participate in ATGL recruitment to LD (200). More recently, the Golgi has also been identified as a site of metabolic control over ATGL (182). A study from Liangong et al. shows that lipase activity is regulated within that organelle by a glucose-sensitive phosphatidylinositol 4-phosphate

(PtdIns4P)-CUL7-FBXW8 pathway; when intracellular glucose drops, Golgi PtdIns4P decreases, assembly of the CUL7-FBXW8 E3 ligase complex is reduced, ATGL polyubiquitylation in the Golgi declines, and ATGL-driven lipolysis is enhanced. (182).

PKD2 contributes to maintenance of Golgi apparatus function, but primarily by regulating secretory trafficking at the TGN. Mechanistically, ARF1 binds PKD2 and recruits it to the TGN, where PKD2 membrane association depends on both, ARF1 interaction and DAG-dependent anchoring, and this localization is required for post-Golgi protein transport (201). Beyond recruitment, PKD2 promotes assembly of an ARF1-ARL1-Arfaptin2 complex at the TGN that supports constitutive carrier formation and cargo secretion (202). PKD activity also influences Golgi morphology, as local activation of PKD accompanies nocodazole-induced Golgi fragmentation, whereas PKD inhibition or depletion preserves Golgi integrity under these conditions (203). ARF1 could be therefore a candidate protein joining ATGL stationing at the Golgi on its trafficking way towards LD with PKD2 function. That concept could be examined in the future via, e.g. immunofluorescent co-staining of these three proteins or protein co-immunoprecipitation. Our study is, according to our knowledge, the first reporting the role of PKD2 in Golgi apparatus Following the investigation around the Golgi is definitely supported by the visual proof (with TEM and IF staining) which we provide, i.e., altered organization of stacks of cisternae of the Golgi and to our knowledge, our study is the first reporting the relevance of PKD2 in structural organization of that subcellular compartment. Moreover, we identified the presence of PKD2 together with some Golgi-associated marker proteins within LD fraction. Intriguing in that context is also a study from Krahmer et al., demonstrating that in diet-induced fatty liver, proteins of the secretory pathway are extensively redistributed, the Golgi apparatus becomes closely associated with LD, together with redistribution of PKD3 and hepatic protein secretion is reduced (185). Quite similar phenotype to enterocyte PKD2-depleted mice, i.e. reduced chylomicron secretion, increased LD deposition in the intestine, structural reorganization of the Golgi and impaired delivery of ATGL to LD surface was already shown in *Grasp*$^{-/-}$ null mice (137), further supporting the idea of considering Golgi apparatus as a central organelle coordinating lipid secretion and storage in enterocytes of the small intestine.

Nevertheless, not Golgi-LD but ER-LD junctions are the organelle interfaces that now are rather recognized to mediate final protein exchange between the ER bilayer and the LD monolayer, although the complete molecular details remain unresolved (204). ER-associated regulators also influence ATGL residence at LDs, because the ER and LD protein , UBXD8, and the ER-

resident factor UBAC2 control UBXD8 partitioning to LDs, where UBXD8 can bind ATGL, recruit p97/VCP, and alter ATGL-CGI-58 interactions (183). The morpholohy or trafficking efficiency in that cellular compartment has not been evaluated by us, which should be complemented as an alternative protein trafficking default explanation. Our data from experiments evaluating ATGL activity in vitro suggest that lipase enzymatic competency is also hampered by PKD2 deficiency. That is in line with a current understanding of ATGL activity acquisition which is largely associated with protein localization at the LDs and via direct co-activation by CGI-58, whereas phosphorylation (such as of Thr372 in the C-terminal hydrophobic region) and inhibitory proteins such as G0S2 or HILPDA modulate the extent of lipase activity rather than serving as the sole activating switch (205–207). With approach that we used in this work, lipase activity is measured without an organelle interaction context (all cellular membranes are solubilized and the protein is free). Ideally would be to compare ATGL activity probed with isolated LDs with intact proteomes, collected from *Pkd2*$^{flox/flox}$ and *Pkd2*$^{gut\Delta/\Delta}$ mouse intestines, a method which was described by Schweiger et al. (189) and which would bring a direct insight on lipolysis performance upon PKD2 deficiency. Another aspect which should be examined is whether PKD2 affects the process of ATGL protein translation or – what is even more likely if considering PKD2 as a kinase – its posttranslational modification, such as phosphorylation and thereby influences ATGL activity. We did not verify if ATGL is a direct phosphorylation substrate of PKD2, however it a is possible direction to follow as ATGL contains a phosphorylation motif recognized by PKD2 (i.e., RxxS/T which is Ser404).

Consistently between all tested models (mouse, intestinal organoids, Caco-2 cells) we observed an activation of PKD2 after treatment with olive oil (in vivo) or oleic acid (in vitro). It is clear that lipid signalling is essential for PKD2 activation (phosphorylation), as was already broadly described in the ‘Introduction’, but briefly, that is executed primarily through recruitment to DAG-enriched membranes, especially at TGN. It was not explored if FA uptake-induced activation of PKD2 is also dependent on DAG, presumably synthesized *de novo* from taken up external substrate, relies on a direct kinase activation by FA intracellularly, or is mediated via cell-surface embedded receptor binding FA and participating in signal transduction. Once identifying the mechanism of PKD2 activation pathway, it would be interesting to determine if that rapid response is required to exert the kinase role in chylomicron synthesis/secretion and LD homeostasis. This could be also verified by short-term blockage of PKD2, via administering a PKD inhibitor such as CRT0066101.

To sum up that part of the study, we uncover a novel function of PKD2 in maintenance of intestinal lipid homeostasis via regulation of LD lipolytic degradation, while kinase deficiency leads to enlarged LD size. That is observed under acute challenge with dietary lipids (olive oil gavage) and chronic fat exposure of the intestine (feeding with HFD), but not during fasting, suggesting that a certain stress of the intestine caused by externally-derived lipids is required to reveal altered LD morphology. At least partial mechanistic explanation for that phenotype is hampered access of ATGL to LD surface which is likely to be caused by fragmentation of the Golgi apparatus. Complementary to our previous study showing a promoting role of PKD2 in CM secretion, are the data presented here, suggesting that PKD2 might be rather releveant for post-synthesis steps in CM trafficking, according to observed a vast lipoprotein accumulation uder lamina propria, in the extracellular space.

In a second part, we describe a physiological event of a targeted degradation of ATGL, presumably also HSL, evoked by ingestion of dietary fats in the epithelium of small intestine. PKD2 seem to play a permissive function for that event as kinase deficiency prevents the degradation. Moreover, independently of PKD2 presence, we found that lipid intake evokes a robust remodeling of the proteome in small intestine, with clusters of proteins being either significantly upregulated or downregulated. Physiological releveance of our finfings has been further supported by analogical observations during refeeding with high-fat, but not fat-free diet in wild-type animals. The specificity of that reaction to ingestion of lipids, but not other nutrients, suggests that ATGL degradation is not associated with a general improvement of energetic status in the cell but rather a lipid-unique metabolic reorganization of enterocyte.

Nutrients availability is well described to shape the proteome stability, where, in general, a high energetic status activates mTORC1 signaling and suppresses autophagy, whereas nutrient or energy deprivation inhibits mTORC1 and activates AMPK, thereby stimulating autophagic degradation of intracellular constituents to preserve metabolic homeostasis (208,209). In parallel, nutrient-responsive ubiquitination selectively modulates the turnover of transporters, transcription factors, and signaling proteins, allowing rapid remodeling of the proteome in response to nutrient stress (210). Amino acids are among the strongest nutrient regulators of both bulk autophagy and selective proteasomal proteolysis, with leucine being a particularly prominent anti-proteolytic signal (211,212). Low glucose/energy activates AMPK-linked catabolism and generally promotes autophagy, while glucose refeeding can trigger selective degradation programs (209,213). Fatty acids differentially regulate autophagy depending on th

lipid species and can also promote proteasomal degradation of lipogenic enzymes such as fatty acid synthase (214,215). By contrast, cholesterol provides a example of nutrient-sensitive protein stability control, as sterol depletion promotes proteasomal degradation of INSIG1 (an ER-resident protein involved in cholesterol metabolism) and activates autophagy, whereas sterol abundance stabilizes INSIG1 and restrains SREBP signaling (216–219). Oleic acid, a fatty acids which seem to be at least one secure ATGL-degradation inducer, was also shown to mediate protein degradation. In macrophages, *cis*-isomer of oleic acid triggers a degradation of cholesterol transporter ABCA1, which results in decreased ABCA1-mediated cholesterol efflux to apoA-I enriched particles, while its isomer *trans* – elaidic acid stabilizes ABCA1 (220). It would be interesting to determine if such *cis* versus *trans* variability also applies to our model, especially given that increased consumption of *trans* fatty acids that are present in hydrogenated vegetable oils (such as margarin) is associated with increased atherogenic plaques formation and cardiovascular risk, while forms *cis*, including oleic acid, exert opposite functions and act anti-iflammatory. Worth noting is also a fact that the impact of lipid intake on ATGL protein abundance is associated with an opposite trend regarding mRNA expression levels of *Pnpla2*, which suggests a post-translational regulation and that transcript abundance cannot serve to predict protein output for this gene under these conditions.

Effective blockage of ATGL removal after administering respective inhibitors of UPS and autophagy – MG132 and Bafilomycin A1 suggests that activity of both mechanisms is needed to evoke the loss of ATGL. In fact, UPS and autophagy are functionally interconnected components of one cellular proteostasis network (221), therefore our findings should not be considered as contradictory. The crosstalk of these pathways is mediated partially by adaptor proteins such as SQSTM1/p62, which bind ubiquitinated cargo and facilitate its delivery to the autophagic machinery, while also influencing the turnover and accumulation of ubiquitinated proteins more broadly (222).

Importantly, several proteins have been shown to undergo degradation through both autophagy and the UPS, proving that the contribution of each pathway depends on substrate conformation, aggregation state, and cellular context. One well-established example is α-synuclein, which can be degraded by both autophagy and the proteasome, with autophagy becoming especially important when the protein accumulates in more aggregation-prone forms (223). Tau protein provides another example of dual pathway usage, as both proteasomal and autophagic mechanisms contribute to its turnover, with some specific tau species displaying a preferential

routing to one system. Of note, caspase-cleaved tau appears to rely more strongly on autophagic degradation than full-length tau (224,225).

The functional relationship between these pathways is further illustrated by the fact that one degradative system can directly regulate the other. Under conditions of cellular stress, proteasomes themselves may become ubiquitinated and selectively degraded through p62-dependent autophagy, which is known as proteaphagy (226). Additionally, HIF-1α, a protein classically recognized as a proteasomal substrate, was also shown to be a subject of CMA in a STUB1/CHIP-dependent manner, demonstrating that even apparently conserved UPS substrates may be rerouted to autophagic pathways (227). Taken together, these findings support the concept that autophagy and the UPS operate as partially overlapping and coordinated degradation systems, with substrate partitioning determined by biochemical state and ubiquitin signaling (221,228). If both systems are engaged in protein degradation in sequence, then ubiquitination is a 'meeting-point' of both. MG132 which we used to hamper UPS, does not interfere with protein ubiquitination and blocks the final degradation step by inhibiting 20S proteasome subunit. A concomitant effective blockage of ATGL loss by Bafilomycin A1 treatment suggest rather that UPS and autophagy may target distinct pools of ATGL, for example, displaying different subcelllar localization, form (e.g., aggregated or not) or lipase activity status. Interesting is the fact that we showed by IF staining an accumulation of LC3 puncta colocalizing with ATGL in enterocytes of *Pkd2*$^{ki/ki}$ mice suggesting a blockage of autophagy-mediated clearance of lipase. Given that ATGL delivery to LD is partially determined by PKD2 it would be interesting to determine if that particular portion of ATGL, i.e. non-LD resident, avoids autophagy-mediated degradation specifically. Further, it should be determined how autophagy or UPS inhibition affect ATGL abundance in *Pkd2*$^{ki/ki}$ or *Pkd2*$^{gut\Delta/\Delta}$ animals with following olive oil gavage which would give an insight on which pathway exerts its functionality despite the lack of PKD2 and/or impaired ATGL localization/activity. There are litrature data supporting the hypothesis that subcellular localization strongly affects the susceptibility to degradation as it governs whether a protein can physically access proteasomes, autophagic membranes, lysosomes, and the compartment-specific ubiquitin ligases or cargo receptors that sort it into one pathway or the other (229,230). As a rule, soluble proteins in the cytosol and nucleus are more readily handled by the ubiquitin-proteasome system (UPS), whereas proteins trapped in aggregates, membranes, vesicles, or organelles are more often directed to autophagic or endolysosomal degradation routes (231–233). A spatial recognition regarding ATGL degradation and responsible pathway could be acquired via enterocyte ATGL co-staining with different organelles (LD, ER, Golgi,

lysosomes) after autophagy and UPS inhibition. In addition, it would be also interesting to find if autophagy-mediated ATGL removal is associated with lipophagy, if that event is triggered by lipid ingestion at all. One more direction worth considering is to determine if altered ATGL trafficking to LD results in a compensatory increase in activity of one of the degradation systems, using PKD2-deficient animals as a model.

An intriguing question that arises from our observations of ATGL degradation in response to dietary fat intake is what might be the physiological relevance of that cellular response. We consider that issue in the context of intestinal fat absorption and maintenance of intestinal epithelium homeostasis as well. Small intestine is an organ encountering a tremendous fluctuations in nutrients availability with each meal ingested. Enterocytes, being the first-line layer facing these variations, should be equipped in adaptative mechanisms allowing to ameliorate the resulting rapid changes in energetic status of the cell. Among the macronutrients (carbohydrates, lipids, protein) when consumed in excess, lipids pose the highest risk of toxicity, both on a whole-organism scale (mainly through hypertriglyceridemia-associated pancreatitis) (234) and on a cellular level (as free fatty acids), although *in vitro* it is most often modeled with palmitate, which commonly induces reduced viability, mitochondrial dysfunction, generation of reactive oxygen species, ER stress, ceramide accumulation, and apoptosis (190,235,236). We hypothesize that ATGL degradation might alleviate lipotoxicity risk occurring during intestinal fat absorption on a whole-body and enterocyte level.

Efficient TG resynthesis from taken up FFA after meal, followed by packaging into CM or LD can be already perceived as astrategies to limit the lipotoxicity risk since TG are neutral lipid form for cellular homeostasis. However, sustained lipolysis (governed by ATGL) would contribute to increased intracellular concentration of FFA while their influx from the gut lumen is poorly controllable (i.e., only partially mediated by membrane transporters but mostly – via passive diffusion). Rapid cutoff in delivery of FFA derived from lipolysis by degradation of ATGL could be therefore a preventive strategy. First, it could ameliorate the overall abundance of available FFA, resynthesized further into TG, incorporated into CM, thus reducing the risk of postprandial hipertriglycerydemia. Second, in the context of enterocyte function itself, ATGL degradation and resulting inhibition of LD catabolism could be perceived as a mechanism facilitating the physiologically occurring formation of LD after dietary fat intake. TG building-up the LD core are composed or a fatty acid mixture – and include both saturated long chain (SFA), mono- and polyunsaturated fatty acid species (PUFA). As already briefly

mentioned above, lipotoxic effects for the cell are primarily associated with elevated SFA concentrations. Particularly palmitate and stearate, elicit a classical lipotoxic response characterized by ER stress, mitochondrial dysfunction, accumulation of bioactive lipid intermediates, oxidative stress, inflammatory activation, and apoptotic cell death (237–240). By contrast, excessive exposure to PUFAs is detrimental primarily due to their high susceptibility to peroxidation, thereby promoting the formation of oxidized lipid species that destabilize membranes, impair mitochondrial function, damage DNA, and trigger apoptosis or ferroptosis under oxidation-promoting conditions (192,193,241,242).

Therefore, a quick reduction of lipolytic degradation of pre-existing LD in postprandial period, during enhanced FFA influx to enterocyte would ameliorate a broad spectrum of excessive FFA detrimental outcomes for the cell. To clarify if our hypotheses are valid, one should determine what are the consequences of impaired ATGL degradation, in the context of fat absorption and enterocyte functions or viability. To achieve this, a model or models of degradation-resistant ATGL are required. Although in PKD2-deficient animals ATGL escapes the degradation, it cannot serve as a model here, since enzyme's activity is abolished already at basal conditions. If indeed, UPS and autophagy govern ATGL degradation in parallel, these two pathways should be rendered separately. Proteasomal degradation could be stabilized via inactivation of degron, a signaling element that directs a protein towards degradation, in which point mutations or short deletions weaken or abolish the degron required for recruitment of the respective ubiquitin ligase, thereby prolonging protein half-life (243).
A second common strategy would be a mutation of key ubiquitin-acceptor lysines, by lysine-to-arginine substitution, especially if ATGL degradation would depend on a limited number of dominant lysine residues rather than on a highly redundant ubiquitination (244).
Resistance to autophagic degradation would need to be engineered according to the specific lysosomal pathway by which ATGL is selected (macroautophagy, CMA, microautophagy) since they rely on distinct recognition mechanisms (245). For selective macroautophagy, one rational strategy is to disrupt the interaction with ATG8-family proteins such as LC3 or GABARAP by mutating the core residues of the LC3-interacting region, since structural studies have established that LIR motifs function as sequence-specific docking modules required for efficient autophagic recruitment (246) and LIR motif has been identified in ATGL sequence (247). If ATGL is recognized by CMA the most direct strategy is mutation of the KFERQ-like targeting motif, as that motif is recognized by Hsc70 and required for delivery of the substrate to the lysosomal membrane (245,248). Since KFERQ-like motifs can also contribute to Hsc70-

dependent endosomal microautophagic targeting, manipulation of this sequence may suppress more than one lysosomal entry route simultaneously (245,248). From experimental point of view, the preferred strategy is not to abolish global proteostasis, but rather to introduce the smallest possible sequence change that selectively disrupts substrate recognition while preserving ATGL folding, subcellular localization, and biological activity (243,245). Ideally would be to generate a mouse model carrying a sequence of degradation-resistant ATGL specifically in the enterocytes of the small and subject those animals to olive oil gavage or HFD feeding. Particularly interesting would be to determine if the blockage of ATGL removal predisposes to post-prandial hipertriglycerydemia/hipercholesterolemia or increased chylomicron size or particle count, which may bring an insight into the role of lipolysis-derived FFA as chylomicron TG synthesis substrate. In a short term perspective, it would be also worth investigating if the lack of ATGL removal after FA uptake has any detrimental consequences for enterocyte homeostasis. We ask this question in the context of a previously hypothesized toxic impact of excessive SFA and PUFA for the cell. That could be determined by for example, measurement of ER stress markers (such as CHOP, ATF4, BiP proteins levels), apoptosis (by cleaved caspase 3 or annexin 5 staining) or ferroptosis markers via measurement of lipid peroxidation products concentration (such as malonodialdehyde or 4-hydroxynonenal). If constant ATGL activity indeed results in increased risk of epithelium injury, a following question would be how it translates into a regenerative potential of the tissue and therefore – the permeability of intestinal barier. Verification of these hypotheses could enrich our understanding of adaptative responses of intestinal epithelium and potentially may bridge in explanation of certain intestinal pathologies.

SUMMARY AND CONCLUSION

To sum up, the findings coming from this study can be subdivided into several, apparently interdependent scenarios, which eventually prove to be parts of one consistent mechanism. First of all, we showed that PKD2, in addition to playing an immense role in chylomicron-mediated fat absorption (52), is also a critical determinant of LD turnover in enterocytes of the small intestine. Intestine-specific deficiency or whole body inactivation of PKD2 results in accumulation of LD in mouse enterocytes or intestinal organoids. That is observed either upon acute oral challenge with dietary fat, such as olive oil, or during continuous feeding with HFD, thereby highlighting a required lipid overload stress of the intestine to reveal the phenotype. At least one mechanism standing behind that outcome is a deficit in LD catabolism, dependent on ATGL lipase function (Fig. 31). We show that delivery of ATGL, a key enzyme initiating TG breakdown, to the LD coat is largely impaired if PKD2 is not functional. In parallel, we observe that kinase deficiency causes a partial rupture of the Golgi apparatus, a hub for protein trafficking and maturation in the cell. ATGL transfer to LD is mediated by COPI complex, which involves the Golgi therefore, it is likely that the primary blockage site in the lipase transfer route and dependent on PKD2 is the Golgi apparatus.

Second, we found and partially characterized a physiological event of dietary fat absorption-induced degradation of ATGL, and likely, also HSL, in enterocytes of the mouse small intestine. We show that this event is specific to the intake of dietary fat but not other nutrients (i.e., carbohydrates, protein). We characterize certain determinants of ATGL loss, such as uptake of FFA by enterocytes, unaltered co-occurring chylomicron synthesis, or LD formation. Using proteomics, we identified that lipid intake is associated with a robust remodeling of the enterocyte proteome, not limited strictly to LD function. Our data suggest that ATGL degradation might be dependent on proteasomal and autophagic machineries (Fig. 32). PKD2 deficiency prevents ATGL loss, which we associate with altered subcellular localization of the enzyme.

A plethora of questions arise from our study, which offer at least a few directions for future investigations (Fig. 48 A, B, C). A major question concerns the physiological relevance of identified targeted protein degradation. One scenario we speculate is that it may serve as an FFA-overload protecting mechanism for a cell already encountering an influx of lipids derived

from a diet. Excessive presence of FFA in the cytosol poses a risk of lipotoxicity (190,191), while in addition, elevated polyunsaturated fatty acid (PUFA) abundance increases a risk of lipid peroxidation, membrane damage, and ultimate cell death via ferroptosis (192,193). Hierarchically, first stands a question of how the fatty acid uptake is translated into a signal towards ATGL lipase degradation and how it mediates PKD2 activation. Second, how does the correct, ie. LD-localization of ATGL determines the lipase susceptibility to degradation, which next prompts to ask about the role of PKD2 in degradation process. Another point is to determine the mechanism of ATGL proteolysis and experimental proposal is described earlier in 'Discussion'. Identification of degradation pathway to target this process and model the physiological consequences of lack of degradation is a leading aim of future studies.

A.

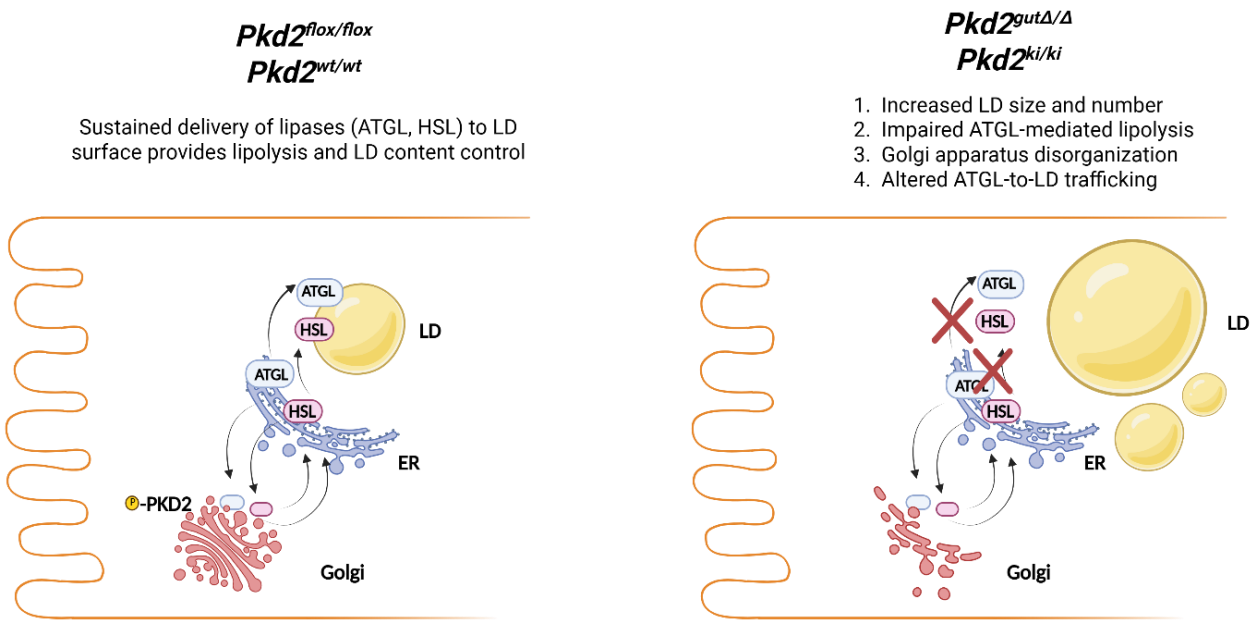

B.

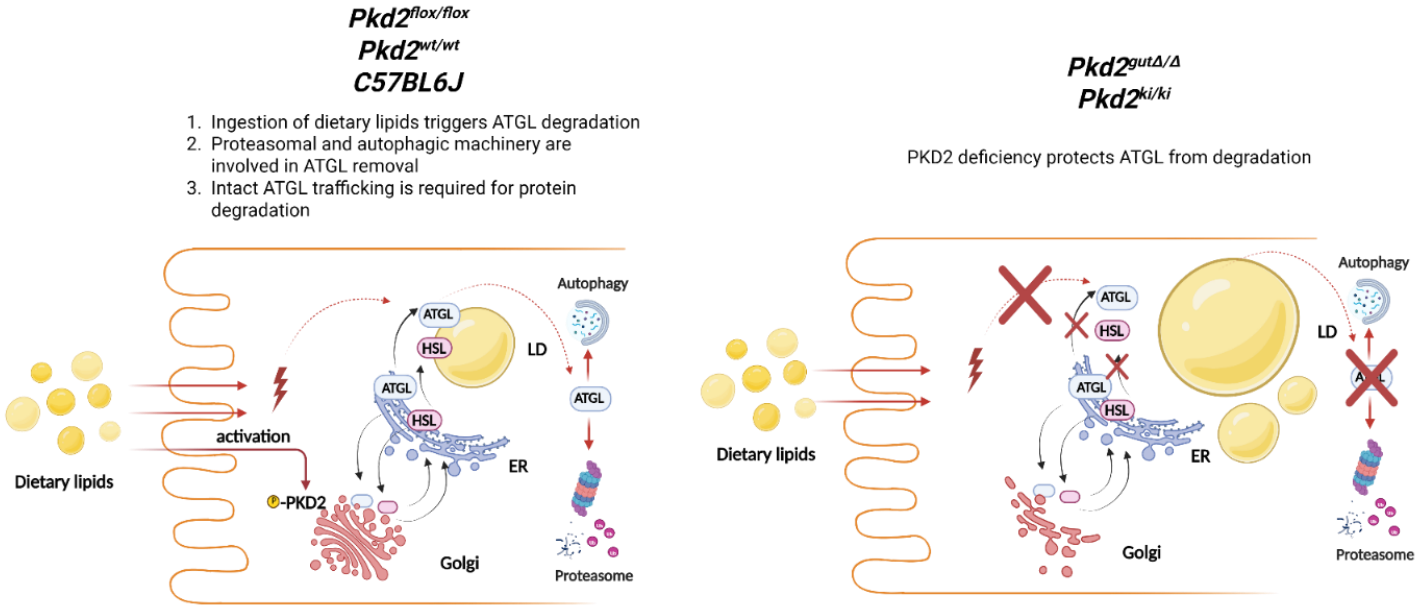

C.

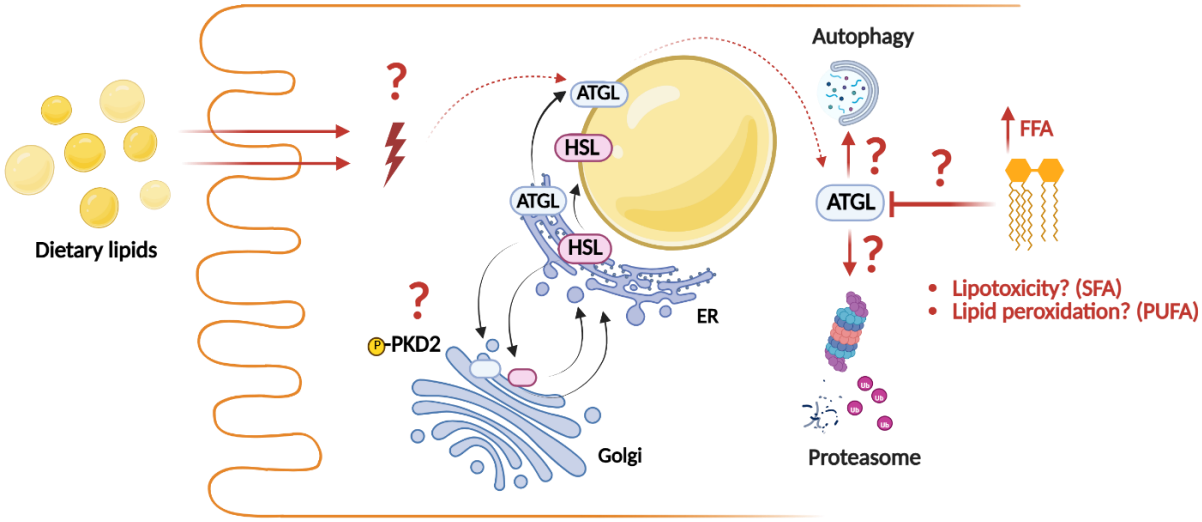

Fig. 48. Schematic summary depicting the role of PKD2 in maintenance of LD homeostasis in small intestine. A. A model summarizing the LD phenotype in PKD2-inactive or deficient enterocytes. B. A model joining the LD phenotype with independently

occurring ATGL degradation after dietary fat intake. C. A speculated model of cellular consequences upon the blockage of ATGL degradation. Figure created with BioRender.

BIBLIOGRAPHY

1. Liu H, Wang S, Wang J, Guo X, Song Y, Fu K, et al. Energy metabolism in health and diseases. Signal Transduct Target Ther. 2025 Jun;10(1). doi:10.1038/s41392-025-02141-x PubMed PMID: 39966374.
2. Vettor R, Vincenzo A Di, Maffei P, Rossato M. Regulation of energy intake and mechanisms of metabolic adaptation or maladaptation after caloric restriction. Rev Endocr Metab Disord. 2020 Jun;21(3):399–409. doi:10.1007/s11154-020-09565-6 PubMed PMID: 32451880.
3. Hall KD, Farooqi IS, Friedman JM, Klein S, Loos RJF, Mangelsdorf DJ, et al. The energy balance model of obesity: beyond calories in, calories out. American Journal of Clinical Nutrition. 2022 Jun;115(5):1243–54. doi:10.1093/ajcn/nqac031 PubMed PMID: 35134825.
4. Klingenspor M, Fromme T. Brown adipose tissue. Adipose Tissue Biology. 2012 Jun;39–69. doi:10.1007/978-1-4614-0965-6_3 PubMed PMID: 41817569.
5. Ogobuiro I, Tuma F. Physiology, Gastrointestinal. StatPearls. 2019. PubMed PMID: 30725788.
6. Shen L. Functional morphology of the gastrointestinal tract. Curr Top Microbiol Immunol. 2009;337(1):1–35. doi:10.1007/978-3-642-01846-6_1 PubMed PMID: 19812978.
7. Meerveld BGV, Johnson AC, Grundy D. Gastrointestinal physiology and function. Handb Exp Pharmacol. 2017 Jun;239. doi:10.1007/164_2016_118 PubMed PMID: 28176047.
8. Berthoud HR, Blackshaw LA, Brookes SJH, Grundy D. Neuroanatomy of extrinsic afferents supplying the gastrointestinal tract. Neurogastroenterology and Motility. 2004 Jun;16(SUPPL. 1):28–33. doi:10.1111/j.1743-3150.2004.00471.x PubMed PMID: 15066001.
9. Wan T, Wang Y, He K, Zhu S. Microbial sensing in the intestine. Protein Cell. 2023 Jun;14(11):824–60. doi:10.1093/procel/pwad028 PubMed PMID: 37191444.
10. Duca FA, Waise TMZ, Peppler WT, Lam TKT. The metabolic impact of small intestinal nutrient sensing. Nat Commun. 2021 Jun;12(1). doi:10.1038/s41467-021-21235-y PubMed PMID: 33568676.
11. Wit M, Trujillo-Viera J, Strohmeyer A, Klingenspor M, Hankir M, Sumara G. When fat meets the gut—focus on intestinal lipid handling in metabolic health and disease. EMBO Mol Med. 2022 Jun;14(5). doi:10.15252/emmm.202114742 PubMed PMID: 35437952.
12. de Wit NJW, Bosch-Vermeulen H, de Groot PJ, Hooiveld GJEJ, Bromhaar MMG, Jansen J, et al. The role of the small intestine in the development of dietary fat-induced obesity and insulin resistance in C57BL/6J mice. BMC Med Genomics. 2008 Jun;1(1). doi:10.1186/1755-8794-1-14 PubMed PMID: 18457598.
13. Wei L, Singh R, Ro S, Ghoshal UC. Gut microbiota dysbiosis in functional gastrointestinal disorders: Underpinning the symptoms and pathophysiology. JGH Open. 2021 Jun;5(9):976–87. doi:10.1002/jgh3.12528 PubMed PMID: 34584964.
14. Allin KH, Tremaroli V, Caesar R, Jensen BAH, Damgaard MTF, Bahl MI, et al. Aberrant intestinal microbiota in individuals with prediabetes. Diabetologia. 2018 Jun;61(4):810–20. doi:10.1007/s00125-018-4550-1 PubMed PMID: 29379988.
15. Gruber L, Kisling S, Lichti P, Martin FP, May S, Klingenspor M, et al. High Fat Diet Accelerates Pathogenesis of Murine Crohn's Disease-Like Ileitis Independently of

Obesity. PLoS One. 2013 Jun;8(8). doi:10.1371/journal.pone.0071661 PubMed PMID: 23977107.
16. Luck H, Tsai S, Chung J, Clemente-Casares X, Ghazarian M, Revelo XS, et al. Regulation of obesity-related insulin resistance with gut anti-inflammatory agents. Cell Metab. 2015 Jun;21(4):527–42. doi:10.1016/j.cmet.2015.03.001 PubMed PMID: 25863246.
17. Font-Burgada J, Sun B, Karin M. Obesity and Cancer: The Oil that Feeds the Flame. Cell Metab. 2016 Jun;23(1):48–62. doi:10.1016/j.cmet.2015.12.015 PubMed PMID: 26771116.
18. Murphy N, Jenab M, Gunter MJ. Adiposity and gastrointestinal cancers: epidemiology, mechanisms and future directions. Nat Rev Gastroenterol Hepatol. 2018 Jun;15(11):659–70. doi:10.1038/s41575-018-0038-1 PubMed PMID: 29970888.
19. Stahel P, Xiao C, Nahmias A, Lewis GF. Role of the Gut in Diabetic Dyslipidemia. Front Endocrinol (Lausanne). 2020 Jun;11. doi:10.3389/fendo.2020.00116 PubMed PMID: 32231641.
20. Ghanem M, Lewis GF, Xiao C. Recent advances in cytoplasmic lipid droplet metabolism in intestinal enterocyte. Biochim Biophys Acta Mol Cell Biol Lipids. 2022 Jun;1867(10). doi:10.1016/j.bbalip.2022.159197 PubMed PMID: 35820577.
21. Stahel P, Xiao C, Davis X, Tso P, Lewis GF. Glucose and GLP-2 (Glucagon-Like Peptide-2) Mobilize Intestinal Triglyceride by Distinct Mechanisms. Arterioscler Thromb Vasc Biol. 2019 Jun;39(8):1565–73. doi:10.1161/ATVBAHA.119.313011 PubMed PMID: 31294621.
22. Altmann GG. Influence of starvation and refeeding on mucosal size and epithelial renewal in the rat small intestine. American Journal of Anatomy. 1972;133(4):391–400. doi:10.1002/aja.1001330403 PubMed PMID: 5016502.
23. Xiao C, Dash S, Morgantini C, Adeli K, Lewis GF. Gut peptides are novel regulators of intestinal lipoprotein secretion: Experimental and pharmacological manipulation of lipoprotein metabolism. Diabetes. 2015 Jun;64(7):2310–8. doi:10.2337/db14-1706 PubMed PMID: 26106188.
24. Stahel P, Xiao C, Nahmias A, Tian L, Lewis GF. Multi-organ Coordination of Lipoprotein Secretion by Hormones, Nutrients and Neural Networks. Endocr Rev. 2021 Jun;42(6):815–38. doi:10.1210/endrev/bnab008 PubMed PMID: 33743013.
25. Haber AL, Biton M, Rogel N, Herbst RH, Shekhar K, Smillie C, et al. A single-cell survey of the small intestinal epithelium. Nature. 2017 Jun;551(7680):333–9. doi:10.1038/nature24489 PubMed PMID: 29144463.
26. Flier LG Van Der, Clevers H. Stem cells, self-renewal, and differentiation in the intestinal epithelium. Annu Rev Physiol. 2009 Jun;71:241–60. doi:10.1146/annurev.physiol.010908.163145 PubMed PMID: 18808327.
27. Williams JM, Duckworth CA, Burkitt MD, Watson AJM, Campbell BJ, Pritchard DM. Epithelial Cell Shedding and Barrier Function: A Matter of Life and Death at the Small Intestinal Villus Tip. Vet Pathol. 2015 Jun;52(3):445–55. doi:10.1177/0300985814559404 PubMed PMID: 25428410.
28. Cornick S, Tawiah A, Chadee K. Roles and regulation of the mucus barrier in the gut. Tissue Barriers. 2015;3(1). doi:10.4161/21688370.2014.982426 PubMed PMID: 25838985.
29. Johansson ME V, Jakobsson HE, Holmén-Larsson J, Schütte A, Ermund A, Rodríguez-Piñeiro AM, et al. Normalization of host intestinal mucus layers requires long-term microbial colonization. Cell Host Microbe. 2015 Jun;18(5):582–92. doi:10.1016/j.chom.2015.10.007 PubMed PMID: 26526499.

30. Sato T, Stange DE, Ferrante M, Vries RGJ, Es JH Van, Brink S Van Den, et al. Long-term expansion of epithelial organoids from human colon, adenoma, adenocarcinoma, and Barrett's epithelium. Gastroenterology. 2011;141(5):1762–72. doi:10.1053/j.gastro.2011.07.050 PubMed PMID: 21889923.
31. Fu Y, Lyu J, Wang S. The role of intestinal microbes on intestinal barrier function and host immunity from a metabolite perspective. Front Immunol. 2023;14. doi:10.3389/fimmu.2023.1277102 PubMed PMID: 37876938.
32. Fung C, Fraser LM, Barrón GM, Gologorsky MB, Atkinson SN, Gerrick ER, et al. Tuft cells mediate commensal remodeling of the small intestinal antimicrobial landscape. Proc Natl Acad Sci U S A. 2023 Jun;120(23). doi:10.1073/pnas.2216908120 PubMed PMID: 37253002.
33. Mansbach CM, Siddiqi SA. The biogenesis of chylomicrons. Annu Rev Physiol. 2009 Jun;72:315–33. doi:10.1146/annurev-physiol-021909-135801 PubMed PMID: 20148678.
34. Kulkarni B V, Mattes RD. Lingual lipase activity in the orosensory detection of fat by humans. Am J Physiol Regul Integr Comp Physiol. 2014 Jun;306(12). doi:10.1152/ajpregu.00352.2013 PubMed PMID: 24694384.
35. Hoyle T. The digestive system: linking theory and practice. Br J Nurs. 1997;6(22):1285–91. doi:10.12968/bjon.1997.6.22.1285 PubMed PMID: 9470654.
36. Hooton D, Lentle R, Monro J, Wickham M, Simpson R. The secretion and action of brush border enzymes in the mammalian small intestine. Rev Physiol Biochem Pharmacol. 2015;168:59–118. doi:10.1007/112_2015_24 PubMed PMID: 26345415.
37. Phan CT, Tso P. Intestinal lipid absorption and transport. Front Biosci. 2001;6. doi:10.2741/a612 PubMed PMID: 11229876.
38. Hussain MM. Intestinal lipid absorption and lipoprotein formation. Curr Opin Lipidol. 2014;25(3):200–6. doi:10.1097/MOL.0000000000000084 PubMed PMID: 24751933.
39. Dash S, Clarke G, Berk M, Jacka FN. The gut microbiome and diet in psychiatry: Focus on depression. Curr Opin Psychiatry. 2015 Jun;28(1):1–6. doi:10.1097/YCO.0000000000000117 PubMed PMID: 25415497.
40. Abumrad NA, Davidson NO. Role of the gut in lipid homeostasis. Physiol Rev. 2012 Jun;92(3):1061–85. doi:10.1152/physrev.00019.2011 PubMed PMID: 22811425.
41. Xiao C, Stahel P, Carreiro AL, Buhman KK, Lewis GF. Recent Advances in Triacylglycerol Mobilization by the Gut. Trends in Endocrinology and Metabolism. 2018 Jun;29(3):151–63. doi:10.1016/j.tem.2017.12.001 PubMed PMID: 29306629.
42. Hui DY, Howles PN. Molecular mechanisms of cholesterol absorption and transport in the intestine. Semin Cell Dev Biol. 2005;16(2):183–92. doi:10.1016/j.semcdb.2005.01.003 PubMed PMID: 15797829.
43. Demignot S, Beilstein F, Morel E. Triglyceride-rich lipoproteins and cytosolic lipid droplets in enterocytes: Key players in intestinal physiology and metabolic disorders. Biochimie. 2014;96(1):48–55. doi:10.1016/j.biochi.2013.07.009 PubMed PMID: 23871915.
44. Zembroski AS, Xiao C, Buhman KK. The Roles of Cytoplasmic Lipid Droplets in Modulating Intestinal Uptake of Dietary Fat. Annu Rev Nutr. 2021;41:79–104. doi:10.1146/annurev-nutr-110320-013657 PubMed PMID: 34283920.
45. Kindel T, Lee DM, Tso P. The mechanism of the formation and secretion of chylomicrons. Atheroscler Suppl. 2010;11(1):11–6. doi:10.1016/j.atherosclerosissup.2010.03.003 PubMed PMID: 20493784.
46. Visser A, Hussain MM, Kuivenhoven JA. The intracellular chylomicron highway: novel insights into chylomicron biosynthesis, trafficking, and secretion. Curr Opin

Lipidol. 2025 Jun;36(3):145–52. doi:10.1097/MOL.0000000000000983 PubMed PMID: 40152288.
47. Xie Y, Matsumoto H, Nalbantoglu Ilk, Kerr TA, Luo J, Rubin DC, et al. Intestine-Specific Mttp Deletion Increases the Severity of Experimental Colitis and Leads to Greater Tumor Burden in a Model of Colitis Associated Cancer. PLoS One. 2013 Jun;8(6). doi:10.1371/journal.pone.0067819 PubMed PMID: 23805328.
48. Peng H, Chiu TY, Liang YJ, Lee CJ, Liu CS, Suen CS, et al. PRAP1 is a novel lipid-binding protein that promotes lipid absorption by facilitating MTTP-mediated lipid transport. Journal of Biological Chemistry. 2021 Jun;296. doi:10.1074/jbc.RA120.015002 PubMed PMID: 33168624.
49. Giammanco A, Cefalù AB, Noto D, Averna MR. The pathophysiology of intestinal lipoprotein production. Front Physiol. 2015;6(MAR). doi:10.3389/fphys.2015.00061 PubMed PMID: 25852563.
50. Gonzalez-Vallina R, Wang H, Zhan R, Berschneider HM, Lee RM, Davidson NO, et al. Lipoprotein and apolipoprotein secretion by a newborn piglet intestinal cell line (IPEC-1). Am J Physiol Gastrointest Liver Physiol. 1996;271(2 34-2). doi:10.1152/ajpgi.1996.271.2.g249 PubMed PMID: 8770040.
51. Wang F, Kohan AB, Kindel TL, Corbin KL, Nunemaker CS, Obici S, et al. Apolipoprotein A-IV improves glucose homeostasis by enhancing insulin secretion. Proc Natl Acad Sci U S A. 2012 Jun;109(24):9641–6. doi:10.1073/pnas.1201433109 PubMed PMID: 22619326.
52. Trujillo-Viera J, El-Merahbi R, Schmidt V, Karwen T, Loza-Valdes A, Strohmeyer A, et al. Protein Kinase D2 drives chylomicron-mediated lipid transport in the intestine and promotes obesity. EMBO Mol Med. 2021 Jun;13(5). doi:10.15252/emmm.202013548 PubMed PMID: 33949105.
53. Jaschke A, Chung B, Hesse D, Kluge R, Zahn C, Moser M, et al. The gtpase ARFRP1 controls the lipidation of chylomicrons in the golgi of the intestinal epithelium. Hum Mol Genet. 2012 Jun;21(14):3128–42. doi:10.1093/hmg/dds140 PubMed PMID: 22505585.
54. Marat AL, Dokainish H, McPherson PS. DENN domain proteins: Regulators of Rab GTPases. Journal of Biological Chemistry. 2011 Jun;286(16):13791–800. doi:10.1074/jbc.R110.217067 PubMed PMID: 21330364.
55. Gordon SM, Neufeld EB, Yang Z, Pryor M, Freeman LA, Fan X, et al. DENND5B Regulates Intestinal Triglyceride Absorption and Body Mass. Sci Rep. 2019 Jun;9(1). doi:10.1038/s41598-019-40296-0 PubMed PMID: 30837651.
56. Ma T, Jayaraman S, Wang KS, Song Y, Yang B, Li J, et al. Defective dietary fat processing in transgenic mice lacking aquaporin-1 water channels. Am J Physiol Cell Physiol. 2001;280(1 49-1). doi:10.1152/ajpcell.2001.280.1.c126 PubMed PMID: 11121384.
57. Dixon JB. Mechanisms of chylomicron uptake into lacteals. Ann N Y Acad Sci. 2010;1207(SUPPL.1). doi:10.1111/j.1749-6632.2010.05716.x PubMed PMID: 20961306.
58. Sané AT, Seidman E, Peretti N, Kleme ML, Delvin E, Deslandres C, et al. Understanding chylomicron retention disease through Sar1B Gtpase gene disruption: Insight from cell culture. Arterioscler Thromb Vasc Biol. 2017;37(12):2243–51. doi:10.1161/ATVBAHA.117.310121 PubMed PMID: 28982670.
59. Whitfield AJ, Barrett PHR, Bockxmeer FM Van, Burnett JR. Lipid disorders and mutations in the APOB gene. Clin Chem. 2004 Jun;50(10):1725–32. doi:10.1373/clinchem.2004.038026 PubMed PMID: 15308601.

60. Dunn E, Zhang B, Sahota VK, Augustin H. Potential benefits of medium chain fatty acids in aging and neurodegenerative disease. Front Aging Neurosci. 2023;15. doi:10.3389/fnagi.2023.1230467 PubMed PMID: 37680538.
61. Wang F, Kohan AB, Dong HH, Yang Q, Xu M, Huesman S, et al. Overexpression of apolipoprotein C-III decreases secretion of dietary triglyceride into lymph. Physiol Rep. 2014 Jun;2(3). doi:10.1002/phy2.247 PubMed PMID: 24760506.
62. Zhang LJ, Wang C, Yuan Y, Wang H, Wu J, Liu F, et al. Cideb facilitates the lipidation of chylomicrons in the small intestine. J Lipid Res. 2014;55(7):1279–87. doi:10.1194/jlr.M046482 PubMed PMID: 24831470.
63. McManaman JL, Bales ES, Orlicky DJ, Jackman M, MacLean PS, Cain S, et al. Perilipin-2-null mice are protected against diet-induced obesity, adipose infl ammation, and fatty liver disease. J Lipid Res. 2013 Jun;54(5):1346–59. doi:10.1194/jlr.M035063 PubMed PMID: 23402988.
64. Weaver T, Auclair PL, Taybos GM. An amalgam tattoo causing local and systemic disease? Oral Surgery, Oral Medicine, Oral Pathology. 1987;63(1):137–40. doi:10.1016/0030-4220(87)90355-0 PubMed PMID: 3543795.
65. Walther TC, Chung J, Farese R V. Lipid droplet biogenesis. Annu Rev Cell Dev Biol. 2017 Jun;33:491–510. doi:10.1146/annurev-cellbio-100616-060608 PubMed PMID: 28793795.
66. Kumari RM, Khatri A, Chaudhary R, Choudhary V. Concept of lipid droplet biogenesis. Eur J Cell Biol. 2023 Jun;102(4). doi:10.1016/j.ejcb.2023.151362 PubMed PMID: 37742390.
67. Wit M, Belykh A, Sumara G. Protein kinase D (PKD) on the crossroad of lipid absorption, synthesis and utilization. Biochim Biophys Acta Mol Cell Res. 2024 Jun;1871(2). doi:10.1016/j.bbamcr.2023.119653 PubMed PMID: 38104800.
68. Mathiowetz AJ, Olzmann JA. Lipid droplets and cellular lipid flux. Nat Cell Biol. 2024 Jun;26(3):331–45. doi:10.1038/s41556-024-01364-4 PubMed PMID: 38454048.
69. Olarte MJ, Kim S, Sharp ME, Swanson JMJ, Farese R V, Walther TC. Determinants of Endoplasmic Reticulum-to-Lipid Droplet Protein Targeting. Dev Cell. 2020 Jun;54(4):471-487.e7. doi:10.1016/j.devcel.2020.07.001 PubMed PMID: 32730754.
70. Sztalryd C, Brasaemle DL. The perilipin family of lipid droplet proteins: Gatekeepers of intracellular lipolysis. Biochim Biophys Acta Mol Cell Biol Lipids. 2017 Jun;1862(10):1221–32. doi:10.1016/j.bbalip.2017.07.009 PubMed PMID: 28754637.
71. Zadoorian A, Du X, Yang H. Lipid droplet biogenesis and functions in health and disease. Nat Rev Endocrinol. 2023 Jun;19(8):443–59. doi:10.1038/s41574-023-00845-0 PubMed PMID: 37221402.
72. Zechner R, Kienesberger PC, Haemmerle G, Zimmermann R, Lass A. Adipose triglyceride lipase and the lipolytic catabolism of cellular fat stores. J Lipid Res. 2009;50(1):3–21. doi:10.1194/jlr.R800031-JLR200 PubMed PMID: 18952573.
73. Schreiber R, Xie H, Schweiger M. Of mice and men: The physiological role of adipose triglyceride lipase (ATGL). Biochim Biophys Acta Mol Cell Biol Lipids. 2019 Jun;1864(6):880–99. doi:10.1016/j.bbalip.2018.10.008 PubMed PMID: 30367950.
74. Sharma AK, Khandelwal R, Wolfrum C. Futile lipid cycling: from biochemistry to physiology. Nat Metab. 2024 Jun;6(5):808–24. doi:10.1038/s42255-024-01003-0 PubMed PMID: 38459186.
75. Soni KG, Mardones GA, Sougrat R, Smirnova E, Jackson CL, Bonifacino JS. Coatomer-dependent protein delivery to lipid droplets. J Cell Sci. 2009 Jun;122(11):1834–41. doi:10.1242/jcs.045849 PubMed PMID: 19461073.
76. Takashima K, Saitoh A, Hirose S, Nakai W, Kondo Y, Takasu Y, et al. GBF1-Arf-COPI-ArfGAP-mediated Golgi-to-ER transport involved in regulation of lipid

homeostasis. Cell Struct Funct. 2011;36(2):223–35. doi:10.1247/csf.11035 PubMed PMID: 22185782.
77. Yu L, Li Y, Grisé A, Wang H. CGI-58: Versatile regulator of intracellular lipid droplet homeostasis. Adv Exp Med Biol. 2020;1276:197–222. doi:10.1007/978-981-15-6082-8_13 PubMed PMID: 32705602.
78. Subramanian V, Garcia A, Sekowski A, Brasaemle DL. Hydrophobic sequences target and anchor perilipin A to lipid droplets. J Lipid Res. 2004 Jun;45(11):1983–91. doi:10.1194/jlr.M400291-JLR200 PubMed PMID: 15342676.
79. Yamaguchi T, Omatsu N, Matsushita S, Osumi T. CGI-58 interacts with perilipin and is localized to lipid droplets: Possible involvement of CGI-58 mislocalization in Chanarin-Dorfman syndrome. Journal of Biological Chemistry. 2004 Jun;279(29):30490–7. doi:10.1074/jbc.M403920200 PubMed PMID: 15136565.
80. Zagani R, El-Assaad W, Gamache I, Teodoro JG. Inhibition of adipose triglyceride lipase (ATGL) by the putative tumor suppressor G0S2 or a small molecule inhibitor attenuates the growth of cancer cells. Oncotarget. 2015;6(29):28282–95. doi:10.18632/oncotarget.5061 PubMed PMID: 26318046.
81. Das KMP, Wechselberger L, Liziczai M, Rodriguez MDLR, Grabner GF, Heier C, et al. Hypoxia-inducible lipid droplet-associated protein inhibits adipose triglyceride lipase. J Lipid Res. 2018;59(3):531–41. doi:10.1194/jlr.M082388 PubMed PMID: 29326160.
82. BasuRay S, Smagris E, Cohen JC, Hobbs HH. The PNPLA3 variant associated with fatty liver disease (I148M) accumulates on lipid droplets by evading ubiquitylation. Hepatology. 2017 Jun;66(4):1111–24. doi:10.1002/hep.29273 PubMed PMID: 28520213.
83. Watt MJ, Holmes AG, Pinnamaneni SK, Garnham AP, Steinberg GR, Kemp BE, et al. Regulation of HSL serine phosphorylation in skeletal muscle and adipose tissue. Am J Physiol Endocrinol Metab. 2006 Jun;290(3). doi:10.1152/ajpendo.00361.2005 PubMed PMID: 16188906.
84. Hayashi Y. Glucagon regulates lipolysis and fatty acid oxidation through inositol triphosphate receptor 1 in the liver. J Diabetes Investig. 2021 Jun;12(1):32–4. doi:10.1111/jdi.13315 PubMed PMID: 32506830.
85. Chakrabarti P, Kim JY, Singh M, Shin YK, Kim J, Kumbrink J, et al. Insulin Inhibits Lipolysis in Adipocytes via the Evolutionarily Conserved mTORC1-Egr1-ATGL-Mediated Pathway. Mol Cell Biol. 2013 Jun;33(18):3659–66. doi:10.1128/mcb.01584-12 PubMed PMID: 23858058.
86. Zechner R, Zimmermann R, Eichmann TO, Kohlwein SD, Haemmerle G, Lass A, et al. FAT SIGNALS - Lipases and lipolysis in lipid metabolism and signaling. Cell Metab. 2012 Jun;15(3):279–91. doi:10.1016/j.cmet.2011.12.018 PubMed PMID: 22405066.
87. Snel M, Jonker JT, Schoones J, Lamb H, Roos A De, Pijl H, et al. Ectopic fat and insulin resistance: Pathophysiology and effect of diet and lifestyle interventions. Int J Endocrinol. 2012;2012. doi:10.1155/2012/983814 PubMed PMID: 22675355.
88. Large V, Peroni O, Letexier D, Ray H, Beylot M. Metabolism of lipids in human white adipocyte. Diabetes Metab. 2004;30(4):294–309. doi:10.1016/S1262-3636(07)70121-0 PubMed PMID: 15525872.
89. Schweiger M, Schoiswohl G, Lass A, Radner FPW, Haemmerle G, Malli R, et al. The C-terminal region of human adipose triglyceride lipase affects enzyme activity and lipid droplet binding. Journal of Biological Chemistry. 2008 Jun;283(25):17211–20. doi:10.1074/jbc.M710566200 PubMed PMID: 18445597.

90. Grabner GF, Xie H, Schweiger M, Zechner R. Lipolysis: cellular mechanisms for lipid mobilization from fat stores. Nat Metab. 2021 Jun;3(11):1445–65. doi:10.1038/s42255-021-00493-6 PubMed PMID: 34799702.
91. Singh R, Cuervo AM. Lipophagy: Connecting autophagy and lipid metabolism. Int J Cell Biol. 2012. doi:10.1155/2012/282041 PubMed PMID: 22536247.
92. Shin DW. Lipophagy: Molecular Mechanisms and Implications in Metabolic Disorders. Mol Cells. 2020 Jun;43(8):686–93. doi:10.143Fig/molcells.2020.0046 PubMed PMID: 32624503.
93. Martinez-Lopez N, Singh R. Autophagy and Lipid Droplets in the Liver. Annu Rev Nutr. 2015 Jun;35(1):215–37. doi:10.1146/annurev-nutr-071813-105336 PubMed PMID: 26076903.
94. Zhang S, Peng X, Yang S, Li X, Huang M, Wei S, et al. The regulation, function, and role of lipophagy, a form of selective autophagy, in metabolic disorders. Cell Death Dis. 2022 Jun;13(2). doi:10.1038/s41419-022-04593-3 PubMed PMID: 35136038.
95. Chung J, Park J, Lai ZW, Lambert TJ, Richards RC, Zhang J, et al. The Troyer syndrome protein spartin mediates selective autophagy of lipid droplets. Nat Cell Biol. 2023 Jun;25(8):1101–10. doi:10.1038/s41556-023-01178-w PubMed PMID: 37443287.
96. Kaushik S, Cuervo AM. Degradation of lipid droplet-associated proteins by chaperone-mediated autophagy facilitates lipolysis. Nat Cell Biol. 2015 Jun;17(6):759–70. doi:10.1038/ncb3166 PubMed PMID: 25961502.
97. Kaushik S, Cuervo AM. AMPK-dependent phosphorylation of lipid droplet protein PLIN2 triggers its degradation by CMA. Autophagy. 2016 Jun;12(2):432–8. doi:10.1080/15548627.2015.1124226 PubMed PMID: 26902588.
98. Farese R V, Walther TC. Essential Biology of Lipid Droplets. Annu Rev Biochem. 2025 Jun;94(1):447–77. doi:10.1146/annurev-biochem-091724-013733 PubMed PMID: 40169008.
99. Minami Y, Hoshino A, Higuchi Y, Hamaguchi M, Kaneko Y, Kirita Y, et al. Liver lipophagy ameliorates nonalcoholic steatohepatitis through extracellular lipid secretion. Nat Commun. 2023 Jun;14(1). doi:10.1038/s41467-023-39404-6 PubMed PMID: 37443159.
100. Liu K, Czaja MJ. Regulation of lipid stores and metabolism by lipophagy. Cell Death Differ. 2013 Jun;20(1):3–11. doi:10.1038/cdd.2012.63 PubMed PMID: 22595754.
101. Seok S, Kim Y, Zhang Y, Kong B, Guo G, Ma J, et al. Feeding activates FGF15-SHP-TFEB-mediated lipophagy in the gut. EMBO J. 2022 Jun;41(17). doi:10.15252/embj.2021109997 PubMed PMID: 35686465.
102. Amir R, Ciechanover A, Cohen S. The ubiquitin-proteasome system: the relationship between protein degradation and human diseases. Harefuah. 2001;140(12). PubMed PMID: 11789303.
103. Guha S, Padh H. Cathepsins: Fundamental effectors of endolysosomal proteolysis. Indian J Biochem Biophys. 2008 Jun;45(2):75–90. PubMed PMID: 21086720.
104. Nazarko VY, Zhong Q. ULK1 targets Beclin-1 in autophagy. Nat Cell Biol. 2013 Jun;15(7):727–8. doi:10.1038/ncb2797 PubMed PMID: 23817237.
105. Nguyen KT, Lee CS, Mun SH, Truong NT, Park SK, Hwang CS. N-terminal acetylation and the N-end rule pathway control degradation of the lipid droplet protein PLIN2. Journal of Biological Chemistry. 2019 Jun;294(1):379–88. doi:10.1074/jbc.RA118.005556 PubMed PMID: 30425097.
106. Takahashi Y, Shinoda A, Kamada H, Shimizu M, Inoue J, Sato R. Perilipin2 plays a positive role in adipocytes during lipolysis by escaping proteasomal degradation. Sci Rep. 2016 Jun;6. doi:10.1038/srep20975 PubMed PMID: 26876687.

107. Xu J, Liu Z, Zhang J, Chen S, Wang W, Zhao X, et al. N-end Rule–Mediated Proteasomal Degradation of ATGL Promotes Lipid Storage. Diabetes. 2023 Jun;72(2):210–22. doi:10.2337/db22-0362 PubMed PMID: 36346641.
108. Ghosh M, Niyogi S, Bhattacharyya M, Adak M, Nayak DK, Chakrabarti S, et al. Ubiquitin Ligase COP1 controls hepatic fat metabolism by targeting ATGL for degradation. Diabetes. 2016 Jun;65(12):3561–72. doi:10.2337/db16-0506 PubMed PMID: 27658392.
109. Zheng P, Obara CJ, Szczesna E, Nixon-Abell J, Mahalingan KK, Roll-Mecak A, et al. ER proteins decipher the tubulin code to regulate organelle distribution. Nature. 2022 Jun;601(7891):132–8. doi:10.1038/s41586-021-04204-9 PubMed PMID: 34912111.
110. Niyogi S, Ghosh M, Adak M, Chakrabarti P. PEDF promotes nuclear degradation of ATGL through COP1. Biochem Biophys Res Commun. 2019 Jun;512(4):806–11. doi:10.1016/j.bbrc.2019.03.111 PubMed PMID: 30926171.
111. Dai Z, Qi W, Li C, Lu J, Mao Y, Yao Y, et al. Dual regulation of adipose triglyceride lipase by pigment epithelium-derived factor: A novel mechanistic insight into progressive obesity. Mol Cell Endocrinol. 2013 Jun;377(1–2):123–34. doi:10.1016/j.mce.2013.07.001 PubMed PMID: 23850519.
112. Wallner B, Palmieri N, Vogl C, Rigler D, Bozlak E, Druml T, et al. Y Chromosome Uncovers the Recent Oriental Origin of Modern Stallions. Current Biology. 2017 Jun;27(13):2029-2035.e5. doi:10.1016/j.cub.2017.05.086 PubMed PMID: 28669755.
113. Khan SA, Wollaston-Hayden EE, Markowski TW, Higgins LA, Mashek DG. Quantitative analysis of the murine lipid dropletassociated proteome during diet-induced hepatic steatosis. J Lipid Res. 2015 Jun;56(12):2260–72. doi:10.1194/jlr.M056812 PubMed PMID: 26416795.
114. Scorletti E, Carr RM. A new perspective on NAFLD: Focusing on lipid droplets. J Hepatol. 2022 Jun;76(4):934–45. doi:10.1016/j.jhep.2021.11.009 PubMed PMID: 34793866.
115. Crunk AE, Monks J, Murakami A, Jackman M, MacLean PS, Ladinsky M, et al. Dynamic Regulation of Hepatic Lipid Droplet Properties by Diet. PLoS One. 2013 Jun;8(7). doi:10.1371/journal.pone.0067631 PubMed PMID: 23874434.
116. Cao X, Wang N, Yang M, Zhang C. Lipid Accumulation and Insulin Resistance: Bridging Metabolic Dysfunction-Associated Fatty Liver Disease and Chronic Kidney Disease. Int J Mol Sci. 2025 Jun;26(14). doi:10.3390/ijms26146962 PubMed PMID: 40725208.
117. Yu XH, Fu YC, Zhang DW, Yin K, Tang CK. Foam cells in atherosclerosis. Clinica Chimica Acta. 2013 Jun;424:245–52. doi:10.1016/j.cca.2013.06.006 PubMed PMID: 23782937.
118. Moore KJ, Tabas I. Macrophages in the pathogenesis of atherosclerosis. Cell. 2011 Jun;145(3):341–55. doi:10.1016/j.cell.2011.04.005 PubMed PMID: 21529710.
119. Zhang Y, Chen Y, Zhuang C, Qi J, Zhao RC, Wang J. Lipid droplets in the nervous system: involvement in cell metabolic homeostasis. Neural Regen Res. 2025 Jun;20(3):740–50. doi:10.4103/NRR.NRR-D-23-01401 PubMed PMID: 38886939.
120. Farmer BC, Walsh AE, Kluemper JC, Johnson LA. Lipid Droplets in Neurodegenerative Disorders. Front Neurosci. 2020 Jun;14. doi:10.3389/fnins.2020.00742 PubMed PMID: 32848541.
121. Papapanagiotou O, Cotton K, Edwards C, Michod D, Crompton L, Craig T, et al. Lipid droplets in neurodegenerative diseases: pathological drivers and therapeutic vulnerabilities. Cell Death Discov. 2026 Jun;12(1). doi:10.1038/s41420-026-03096-w PubMed PMID: 41956992.

122. Haney MS, Pálovics R, Munson CN, Long C, Johansson PK, Yip O, et al. APOE4/4 is linked to damaging lipid droplets in Alzheimer's disease microglia. Nature. 2024 Jun;628(8006):154–61. doi:10.1038/s41586-024-07185-7 PubMed PMID: 38480892.
123. ru Zhao X, ying Gu Y, yi Wang J, Yi Y, qiu Zhang Y, hang Shao Q, et al. The interplay between lipid droplets and Parkinson's disease. Biochim Biophys Acta Mol Basis Dis. 2025 Jun;1871(7). doi:10.1016/j.bbadis.2025.167953 PubMed PMID: 40516715.
124. Bosma M. Lipid droplet dynamics in skeletal muscle. Exp Cell Res. 2016 Jun;340(2):180–6. doi:10.1016/j.yexcr.2015.10.023 PubMed PMID: 26515552.
125. Nielsen J, Christensen AE, Nellemann B, Christensen B. Lipid droplet size and location in human skeletal muscle fibers are associated with insulin sensitivity. Am J Physiol Endocrinol Metab. 2017 Jun;313(6):E721–30. doi:10.1152/ajpendo.00062.2017 PubMed PMID: 28743757.
126. Yue F, Oprescu SN, Qiu J, Gu L, Zhang L, Chen J, et al. Lipid droplet dynamics regulate adult muscle stem cell fate. Cell Rep. 2022 Jun;38(3). doi:10.1016/j.celrep.2021.110267 PubMed PMID: 35045287.
127. Uchida A, Lee HJ, Cheng JX, Buhman KK. Imaging cytoplasmic lipid droplets in enterocytes and assessing dietary fat absorption. Methods Cell Biol. 2013;116:151–66. doi:10.1016/B978-0-12-408051-5.00014-0 PubMed PMID: 24099292.
128. Beilstein F, Carrière V, Leturque A, Demignot S. Characteristics and functions of lipid droplets and associated proteins in enterocytes. Exp Cell Res. 2016 Jun;340(2):172–9. doi:10.1016/j.yexcr.2015.09.018 PubMed PMID: 26431584.
129. Auclair N, Melbouci L, St-Pierre D, Levy E. Gastrointestinal factors regulating lipid droplet formation in the intestine. Exp Cell Res. 2018 Jun;363(1):1–14. doi:10.1016/j.yexcr.2017.12.031 PubMed PMID: 29305172.
130. Zembroski AS, D'Aquila T, Buhman KK. Characterization of cytoplasmic lipid droplets in each region of the small intestine of lean and diet-induced obese mice in response to dietary fat. Am J Physiol Gastrointest Liver Physiol. 2021 Jun;321(1):G75–86. doi:10.1152/AJPGI.00084.2021 PubMed PMID: 34009042.
131. D'Aquila T, Sirohi D, Grabowski JM, Hedrick VE, Paul LN, Greenberg AS, et al. Characterization of the proteome of cytoplasmic lipid droplets in mouse enterocytes after a dietary fat challenge. PLoS One. 2015 Jun;10(5). doi:10.1371/journal.pone.0126823 PubMed PMID: 25992653.
132. Ng YM, Voo P, Maakip I. Psychosocial factors, depression, and musculoskeletal disorders among teachers. BMC Public Health. 2019 Jun;19(1). doi:10.1186/s12889-019-6553-3 PubMed PMID: 30808335.
133. Syed-Abdul MM, Stahel P, Zembroski A, Tian L, Xiao C, Nahmias A, et al. Glucagon-like Peptide-2 Acutely Enhances Chylomicron Secretion in Humans without Mobilizing Cytoplasmic Lipid Droplets. Journal of Clinical Endocrinology and Metabolism. 2023 Jun;108(5):1084–92. doi:10.1210/clinem/dgac690 PubMed PMID: 36458872.
134. Mukherjee K, Xiao C. GLP-2 regulation of intestinal lipid handling. Front Physiol. 2024;15. doi:10.3389/fphys.2024.1358625 PubMed PMID: 38426205.
135. Korbelius M, Vujic N, Sachdev V, Obrowsky S, Rainer S, Gottschalk B, et al. ATGL/CGI-58-Dependent Hydrolysis of a Lipid Storage Pool in Murine Enterocytes. Cell Rep. 2019 Jun;28(7):1923-1934.e4. doi:10.1016/j.celrep.2019.07.030 PubMed PMID: 31412256.
136. Obrowsky S, Chandak PG, Patankar J V, Povoden S, Schlager S, Kershaw EE, et al. Adipose triglyceride lipase is a TG hydrolase of the small intestine and regulates intestinal PPARα signaling. J Lipid Res. 2013 Jun;54(2):425–35. doi:10.1194/jlr.M031716 PubMed PMID: 23220585.

137. Kim J, Kim H, Noh SH, Jang DG, Park SY, Min D, et al. Grasp55 −/− mice display impaired fat absorption and resistance to high-fat diet-induced obesity. Nat Commun. 2020 Jun;11(1). doi:10.1038/s41467-020-14912-x PubMed PMID: 32184397.
138. Maresch LK, Benedikt P, Feiler U, Eder S, Zierler KA, Taschler U, et al. Intestine-Specific Overexpression of Carboxylesterase 2c Protects Mice From Diet-Induced Liver Steatosis and Obesity. Hepatol Commun. 2019 Jun;3(2):227–45. doi:10.1002/hep4.1292 PubMed PMID: 30766961.
139. Prosniak M, Harshyne LA, Gorky J, Curtis MT, Kenyon LC, Schwaber JS, et al. Systemic Immune Bias Delineates Malignant Astrocytoma Survival Cohorts. The Journal of Immunology. 2021 Jun;206(7):1483–92. doi:10.4049/jimmunol.2000901 PubMed PMID: 33685995.
140. Liu R, Giddens J, McClung CM, Magnelli PE, Wang LX, Guthrie EP. Evaluation of a glycoengineered monoclonal antibody via LC-MS analysis in combination with multiple enzymatic digestion. MAbs. 2016 Jun;8(2):340–6. doi:10.1080/19420862.2015.1113361 PubMed PMID: 26514686.
141. Ocvirk S, O'Keefe SJD. Dietary fat, bile acid metabolism and colorectal cancer. Semin Cancer Biol. 2021 Jun;73:347–55. doi:10.1016/j.semcancer.2020.10.003 PubMed PMID: 33069873.
142. Kwon SJ, Khan MS, Kim SG. Intestinal Inflammation and Regeneration–Interdigitating Processes Controlled by Dietary Lipids in Inflammatory Bowel Disease. Int J Mol Sci. 2024 Jun;25(2). doi:10.3390/ijms25021311 PubMed PMID: 38279309.
143. Zhong J, Guo J, Zhang X, Feng S, Di W, Wang Y, et al. The remodeling roles of lipid metabolism in colorectal cancer cells and immune microenvironment. Oncol Res. 2022;30(5):231–42. doi:10.32604/or.2022.027900 PubMed PMID: 37305350.
144. Ocvirk S, O'Keefe SJ. Influence of Bile Acids on Colorectal Cancer Risk: Potential Mechanisms Mediated by Diet-Gut Microbiota Interactions. Curr Nutr Rep. 2017 Jun;6(4):315–22. doi:10.1007/s13668-017-0219-5 PubMed PMID: 29430336.
145. Nagengast FM, Grubben MJAL, van Munster IP. Role of bile acids in colorectal carcinogenesis. Eur J Cancer. 1995;31(7–8):1067–70. doi:10.1016/0959-8049(95)00216-6 PubMed PMID: 7576993.
146. Zeng H, Umar S, Rust B, Lazarova D, Bordonaro M. Secondary bile acids and short chain fatty acids in the colon: A focus on colonic microbiome, cell proliferation, inflammation, and cancer. Int J Mol Sci. 2019 Jun;20(5). doi:10.3390/ijms20051214 PubMed PMID: 30862015.
147. Ocvirk S, Wilson AS, Appolonia CN, Thomas TK, O'Keefe SJD. Fiber, Fat, and Colorectal Cancer: New Insight into Modifiable Dietary Risk Factors. Curr Gastroenterol Rep. 2019 Jun;21(11). doi:10.1007/s11894-019-0725-2 PubMed PMID: 31792624.
148. Marra F, Svegliati-Baroni G. Lipotoxicity and the gut-liver axis in NASH pathogenesis. J Hepatol. 2018 Jun;68(2):280–95. doi:10.1016/j.jhep.2017.11.014 PubMed PMID: 29154964.
149. Harsh S, Heryanto C, Eleftherianos I. Intestinal lipid droplets as novel mediators of host-pathogen interaction in Drosophila. Biol Open. 2019;8(7). doi:10.1242/bio.039040 PubMed PMID: 31278163.
150. Engin ED. Microbiota and Lipotoxicity. Adv Exp Med Biol. 2024;1460:357–72. doi:10.1007/978-3-031-63657-8_12 PubMed PMID: 39287858.
151. Yu AG, Wei XL, Zito E, Zheng H, Zhong CC, Gong YL, et al. Oxidative stress and caspase 3/Gsdme-dependent pyroptosis contributes to high fat diet induced-intestinal inflammation and lipotoxicity via Srebp1 cleavage at D444 site by caspase 3. Journal

of Nutritional Biochemistry. 2025 Jun;145. doi:10.1016/j.jnutbio.2025.110033 PubMed PMID: 40669570.
152. Kolczynska K, Loza-Valdes A, Hawro I, Sumara G. Diacylglycerol-evoked activation of PKC and PKD isoforms in regulation of glucose and lipid metabolism: A review. Lipids Health Dis. 2020 Jun;19(1). doi:10.1186/s12944-020-01286-8 PubMed PMID: 32466765.
153. Sumara G, Formentini I, Collins S, Sumara I, Windak R, Bodenmiller B, et al. Regulation of PKD by the MAPK p38δ in Insulin Secretion and Glucose Homeostasis. Cell. 2009 Jun;136(2):235–48. doi:10.1016/j.cell.2008.11.018 PubMed PMID: 19135240.
154. Löffler MC, Mayer AE, Viera JT, Valdes AL, El-Merahbi R, Ade CP, et al. Protein kinase D1 deletion in adipocytes enhances energy dissipation and protects against adiposity. EMBO J. 2018 Jun;37(22). doi:10.15252/embj.201899182 PubMed PMID: 30389661.
155. Loza-Valdes A, Mayer AE, Kassouf T, Trujillo-Viera J, Schmitz W, Dziaczkowski F, et al. A phosphoproteomic approach reveals that PKD3 controls PKA-mediated glucose and tyrosine metabolism. Life Sci Alliance. 2021 Jun;4(8). doi:10.26508/LSA.202000863 PubMed PMID: 34145024.
156. Mayer AE, Löffler MC, Valdés AEL, Schmitz W, El-Merahbi R, Viera JT, et al. The kinase PKD3 provides negative feedback on cholesterol and triglyceride synthesis by suppressing insulin signaling. Sci Signal. 2019 Jun;12(593). doi:10.1126/scisignal.aav9150 PubMed PMID: 31387939.
157. Genders AJ, Connor T, Morrison S, Bond ST, Drew BG, Meikle PJ, et al. Reducing hepatic PKD activity lowers circulating VLDL cholesterol. Journal of Endocrinology. 2020 Jun;246(3):265–76. doi:10.1530/JOE-19-0548 PubMed PMID: 32698129.
158. Yanai H, Adachi H, Hakoshima M, Katsuyama H. Postprandial Hyperlipidemia: Its Pathophysiology, Diagnosis, Atherogenesis, and Treatments. Int J Mol Sci. 2023 Jun;24(18). doi:10.3390/ijms241813942 PubMed PMID: 37762244.
159. Laronha H, Caldeira J. Structure and function of human matrix metalloproteinases. Cells. 2020 Jun;9(5). doi:10.3390/cells9051076 PubMed PMID: 32357580.
160. McCann MR, la Rosa MVG De, Rosania GR, Stringer KA. L-carnitine and acylcarnitines: Mitochondrial biomarkers for precision medicine. Metabolites. 2021 Jun;11(1):1–21. doi:10.3390/metabo11010051 PubMed PMID: 33466750.
161. Smolková K, Gotvaldová K. Fatty Acid Trafficking Between Lipid Droplets and Mitochondria: An Emerging Perspective. Int J Biol Sci. 2025;21(5):1863–73. doi:10.7150/ijbs.105361 PubMed PMID: 40083687.
162. Enkler L, Spang A. Functional interplay of lipid droplets and mitochondria. FEBS Lett. 2024 Jun;598(10):1235–51. doi:10.1002/1873-3468.14809 PubMed PMID: 38268392.
163. Moschandrea C, Kondylis V, Evangelakos I, Herholz M, Schneider F, Schmidt C, et al. Mitochondrial dysfunction abrogates dietary lipid processing in enterocytes. Nature. 2024 Jun;625(7994):385–92. doi:10.1038/s41586-023-06857-0 PubMed PMID: 38123683.
164. Rambold AS, Kostelecky B, Elia N, Lippincott-Schwartz J. Tubular network formation protects mitochondria from autophagosomal degradation during nutrient starvation. Proc Natl Acad Sci U S A. 2011 Jun;108(25):10190–5. doi:10.1073/pnas.1107402108 PubMed PMID: 21646527.
165. Gomes LC, Scorrano L. Mitochondrial elongation during autophagy: A stereotypical response to survive in difficult times. Autophagy. 2011;7(10):1251–3. doi:10.4161/auto.7.10.16771 PubMed PMID: 21743300.

166. Heck AM, Yanovski JA, Calis KA. Orlistat, a new lipase inhibitor for the management of obesity. Pharmacotherapy. 2000;20(3):270–9. doi:10.1592/phco.20.4.270.34882 PubMed PMID: 10730683.
167. Hvizdos KM, Markham A. Orlistat. A review of its use in the management of obesity. Drugs. 1999;58(4):743–60. doi:10.2165/00003495-199958040-00015 PubMed PMID: 10551441.
168. Dow RL, Li JC, Pence MP, Gibbs EM, Laperle JL, Litchfield J, et al. Discovery of PF-04620110, a potent, selective, and orally bioavailable inhibitor of DGAT-1. ACS Med Chem Lett. 2011 Jun;2(5):407–12. doi:10.1021/ml200051p PubMed PMID: 24900321.
169. Futatsugi K, Cabral S, Kung DW, Huard K, Lee E, Boehm M, et al. Discovery of Ervogastat (PF-06865571): A Potent and Selective Inhibitor of Diacylglycerol Acyltransferase 2 for the Treatment of Non-alcoholic Steatohepatitis. J Med Chem. 2022 Jun;65(22):15000–13. doi:10.1021/acs.jmedchem.2c01200 PubMed PMID: 36322383.
170. Sharma AK, Wolfrum C. DGAT inhibition at the post-absorptive phase reduces plasma FA by increasing FA oxidation . EMBO Mol Med. 2023 Jun;15(11). doi:10.15252/emmm.202318209 PubMed PMID: 37789773.
171. Janecek M, Bozdech Z, Sklensky M. Reconstruction of the wrist by the patient's own fibula in tumours of the distal radius. Acta Chir Orthop Traumatol Cech. 1988;55(6):549–55. PubMed PMID: 3218439.
172. Spitler KM, Shetty SK, Davies BSJ. Effects of age and diet on triglyceride metabolism in mice. J Lipid Res. 2025 Jun;66(1). doi:10.1016/j.jlr.2024.100706 PubMed PMID: 39566846.
173. Eckel-Mahan K, Sassone-Corsi P. Phenotyping Circadian Rhythms in Mice. Curr Protoc Mouse Biol. 2015 Jun;5(3):271–81. doi:10.1002/9780470942390.mo140229 PubMed PMID: 26331760.
174. Li Y, Li S, Wu H. Ubiquitination-Proteasome System (UPS) and Autophagy Two Main Protein Degradation Machineries in Response to Cell Stress. Cells. 2022 Jun;11(5). doi:10.3390/cells11050851 PubMed PMID: 35269473.
175. Harwood SM, Yaqoob MM, Allen DA. Caspase and calpain function in cell death: Bridging the gap between apoptosis and necrosis. Ann Clin Biochem. 2005 Jun;42(6):415–31. doi:10.1258/000456305774538238 PubMed PMID: 16259792.
176. Mauvezin C, Neufeld TP. Bafilomycin A1 disrupts autophagic flux by inhibiting both V-ATPase-dependent acidification and Ca-P60A/SERCA-dependent autophagosome-lysosome fusion. Autophagy. 2015 Jun;11(8):1437–8. doi:10.1080/15548627.2015.1066957 PubMed PMID: 26156798.
177. Raffeiner M, Zhu S, González-Fuente M, Üstün S. Interplay between autophagy and proteasome during protein turnover. Trends Plant Sci. 2023 Jun;28(6):698–714. doi:10.1016/j.tplants.2023.01.013 PubMed PMID: 36801193.
178. Lippai M, Low P. The role of the selective adaptor p62 and ubiquitin-like proteins in autophagy. Biomed Res Int. 2014;2014. doi:10.1155/2014/832704 PubMed PMID: 25013806.
179. Tanida I, Ueno T, Kominami E. LC3 and autophagy. Methods in Molecular Biology. 2008;445:77–88. doi:10.1007/978-1-59745-157-4_4 PubMed PMID: 18425443.
180. Rosenfeldt MT, Nixon C, Liu E, Mah LY, Ryan KM. Analysis of macroautophagy by immunohistochemistry. Autophagy. 2012;8(6):963–9. doi:10.4161/auto.20186 PubMed PMID: 22562096.
181. Zhang X, Connelly J, Chao Y, Wang QJ. Multifaceted functions of protein kinase d in pathological processes and human diseases. Biomolecules. 2021 Jun;11(3). doi:10.3390/biom11030483 PubMed PMID: 33807058.

182. Ding L, Huwyler F, Long F, Yang W, Binz J, Wernlé K, et al. Glucose controls lipolysis through Golgi PtdIns4P-mediated regulation of ATGL. Nat Cell Biol. 2024 Jun;26(4):552–66. doi:10.1038/s41556-024-01386-y PubMed PMID: 38561547.
183. Olzmann JA, Richter CM, Kopito RR. Spatial regulation of UBXD8 and p97/VCP controls ATGL-mediated lipid droplet turnover. Proc Natl Acad Sci U S A. 2013 Jun;110(4):1345–50. doi:10.1073/pnas.1213738110 PubMed PMID: 23297223.
184. Kao SH, Wang WL, Chen CY, Chang YL, Wu YY, Wang YT, et al. Analysis of Protein Stability by the Cycloheximide Chase Assay. Bio Protoc. 2015;5(1). doi:10.21769/bioprotoc.1374 PubMed PMID: 29082276.
185. Krahmer N, Najafi B, Schueder F, Quagliarini F, Steger M, Seitz S, et al. Organellar Proteomics and Phospho-Proteomics Reveal Subcellular Reorganization in Diet-Induced Hepatic Steatosis. Dev Cell. 2018 Jun;47(2):205-221.e7. doi:10.1016/j.devcel.2018.09.017 PubMed PMID: 30352176.
186. Xu M, Chen ZY, Li Y, Li Y, Guo G, Dai RZ, et al. Rab2A-mediated Golgi-lipid droplet interactions support very-low-density lipoprotein secretion in hepatocytes. EMBO Journal. 2024 Jun;43(24):6383–409. doi:10.1038/s44318-024-00288-x PubMed PMID: 39496977.
187. Du Y, Hu X, Chang W, Deng L, Ji WK, Xiong J. A Possible Role of VPS13B in the Formation of Golgi-Lipid Droplet Contacts Associating with the ER. Contact. 2023 Jun;6. doi:10.1177/25152564231195718 PubMed PMID: 38090145.
188. Pagnon J, Matzaris M, Stark R, Meex RCR, Macaulay SL, Brown W, et al. Identification and functional characterization of protein kinase A phosphorylation sites in the major lipolytic protein, adipose triglyceride lipase. Endocrinology. 2012 Jun;153(9):4278–89. doi:10.1210/en.2012-1127 PubMed PMID: 22733971.
189. Schweiger M, Eichmann TO, Taschler U, Zimmermann R, Zechner R, Lass A. Measurement of lipolysis. Methods Enzymol. 2014;538:171–93. doi:10.1016/B978-0-12-800280-3.00010-4 PubMed PMID: 24529439.
190. Piccolis M, Bond LM, Kampmann M, Pulimeno P, Chitraju C, Jayson CBK, et al. Probing the Global Cellular Responses to Lipotoxicity Caused by Saturated Fatty Acids. Mol Cell. 2019 Jun;74(1):32-44.e8. doi:10.1016/j.molcel.2019.01.036 PubMed PMID: 30846318.
191. Obaseki E, Adebayo D, Bandyopadhyay S, Hariri H. Lipid droplets and fatty acid-induced lipotoxicity: in a nutshell. FEBS Lett. 2024 Jun;598(10):1207–14. doi:10.1002/1873-3468.14808 PubMed PMID: 38281809.
192. Mortensen MS, Ruiz J, Watts JL. Polyunsaturated Fatty Acids Drive Lipid Peroxidation during Ferroptosis. Cells. 2023 Jun;12(5). doi:10.3390/cells12050804 PubMed PMID: 36899940.
193. Yang WS, Kim KJ, Gaschler MM, Patel M, Shchepinov MS, Stockwell BR. Peroxidation of polyunsaturated fatty acids by lipoxygenases drives ferroptosis. Proc Natl Acad Sci U S A. 2016 Jun;113(34):E4966–75. doi:10.1073/pnas.1603244113 PubMed PMID: 27506793.
194. Ye J, Li JZ, Liu Y, Li X, Yang T, Ma X, et al. Cideb, an ER- and Lipid Droplet-Associated Protein, Mediates VLDL Lipidation and Maturation by Interacting with Apolipoprotein B. Cell Metab. 2009 Jun;9(2):177–90. doi:10.1016/j.cmet.2008.12.013 PubMed PMID: 19187774.
195. Shin JY, Hernandez-Ono A, Fedotova T, Östlund C, Lee MJ, Gibeley SB, et al. Nuclear envelope–localized torsinA-LAP1 complex regulates hepatic VLDL secretion and steatosis. Journal of Clinical Investigation. 2019;129(11):4885–900. doi:10.1172/JCI129769 PubMed PMID: 31408437.

196. Bianco V, Korbelius M, Vujic N, Akhmetshina A, Amor M, Kolb D, et al. Impact of (intestinal) LAL deficiency on lipid metabolism and macrophage infiltration. Mol Metab. 2023 Jun;73. doi:10.1016/j.molmet.2023.101737 PubMed PMID: 37182562.
197. Díaz LA, Llinás G, Vázquez A, Tenorio A, Contigiani MS. Silent circulation of St. Louis encephalitis virus prior to an encephalitis outbreak in Cordoba, Argentina (2005). PLoS Negl Trop Dis. 2012 Jun;6(1). doi:10.1371/journal.pntd.0001489 PubMed PMID: 22303490.
198. Chen CW, Sowden M, Zhao Q, Wiedmer T, Sims PJ. Nuclear phospholipid scramblase 1 prolongs the mitotic expansion of granulocyte precursors during G-CSF-induced granulopoiesis. J Leukoc Biol. 2011 Jun;90(2):221–33. doi:10.1189/jlb.0111006 PubMed PMID: 21447647.
199. Hung YH, Carreiro AL, Buhman KK. Dgat1 and Dgat2 regulate enterocyte triacylglycerol distribution and alter proteins associated with cytoplasmic lipid droplets in response to dietary fat. Biochim Biophys Acta Mol Cell Biol Lipids. 2017 Jun;1862(6):600–14. doi:10.1016/j.bbalip.2017.02.014 PubMed PMID: 28249764.
200. Ellong EN, Soni KG, Bui QT, Sougrat R, Golinelli-Cohen MP, Jackson CL. Interaction between the triglyceride lipase ATGL and the arf1 activator GBF1. PLoS One. 2011;6(7). doi:10.1371/journal.pone.0021889 PubMed PMID: 21789191.
201. Pusapati GV, Krndija D, Armacki M, Wichert G Von, Blume J Von, Malhotra V, et al. Role of the second cysteine-rich domain and Pro275 in protein kinase D2 interaction with ADP-ribosylation factor 1, trans-Golgi network recruitment, and protein transport. Mol Biol Cell. 2010 Jun;21(6):1011–22. doi:10.1091/mbc.E09-09-0814 PubMed PMID: 20089835.
202. Eiseler T, Wille C, Koehler C, Illing A, Seufferlein T. Protein kinase D2 assembles a multiprotein complex at the trans-Golgi network to regulate matrix metalloproteinase secretion. Journal of Biological Chemistry. 2016 Jun;291(1):462–77. doi:10.1074/jbc.M115.673582 PubMed PMID: 26507660.
203. Fuchs YF, Eisler SA, Link G, Schlicker O, Bunt G, Pfizenmaier K, et al. A Golgi PKD activity reporter reveals a crucial role of PKD in nocodazole-induced Golgi dispersal. Traffic. 2009;10(7):858–67. doi:10.1111/j.1600-0854.2009.00918.x PubMed PMID: 19416469.
204. Choudhary V, Schneiter R. A Unique Junctional Interface at Contact Sites Between the Endoplasmic Reticulum and Lipid Droplets. Front Cell Dev Biol. 2021 Jun;9. doi:10.3389/fcell.2021.650186 PubMed PMID: 33898445.
205. Yang X, Heckmann BL, Zhang X, Smas CM, Liu J. Distinct mechanisms regulate ATGL-mediated adipocyte lipolysis by lipid droplet coat proteins. Molecular Endocrinology. 2013;27(1):116–26. doi:10.1210/me.2012-1178 PubMed PMID: 23204327.
206. Gruber A, Cornaciu I, Lass A, Schweiger M, Poeschl M, Eder C, et al. The N-terminal region of comparative gene identification-58 (CGI-58) is important for lipid droplet binding and activation of adipose triglyceride lipase. Journal of Biological Chemistry. 2010 Jun;285(16):12289–98. doi:10.1074/jbc.M109.064469 PubMed PMID: 20164531.
207. Mason RR, Meex RCR, Lee-Young R, Canny BJ, Watt MJ. Phosphorylation of adipose triglyceride lipase Ser404 is not related to 5′-AMPK activation during moderate-intensity exercise in humans. Am J Physiol Endocrinol Metab. 2012 Jun;303(4). doi:10.1152/ajpendo.00082.2012 PubMed PMID: 22713505.
208. Chang YY, Juhász G, Goraksha-Hicks P, Arsham AM, Mallin DR, Muller LK, et al. Nutrient-dependent regulation of autophagy through the target of rapamycin pathway.

Biochem Soc Trans. 2009;37(1):232–6. doi:10.1042/BST0370232 PubMed PMID: 19143638.
209. He C. Balancing nutrient and energy demand and supply via autophagy. Current Biology. 2022 Jun;32(12):R684–96. doi:10.1016/j.cub.2022.04.071 PubMed PMID: 35728554.
210. Mackinnon E, Stone SL. The Ubiquitin Proteasome System and Nutrient Stress Response. Front Plant Sci. 2022 Jun;13. doi:10.3389/fpls.2022.867419 PubMed PMID: 35665152.
211. Sadiq F, Hazlerigg DG, Lomax MA. Amino acids and insulin act additively to regulate components of the ubiquitin-proteasome pathway in C2C12 myotubes. BMC Mol Biol. 2007 Jun;8. doi:10.1186/1471-2199-8-23 PubMed PMID: 17371596.
212. Chotechuang N, Azzout-Marniche D, Bos C, Chaumontet C, Gaudichon C, Tomé D. Down-regulation of the ubiquitin-proteasome proteolysis system by amino acids and insulin involves the adenosine monophosphate-activated protein kinase and mammalian target of rapamycin pathways in rat hepatocytes. Amino Acids. 2011 Jun;41(2):457–68. doi:10.1007/s00726-010-0765-2 PubMed PMID: 20957397.
213. Singh R, Cuervo AM. Autophagy in the cellular energetic balance. Cell Metab. 2011 Jun;13(5):495–504. doi:10.1016/j.cmet.2011.04.004 PubMed PMID: 21531332.
214. Wójcik C, Lohe K, Kuang C, Xiao Y, Jouni Z, Poels E. Modulation of adipocyte differentiation by omega-3 polyunsaturated fatty acids involves the ubiquitin-proteasome system. J Cell Mol Med. 2014;18(4):590–9. doi:10.1111/jcmm.12194 PubMed PMID: 24834523.
215. Reginato A, Siqueira BP, Miyamoto JÉ, Portovedo M, de Oliveira Costa S, de Fante T, et al. Acute effects of fatty acids on autophagy in NPY neurones. J Neuroendocrinol. 2020 Jun;32(10). doi:10.1111/jne.12900 PubMed PMID: 33040385.
216. Gong Y, Lee JN, Lee PCW, Goldstein JL, Brown MS, Ye J. Sterol-regulated ubiquitination and degradation of Insig-1 creates a convergent mechanism for feedback control of cholesterol synthesis and uptake. Cell Metab. 2006 Jun;3(1):15–24. doi:10.1016/j.cmet.2005.11.014 PubMed PMID: 16399501.
217. Joon NL, Song B, DeBose-Boyd RA, Ye J. Sterol-regulated degradation of insig-1 mediated by the membrane-bound ubiquitin ligase gp78. Journal of Biological Chemistry. 2006 Jun;281(51):39308–15. doi:10.1074/jbc.M608999200 PubMed PMID: 17043353.
218. Cheng J, Ohsaki Y, Tauchi-Sato K, Fujita A, Fujimoto T. Cholesterol depletion induces autophagy. Biochem Biophys Res Commun. 2006 Jun;351(1):246–52. doi:10.1016/j.bbrc.2006.10.042 PubMed PMID: 17056010.
219. Shapira KE, Shapira G, Schmukler E, Pasmanik-Chor M, Shomron N, Pinkas-Kramarski R, et al. Autophagy is induced and modulated by cholesterol depletion through transcription of autophagy-related genes and attenuation of flux. Cell Death Discov. 2021 Jun;7(1). doi:10.1038/s41420-021-00718-3 PubMed PMID: 34716312.
220. Shao F, Ford DA. Differential regulation of ABCA1 and macrophage cholesterol efflux by elaidic and oleic acids. Lipids. 2013 Jun;48(8):757–67. doi:10.1007/s11745-013-3808-0 PubMed PMID: 23800855.
221. Chen D, Xia D, Li X, Zhu Q, Yu H, Zhu C, et al. Comparative study of Pluronic® F127-modified liposomes and chitosan-modified liposomes for mucus penetration and oral absorption of cyclosporine A in rats. Int J Pharm. 2013 Jun;449(1–2):1–9. doi:10.1016/j.ijpharm.2013.04.002 PubMed PMID: 23583840.
222. Liu WJ, Ye L, Huang WF, Guo LJ, Xu ZG, Wu HL, et al. p62 links the autophagy pathway and the ubiqutin-proteasome system upon ubiquitinated protein degradation.

Cell Mol Biol Lett. 2016 Jun;21(1). doi:10.1186/s11658-016-0031-z PubMed PMID: 28536631.
223. Webb JL, Ravikumar B, Atkins J, Skepper JN, Rubinsztein DC. α-synuclein Is Degraded by Both Autophagy and the Proteasome. Journal of Biological Chemistry. 2003 Jun;278(27):25009–13. doi:10.1074/jbc.M300227200 PubMed PMID: 12719433.
224. Wang Y, Mandelkow E. Degradation of tau protein by autophagy and proteasomal pathways. Biochem Soc Trans. 2012 Jun;40(4):644–52. doi:10.1042/BST20120071 PubMed PMID: 22817709.
225. Dolan PJ, Johnson GVW. A caspase cleaved form of tau is preferentially degraded through the autophagy pathway. Journal of Biological Chemistry. 2010 Jun;285(29):21978–87. doi:10.1074/jbc.M110.110940 PubMed PMID: 20466727.
226. Cohen-Kaplan V, Livneh I, Avni N, Fabre B, Ziv T, Kwon YT, et al. p62- and ubiquitin-dependent stress-induced autophagy of the mammalian 26S proteasome. Proc Natl Acad Sci U S A. 2016 Jun;113(47):E7490–9. doi:10.1073/pnas.1615455113 PubMed PMID: 27791183.
227. Ferreira JV, Fofo H, Bejarano E, Bento CF, Ramalho JS, Girao H, et al. STUB1/CHIP is required for HIF1A degradation by chaperone-mediated autophagy. Autophagy. 2013;9(9):1349–66. doi:10.4161/auto.25190 PubMed PMID: 23880665.
228. Wang X, Fan H, Ying Z, Li B, Wang H, Wang G. Degradation of TDP-43 and its pathogenic form by autophagy and the ubiquitin-proteasome system. Neurosci Lett. 2010 Jun;469(1):112–6. doi:10.1016/j.neulet.2009.11.055 PubMed PMID: 19944744.
229. Lei L, Wu Z, Winklhofer KF. Protein quality control by the proteasome and autophagy: A regulatory role of ubiquitin and liquid-liquid phase separation. Matrix Biology. 2021 Jun;100–101:9–22. doi:10.1016/j.matbio.2020.11.003 PubMed PMID: 33259919.
230. Janse DM, Crosas B, Finley D, Church GM. Localization to the proteasome is sufficient for degradation. Journal of Biological Chemistry. 2004 Jun;279(20):21415–20. doi:10.1074/jbc.M402954200 PubMed PMID: 15039430.
231. Lu K, den Brave F, Jentsch S. Pathway choice between proteasomal and autophagic degradation. Autophagy. 2017 Jun;13(10):1799–800. doi:10.1080/15548627.2017.1358851 PubMed PMID: 28813181.
232. Fregno I, Molinari M. Proteasomal and lysosomal clearance of faulty secretory proteins: ER-associated degradation (ERAD) and ER-to-lysosome-associated degradation (ERLAD) pathways. Crit Rev Biochem Mol Biol. 2019 Jun;54(2):153–63. doi:10.1080/10409238.2019.1610351 PubMed PMID: 31084437.
233. Pryor PR, Luzio JP. Delivery of endocytosed membrane proteins to the lysosome. Biochim Biophys Acta Mol Cell Res. 2009 Jun;1793(4):615–24. doi:10.1016/j.bbamcr.2008.12.022 PubMed PMID: 19167432.
234. Yang AL, McNabb-Baltar J. Hypertriglyceridemia and acute pancreatitis. Pancreatology. 2020 Jun;20(5):795–800. doi:10.1016/j.pan.2020.06.005 PubMed PMID: 32571534.
235. Ciregia F, Bugliani M, Ronci M, Giusti L, Boldrini C, Mazzoni MR, et al. Palmitate-induced lipotoxicity alters acetylation of multiple proteins in clonal β cells and human pancreatic islets. Sci Rep. 2017 Jun;7(1). doi:10.1038/s41598-017-13908-w PubMed PMID: 29044173.
236. Moliterni C, Vari F, Schifano E, Tacconi S, Stanca E, Friuli M, et al. Lipotoxicity of palmitic acid is associated with DGAT1 downregulation and abolished by PPARα activation in liver cells. J Lipid Res. 2024 Jun;65(12). doi:10.1016/j.jlr.2024.100692 PubMed PMID: 39505261.

237. Listenberger LL, Ory DS, Schaffer JE. Palmitate-induced Apoptosis Can Occur through a Ceramide-independent Pathway. Journal of Biological Chemistry. 2001 Jun;276(18):14890–5. doi:10.1074/jbc.M010286200 PubMed PMID: 11278654.
238. Xu S, Nam SM, Kim JH, Das R, Choi SK, Nguyen TT, et al. Palmitate induces ER calcium depletion and apoptosis in mouse podocytes subsequent to mitochondrial oxidative stress. Cell Death Dis. 2015;6(11). doi:10.1038/cddis.2015.331 PubMed PMID: 26583319.
239. Yin J, Wang Y, Gu L, Fan N, Ma Y, Peng Y. Palmitate induces endoplasmic reticulum stress and autophagy in mature adipocytes: Implications for apoptosis and inflammation. Int J Mol Med. 2015 Jun;35(4):932–40. doi:10.3892/ijmm.2015.2085 PubMed PMID: 25647410.
240. Harvey KA, Walker CL, Pavlina TM, Xu Z, Zaloga GP, Siddiqui RA. Long-chain saturated fatty acids induce pro-inflammatory responses and impact endothelial cell growth. Clinical Nutrition. 2010 Jun;29(4):492–500. doi:10.1016/j.clnu.2009.10.008 PubMed PMID: 19926177.
241. Kalyankrishna S, Parmentier JH, Malik KU. Arachidonic acid-derived oxidation products initiate apoptosis in vascular smooth muscle cells. Prostaglandins Other Lipid Mediat. 2002 Jun;70(1–2):13–29. doi:10.1016/S0090-6980(02)00010-2 PubMed PMID: 12428675.
242. Lindskog M, Gleissman H, Ponthan F, Castro J, Kogner P, Johnsen JI. Neuroblastoma cell death in response to docosahexaenoic acid: Sensitization to chemotherapy and arsenic-induced oxidative stress. Int J Cancer. 2006 Jun;118(10):2584–93. doi:10.1002/ijc.21555 PubMed PMID: 16353135.
243. Kampmeyer C, Larsen-Ledet S, Wagnkilde MR, Michelsen M, Iversen HKM, Nielsen S V, et al. Disease-linked mutations cause exposure of a protein quality control degron. Structure. 2022 Jun;30(9):1245-1253.e5. doi:10.1016/j.str.2022.05.016 PubMed PMID: 35700725.
244. Rodriguez MS, Desterro JMP, Lain S, Lane DP, Hay RT. Multiple C-Terminal Lysine Residues Target p53 for Ubiquitin-Proteasome-Mediated Degradation. Mol Cell Biol. 2000 Jun;20(22):8458–67. doi:10.1128/mcb.20.22.8458-8467.2000 PubMed PMID: 11046142.
245. Valdor R, Martinez-Vicente M. The Role of Chaperone-Mediated Autophagy in Tissue Homeostasis and Disease Pathogenesis. Biomedicines. 2024 Jun;12(2). doi:10.3390/biomedicines12020257 PubMed PMID: 38397859.
246. Suzuki H, Tabata K, Morita E, Kawasaki M, Kato R, Dobson RCJ, et al. Structural basis of the autophagy-related LC3/Atg13 LIR complex: Recognition and interaction mechanism. Structure. 2014 Jun;22(1):47–58. doi:10.1016/j.str.2013.09.023 PubMed PMID: 24290141.
247. Martinez-Lopez N, Garcia-Macia M, Sahu S, Athonvarangkul D, Liebling E, Merlo P, et al. Autophagy in the CNS and Periphery Coordinate Lipophagy and Lipolysis in the Brown Adipose Tissue and Liver. Cell Metab. 2016 Jun;23(1):113–27. doi:10.1016/j.cmet.2015.10.008 PubMed PMID: 26698918.
248. Seike T, Terasawa K, Iwata T, Guan JL, Watabe T, Yokoyama S, et al. Site-specific photo-crosslinking of Hsc70 with the KFERQ pentapeptide motif in a chaperone-mediated autophagy and microautophagy substrate in mammalian cells. Biochem Biophys Res Commun. 2024 Jun;736. doi:10.1016/j.bbrc.2024.150515 PubMed PMID: 39128268.
249. Ishikawa E, Kosako H, Yasuda T, Ohmuraya M, Araki K, Kurosaki T, et al. Protein kinase D regulates positive selection of CD4+ thymocytes through phosphorylation of

SHP-1. Nat Commun. 2016 Jun;7. doi:10.1038/ncomms12756 PubMed PMID: 27670070.
250. Konopatskaya O, Matthews SA, Harper MT, Gilio K, Cosemans JMEM, Williams CM, et al. Protein kinase C mediates platelet secretion and thrombus formation through protein kinase D2. Blood. 2011 Jun;118(2):416–24. doi:10.1182/blood-2010-10-312199 PubMed PMID: 21527521.
251. Xu G, Zhao Z, Wysham WZ, Roque DR, Fang Z, Sun W, et al. Orlistat exerts anti-obesity and anti-tumorigenic effects in a transgenic mouse model of endometrial cancer. Front Oncol. 2023;13. doi:10.3389/fonc.2023.1219923 PubMed PMID: 37601677.
252. Takemoto K, Fukasaka Y, Yoshimoto R, Nambu H, Yukioka H. Diacylglycerol acyltransferase 1/2 inhibition induces dysregulation of fatty acid metabolism and leads to intestinal barrier failure and diarrhea in mice. Physiol Rep. 2020 Jun;8(15). doi:10.14814/phy2.14542 PubMed PMID: 32786057.
253. Nash DR, Steingrube VA, Warrington RJ. Primary immune responsiveness and other observations in mice given oral dimethyl sulfoxide. Immunopharmacology. 1983;6(3):191–201. doi:10.1016/0162-3109(83)90020-6 PubMed PMID: 6355008.
254. Wang Y, Ghoshal S, Ward M, de Villiers W, Woodward J, Eckhardt E. Chylomicrons promote intestinal absorption and systemic dissemination of dietary antigen (Ovalbumin) in mice. PLoS One. 2009;4(12). doi:10.1371/journal.pone.0008442 PubMed PMID: 20041190.
255. Caron AZ, Haroun S, Leblanc É, Trensz F, Guindi C, Amrani A, et al. The proteasome inhibitor MG132 reduces immobilization-induced skeletal muscle atrophy in mice. BMC Musculoskelet Disord. 2011;12. doi:10.1186/1471-2474-12-185 PubMed PMID: 21843349.
256. Yuan N, Song L, Zhang S, Lin W, Cao Y, Xu F, et al. Bafilomycin A1 targets both autophagy and apoptosis pathways in pediatric B-cell acute lymphoblastic leukemia. Haematologica. 2015;100(3):345–56. doi:10.3324/haematol.2014.113324 PubMed PMID: 25512644.
257. Zhang C, Wei B, Liu Z, Yao W, Li Y, Lu J, et al. Bafilomycin A1 inhibits SARS-CoV-2 infection in a human lung xenograft mouse model. Virol J. 2023 Jun;20(1). doi:10.1186/s12985-023-01971-x PubMed PMID: 36721152.
258. Ding Y, Zhang S, Yang L, Na H, Zhang P, Zhang H, et al. Isolating lipid droplets from multiple species. Nat Protoc. 2013 Jun;8(1):43–51. doi:10.1038/nprot.2012.142 PubMed PMID: 23222457.
259. Brasaemle DL, Wolins NE. Isolation of lipid droplets from cells by density gradient centrifugation. Curr Protoc Cell Biol. 2016;2016:3.15.1-3.15.13. doi:10.1002/cpcb.10 PubMed PMID: 27580706.
260. Hughes CS, Moggridge S, Müller T, Sorensen PH, Morin GB, Krijgsveld J. Single-pot, solid-phase-enhanced sample preparation for proteomics experiments. Nat Protoc. 2019 Jun;14(1):68–85. doi:10.1038/s41596-018-0082-x PubMed PMID: 30464214.

PUBLICATIONS RECORD OF THE CANDIDATE

- Experimental:

1. Trujillo-Viera J, El-Merahbi R, Schmidt V, Karwen T, Loza-Valdes A, Strohmeyer A, Reuter S, Noh M, **Wit M**, Hawro I, Mocek S, Fey C, Mayer AE, Löffler MC, Wilhelmi I, Metzger M, Ishikawa E, Yamasaki S, Rau M, Geier A, Hankir M, Seyfried F, Klingenspor M, Sumara G. Protein Kinase D2 drives chylomicron-mediated lipid transport in the intestine and promotes obesity. EMBO Mol Med. 2021 May 7;13(5):e13548. doi: 10.15252/emmm.202013548. Epub 2021 May 5. PMID: 33949105; PMCID: PMC8103097.

2. Karwen T, Kolczynska-Matysiak K, Gross C, Löffler MC, Friedrich M, Loza-Valdes A, Schmitz W, **Wit M**, Dziaczkowski F, Belykh A, Trujillo-Viera J, El-Merahbi R, Deppermann C, Nawaz S, Hastoy B, Demczuk A, Erk M, Wieckowski MR, Rorsman P, Heinze KG, Stegner D, Nieswandt B, Sumara G. Platelet-derived lipids promote insulin secretion of pancreatic β cells. EMBO Mol Med. 2023 Sep 11;15(9):e16858. doi: 10.15252/emmm.202216858. Epub 2023 Jul 25. PMID: 37490001; PMCID: PMC10493578.

- Review:

1**. Wit M**, Trujillo-Viera J, Strohmeyer A, Klingenspor M, Hankir M, Sumara G. When fat meets the gut-focus on intestinal lipid handling in metabolic health and disease. EMBO Mol Med. 2022 May 9;14(5):e14742. doi: 10.15252/emmm.202114742. Epub 2022 Apr 19. PMID: 35437952; PMCID: PMC9081902.

2. **Wit M**, Belykh A, Sumara G. Protein kinase D (PKD) on the crossroad of lipid absorption, synthesis and utilization. Biochim Biophys Acta Mol Cell Res. 2024 Feb;1871(2):119653. doi: 10.1016/j.bbamcr.2023.119653. Epub 2023 Dec 15. PMID: 38104800.